On dew and micrometeorology in an arid coastal ecosystem

Bert G. Heusinkveld

Promotor:

Prof. dr. A.A.M. Holtslag	Hoogleraar in de meteorologie Leerstoelgroep Meteorologie en Luchtkwaliteit, Wageningen Universiteit

Co-promotor:

Dr. ir. A.F.G. Jacobs	Universitair hoofddocent Leerstoelgroep Meteorologie en Luchtkwaliteit Wageningen Universiteit

Samenstelling promotiecommissie:

Prof. dr. A. Kaplan	Hebrew University, Jerusalem, Israel
Prof. dr. T. Foken	University of Bayreuth, Germany
Prof. dr. ir. B.J.J.M. v.d. Hurk	Universiteit Utrecht, KNMI, De Bilt
Prof. dr. ir. S.E.A.T.M. van der Zee	Wageningen Universiteit

Dit onderzoek is uitgevoerd binnen de onderzoeksschool Productie Ecologie.

On dew and micrometeorology in an arid coastal ecosystem

Bert G. Heusinkveld

Proefschrift
ter verkrijging van de graad van doctor
op gezag van de rector magnificus
van Wageningen Universiteit,
Prof. dr. M.J. Kropff,
in het openbaar te verdedigen
op woensdag 4 juni 2008
des namiddags te vier uur in de Aula

CIP-data Koninklijke Bibliotheek, Den Haag

On dew and micrometeorology in an arid coastal ecosystem

Heusinkveld, B.G., 2008

PhD thesis, Wageningen University, The Netherlands
With references – with summaries in English and Dutch

ISBN 978-90-8504-932-6

Voorwoord

Dankbaar en blij dat het proefschrift klaar is wil ik beginnen met een voorwoord om al die mensen nog eens naar voren te halen die op een of andere manier hebben bijgedragen tot deze mijlpaal.

Promotor Bert Holtslag wil ik danken voor de inhoudelijke discussies en de stimulering die daarvan uitging. Mijn co-promotor Adrie Jacobs wil ik bedanken voor zijn toegewijde begeleiding en zijn altijd bijzonder positieve instelling. Adrie, wat hebben we eigenlijk veel samen beleefd, of moet ik zeggen overleefd? Als ik zo terugkijk, dan begon het eigenlijk met zo'n reisje op de Rijn, maar dan wel hartje winter en hoogste waterstand. Ja, om een system beter te leren kennen moeten soms extremen opgezocht worden. Ook in het onderzoek ging dat op, want we zijn uiteindelijk een droge woestijn in gegaan voor het dauw onderzoek. Dat we daarbij ook bij nacht en ontij onze metingen moesten verrichten maakte het ook weer avontuurlijk. Het onderzoek in de Negev woestijn was niet mogelijk geweest zonder de enorme toewijding en motivatie van mijn Israelische vriend Simon Berkowicz. Simon, you are a fantastic friend and your enthousiasm has always pushed the research forward. Your Jewish mother instinct has helped me through hard times! Aron Kaplan, thank you for providing the experimental site and support. Eyal Sachs, you logistics support and humor was very much appreciated. Ariel Cohen and Shy Ron, thank you for watching after us and helping out during noctural measurements, shalom! Jos van Dam je hebt me geweldig geholpen met het bepalen van de vochtkarakteristieken! Peter Felix-Henningson möchte ich danken für die Luftnahe Bodenschicht Beratung.

Wat een geweldige werksfeer bij MAQ. Gerrie van den Brink, je was altijd een steun en toeverlaat. Kees Stigter, wat heb ik een respect voor jouw werk in Afrika gekregen. Kees, je hebt me het belang van wetenschappelijk onderzoek naar soms vanzelfsprekende landbouwmeteorologische methoden laten zien. Kees van den Dries, dank dat je altijd klaar staat voor allerlei hulp, ook als het niet met een computer te maken heeft! Frits Antonijsen, je was altijd een steun en toeverlaat tijdens de veldexperimenten. Willy Hillen, wat kun je mooie dingen maken uit een blokje metaal of kunststof. Joost Nieveen, dank voor jouw bijdrage in het opstarten van dit STW (Stichting Technische Wetenschappen) project. En hierbij wil ik dan ook tevens technologiestichting STW danken voor de sponsoring van dit onderzoek. Arjan van Dijken, je hebt een grote bijdrage geleverd aan het fundamenteel uitwerken en opzetten van de software voor de verwerking van turbulentie metingen en jouw discussies worden zeer gemist. Henk de Bruin, dankzij jou heb ik veel geleerd van de vele internationale veldexperimenten. Wim Kohsiek, ik genoot altijd van de discussies over instrumentele ontwikkeling. Rushdi M. M. El-Kilani, thanks for the interesting

discussions and salam aleikum, we miss you! Krijn Paaimans, ik zal niet gauw onze muggensafari vergeten! Jordi Villa, Leo Kroon, Arnold Moene, Wouter Meijninger, Oscar Hartogensis, Bas van de Wiel, Gert Jan Steeneveld, Bert van Hove, Roy Wichink Kruit wil ik danken voor de prettige samenwerking. Joel Schröter, vielen Dank für die Interesse an meiner Arbeit! Peter Hofschreuder, jouw inbreng verlevendigt de groep. Maarten Krol zet je strijd voort voor betere luchtkwaliteit ook op de vakgroep. Chiel van Heerwaarden, dank voor het inwijden in de vele fiets cols in Limburg.

Verder wil ik mijn vrienden bij Ibex vermelden, want tijdens het klimmen wordt steeds weer veel nieuwe energie opgedaan. Johan Koelman, wat een geweldige boulderproblemen hebben we al opgelost. Het benodigde doorzettingsvermogen daarvoor blijkt ook te werken voor het afronden van het proefschrift. Toru Furukubo you are a very good friend, sayonara, and see you soon! Ook niet te vergeten zijn de mooie en soms stormachtige zeiltochten met Marcel Wokke en de Aqua's. Saakje Hazenberg, thanks for the relaxing long distance ski touring weekends! Hans Kleingeld, je hebt me een tijdje moeten missen op het water vanwege mijn schrijfwerk, maar binnenkort hoop ik het speeden weer met je te kunnen delen!

Tenslotte wil ik mijn lieve ouders en broer Robbie bedanken voor de steun en toeverlaat.

Abstract

This study investigated intriguing aspects of dew within a sandy arid ecosystem situated in the NW Negev desert, Israel. The goal was to quantify dew formation and evaporation processes through sensor design, field measurements and modelling. To do this, two new sensors were developed. The first sensor is an automated microlysimeter for measurements of water content changes within the upper soil layer. This sensor uses a sensitive inexpensive Load Cell to provide daily records of dew input and evaporation. Dew amounts reached almost 0.4 mm day^{-1} but were found to depend strongly on the soil type. The second sensor developed was a remote optical surface wetness sensor that was designed and tested in the laboratory and in the Negev desert. The novelty of the sensor is that it measures surface wetness directly at the interface of the atmosphere, it is non-destructive and allows for repetitive measurements on the same sample, and it can operate outdoors without being affected by direct sunlight. The sensor was found to be capable of measuring leaf water content and near soil surface water content. Data obtained for an *Anabasis articulata* bush showed that leaves change their leaf water content during the evening.

In general, errors in flux measurements can lead to difficulties in closing the energy balance at the surface, especially if turbulent flux or soil heat flux measurements are underestimated. Soil heat flux was assessed during the field experiments using a new approach. By placing the soil heat flux sensor near the surface, depth corrections are no longer needed. It is shown that the large soil heat fluxes in hot desert regions are very important in energy balance studies. The soil heat flux measurements led to a very good closure of the surface energy balance and highlighted the importance for careful soil heat flux measurements.An analysis of dew formation conditions revealed that the actual dew is greater than the calculated potential dew. The dew formation process seems to be enhanced by the extreme dryness of the soil. The dry soil pores reduce vapour pressure and increase the downward vapour flux. This is demonstrated by using a Penman model and incorporating the vapour pressure reduction of the soil surface.

The dew amount that is available within a soil is limited by the soil physical properties. The term FAD "Free Available Dew" is introduced to define the amount of water available for biological activity. The FAD would be higher for a biological crust with cyanobacteria than for vascular plant roots. The FAD for cyanobacteria is around 20% of total dew. To improve our understanding of the distribution and flow of dew water within a sandy soil covered with a biological crust, a multilayer soil model was constructed. The model was tested with the microlysimeter data and gravimetric soil moisture profile measurements. Diurnal soil moisture variation was found to be

confined to the top 15 mm. The FAD is available in the upper half of a 4 mm thick biological crust only and limited to < 25% of the day.

The possibility of harvesting dew from an artificial flat surface within the interdune was investigated by constructing a dew collector and analyzing the measurements. This resulted in a detailed dew model to simulate dew yield in general. Dew yields of 0.30 mm day^{-1} are possible in the NW Negev desert at a location 40 km from the coast at the end of the dry season. The artificial flat surface tested here provided 0.10 mm day-1. Modelled yields were found to be larger near the coastline.

Open path gas analyzers and ultrasonic anemometers have been used to measure water vapour fluxes. Dew can affect the performance of open path gas analyzers and thus affect data quality in an arid environment. A field experiment showed that additional sensor heating can avoid dew problems and yet greatly improve the quality of flux measurements. A detailed energy balance model of the gas analyzer window housings is presented so that existing datasets can be filtered for dew contamination events on the windows. Additional heating does influence the measured concentration but the effect is very minor.

Table of contents

1 General introduction 1

2 Surface energy balance closure in an arid region: Role of soil heat flux 15

3 An automated microlysimeter to study dew formation and evaporation in arid and semi-arid regions 43

4 A new remote optical wetness sensor and its applications.....61

5 Dewfall and soil water flow in a sand dune ecosystem possessing biological soil crusts 91

6 Observations and model calculations for dew collection on a flat surface in the NW Negev desert, Israel 123

7 Effect of open path gas analyzer wetness on eddy covariance flux measurements; a proposed solution 145

8 Summary and perspectives on future research 171

1 General introduction

1.1 Background

Dew is the result of condensation of water vapour onto relatively cool surfaces. It can originate from separate sources; the air ("dew-fall") and from the moist soil where the evaporating water condenses on nearby relatively cool natural surfaces such as plant leaves (Monteith, 1957). In deserts, which are characterized by very low soil moisture, "dew-fall" is the predominant source of such moisture.

Environmental importance

Dew plays a special role in many ecosystems because of its small but regular supply of moisture to a given surface. Both florae and faunae can profit form dew. Desert soil faunae, such as nematodes, are sensitive to dew deposition on a soil surface (Steinberger et al. 1989). Desert arthropods, such as isopods, ants, and beetles rely on dew as a significant moisture source (Broza 1979; Moffett 1985) and desert landsnails become active when the soil is wet from dew (Nevo et al. 1981). Spider webs can be laden with dew on heavy dew evenings, contributing to webs breaking due to the increased load (Brackenbury 1997). Larmuth and Harvey (1978) found that desert seedling distribution in a reg desert of Morocco was greatest near a stone, and speculated on the role of stones as both a dew collector and funnel of dew. Dew may also contribute to seed germination and assist in the adhesion of dust and fine materials to surfaces. Gutterman and Shem-Tov (1997) noted that certain desert plants have seeds that develop a mucilaginous layer when wetted and can then adhere to a soil surface. They believe that although dew wetting is insufficient to cause seed germination, it may help in priming the seed. Recent studies on dew deposition, plant water relations, and diurnal variations of photosynthesis in some Mediterranean shrubs and plants found that the leaves were able to absorb dew and thus restore plant water status (Munne-Bosch et al., 1999; Munne-Bosch & Alegre, 1999). Dew can affect understorey plant species in forests (Barradas & Glez-Medellin, 1999).

Surface wetness is an important parameter in arid to Mediterranean ecosystems, where dew and/or fog are usually the only source of water input during the hot or rainless periods. Arid and semi-arid sand dune ecosystems may contain biotic crusts, up to several mm thick, composed of cyanobacteria, mosses, lichens, and algae (Lange et al., 1992). The development of such crusts is largely determined by water availability for the crust organisms, in addition to temperature and light conditions, which is the key parameter controlling the activity of the microbial crust community (Harel et al. 2004). Nocturnal dew can be a major source of water for these organisms (Jacobs et al. 2000). The crusts help stabilize the dunes (Danin et al.,

1989), inhibit rain infiltration (Yair, 1990) as well as evaporation from the soil due to its protective cover (Jacobs et al., 1999, 2000).

Aeolian sand transport is highly dependant on soil surface moisture. Wiggs et al., (2003) investigated the influence of changes in surface moisture content on sand entrainment and transport on a meso-tidal beach.

In agriculture, leaf surface wetness is well-known for contributing to the development of plant pathogens, foliar bacteria, crop epidemics and pests (Baier, 1966, Bass et al., 1991; Hatefield & Thomases, 1982; Huber & Gillespie, 1992; Jacobs et al., 1990; Lou & Goudriaan, 2000; Wallin, 1963, 1967), with severe economic repercussions. *Botrytis-spp.* in lilies and *Phytophthora infestans* in potatoes are feared for their rapid destructive work (Doornik & Bergman, 1974; Shoemaker & Lorbeer, 1977; Royle & Butler, 1986). Farmers avoid crop risks by preventive spraying of costly fungicides/pesticides on a very regular time schedule. These sprayings can be considerably reduced if reliable prognostic estimates can be made of actual leaf wetness duration (e.g. Norman, 1982; Weiss & Norman, 1987) and can be applied to both field crops and greenhouses. This would decrease farming costs and reduce the amount of chemicals introduced into the environment.

Surface wetness has a great effect on evaporation and surface temperature, (Monteith, 1981; Holtslag and De Bruin, 1988). Kiondo (1990) showed how the partitioning of the surface energy balance components depends on soil moisture content.

Dew measurement challenges

Insights into the exchange processes of heat and mass in arid and semi-arid environments require that reliable measurements can be made of dew and its subsequent evaporation. The absolute amounts, however, are small and are not likely to exceed 0.4 mm per evening (Jacobs et al. 2000). As noted by Zangvil (1996), dew formation has been a neglected area of desert meteorology. It is thus not surprising that attempts to evaluate the multiple role dew plays in the environment and in ecosystems have been hindered by the very difficulty of dew measurement. Approaches have included destructive sampling, moisture-absorbing material, dew-drop size calibrations, electrical surface wetness circuits, and assessment of dew on proxy surfaces (Berkowicz et al. 2001, Richards 2004 and Agam & Berliner 2006). Single measurements taken near sunrise will, at best, provide only maximum dew amounts for the particular surface under study. This does not take into account possible drying during the evening. However, dew onset, accumulation (and rate), and evaporation, can be of primary interest, for example, in agriculture where dew is a factor in the development of plant diseases (Wallin 1967). There is a need for dew sensors to allow repetitive measurements to be performed, but with a capability for automated recording at desired time intervals.

The ability to detect and measure moisture upon surfaces has intrigued scientists for decades. Concise reviews covering several aspects of this issue are contained in Berkowicz et al. (2001), Richards (2004) and Agam & Berliner (2006). If the source of the moisture is dew (and to some extent fog), then surface properties will heavily influence the formation, rate and amount of condensation. Soils, tree/plant leaves, rocks, and man-made materials (cement, ceramic, metals, glass) have different inherent thermal and physical properties. Surfaces moistened by rain may also be of interest.

Attempts to directly detect/measure surface moisture have been greatly hindered by a lack of suitable sensors. Over the past 50 years, much attention has been given to the development of techniques (i.e. numerical models) and instruments to make reliable estimates of dew amounts and leaf wetness duration (Wallin, 1963; Burrage, 1972). Such instruments are based, however, on indirect approaches. For example, dew drops forming on wooden blocks (e.g. Duvdevani, 1947), electrical resistance grids (e.g. Gillespie & Kidd, 1978).

Deserts offer unusual research possibilities for dew research

Dew has received less attention by hydrologists and ecologists, primarily because of their far-smaller quantitative output relative to rainfall. There were several considerations in working in a desert area for the purposes of this research. First, the study site in the NW Negev desert of Israel experiences dew approximately 200 evenings per year (Evenari 1982; Zangvil 1996), mainly in summer. In addition, the hot rainless period is usually 6 to 7 consecutive months (i.e. from April to October), but up to 9 consecutive months during a drought year (Berkowicz 2003). The drying of the upper soil simplifies the research since noe may focus on the dew input condensing at the surface. Thus an intensive field campaign during the late summer could generate considerable data within a short period of time.

Early studies in the Negev desert, though crude, showed that the frequency and amount of dew depended on distance from the sea (Ashbel, 1949). Ashbel (1949) found that the annual number of dew nights by the coast was up to 250 and the amount up to 150 mm. The amount of dew is unreasonable but is likely related to how Ashbel performed his measurements. Moist air is the source for dew and it can be expected that this is not a limiting factor near the sea.

Biological Soil Crusts within a fragile ecosystem

In arid and semi-arid regions, biological soil crusts (BSC) often constitute more than 70% of the living cover (Belnap, 1995). These crusts are prominent in many drylands and can be found in diverse parts of the globe including the major desert regions in the USA (Arizona, New Mexico, Colorado), Chile (Atacama desert), South Africa, and the Negev desert. The BSC have a photosynthetic active layer on

the soil bulk material and serve as an interface between soil and atmosphere. Dew can provide a regular supply of moisture to generate crust activity.

The pioneers in colonising the soil surface are the cyanobacteria; green algae, mosses and lichens (Lange et al., 1992). Heterotrophic communities of microfungi and bacteria are associated with and supported by the photosynthetic layer.

High rates of assimilation for such crusts in the Negev desert of Israel were measured along dune slopes. The extensive cover of even a thin layer of photo synthetically active organisms was shown to be an important basis for carbon fixation in an environment where primary production is low (Zaady et al., 2000 and Lange et al., 1992). Especially in coastal deserts (Namib, Negev, Atacama) where locally generated wind patterns transport moist air inland, nocturnal radiative cooling can generate a substantial amount of dew. Although these moist conditions may favour photosynthetic activity during a brief early morning window when moisture and light briefly coincide, the rising sun soon desiccates the active crust into a dormant state.

In a dryland dune ecosystem, BSC can be up to 4 mm thick and can stabilize sand and sand dune movement, thus hindering soil degradation and promoting recovery following disturbance. The BSC influence local hydrology and can create their own microclimate. These factors improve soil quality because they contribute to nitrate and carbons to the soils, and to the establishment of higher order vascular plant species (Belnap, 1995, 2003).

The impact of crusting on a desert ecosystem can be illustrated by a satellite image (Fig. 1.1) showing the northern Negev desert in Israel and Egyptian Sinai; the border is clearly recognized due to different albedo. This image illustrates the impact of different land use practices in a sandy desert with biological crusting. Winter-rain agriculture and grazing have removed most vegetation and the protective crust on the Egyptian side (i.e. higher albedo and drifting sand dunes), while the Israeli side ceased all such activity since 1982 (i.e. crust recovery, vegetation growth and stabilisation of the dunes).

Figure 1.1: Satellite image (Google earth, 4.3 km^2) of the northern Negev desert. The study area is the square with linear dune systems. Clearly visible is the border line between Egypt and Israel.

Although dew does not directly input water to deeper soil layers, dew can contribute to the water balance of the near soil surface and supply a BSC with water on a regular basis, whereas rain input is restricted and confined to part of the year. It is important to note that research on crust photosynthesis has been conducted primarily under laboratory conditions. A better understanding is needed of the meteorological conditions contributing to biological crust formation and growth.

1.2 The Negev field experiments

The north-western part of the Negev desert of Israel (see box in Fig. 1.1 and Fig. 1.2) was selected for the dew field experiments. The proximity to the Mediterranean Sea qualifies the Negev desert as a coastal desert and the northern part experiences frequent dew occurrences throughout the year especially during the long, hot summer. Zangvil (1996) outlined the synoptic conditions promoting dew formation in this region. The land-sea breeze transports moist air inland during daytime and it is a local wind circulation pattern driven by the surface temperature

difference between the land surface and sea. The thermal radiative heat loss cools moist air during the night and maintains the dew formation process during the night.

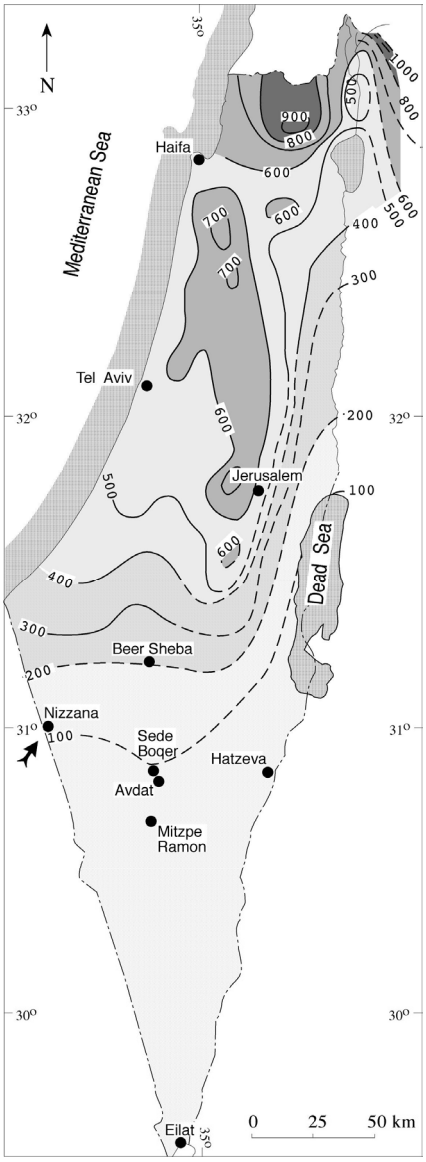

Figure 1.2: Location map showing annual average rainfall isohyets for 1961 - 1990 (after Israel Meteorological Service), and study site (bold arrow).

A transect crossing through the linear dune system within the study area, reveals three main landscape components (Fig. 1.3):

1. Mobile crest (from 0-10 and 230 .. 240 m)
2. Dune slopes with biological crusting (from 10 - 50 m and 190 – 230 m)
3. Interdune containing playa soils (60 .. 190 m)

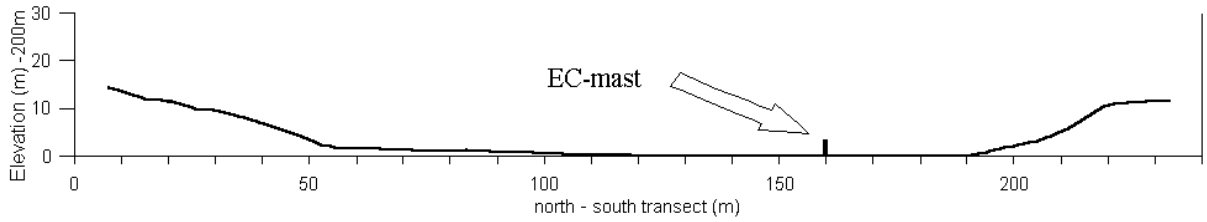

Figure 1.3: Cross-section of study area, EC = location of the ultrasonic anemometer mast.

A biological crust in area 2 can be identified as a thin mat of a few mm thickness covering the mobile sand. The crust acts as a boundary between the underlaying sand and the atmosphere and this influences gas and water exchange in the soil and the air above (Belnap et al., 2003). Dew (or fog interception) directly inputs water to the soil curst. The crust swells when wet, leading to a blockage of the access pores and this leads to an increased runoff and a reduction in evaporation in the sand below (Verrecchia et al., 1995). Area 3 has a physical crust and thus the soil composition has a higher silt and clay content.

The microclimatic differences are great between a bare soil and a soil covered by vegetation. Figure 2 shows an example comparing the mid-latitude grassland Wageningen University Haarweg meteorological station with the Negev desert for the same incoming solar radiation; there is a 50% difference in shortwave radiation reflection and the emitted thermal radiation is far larger from the bare soil because of the lack of evaporative cooling.

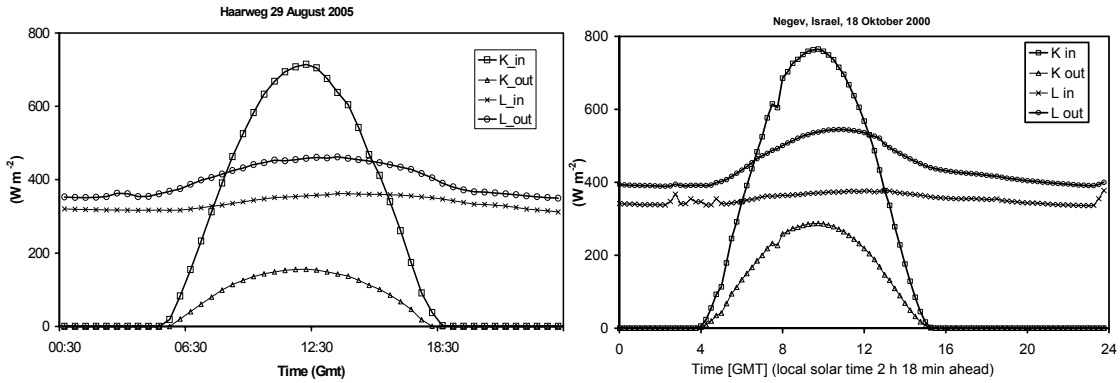

Figure 1.4: Shortwave and longwave radiation balance components of a grass cover at Haarweg meteorological station, the Netherlands (August 29, 2005) (left panel) and Negev desert, Israel (right panel).

The nocturnal heat-loss by the thermal infrared radiation is larger for the Negev site. Whether this will lead to dew formation will depend on various factors (Monteith, 1957). The nocturnal radiative heat loss will cool the soil and air whereby atmospheric moisture might condense and limit further cooling. This can be described by the surface energy balance. At the surface, the net radiative energy flux (Q^*) should be balanced by the soil heat flux (G), sensible heat flux (H), and latent heat flux (L_vE) (Eq. 1.1):

$$Q^* = H + L_v E + G \tag{1.1}$$

Both the sensible heat flux that cools the air during the night and the soil heat released during the night limit the available cooling energy for condensation. Changes in land cover will have a direct effect on the partitioning of the energy balance fluxes. Climate change may have an effect on desertification and this will likely increase. Since the biological crusts are photosynthetically active, a decline in their global presence or activity may have a negative impact on the global carbon budgets and this can lead to a positive feedback on climate change. However, the resulting increase in albedo may suppress global warming.

1.3 Objectives and research questions

This study focuses on the microclimate of a sandy desert ecosystem with biological soil crusts (BSC). Two measurement programmes were initiated that focussed on the microclimate conditions favouring dew. The first was carried out in 1997 to obtain a good overview of the dew process. In 2000, the micrometeorological factors controlling dew formation and drying were studied.

Because the microclimatic conditions favouring dew are complex and the amounts are low, this dew research required special instrumentation to quantify the amount of dew. A new microlysimeter was thus developed. The detection of the condensation process without instrumentation interference was another challenge and required the design of a novel sensor for remote sensing of surface wetness conditions.

An intriguing aspect of dew is its movement in the top soil layer of a sandy desert. The field campaigns enabled detailed information to be gained about the dew formation and drying process, and dew water penetration into a soil covered with a biological crust. As it is not clear what effect climate change will have on ecosystems with biological crusting, it is essential to acquire good quality dew input data.

In summary the research was directed at:

1. The role of soil heat flux in the energy balance in a coastal desert ecosystem,
2. Quantifing (through sensor development and measurements) dew deposition and evaporation in a coastal desert ecosystem,
3. Analyzing the conditions that favour dew formation,
4. Developing and validating a numerical model to investigate dew water flows within a soil surface.

1.4 Organisation of this thesis

Soil heat flux plays a major role in the surface energy balance (Eq. 1.1). This soil heat flux was thus assessed in the field site and is discussed in Chapter 2. New instruments were needed to quantify the amount of dew and lead to the design of two instruments; an automated microlysimeter and a remote optical wetness detector. The microlysimeter is described in Chapter 3 and contains data comparing dew formation in two soil types in the research site (Fig. 1.3). Chapter 4 reports on the design and experimental data of a novel sensor for remote sensing of surface moisture conditions. The processes involved in dew formation and evaporation and the migration of water into the soil are studied in detail in chapter 5. Experimental results from chapter 3 and 4 are used, as well as additional measurements of soil water content. A soil model was constructed to simulate water flows in the upper soil layer and a second model was constructed to understand the dew formation process (Chapter 5).

The potential of harvesting dew in a coastal desert region is presented in Chapter 6. A flat isolated plate of 2.5 m^2 was used to test dew collection conditions on an artificial surface. A model was constructed to simulate the collector performance under various conditions. The collection method can be used as a potential source of clean water.

Chapter 7 discusses problems associated with dew formation on optical instruments for the detection of water vapour and CO_2. Such a sensor was operated during the second measurement campaign to study latent heat fluxes.

References

Agam, N., Berliner P.R., 2006. Dew formation and water vapor adsorption in semi-arid environments- A review. J. Arid Environ. 65, 572-590.

Ashbel, D., 1949. Frequency and distribution of dew in Palestine. Geographical Review, 34 (2); 291-297.

Barradas, V.L., Glez-Medellin, M.G., 1999. Dew and its effect on two heliophile understorey species of a tropical dry deciduous forest in Mexico. Int. J. Biometeorol. 43, 1-7.

Baier, W., 1966. Studies on dew formation under semiarid conditions. Agric. Meteorol. 3, 103-112.

Bass, B., Savdie, I., Gillespie, T.J., 1991. Simulation of leaf wetness duration for field corn. Agric. For. Meteorol. 57, 69-84.

Belnap J., Hawkes, C.V., Firestone, M.K., 2003. Boundaries in miniature: Two examples from soil. Bioscience 53, 739-749.

Belnap, J., Prasse R., Harper, K.T., 2003. Influence of biological soilcrusts on soil environments and vascular plants. In: Belnap J, Lange OL (eds) Biological soil crusts: structure, function, and management. Springer, Berlin Heidelberg New York, pp 281–300.

Belnap J., Phillips, S.L., Miller, M.E., 2004. Response of desert biological soil crusts to alterations in precipitation frequency. Oecologia (2004) 141: 306–316, DOI 10.1007/s00442-003-1438-6.

Belnap J (1995). Surface disturbances: their role in accelerating desertification. Environ Monit Assess 37:9–57.

Berkowicz, S.M., Heusinkveld, B.G., and Jacobs, A.F.G., 2001: Dew in an arid ecosystem: Ecological aspects and problems in dew measurement. Proc., 2nd International Conference on Fog and Fog Collection,15-20 July 2001, St. John's, Newfoundland, Canada. pp 301-304.

Berkowicz, S.M., 2003: Nizzana rainfall data summary. Unpublished internal report. Arid Ecosystems Research Centre, Hebrew University of Jerusalem, Jerusalem, Israel.

Brackenbury, J.H., 1997: Spider webs: dew loading of the linyphid sheet-web. *J. Zool. London*, 242, 131-136.

Broza, M., 1979: Dew, fog and hygroscopic food as a source of water for desert arthropods. *J. Arid Environ.*, **2**, 43-49.

Burrage, S.W., 1972. Dew on wheat. Agric. Meteorol. 10, 3-12.

Danin, A., Bar-Or, Y., Dor, I., Yisraeli, T., 1989. The role of cyanobacteria in stabilisation of sand dunes in southern Israel. Ecol. Mediter. XV, 55-64.

Doornik A.W., Bergman, B.H.H., 1974. Infection of tulip bulbs by botrytis-Tulipae originating from spores or contaminated soil. J. Horticult. Sci. Biotech. 49, 203-207.

Duvdevani, S., 1953: Dew gradients in relation to climate, soil and topography. Proceedings of the International Symposium on Desert Research. Research Council of Israel, special public. No. 2, 136-148

Evenari, M., Shanan, I., and Tadmor, N., 1982: *The Negev: Challenge of a Desert*. University Press, Cambridge Mass., 284 pp.

Gillespie, T.J., Kidd, G.E., 1978. Sensing duration of leaf moisture retention using electrical impedance grids. Can. J. Plant Sci. 58, 179-187.

Gutterman, Y., and Shem-Tov, S., 1997: Mucilaginous seed coat structure of *Carrichtera annua* and *Anastatica hierochuntica* from the Negev Desert highlands of Israel, and its adhesion to the soil crust. *J. Arid Environ.*, 35, 695-705

Harel, Y., Ohad, I., and Kaplan, A., 2004: Activation of photosynthesis and resistance to photoinhibition in cyanobacteria within biological desert crust. *Plant Physiology*, 136, 3070-3079.

Hatefield, J., Thomases I., 1982. (eds.). Biometeorology in Integrated Pest Management. Academic Press, New York. 491 pp.

Holtslag, A.A.M., DeBruin, H.A.R., 1988. Applied modeling of the nighttime surface-energy balance over land. J. of Appl. Meteorol. 27, 689-704.

Huber, L., Gillespie, T.J., 1992. Modelling leaf wetness in relation to plant disease epidemiology. Annual Rev. Phytopathology 30, 553–77.

Jacobs, A.F.G., Van Pul, W.A.J., Van Dijken, A., 1990. Similarity dew profiles within a corn canopy. J. Applied Meteorol. 29, 1300-1306.

Jacobs,A.F.G., Heusinkveld, B.G., Berkowicz, S.M., 1999. Dew deposition and drying in a desert system: a simple simulation model. *J. Arid Environments* 42,211-222.

Jacobs, A.F.G., Heusinkveld, B.G.,Berkowicz, S.M., 2000. Force-restore technique for ground surface temperature and moisture content in a dry desert system. Water Resour. Res. 36: 1261-1268.

Kiondo, J., Saigura, M., Sato, T., 1990. A parameterisation of evaporation from bare soil surfaces. J. Appl. Meteorol. 29, 385-389.

Lange, O.L., Kidron, G, Büdel, B., Meyer, A., Kilian, E., Abeliovich, A., 1992. Taxonomic composition and photosynthetic characteristics of the 'biological crusts' covering sand dunes in the western Negev desert. Functional Ecology 6, 519-527.

Larmuth, J., and Harvey, J., 1978: Aspects of the occurrence of desert plants. *J. Arid Environ.*, **1**, 129-133.

Lou, W., Goudriaan, J., 2000. Dew formation on rice under varying durations of nocturnal radiative loss. Agric. For. Meteorol. 104, 303–313.

Monteith, J.L., 1957: Dew. Quart. J. Roy. Meteorol. Soc., 83:322-341.

Monteith, J.L., 1981. Evaporation and surface temperature. Quart. J. Roy. Meteor. Soc. 107, 1-27.

Munne-Bosch S., and Alegre, L., 1999: Role of dew on the recovery of water-stressed Melissa officinalis L-plants *J. Plant Physiol*., 154, 759-766.

Nevo, E., Bar-El, C., Bar, Z., and Beiles, A., 1981: Genetic structure and climatic correlates of desert landsnails. *Oecologia (Berl),* 48, 199-208.

Norman, J. M., 1982. Simulation of microclimates. In: J. Hatefield & I. Thomases (eds.), Biometeorology in Integrated Pest Management. Academic Press, New York, pp. 65-99.

Richards, K., 2004: Observation and simulation of dew in rural and urban environments. *Prog. Physical Geog.*, 28, 76–94.

Royle, D.J., Butler, D.R., 1986. Epidemiological significance of liquid water in crop canopies and its role in disease forecasting. In: P.G. Ayres & Boddy, L. (eds.), Water, Fungi and Plants. Cambridge Univ. Press, Cambridge, pp. 139-156.

Shoemaker, P.B., Lorbeer, J.W., 1977. Role of dew and temperature in epidemiology of botrytis leaf-blight of onion. Phytopathology 67, 1267-1272.

Steinberger, Y., Loboda, I., and Garner, W., 1989: The influence of autumn dewfall on spatial and temporal distribution of nematodes in the desert ecosystem. *J. Arid Environ.*, 16, 177–183.

Verrecchia, E, Yair, A., Kidron, G.J. & Verrecchia, K., 1995. Physical properties of the psammophile cryptogamic crust and their consequences to the water regime of sandy soils, north western Negev Desert, Israel. J. Arid Environ. 29: 427-437.

Wallin, J.R., 1963. Dew, its significance and measurement in phytopathology. Phytopathology 53, 1210-1216.

Weiss, A., Norman, J. M., 1987. Comparison of field measurements and numerical simulations of leaf wetness durations in a bean canopy. 18th AMS Conf. on Agricultural and Forest Meteorology, 13-18 Sept. 1987. Amer. Meteorol. Soc., Boston, Mass. pp. 52-53.

Wiggs, G.F.S., Baird, A.J., Atherton, R.J., 2004. The dynamic effects of moisture on the entrainment and transport of sand by wind. Geomorphology 59, 13-30.

Yair, A., 1990. Runoff generation in a sandy area – The Nizzana sands, western Negev, Israel. Earth Surf. Processes Landforms 15, 597-609.

Zangvil, A., 1996. Six years of dew observations in the Negev desert, Israel. J. Arid Environ. 32, 361-371.

Zaady, E., Kuhn, U., Burkhard, W., Sandoval-Soto, L., Kesselmeier, J., 2000. Patterns of CO_2 exchange in biological soil crusts of successional age

2 Surface energy balance closure in an arid region: Role of soil heat flux

reprinted from*

B.G. Heusinkveld[a], A.F.G. Jacobs[a], A.A.M. Holtslag[a], S.M. Berkowicz[b]

[a] *Wageningen University, Meteorology and Air Quality Group, Duivendaal 2, 6701 AP Wageningen, The Netherlands*

[b] *Hebrew University of Jerusalem, Minerva Arid Ecosystems Research Centre, Institute of Earth Sciences, Givat Ram Campus, Jerusalem, Israel 91904*

*Published in Agricultural and Forest Meteorology (2004), doi:10.1016/j.agrformet.2003.09.005

Abstract

The large soil heat fluxes in hot desert regions are very important in energy balance studies. Surface energy balance observations, however, reveal that there is an imbalance in surface flux measurements and that it is difficult to isolate those flux measurements causing the imbalance errors. In this paper a new approach was tested focusing on a high temporal resolution of soil heat flux measurements at the surface. To determine if improved soil heat flux measurements could be obtained for a sandy desert, a standard soil heat flux sensor was buried at the surface of a playa and covered with less than 1 mm of playa soil, as opposed to burial several cm deep. It was anticipated that this would permit direct surface soil heat flux measurements. A field campaign was carried out in September and October in 1997 and for the same period in 2000, in a sandy desert belt situated in Nizzana, NW Negev, Israel. The research was designed to examine the separate components of the surface energy balance. The location was considered ideal since only the soil heat flux and sensible heat flux are balanced by the net radiation. This new approach was compared to traditional soil heat flux measurements. The resulting energy balance closure was found to be very good. The results suggest that this method could be used as a reference surface soil heat flux measurement. Further examination of the energy balance closure is needed over a range of land surface types.

Keywords: soil heat flux, surface energy balance, measurement, Negev desert, Israel

2.1 Introduction

There is an increasing interest in understanding desert ecosystems, especially in global change research. Although general climatic data is not lacking for desert regions, microclimate research is much more difficult to conduct. This is due to a combination of long-term logistics and access, technician costs, and the need for clear and specific research questions.

Many techniques have been proposed to measure the sensible (H) and latent heat (L_vE) flux (Bowen ratio, Eddy Covariance). The energy flux leaving the surface should be equivalent to the energy flux received at the surface, hence an energy balance closure test can be applied. If a reasonable closure is not obtained, the errors can be attributed to one or more of the separate surface energy flux measurements. Typically, in micro-meteorological studies, independent measurements of the fluxes are only 70-90% of measured net radiation (Q^*), as demonstrated by studies over the past decade. Oncley et al. (2002) noted this problem and attempted to explain the closure error for a vegetated surface energy balance experiment. In general, the failure to achieve closure in the energy balance has been attributed to instrumentation problems and/or an underestimation error in aerodynamic flux measurements, such as flow distortion, limited high frequency response, flux averaging period, etc. (Foken and Oncley, 1995; Spittlehouse and Black, 1981; Stewart and Thom, 1973; Cleugh and Roberts, 1994).

The component of the soil heat flux (G) in the surface energy balance (SEB) of a vegetated surface is usually very small (daytime: 5 - 15% of Q^*, night time: 50% of Q^*) (Stull, 1988). Research has tended to focus on vegetated surfaces because of agricultural interest. This may explain why relatively little attention has been paid to soil heat flux, and is usually reflected in the general budget planning for micrometeorological measurements. A small proportion of funding is dedicated to soil heat flux measurements. The question arises whether current soil heat flux measurement techniques are in fact adequate. To address this issue, a simple setting, such as a dry and bare soil surface, can provide an excellent case study. In a hot desert the absence of a vegetation layer, coupled with little available water to evaporate, limits the turbulent flux measurements only to the sensible heat flux. However, the measurement of the soil heat flux becomes increasingly important since, in a bare soil, it can be more than 50% of the net radiation in the daytime (Idso, et al., 1975).

A new soil heat flux measurement approach is proposed here, whereby the conventional sensor is moved to a location just below the surface. This allows for the direct measurement of $G_{(0)}$. These measurements are compared with a conventional soil heat flux set-up, where the sensor is buried at a depth of 40-60 mm. Although

correction schemes for buried soil heat flux sensors have been proposed (Philip, 1961; Mogensen, 1970; Howell and Tolk, 1990), they have their limitations.

Measurements were carried out within a sandy desert belt situated in the NW Negev, Israel, during two measurement campaigns. The first was carried out in September and October, 1997, and the second campaign in September and October, 2000. The surface soil heat flux measurements were first carried out in 1997, but reliable measurements of latent and sensible heat fluxes were not available. Thus it was not possible to check the surface energy balance closure. The initial measurements, however, pointed to the importance of soil heat flux measurements and thus the experiment was repeated in the same location in 2000 using a reliable flux station. The results from the first campaign show that the placement of soil heat flux sensors very close to the surface works very well. Our measurements during the second campaign indicate that a closure of the surface energy balance can be achieved in a desert region as long as special care is given to the soil heat flux measurement.

2.2 Experimental site and set-up

2.2.1 Site description

The experiment was carried out at the Hebrew University of Jerusalem Minerva Arid Ecosystems Research Centre field station at Nizzana (latitude N $30^0$56' longitude E $34^0$23' elevation above mean sea level 190 m)(Fig. 2.1). The Mediterranean Sea lies about 40 km to the northwest. The average annual rainfall of the region is about 100 mm with a coefficient of variation of about 40%. Rainfall occurs primarily in winter between December and February (Sharon et al., 2002). The dune field encompassing Nizzana (known as Sede Hallamish) consists of sparsely vegetated linear dunes 10 to 25 m high and up to 125 m wide. Although the dune crests are mobile, the dunes themselves are stable and elongate west east, which is the direction of the strongest winds (Sharon et al., 2002). Notwithstanding the arid climate, the dunes can have a perennial vegetation cover of up to 30% on dune slopes and even up to 50% near foot slopes (Tielbörger, 1997). Cryptogamic crusts form on the dune slopes and tend to cover the open areas between shrubs (Littmann and Ginz, 2000). The interdune corridors are between 50-150 m wide and contain a mixture of wide flat playa surfaces, gently sloping stretches, many small hillocks and remnants of eroded ancient dunes (Figs. 2.2 and 2.3).

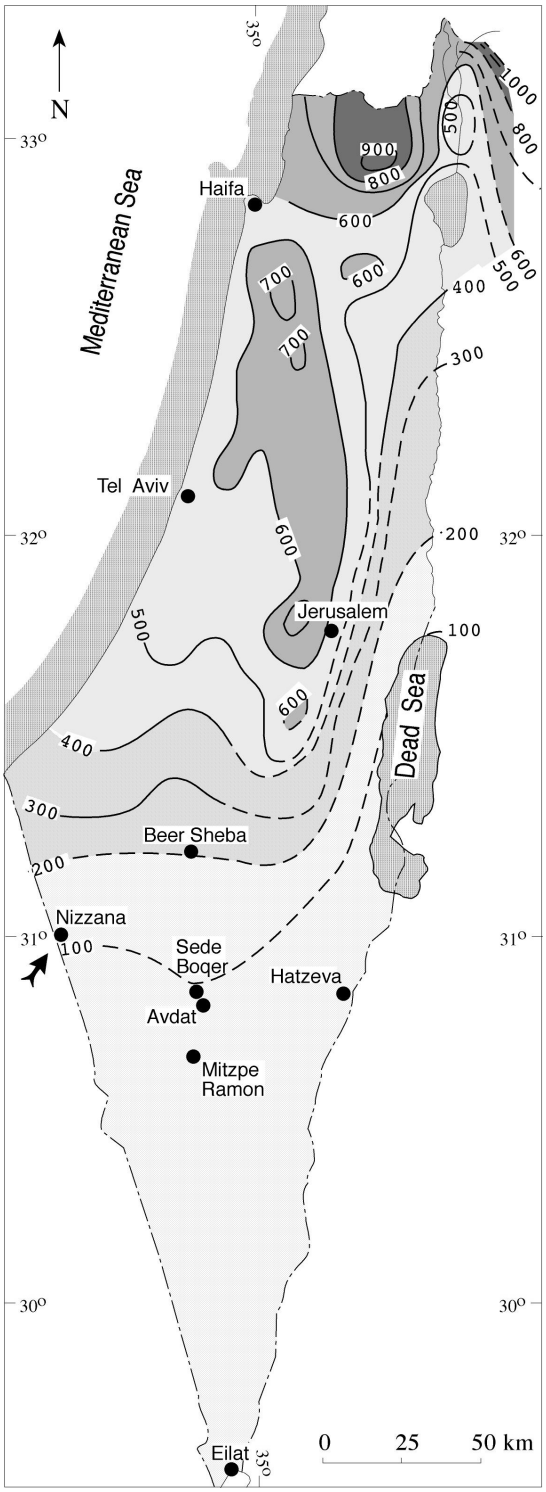

Figure 2.1: Location map showing annual average rainfall isohyets for 1961 - 1990 (after Israel Meteorological Service), and study site (bold arrow).

The flux station was established in the midst of a large, flat playa situated within an interdune corridor. This location was selected due to the playa's homogeneity, minimal vegetation cover, and sufficient distance from the dune crests to avoid wind flow distortion (Figs 2.2 and 2.3).

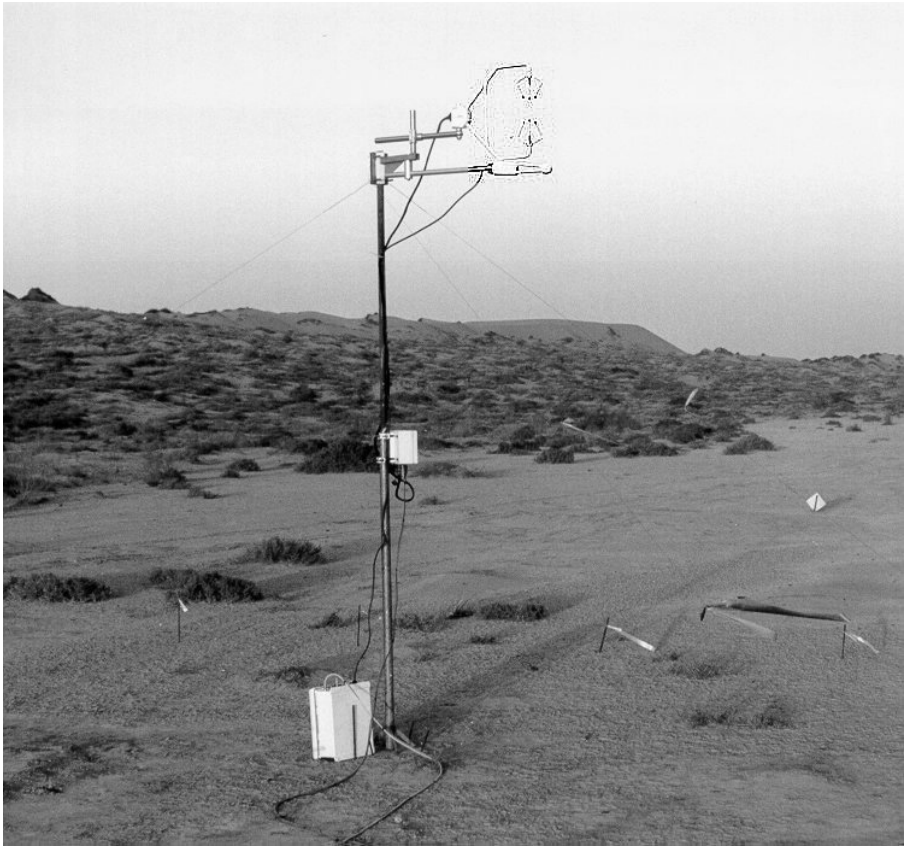

Figure 2.2: Flux station mast (3 m).

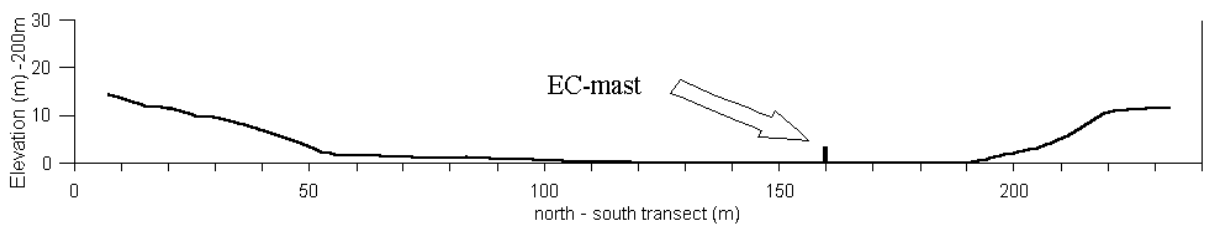

Figure 2.3: North-south transect of experimental site between two linear dunes, showing the elevation above the location of the Eddy Covariance (EC) mast.

The playa soil in the experimental area of the interdune has a thick compacted layer of silt and clay, though the first few mm can contain 35% fine sand (Pfisterer et

al., 1996). This material was deposited during brief inundations after strong winter rains. The very low plant density around the instrumented area, coupled with the flat terrain, made it an excellent test site for our purposes (Figs. 2.2 and 2.3).

Figure 2.3 contains a cross-section of the interdune corridor. The instruments were located at point 160 m of the transect. Three main types of measurements were made; radiation fluxes, convective fluxes (sensible heat and latent heat), and soil heat flux. Data logging took into account the need for slow or fast measurements.

2.2.2 Soil heat flux

Three TNO thermopile soil heat flux sensors (Netherlands Organization for Applied Scientific Research, P.O. Box 155, 2600 AD Delft, the Netherlands) of 4 mm thickness, diameter 150 mm, and a heat conduction of 0.25 W m^{-1} K^{-1} and an error of the calibration constant of 5%, were buried just below the surface near the Eddy Covariance mast, and covered with a very thin layer (<1 mm) of surface playa soil. In addition, one very thin TNO thermopile soil heat flux sensor of 1 mm thickness and a diameter of 150 mm, with a heat conductivity of 0.25 W m^{-1} K^{-1}, was buried at a depth of 46 mm. The heat conductivity of the plates (λ_p = 0.25 W m^{-1} K^{-1}) was very close to that of the soil (λ_s = 0.24 W m^{-1} K^{-1}). The error of the calibration constant is within 5 %. It is important to note that the soil has a very high light extinction coefficient such that the effects of direct short wave radiative sensor heating are minimal. However, this might be a problem for high quartz content sand types. In the 1997 experiment there were extra thermometers (Pt100 sensors) placed near the soil surface, at depths of 10, 15, 34, 50, 100, 150 and 300 mm. The soil heat flux plates were buried in the vicinity of the flux station mast. Shallow soil cuts showed that this area was quite homogeneous with respect to soil type and soil structure. Although it was difficult to establish good thermal contact with the underlying soil due to both soil compaction and cracking that appeared while digging, satisfactory installation was achieved after many attempts. The thermal contact was tested by comparing the three installed sensors. In addition, thermal images were taken of the soil heat flux area using a handheld imaging radiometer (Infrared Solutions Inc., Model 525) as a test of temperature homogeneity.

2.2.3 Radiative and atmospheric energy fluxes

The incoming and outgoing short-wave and long-wave radiation were measured separately using 4 radiometers. One albedo meter (Kipp CM14), measuring separate incoming and reflected short-wave radiation, incorporated two CM11 sensors, with a thermopile consisting of a 100-thermocouple sensor. Spectral range is from 305-2800 nm with an overall error of <3%. The long-wave radiation balance meter, a Kipp CG2, incorporates two Kipp CG1 long-wave radiometers. Spectral range is from 5-50 µm, and has an error of up to 15 W m^{-2} in the form of window

heating at full sunshine (Kipp CG2 specifications). The long-wave radiometers were heated in order to prevent moisture formation on its windows. The radiometers, together with masts measuring temperature and wind profiles, were located in the interdune area. The radiation balance was measured from a height of 1.2 meters. The surface temperature was monitored using 3 thermal infrared thermometers. One sensor was directed onto the bare soil near the Eddy Covariance mast (field of view 0.5 x 0.5 m). The second was aimed at the north-facing slope (both types: KT15, Heimann). The third was an imaging thermal camera (Infrared Solutions Inc., Model 525, 120 x 120 pixels, 18.9° field of view, sensitivity 0.1 °C), mounted on top of the south-facing slope about 160 m away, and overlooking the entire interdune corridor and north-facing slope. The pixel resolution around the Eddy Covariance set-up was about 0.4 m.

The sensible and latent heat fluxes were measured with an EC set-up. The EC system used during the experiment in 1997 was not capable of storing the raw data, hence only rough estimates of fluxes were available from the automatically processed data. For the experiment in 2000, a high quality EC system was added. This particular Eddy Covariance system comprises a fast 3D sonic anemometer (Campbell, CSAT3) and a fast moisture sensor (Li-Cor, Li-7500). The diameter of the sample volume of the sonic anemometer, also referred to as the path length, is 100 mm. The moisture sensor is an open path double beam infrared gas analyser, with a path length of 125 mm. The gas analyser was placed horizontally and below the sonic path. This limits flow distortion from various directions as well as hinders the effect of dew formation or dust accumulation on the windows. The placement of the gas analyser under the sonic made the measurement less affected by wind direction distortion. Hence it was not necessary for the EC system to be aimed at the wind. The centre of the sonic anemometer was at a height of 3 m, with the gas analyser 0.26 m below (Fig. 2.2).

The raw digital sensor data (sampling speed 10 Hz) were collected over 1 minute intervals by a Campbell 23X datalogger and then forwarded at the end of every minute to a laptop computer for storing. The signal response of the open path gas analyser is a bandwidth limited to 0-10Hz. This means that in a flux calculation, eddies of up to 10 Hz will be >seen= by the sensor. It is not the sampling speed but rather the single sample integration time that determines the detection limit of the fastest eddies contributing to the flux (or covariance) calculation. The final flux calculations were executed using a standardized software package EC-Times. The software package comprises all necessary corrections for density (Webb et al., 1980), frequency response, and axis rotation.

Aerodynamic flux measurements require a homogeneous and flat fetch. These needs were provided in the interdune area around the 160 m cross-section point (Fig. 2.3). In this area, the spatial variability of surface temperature was low (less than 1 °C over an area of half a square metre), as confirmed by thermal imaging data. The area

within a radius of at least 30 m (i.e. 10 times the height of the flux station mast of 3 m) was flat and very low in vegetation cover (<3%) (Figs. 2.2 and 2.3). The location of the flux station was selected precisely because the fetch would experience low or no distortion from the nearby sand dunes (about 15 m high). The daily wind pattern would result in a fetch along the corridor between the dunes.

2.3 Methodology

Verification of the flux measurements can be made by doing an energy balance closure test. At the surface, the net radiative energy (Q^*) should be balanced by the soil heat flux (G), sensible heat flux (H), and latent heat flux (L_vE). As these measurements are usually performed at a certain height or depth away from the surface, the energy balance closure test should show an imbalance in favour of the net radiation. To illustrate this, a more complete energy balance equation is presented below in Eq. 2.1.

$$Q_z^* = H_z + L_v E_z + G_d + X \tag{2.1}$$

where $Q^*_{(z)}$, is the net radiation measured at a height z, H is the sensible heat flux, L_vE is the latent heat flux (both measured at height z), G is the soil heat flux, and X represents additional terms. Often X is neglected. Thus Eq. 2.1 assumes an ideal case, where all the components are measured at the interface between surface and atmosphere or corrected as such. Since fluxes are normally measured at a certain distance away from the surface, X can be written as:

$$X = Y + A + h_r \frac{\partial Q^*}{\partial z} + \frac{\partial S_b}{\partial t} \tag{2.2}$$

where:

A = Advection term,

$h_r \frac{\partial Q^*}{\partial z}$ = Radiation flux divergence, where h_r is the height of the radiometer above the Eddy Covariance system. Otherwise it is zero (already accounted for in Y).

$\frac{\partial S_b}{\partial t}$ = Change in biomass energy

and

$$Y = C_s \int_{z_{HFS}}^{0} \frac{\partial T}{\partial t} dz + C_a \int_{0}^{h} \frac{\partial T}{\partial t} dz + L_v \int_{0}^{h} \frac{\partial q}{\partial t} dz \,. \tag{2.3}$$

Here Y represents a change of heat storage over the evaluated time interval. The first term is the change of heat storage above the soil heat flux sensor, the second term is the change of heat storage in the air between the sensor and the soil, and the last term is the change of moisture.

The soil heat flux is usually measured at a certain depth and corrected for heat storage between sensor and surface. The corrected fluxes are then combined in the energy balance equation in its simple form. In general, it is not clear what corrections should be used. Therefore it would be more complete to use the full equation. In a dry desert situation, our new surface soil heat flux approach renders many terms in X and Y as zero. What remains is the advection term and the heat storage between the Eddy Covariance sensors and the surface. The advection term is difficult to estimate, as this would require a large number of flux stations. However, it can be expected that this will be small in a homogeneous fetch area. The measurement height determines the sensitivity to daily variations in the air column temperature below the flux station (installed at 3 m). This can be significant under conditions with low forced convection and a steep change in solar radiation input. The radiation divergence has little effect, since the radiometers were mounted below the eddy covariance system and the temperature profile below this system is constantly monitored (to account for term Y). It is important not to overlook the shape correction (Φ) for soil heat flux sensors (Eq. 2.4) as proposed by Mogensen (1970).

$$\Phi = \frac{1}{1 - 1.7tA^{-0.5}(1 - \varepsilon^{-1})} \tag{2.4}$$

Here t is the thickness of the plate, A is the area of the plate, and ε is the ratio between the thermal conductivity of the plate to that of the soil. A difference in the thermal conductivity of the plate and that of the soil will result in a deviation in the heat flow through them.

The meteorological field experiment conducted in September-October 2000 provided an excellent opportunity to apply the energy balance closure test. In the study site, rainfall occurs mainly from October till March. The October 1999 to March 2000 period had only 35 mm, with 8 mm in March spread out over 4 small showers. The only major rainfall that year to provide significant moisture to the soil occurred in late January 2000 (18 mm). Hence by September 2000 the soil moisture was extremely low. Annual plants had long since disappeared and much of the remaining sparse perennial vegetation enters an above-surface dormant stage in order

to conserve moisture. The 1997 study already revealed that classic soil heat flux measurements were inadequate since, in a dry desert soil, damping depth is low and temperature gradients are steep. The dryness of the soil was similar in 1997 compared to the 2000 study. We present these results in Section 4, below. The surface soil heat flux measurements are compared with 2 classical methods:

-Calorimetric method
-Harmonic analysis

The calorimetric correction to the soil heat flux measurement involves a heat flux plate buried at 0.04-0.08 m depth with a temperature sensor placed halfway between the soil surface and the heat flux plate. In this manner the soil heat storage above the plate can be taken into account. However, by doing so, the soil heat flux may be underestimated and the dynamics of the soil heat flux cannot be measured correctly. Corrections for the buried soil heat flux sensor, based on the so-called calorimetric method, rely on an exact knowledge of the soil thermal properties. As these soil properties are difficult to measure, it can be argued that classical soil heat flux measurements - without reliable soil thermal property data - are unreliable.

The soil heat flux and the temperature wave in the soil are a complex composition of high and low frequencies, and can be described mathematically (Appendix), by harmonic analysis. It is important to keep in mind that the soil damps the temperature wave. The phase of the temperature wave also shifts with increasing depth. A dry soil, as was the case in this experiment, has a very low damping depth less than 70 mm for the daily temperature wave. At this depth only 37% of the daily surface temperature range is visible. This also explains the difficulty to correct a buried soil heat flux sensor for heat storage above the sensor. A temperature sensor will measure a delayed temperature wave, and corrections could be out of phase if the number of temperature sensors above the heat flux sensor is limited.

What remains are the sensible and latent heat fluxes. Since the soil was so dry, the latent heat fluxes were very low and hence their contribution to the energy balance was low. Nevertheless, they could not be neglected during morning hours because latent heat can peak at around 50 W m^{-2}. The only daily water input originated from dew (Jacobs et al., 1999).

2.4 Analysis of soil heat flux measurements

The importance of a correct soil heat flux is illustrated in Fig. 2.4 containing results from the study in 1997. The strong dips in the measured soil surface heat flux are impressive - they are not noise but rather the actual soil heat flux at the surface. How do these surface soil heat flux measurements compare with the classic soil heat

flux measurement approach? From the difference between the two measured soil heat fluxes, the translation of the soil heat flux at 46 mm depth to the surface involves a large correction.

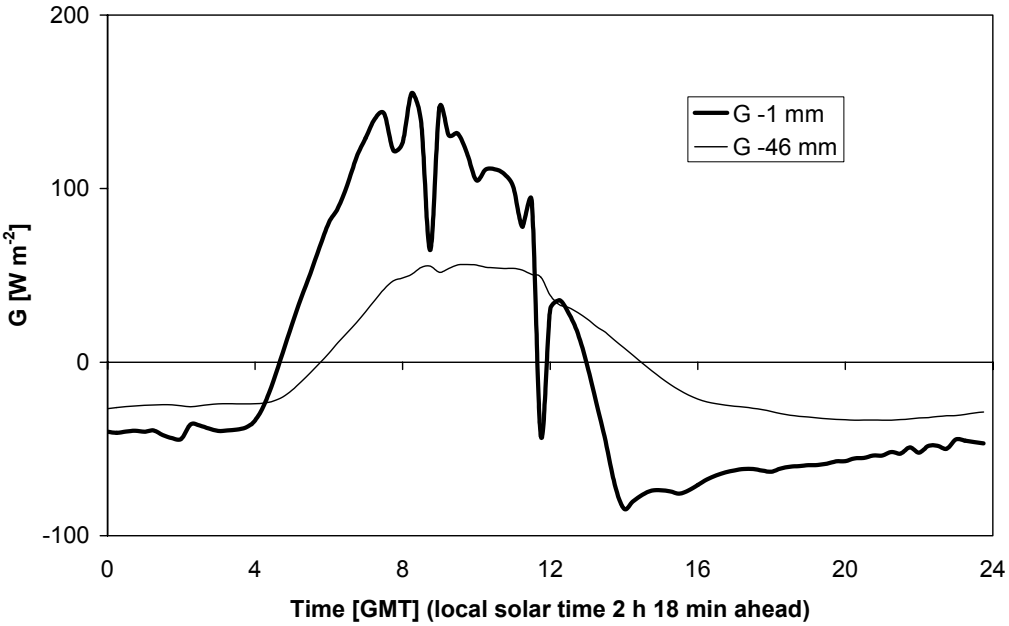

Figure 2.4: Soil heat flux (*G*) measured at two depths (-1 and -46 mm), sampling interval 15 minutes (30 Sept. 1997).

To validate the new soil surface measurement, the data was compared with two other methods. The first method involves the analysis of the temperature wave propagation into the soil (Appendix 1). The second involves the calorimetric method, which basically uses term *Y* in *X* in Eq. 2.1 to convert the measured G_d at a certain depth, to the surface $G_{(0)}$.

The first method requires a homogeneous soil and a set of soil temperature probes buried at various depths. In addition the soil thermal conductivity is needed. This can be derived from an additional measurement of *G* at a certain depth (see also Appendix), or from a thermal conductivity measurement probe (Van Loon et al., 1998). As the measurement of the surface temperature with a buried soil thermometer is difficult, an infrared thermometer was used. The calibrated infrared thermometer was offset by +2□C, based on the overall fit with the temperature measured by the soil thermometers. The offset might originate from solar heating of the sensor housing. However the amplitude of the temperature was expected to be within an acceptable accuracy. It is the temperature wave amplitude that is most important in this calculation. By fitting the temperature depth function (Eq.A6) to the real data, the soil thermal diffusivity (κ) can be found. The length of this time series is important.

Days with similar conditions must be used (i.e. radiation, wind speed, temperature, soil moisture, etc.). If not, then one must analyse longer time series (estimate: >10 days) without including deep (>2x damping depth) soil temperature measurements. In our calculations, 6 days were used (28 September - 3 October 1997). It is favourable to have a highly variable soil heat flux, because this improves the quality of the analysis by revealing in more detail the response of the soil to temperature variations at the surface. The maximum number of harmonics was used for this analysis, since this reveals the soil heat flux for the short sampling interval of 15 minutes. The procedure is as follows. After an initial guess of the thermal diffusivity, the result is compared with the measured temperature profile, and the parameter is adjusted depending on the differences in phase and amplitude. The iteration process stops when the difference in amplitude is less than 3% and the difference in phase is less than 3% in this comparison. The fit with a thermal diffusivity $\kappa = 1.5 \times 10^{-7}$ m^2 s^{-1} (the values for the 6 days varied by only ±5%) gave best results in overall phase and amplitude (Fig. 2.5). From the temperature data, a damping depth can also be calculated (Eq.A7). In our case it was 64 mm. The soil heat conduction can be estimated from a similar iteration process by fitting Eq.A8 to the measured soil heat flux at 46 mm and 1 mm depth (Fig. 2.6) (λ = 0.24 W m^{-1} K^{-1}, the values for the six days varied by only ±5%). With these results the soil heat flux can be calculated for every depth using Eq. A8 (Fig. 2.6). This is an analytical solution of the soil heat flux at any depth. It is interesting to note that these values correspond with published values for a very dry clay soil. In addition, this calculated soil heat conductivity is close to that of the soil heat flux sensors (0.25 W m^{-1} K^{-1}). In this case, the shape correction (Eq. 2.2) is below 1%.

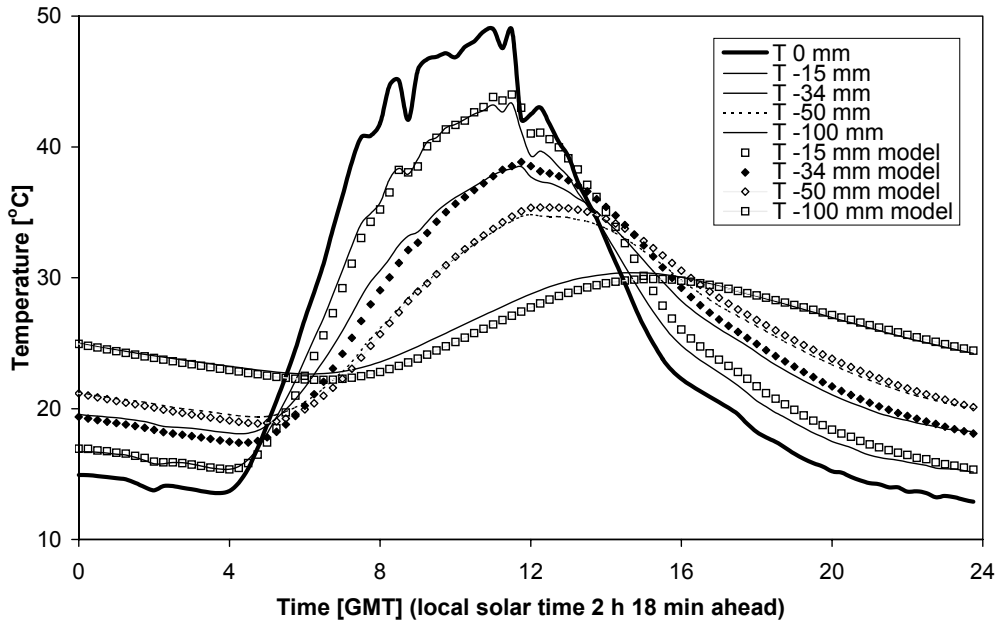

Figure 2.5: Soil temperature wave, measurements and model (harmonic analysis) (30 Sept. 1997).

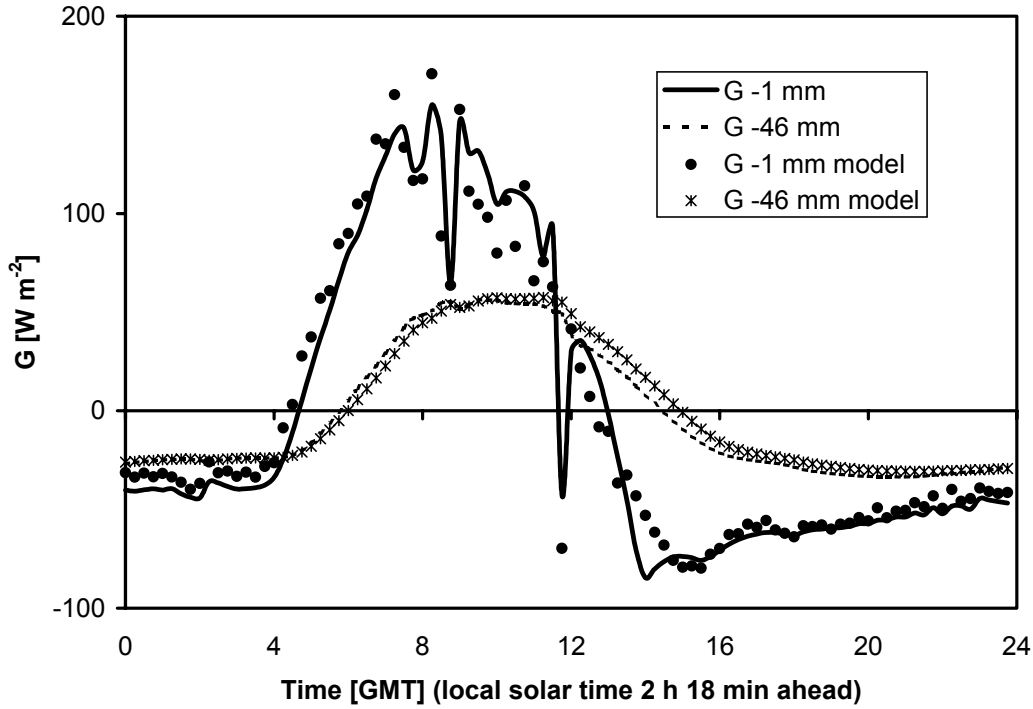

Figure 2.6: Soil heat flux at two depths, measurements and model (harmonic analysis) (30 Sept. 1997).

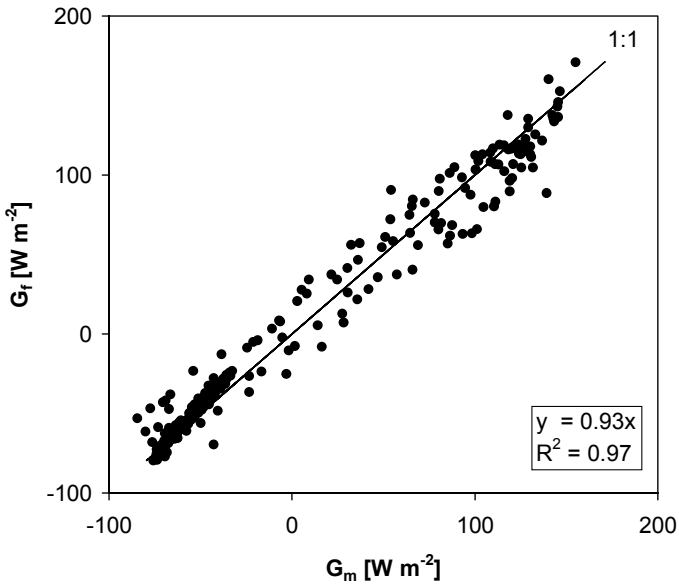

Figure 2.7: Soil heat flux calculated from harmonic analysis (G_f) compared with soil heat flux measured at the surface (G_m) (30 Sept.- 2 Oct. 1997).

Figure 2.7 shows that there is good agreement between the soil heat flux calculated from the analytical (harmonic) solution compared with the measured soil heat flux at the two depths.

The calorimetric method could also be tested. It requires a soil heat flux sensor buried at a certain depth and correction for the heat storage above the plate, an integration of the temperature profile above the sensor, and subsequent calculation of the temperature change of the soil column above the sensor. Usually a limited number of temperature sensors are used for this method. This highlights the difficulties that arise when correcting soil heat flux sensors. The calorimetric method can only work when the soil thermal properties are known. These properties were derived from the temperature profile measurements and the use of the analytical solution (Appendix). This technique only works for a homogeneous soil.

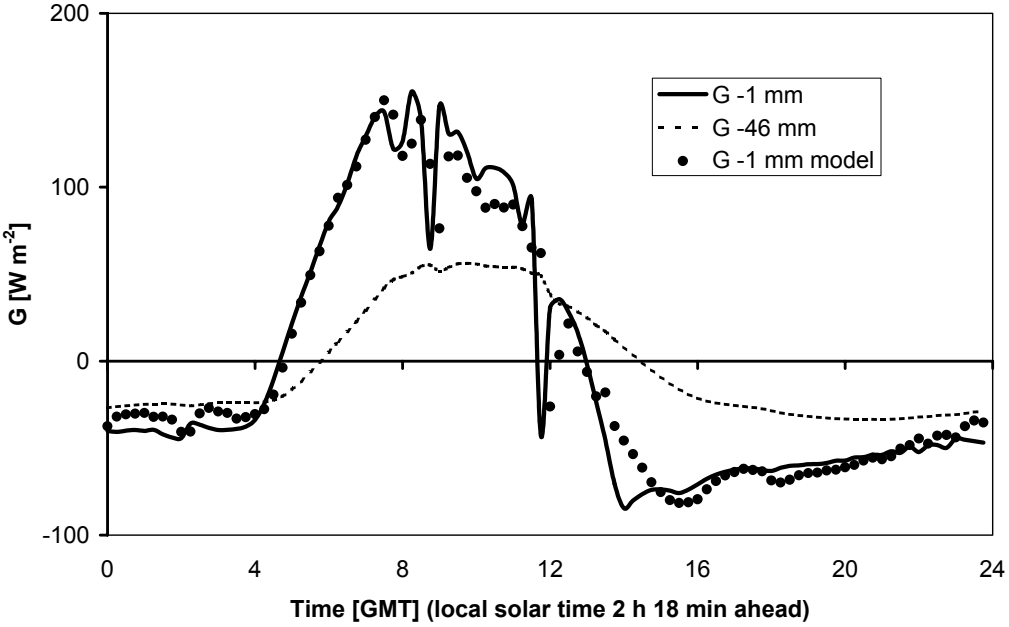

Figure 2.8: Surface soil heat flux calculated from calorimetric method, using a thermometer at -34 mm and a soil heat flux plate at -46 mm (30 Sept. 1997).

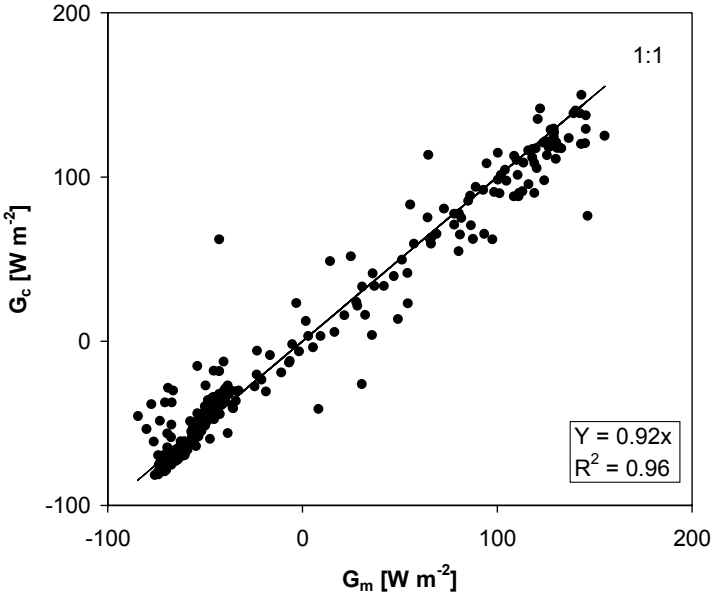

Figure 2.9: Soil heat flux (G_c) calculated from calorimetric method and compared with soil surface heat flux measurements (G_m) (30 Sept. - 2 Oct. 1997)

The results in Fig. 2.8 illustrate that a reasonable result can be attained. In Fig. 2.9, the calorimetric method is compared with the direct soil heat flux measurements

at the surface. Also note that for this analysis we used the thermal properties as calculated from the analytical solution. In practice these extensive analyses are usually omitted in the calorimetric method. The thermal properties are usually estimated from the soil composition and soil moisture. This would further reduce the quality of the calorimetric approach.

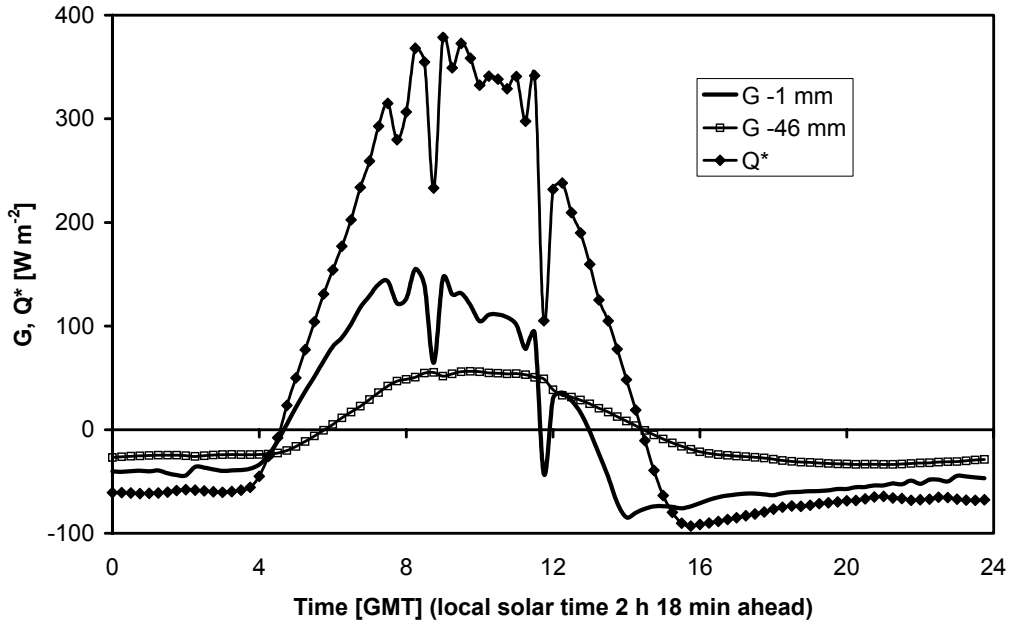

Figure 2.10: Measured soil heat flux at 2 depths (*G* at -1 and -46 mm) and the net radiation (*Q**) (30 Sept. 1997).

The two soil heat flux calculation methods show that the direct measurement of the soil heat flux at the surface seems correct.

Attention should be paid to the strong dips in the soil heat flux in Fig. 2.10. Note how rapidly the soil surface reacts to changes in radiation input. Furthermore, the strong negative peak around sunset is striking. This minimum occurs just before the transition time from an unstable situation ($Q^*>0$) to one that is stable, and can be explained as follows. There is a considerable heat store in a very thin soil layer (damping depth <0.07 m). The soil heat capacity can sustain a high heat release for some time during sunset hours (*T surface>T air*). This energy is effectively released as radiative heat and as convective heat into the air above. While the surface temperature starts dropping, it moves towards a new equilibrium with the sky radiative temperature, and the soil heat flux slowly diminishes during the night. As the atmosphere becomes stable, the heat exchange between the soil and the air above becomes low.

2.5 Surface Energy Balance (SEB) closure

The surface energy balance (Eq. 2.1) can be tested using the collected Eddy Covariance data, the soil heat flux measurements at the surface, and the radiation measurements. The net radiation (Q^*) was calculated from 4 radiometers; global incoming short-wave radiation, reflected short-wave radiation, long-wave incoming radiation and long-wave surface emitted radiation. The long-wave radiometers have a small sensitivity to short-wave radiation (15 W m^{-2} at full sunshine). This was corrected for as follows. The albedo in our testing area was high, 0.4, and resulted in a short-wave radiation sensitivity error in the down facing sensor too. A higher albedo would reduce this noise on the resultant net radiation calculation. The radiation balance was therefore corrected using Eq. 2.5,

$$Q^* = Q^*_m - 15(1-\alpha)\frac{Q_g}{Q_g^{\max}} \tag{2.5}$$

Here α is the albedo of the soil surface (around 0.4), Q^*_m is the measured net radiation, Q_g is the incoming global radiation, and $Q_g^{\max}$ is the maximum possible global radiation (assumed to be 1000 W m^{-2}).

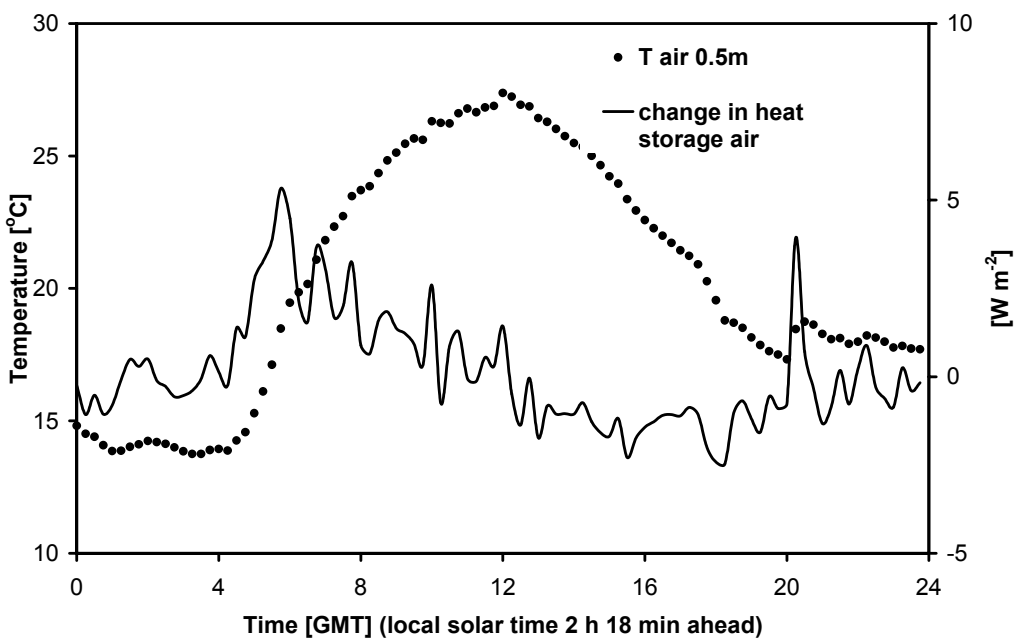

Figure 2.11: Temperature variations in the air column below the flux station is responsible for a correction term in the sensible heat flux as measured by the flux station (at 3m height) (16 Oct. 2000).

The heat storage of the air below the flux station in Eq. 2.1 is included in the surface energy balance closure evaluation. The asymmetric shape of the daily

temperature cycle results in a higher heat storage in the air during the first hours after sunrise than before sunset. The daily wind pattern is responsible for this. The wind picks up at midday due to the sea breeze (Littmann, 1997) and reaches its peak near sunset. This improves mixing and results in a less steep temperature drop at the end of the afternoon (Fig. 2.11).

The advection term in Eq. 2.1 is difficult to estimate since there were no additional measurements in the surrounding area. However, one can assume that this term is relatively small as the area is quite homogeneous. The regression line over a 24-day period (Fig. 2.14) with a R^2 of 0.96 was achieved by including the air heat storage term (Fig. 2.11) and the long-wave radiation corrected for the sensitivity of the radiometers to short-wave radiation (Eq. 2.3). These corrections raised the closure from an initial value of 0.90 to a closure of 0.96. To demonstrate the quality of the field data, Fig. 2.12 shows that the SEB also closes in the case of a very light rain (0.2 mm), which occurred on the preceding evening (15 October 2000), and was followed by heavy dew and stronger evaporation in the morning hours of 16 October 2000. The graphs of the surface energy balance (Fig. 2.12 and 2.13) show that there is a lag in the maximum sensible heat flux caused primarily by the increase in wind speed during the afternoon hours but also in part because of the evaporation of dew in the morning hours. Cloudy days are included in the analysis. Fig. 2.13 shows that the surface energy balance also then reaches closure (even during night time).

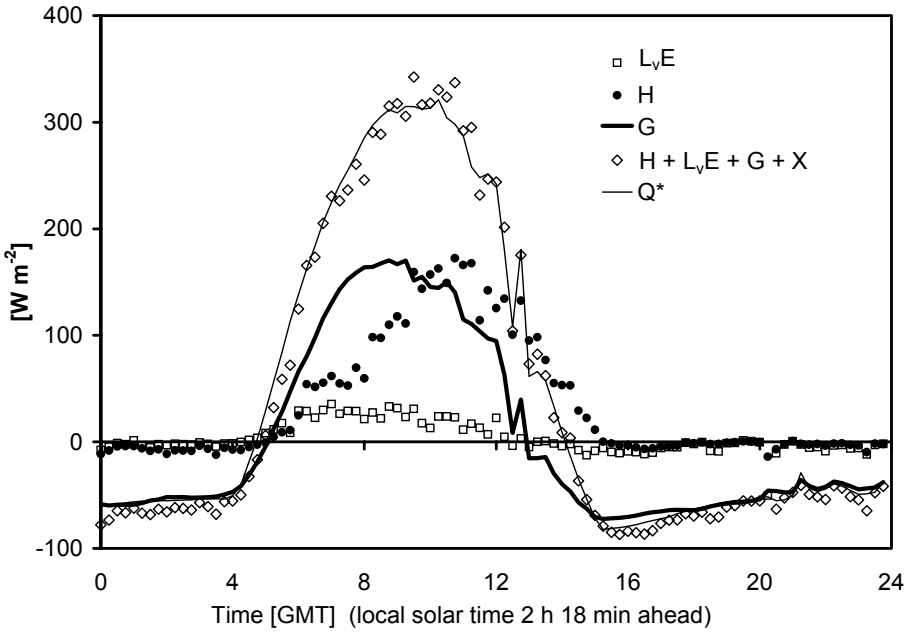

Figure 2.12: Measurements of the energy balance components during an almost clear day, using Eddy Covariance (EC) measurement techniques (sensible (*H*) and latent heat (L_vE) and a soil heat flux plate (*G*) close to the surface (16 Oct. 2000). The

correction term (X) was 5.3 W m^{-2} at maximum around 5:45 h., due to the temperature rise of the air column under the EC sensors (16 Oct. 2000).

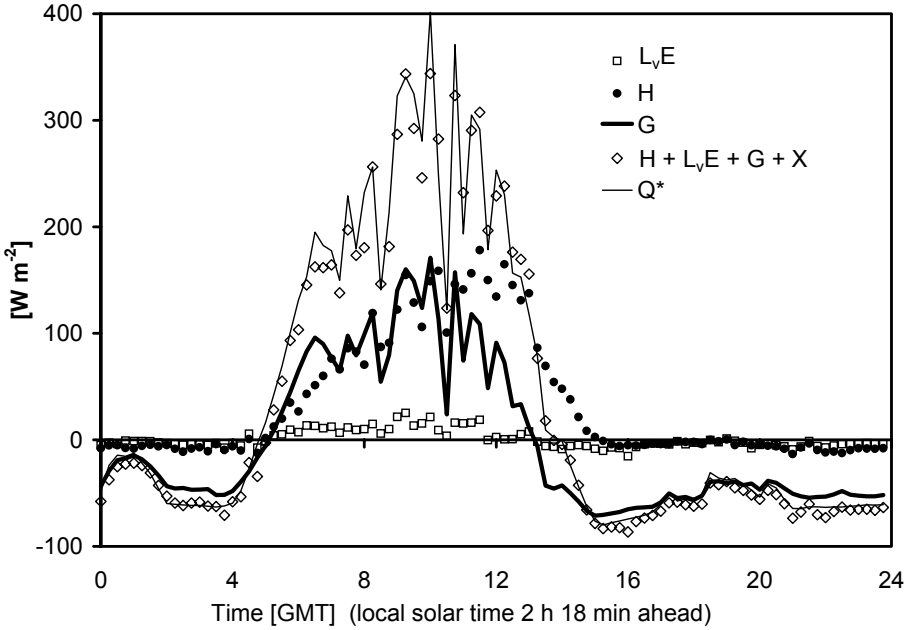

Figure 2.13: Measurements of the energy balance components, using Eddy Covariance (EC) measurement techniques (sensible (H) and latent heat (L_vE) and a soil heat flux plate (G) close to the surface (a day with some cloud cover, 21 Oct. 2000). The correction term (X) was 5.7 W m^{-2} at maximum around 6:15 h., due to the temperature rise of the air column under the EC.

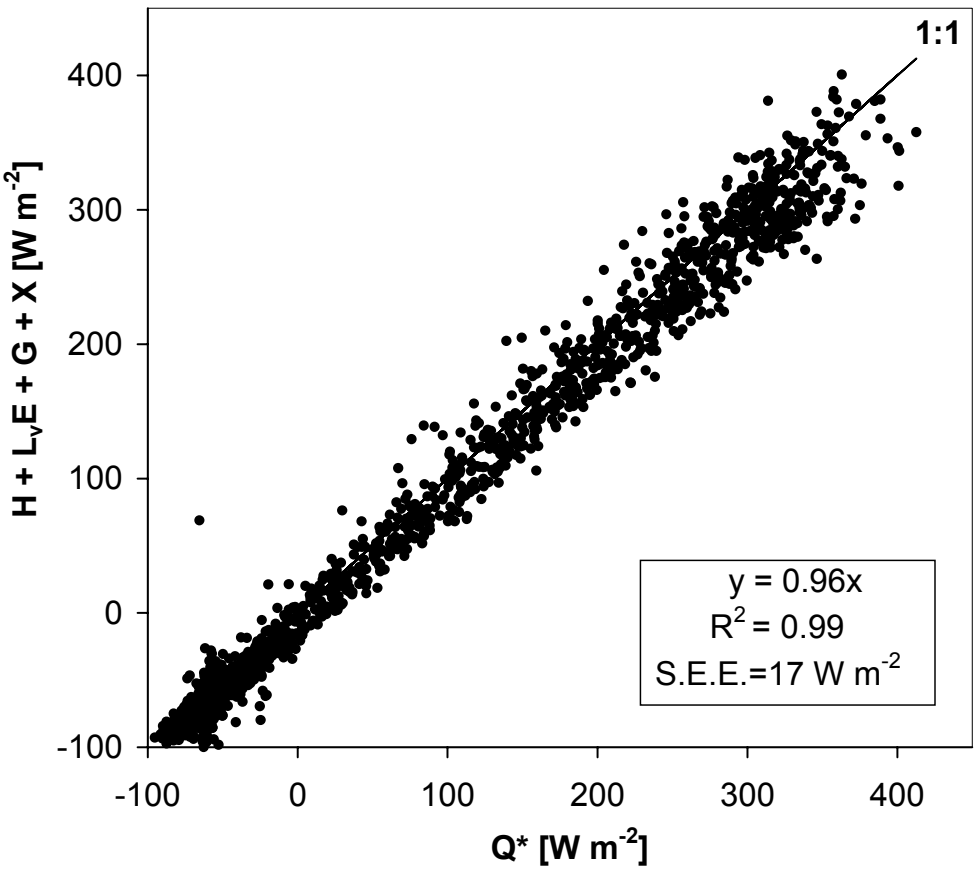

Figure 2.14: Energy balance closure over a 24 day period (28 Sept. – 22 Oct. 2000), as measured by Eddy Covariance (EC) measurement techniques (sensible (*H*) and latent heat (L_vE)) at 3 m, a soil heat flux plate (*G*) at 1 mm depth, and net a radiometer at 1.2 m (*Q**).

The flux averaging time interval for the turbulent fluxes was 15 minutes. As we recognize that shorter averaging time intervals might result in a lower flux, we tested this sensitivity by extending the time interval from a minute to over an hour. For 15-minute flux averages, the deviation from the 30-minute averages was -2% (Fig. 2.15). It was decided not to average the data to half-hour values, because this would mask the dynamic surface energy balance exchange processes.

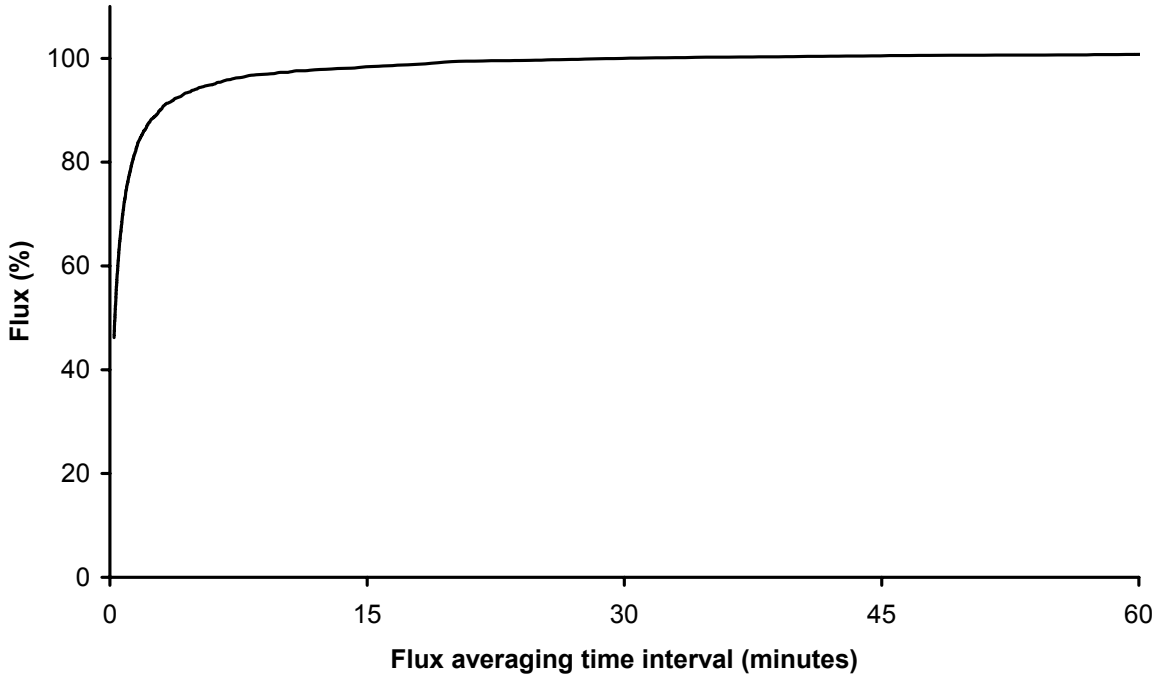

Figure 2.15: Flux as calculated from a time series of 30 min. compared with shorter and longer time series (mid-day period).

2.6 Discussion

The correct measurement of soil thermal properties is very important in estimating soil surface heat flux from a conventional buried heat flux sensor approach because the corrections become very large. In the present paper this becomes very difficult even for an ideal case (homogeneous soil, very low soil moisture). A further complication would be a soil that consists of several layers with different thermal properties. The surface soil heat flux measurement technique proposed here, directly measures the surface soil heat flux, since the sensor is buried very close to the surface. With this method, there is no need for measurements of soil thermal properties.

The analytical solution (Appendix) is shown here to be a fast and powerful tool in performing soil thermal analysis for a homogeneous soil. This only works however, with a very high order harmonic analysis (>30/day). The dynamic nature of the soil heat flux requires a measuring interval of at most 15 minutes. From such analyses, a surface soil heat flux can be reconstructed from the temperature profile and a soil heat flux measurement at a given depth. In addition, the soil thermal properties are solved using this technique.

Although it is common to make a correction for a buried soil heat flux sensor using data from one or more thermometers inserted between the soil heat flux sensor and the surface, such corrections can be as high as a factor of 3 in the case of a soil

heat flux plate buried at 0.046 m depth (damping depth <0.07m). In our case, the thermal properties were calculated using the analytical solution (fitting the measurements of temperature and soil heat waves), which was possible because of the rather homogeneous soil. The calculated soil surface heat flux was found to be reasonable using this procedure, and was achieved owing to good soil thermal property calculations (Figs. 2.8, 2.9). An inadequate number of temperature sensors can lead to an underestimation of the calculated heat flux into the soil because the temperature profile above the soil heat flux sensor is not linear. This error will depend on the higher order dynamics of the surface temperature. They can be greater under partly cloudy sky conditions. Partly cloudy skies will cause step changes in short-wave radiation arriving at the surface and lead to almost stepwise changes in surface temperatures and fluxes. It is shown that these changes in the soil heat flux can be more than 150 W m^{-2} over a 15-minute interval (see Figs. 2.10 and 2.13). The low damping depth makes the soil surface heat flux respond very fast to radiation changes.

It would be interesting if a simple flux partitioning scheme could be derived from these measurements. One simple scheme would assume that G is a fraction of Q^*. However, the time lag between G and Q^* limits the use of such models to longer time intervals. In the morning hours this fraction is more than 60%, whereas the daytime fraction where $Q^*>0$, would be around 30%. The nighttime fraction (24 days analysis) ranged between 75 - 100% of Q^*.

In assessing the energy balance, it is a challenge to correctly measure the day-night changes because they are rapid and contain higher order harmonics that are damped in a shallow soil layer. Furthermore, the heat wave at half-damping depth is time shifted by more than an hour. Small measurement errors will have a large effect on the calculated heat flux at the surface. Since it is very difficult to estimate the sensor depth accurately, it is far easier to move the heat flux sensor to the surface. Our measurements look very convincing when compared with data obtained from conventional techniques. These soil heat flux sensors were covered with a thin layer of playa soil material (d<1 mm), so that their surface albedo would be similar to that of the surrounding soil. However, this might not be possible in quartz sand, because of light penetration. In addition, it is important to check that the soil heat flux sensor remains covered by the material during the day. This was done on a regular basis during our study period and the layer was found to be stable. The application of soil heat flux measurements close to the surface might be limited to a dry bare soil situation. Miniature thermopile sensors with a diameter of 25 mm and a thickness of 1 mm (PU11T, manufactured by TNO, Delft, the Netherlands) are reaching the commercial market. Such sensors might make future measurements possible in less than ideal conditions, i.e. a moist soil with a vegetation cover, but this aspect was not tested in the present study.

2.7 Conclusion

The accurate measurement of soil heat flux is often neglected in energy balance studies. Because in a desert *G* can be as high as the sensible heat flux, this omission will lead to large errors in the calculations. During the night these fluxes are especially dominant. A dry soil will quickly dampen the daily temperature wave to such an extent that a good correction for a buried soil heat flux sensor becomes very difficult and necessitates many additional measurements.

In this paper a harmonic analysis and a calorimetric method are used to obtain the soil surface heat flux in comparison with observations near the surface. It appears that the approach proposed here provides realistic soil heat fluxes. This is confirmed by the perfect closure of the soil surface energy balance under dry desert conditions. The surface energy balance closure test gives less scatter with the directly measured surface soil heat flux measurements than with the corrected data of the two conventional techniques described earlier. This supports the placement of the soil heat flux sensor very close to the surface. In a dry bare soil with a very high soil heat flux, we advise burying the sensor as close as possible to the soil surface.

Acknowledgements

The authors are grateful to both the Minerva Arid Ecosystem Research Centre of the Hebrew University of Jerusalem and the Dutch Organization for Scientific Research (NWO) for assistance in carrying out the field campaign in the Hebrew University Nizzana experimental station. The authors thank Eyal Sachs for technical assistance, and Yariv Har-El and Ariel Cohen for their assistance in the field.

Appendix I - Overview of the harmonic analysis

Harmonic analysis can be used in a homogeneous soil. Although only 1 soil heat flux plate and 1 soil thermometer are required, additional such sensors are preferred. The only unknown parameters are the thermal diffusivity and the soil heat conductivity. These can be found by this method and is explained below.

An analytical solution can be found to calculate the soil heat flux and temperature at any depth. The equations were analysed using the mathematical analysis software package Mathcad (Mathsoft Inc., 2001). For a homogeneous soil, the temperature at depth z can be calculated by solving Eq. A1, (Van Wijk and De Vries, 1963):

$$\frac{\partial T}{\partial t} = \frac{\kappa \partial^2 T}{\partial z^2} \tag{A1}$$

where $\kappa = \dfrac{\lambda}{\rho C_p}$

With a fast fourier expansion of the surface temperature time series, the analytical solution of Eq. A1 can be found. By using the fast fourier transform (fft), the temperature at the surface (or deeper if not available) can be converted into a frequency domain C_j (Eq. A2):

$$C_j = \frac{1}{\sqrt{N}} \sum_{k=0}^{N\text{-}1} T_k \, e^{i(2\pi j / N)k} \tag{A2}$$

where N is the number of elements of temperature T_k and i is the imaginary unit.
Next, the surface temperature can be expressed as a set of complex frequencies:

$$T_{0,t} = \overline{T_0} + \sum_{n=1}^{M} (A_n \sin(n\omega t + \Phi_n)) \tag{A3}$$

Where n is the harmonic wave number, ω is the radial frequency ($2\pi/N$), M is the highest harmonic wave number and A_n is the fourier coefficient vector length:

$$A_n = \frac{2}{\sqrt{N}} |C_n| \tag{A4}$$

Φ is the argument of the fourier coefficient vector:

$$\phi_n = \arctan(a_n / b_n) \tag{A5}$$

where a_n is the real part and b_n is the imaginary part of the fourier coefficient vector C_n.

Inserting Eq. A3 in Eq. A1, the analytical solution becomes:

$$T_{z,t} = \overline{T} + \sum_{n=1}^{M} [A_n e^{-z(n\frac{\omega}{2p\kappa})^{0.5}} \sin(n\omega t + \phi_n - z(n\frac{\omega}{2p\kappa})^{0.5})] \tag{A6}$$

where z is the depth in m, n is the harmonic wave number, ω is the radial frequency, κ is the thermal diffusivity in $m^2\ s^{-1}$, p is the sampling interval time, and M is the highest harmonic wave number.

By fitting the temperature depth function (Eq. A6) to the actual data, the soil diffusivity (κ) can be determined. The soil depth (D) where the amplitude of the daily temperature wave is 37% of that of the surface is called the damping depth. This is related to κ as follows:

$$D = \sqrt{2\frac{\kappa}{\omega}} \tag{A7}$$

Here ω is the angular frequency of the daily temperature wave cycle.

By taking the derivative dT/dz of Eq. A6, and multiplying this by the soil heat conduction coefficient λ (W m^{-1} K^{-1}), the soil heat flux $G_{z,t}$ (W m^{-2}) can be calculated for each depth. However, the soil heat conduction constant is unknown. This can be estimated from a fit of Eq. A8 into the measured soil heat flux. In our case these were two depths, one at the surface and at 46 mm. With these results the soil heat flux can be calculated for every depth using Eq. A8 (Fig. 2.7).

$$G_{z,t} = \sum_{n=1}^{M} [A_n \frac{1}{\kappa}(n\omega\kappa)^{0.5} e^{-z(n\frac{\omega}{2p\kappa})^{0.5}} \sin(n\omega t + \phi_n + \frac{\pi}{4} - z(n\frac{\omega}{2p\kappa})^{0.5})]\frac{\lambda}{10\pi} \tag{A8}$$

Note that measurements of the topsoil surface temperature are not needed to find a solution for the surface soil heat flux using Eqs. A6 and A8. The surface soil heat flux can also be found by inserting temperature data of a certain depth into Eq. A2. Next the surface temperature or surface soil heat flux can be found by inserting a negative depth (z is positive into the soil) into Eqs. A6 and A8. However the accuracy decreases, since the amplitude becomes very small. The analysis should contain a high number of harmonics M, which can now be handled with fast personal computers.

References

Cleugh, H.A., Roberts,T., 1994. Local-scale energy balances and microclimate in the desert ranges of central Australia. *Australian Meteorol. Mag.* 43, 219-228.

Foken, T., Oncley,S.P., 1995. A report on the workshop: Instrumental and methodological problems of land-surface flux measurements. *Bull. Amer. Meteorol. Soc*. 76, 1191-1193.

Idso, S.B., Aase, J. K., Jackson, R.D., 1975. Net radiation-soil heat flux relations as influenced by soil water variations. *Bound.-Layer Meteorol*. 9,113-122.

Howell, T.A., Tolk J.A., 1990. Calibration of heat flux transducers. *Theoret. Appl. Climatol.* 42, 263-272.

Jacobs,A.F.G., Heusinkveld, B.G., Berkowicz, S.M., 1999. Dew deposition and drying in a desert system: a simple simulation model. *J. Arid Environments* 42,211-222.

Littmann, T., 1997. Atmospheric input of dust and nitrogen into the Nizzana sand dune ecosystem, nothwestern Negev, Israel. *J. Arid Environments* 36, 433-457.

Littmann, T. and Ginz, D., 2000. Eolian transport and deposition in a partially vegetated linear sand dune area (northwestern Negev, Israel). *Z. Geomorph. N.F. Suppl.-Bd*. 121, 77-90.

Mogensen, V.O., 1970. The calibration factor of heat flux meters in relation to the thermal conductivity of the surrounding medium. *Agric. For. Meteorol*. 7, 401-410.

Oncley,S.P., Foken,T., Vogt,R., Bernhofer,C., Kohsiek, W., Liu, H., Pitacco, A., Grantz,D., Riberio,L., Weidinger,T. , 2002. The energy balance experiment EBEX 2000. Proceedings 15th Symposium on boundary layers and turbulence, Wageningen, The Netherlands, July 15-19,2002. American Meteorological Society. Pp. 1-4.

Pfisterer, U. Blume, H.-P., Beyer, B., 1996. Distribution pattern, genesis and classification of soils of an arid dune area in northern Negev. *Z. Pflanzenernähr. Bodenk.* 159, 419-428.

Philip, J.R. 1961. The theory of heat flux meters. *J. Geophysical Rese.* 66, 571-579.

Sharon, D., Margalit, A., Berkowicz, S. M., 2002. Locally modified surface winds on linear dunes as derived from directional raingauges. *Earth Surf. Process. Landforms* 27,867-889.

Spittlehouse, D.C., Black, T.A., 1981. Evaluation of the Bowen Ratio/energy balance method for determining forest evaporation. *Atmospheric Oceanographic Technology* 18, 98-116.

Stewart, J.B., Thom, A.S., 1973. Energy budgets in pine forests. *Quart. J. Royal Meteorol. Soc.* 99: 154-170.

Stull, R.B., 1988. An Introduction to Boundary Layer Meteorology. Kluwer Academic Publishers, Dordrecht. 666 pp.

Tielbörger, H., 1997. The vegetation of linear desert dunes in the north-western Negev, Israel. *Flora,* 192, 261-278.

Van Loon, W., Bastings, H.M.H., Moors,, E. J., 1998. Calibration of soil heat flux sensors. *Agric. For. Meteorol.* 29,1-8.

Van Wijk, W.R., De Vries, D.A.,1963. Periodic temperature variations in a homogeneous soil. *Physics of Plant Environment. North Holland Publishers. Amsterdam, pp.* 103-143.

Webb, E.K., Pearman, G.I., Leuning R., 1980. Corrections of flux measurements for density effects due to heat and water vapour transfer. *Quart. J. Royal Meteorol. Soc.* 106, 85-100.

3 An automated microlysimeter to study dew formation and evaporation in arid and semi-arid regions

reprinted from*

Bert G. Heusinkveld[a], Simon M. Berkowicz[b] , Adrie F.G. Jacobs[a], Albert A.M. Holtslag[a] and Willy C.A.M. Hillen[a]

[a] *Wageningen University, Meteorology and Air Quality Group, Duivendaal 2, NL-6701 AP Wageningen, The Netherlands*
[b] *Hebrew University of Jerusalem, Minerva Arid Ecosystems Research Centre, Institute of Earth Sciences, Safra Givat Ram Campus, Jerusalem, Israel 91904*

*Published in Journal of Hydrometeorology (2006), 7: 825-832

ABSTRACT

The development of a simple and low-cost portable weighing microlysimeter is presented, which makes use of a Load Cell for automated recording, for studying daily dew formation, rate of accumulation and subsequent evaporation in arid or semi-arid regions during rainless seasons. The sampling cup is 3.5 cm deep, with the Load Cell itself situated at 20 cm depth to minimize temperature effects. The device was tested in a sand dune experimental station situated near Nizzana, NW Negev desert, Israel, during which extensive micrometeorological measurements were collected. One microlysimeter was placed in a playa and a second was installed on the stabilized midslope of an adjacent linear sand dune. To assess the performance of the Load Cell microlysimeters (LCM), one pair of manual microlysimeters was installed next to each LCM. A third pair was installed at a point between the LCM's and a fourth pair above the midslope LCM. Sixteen overnight measurements were carried out within a 6-week period. The LCM could measure dew with an error of ± 0.02 mm. The daily dew variation in the samples during the 16 overnight measurements ranged up to 0.2 mm on stable dune slopes but up to 0.4 mm on the playa. This difference is attributed to the playa's high silt and clay content and salinity. Dew formation and accumulation was found to occur long before the surface temperature reached the dew point temperature of the air. The cost of building this microlysimeter, excluding labour, is about US$175.

3.1 Introduction

Insights into the exchange processes of heat and mass in arid and semi-arid environments require that reliable measurements can be made of dew and its subsequent evaporation. The absolute amounts, however, are small and are not likely to exceed 0.4 mm per evening (Jacobs et al. 2000a). It is thus not surprising that attempts to evaluate the multiple role dew plays in the environment and in ecosystems have been hindered by the very difficulty of dew measurement. Approaches have included destructive sampling, moisture-absorbing material, dew-drop size calibrations, electrical surface wetness circuits, and assessment of dew on proxy surfaces (Berkowicz et al. 2001; Richards 2004). Single measurements taken near sunrise will, at best, provide only maximum dew amounts for the particular surface under study. This does not take into account possible drying during the evening. However, dew onset, accumulation (and rate), and evaporation, can be of primary interest, for example, in agriculture where dew is a factor in the development of plant diseases (Wallin 1967). There is a need for dew sensors to allow repetitive measurements to be performed, but with a capability for automated recording at desired time intervals.

The exchange process of water between the soil surface and the atmosphere plays an important role in arid regions (Malek et al. 1999), especially during lengthy rainless seasons. In this period dew (and sometimes fog, depending on the location) is the only source of water. Desert arthropods, such as isopods, ants, and beetles rely on dew as a significant moisture source (Broza 1979; Moffett 1985) and desert landsnails become active when the soil is wet from dew (Nevo et al. 1981). Spider webs can be laden with dew on heavy dew evenings, contributing to webs breaking due to the increased load (Brackenbury 1997). Desert soil faunae, such as nematodes, are sensitive to dew deposition on a soil surface (Steinberger et al. 1989). Larmuth and Harvey (1978) found that desert seedling distribution in a reg desert of Morocco was greatest near a stone, and speculated on the role of stones as both a dew collector and funnel of dew. Dew may also contribute to seed germination and assist in the adhesion of dust and fine materials to surfaces. Gutterman and Shem-Tov (1997) noted that certain desert plants have seeds that develop a mucilaginous layer when wetted and can then adhere to a soil surface. They believe that although dew wetting is insufficient to cause seed germination, it may help in priming the seed. Other studies have focused on water stress recovery by desert plants from dew (Munne-Bosch et al. 1999; Munne-Bosch and Alegre 1999). In addition, in many desert areas biological sand crusts play a major role in stabilizing sand dunes (Danin et al. 1989). The development of such crusts is largely determined by water availability for the crust organisms, which is the key parameter controlling the activity of the microbial

crust community (Harel et al. 2004). Nocturnal dew can be a major source of water for these organisms (Jacobs et al. 2000a).

In the present study, dew formation and evaporation on flat surfaces as well as on a slope were of special interest. A search of electronic catalogues led to the investigation of Load Cells as a basic sensor with which to construct a simple and inexpensive weighing microlysimeter. A Load Cell is an electronic device that measures the deformation of a piece of metal by means of a strain gage, i.e. the resistance changes when stretched. Examples of Load Cell use range in applications from Grimmond et al. (1992) for a vegetated surface, Jackson (1996) for an aeolian sediment trap, Scott et al. (2002) on effects of soil trampling on evapotranspiration, and Sear et al. (2000) to record bedload transport in streams.

The advantage of a microlysimeter method is that it is a direct measure of soil water loss/gain. There are a number of studies where microlysimeters have been used for determining evaporation. Daamen et al. (1993) reviewed various microlysimeter designs. They tested microlysimeters that ranged from 51 mm to 214 mm in diameter and 100 to 200 mm in depth. Although they concluded that all of the microlysimeters performed similarly, they did not report if they were sensitive enough to measure dew. Exposure of the edge of the sampling cup cannot be avoided and thus the edge will stick out a few mm above the surrounding soil surface. As edges can enhance turbulent transport, a small diameter lysimeter will have a greater edge-to-diameter ratio. Daamen et al. (1993), however, did not find evidence for this.

There were several considerations in working in a desert area for the purposes of our research. First, the study site in the NW Negev desert of Israel experiences dew approximately 200 evenings per year (Evenari 1982; Zangvil 1996) and can reach up to 0.4 mm per night even in the hot dry summer (Jacobs et al. 2000a). In addition, the hot rainless period is usually 6 to 7 consecutive months (i.e. from April to October), but up to 9 consecutive months during a drought year (Berkowicz 2003).

Meteorological and manual microlysimeter measurements in the research site were first carried out in September-October 1997 (Jacobs et al. 1999, 2000a, 2000b, 2002). The data revealed that the latent heat fluxes are substantial and that they followed a daily pattern resulting from dew. The number of dew evaporation measurements using the manual microlysimeters was limited since the measurements were very time-consuming. It required that the manual microlysimeters soil samples be repeatedly removed from their respective locations and weighed within an on-site shielded sensitive balance (Mettler, PM1200, Switzerland, 0.001 g accuracy), (powered by car batteries and recharged by solar panels) that had been placed inside a box to protect against wind effects. These manual measurements were either initiated

about 2 hours before sunset to about 13:00 local time the following day (until no weight changes occurred), or from about 1 hour before sunrise to about 13:00. The lysimeters were weighed at 30 minute intervals around sunrise and sunset because of rapid dew accumulation/drying, and then at 1 to 2 hour intervals. One difficulty in carrying out such measurements is the need to remove and replace the manual microlysimeters. This required carefully cleaning them before weighing in order to remove any soil material that may have attached itself to the sides or base.

Such measurements are laborious and exhausting, which may partly explain why modern dew research (post-1970) has lagged behind other areas in meteorology. Hence, an inexpensive recording device can be a welcome tool for both short and long-term dew measurements. In this paper, the development of an automated microlysimeter is presented including results obtained from an experimental campaign held in the Negev desert in September-October 2000 to study dew onset, accumulation and evaporation.

3.2 Load Cell Microlysimeter (LCM) Specifications and Design

The instrument was designed as a portable, lightweight and inexpensive sensor that could be used either in the field or under lab conditions. The design and specifications needed were based, in part, on experience and data obtained during a dew measurement field campaign carried out in 1997 (Heusinkveld et al. 2004; Jacobs et al. 1999, 2000a). The Load Cell is manufactured by Vishay Tedea-Huntleigh (Switzerland) (www.tedea-huntleigh.com). A low capacity, single-point Load Cell was used, model 1042, 1 kg rated capacity, made of anodized aluminium with dimensions 150 x 39 x 20 mm. It has a humidity resistant coating. The total error is given as 0.02 % of the applied load. There is internal electronic temperature compensation, but the remaining temperature dependence cannot be neglected. The temperature effect as specified by the manufacturer is +/- 0.001 % K^{-1} on output of load versus temperature, and the effect on the offset is +/- 0.004% K^{-1} of the rated output. Thus for a sampling cup of 140 mm diameter weighing 1 kg, the temperature effect in equivalent units in depth of water as dew is 3.2 μm K^{-1}. This was tested in a temperature-controlled oven over a range of 20-70 ºC and the company specifications were found to be correct.

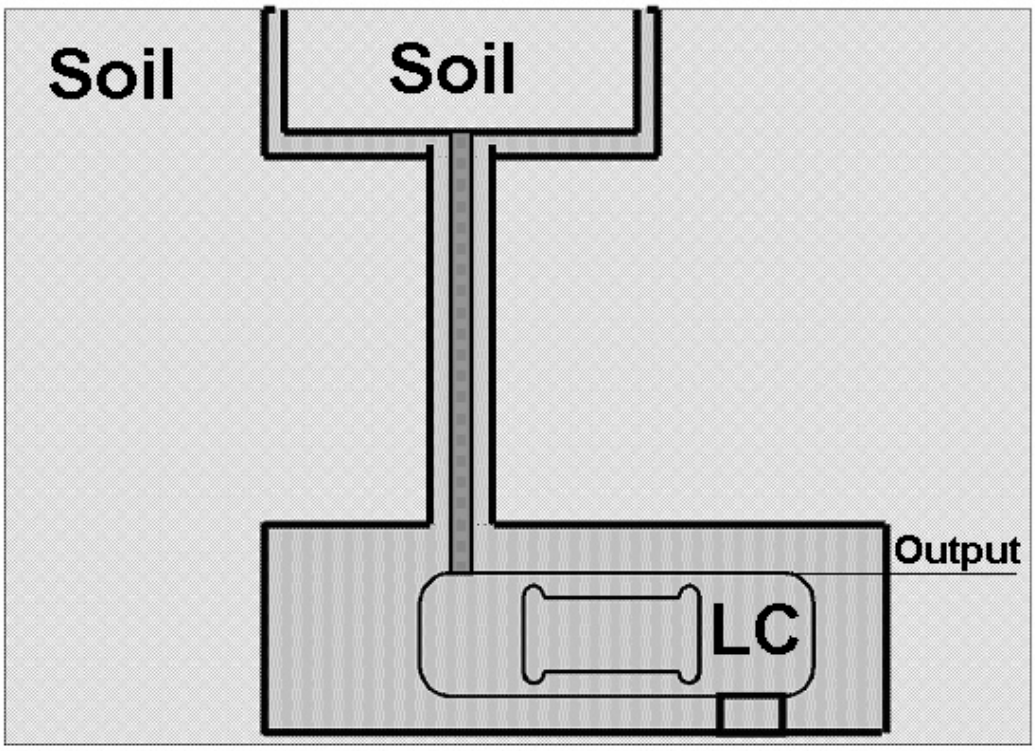

Figure 3.1: Sketch of microlysimeter construction. The top of the Load Cell (LC) is 0.22m below the surface.

Figure 3.2: Left panel: Load Cell affixed to a PVC base plate. An aluminum base plate option is also shown (note the depression to allow the Load Cell to bend). Rightpanel: Microlysimeter showing the empty plastic sampling dish and protective cover for rain or storage.

The LCM was thus designed to avoid these temperature problems. Figure 3.1 contains a sketch of the sensor and Fig. 3.2 shows the LCM on a base plate (left panel) and protective housing (right panel), respectively. The exposed surface area of the LCM contains a transparent plastic polypropylene dish (2 mm thick walls) that can hold a sample 140 mm in diameter and 35 mm deep. Although a larger diameter would reduce aerodynamic edge effects, this would also increase the size and weight of the sample.

The sampling cup depth of 35 mm was based on previous dew measurements at the Nizzana field site, comparing 10, 30 and 75 mm deep manual microlysimeters (polyvinylchloride, diameter 70 mm, walls 3 mm). The results showed that there were no differences between the 30 and 75 mm deep microlysimeters (Jacobs et al. 1999; but see also Evett et al. 1995). A shallower microlysimeter dish, would block vapour transport to deeper soil layers and collect less dew. The dish base has a small cap that fits into a central plastic support pipe to ensure the dish is balanced on the Load Cell below. The plastic pipe has a low heat conduction coefficient, which limits heat conduction towards the load cell. Polyvinylchloride (PVC) material, 5 mm thick, was used to house the Load Cell and protect the sampling dish. Figure 3.2 (right panel) shows the Load Cell attached to the housing base plate. The base plate can be made of

PVC, but also in aluminium to ensure better thermal contact with the soil below. We recognize that this housing material and bottom cap will affect the thermal transfer between the soil and the microlysimeter sample (Evett et al. 1995). A small depression was carved into the base plate (Fig. 3.2, left panel) to allow the Load Cell to bend. A screw can be inserted into a threaded hole in the loading end of the Load Cell for overload protection.

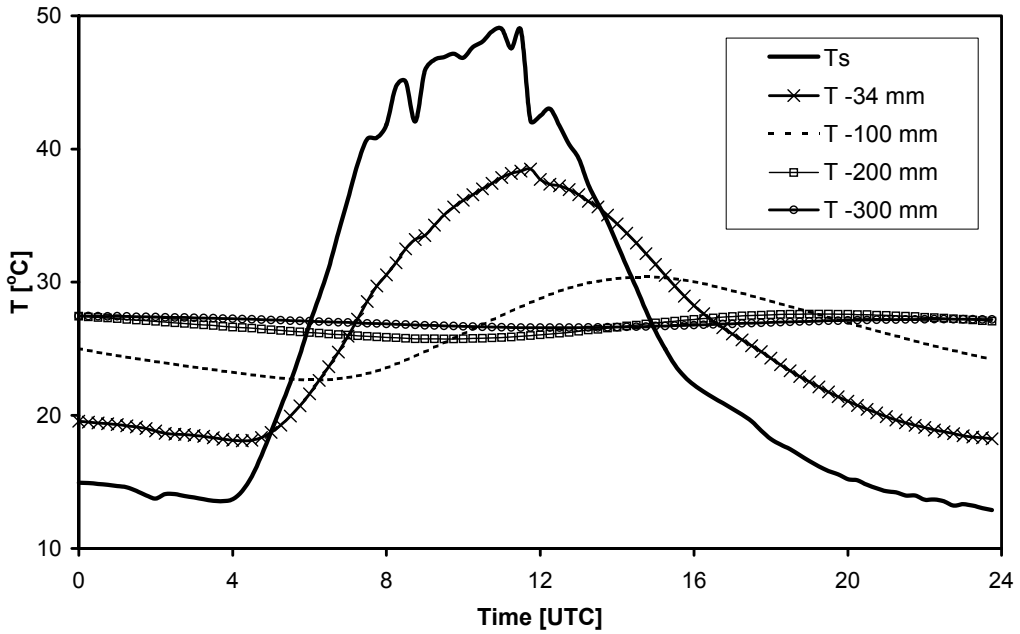

Figure 3.3: Measured temperature variation in a playa soil at the surface, Ts, and at various depths, 30 Sept. 1997. Local solar time is UTC + 2 h 18 min.

The Load Cell itself is installed (Fig. 3.1) at a depth of 220 mm (top of Load Cell), much deeper than the depth of the soil sampling cup. Figure 3.3 shows a typical diurnal pattern of the soil temperature profile variation in the field site to be less than 5° C at 200 mm depth during summer. Assuming that the temperature variation in the Load Cell will be similar to that of the soil below the loadcell, one can estimate a temperature error effect on the Load Cell output (Storlie and Eck 1996), i.e. a maximum error of 0.015 mm of equivalent dew amount. Because of the insulating open space above the Load Cell and the poor temperature-conducting plastic shaft that connects the Load Cell to the soil sampling cup, it is expected that the temperature variation is lower. Therefore, no corrections were made for the remaining temperature effect.

The output was recorded using a Campbell Scientific 21X data logger (Campbell, USA). The measurement technique was a 6 wire full bridge with excitation lead compensation with a resolution of 0.1 grams. The mass was monitored at 5 sec intervals and were averaged every 15 min.

The soil cores for the MLS sampling cup were prepared in the following way. A PVC pipe of the same diameter and depth as the sampling cup, was placed on the study surface. The pipe was then tapped until flush with the surface. The soil around the pipe was then exposed by digging and a flat plate was inserted horizontally at the base of the exposed pipe. The surface was then covered by another plate and the entire core was lifted and inverted. The top plate was removed and the sampling cup was placed over the core and pushed down. Then the core was inverted again revealing the original surface. The dish and protective PVC casing limits heat exchange from the surrounding soil and is obviously not suited for situations under rainfall. In such cases, the dish should be covered with a cap. However our design could be used for light rains of a few mm, as long as the water percolation does not reach the dish base. This can be determined by removing the transparent dish and visual examination of the base.

3.3 Field Site Description

The Load Cell microlysimeters were tested during a 6-week field campaign held in September-October 2000, in the Hebrew University of Jerusalem Minerva Arid Ecosystems Research Center (AERC) sand dune experimental station (lat $30^0$56' N; lon $34^0$23' E; elevation 190 MSL) situated near Nizzana, NW Negev desert, Israel. The Mediterranean Sea lies about 40 km to the northwest. The average annual rainfall of the region is about 100 mm, with a coefficient of variation of about 40 %, and occurs primarily in winter between December to February (Sharon et al., 2002). The measurement campaign took place near the end of the hot, rainless summer. The soil water recharge by rain is low. During the period October 1999–March 2000, the site received only 35 mm of rainfall, with 8 mm in March 2000 distributed over four small showers. The only major rainfall occurred in late January 2000 (18 mm).

The dune field encompassing Nizzana consists of sparsely vegetated linear dunes 10 to 25 m high and up to 125 m wide. The dune crests are mobile but the dunes themselves are stable. The dunes are elongated west-east, which is the resultant of the direction of the strongest winds (Sharon et al. 2002). Although the climate is classified as arid, the dune slopes can have a perennial vegetation cover of up to 30% and even up to 50% near footslopes (Tielbörger 1997). Biological crusts form on the dune slopes and tend to cover the open areas between shrubs (Littmann and Ginz 2000). The interdune corridors are between 50-150 m wide and contain a mixture of wide flat playa surfaces, gently sloping stretches, many small hillocks and remnants of eroded ancient dunes.

Dew formation and evaporation on two terrain types were assessed on a dune slope covered with biological crusts and, in a flat playa area situated near the foot of the dune. The playa consists of a thick compacted layer of silt and clay, though the

first few mm can contain 35% fine sand (Pfister et al.1996). This material was deposited during temporal inundations caused by strong winter rains.

3.4 Field Instrumentation

The meteorological measurements were made 10-30 m away from the microlysimeters, depending on the sensor. Monitoring of the radiation budget, by measuring the short wave and long wave radiation separately, was performed with Kipp radiometers at an interval of 15 minutes. The incoming and reflected short wave radiation was monitored by 2 solarimeters (Kipp CM14, The Netherlands), the incoming and emitted longwave radiation by 2 pyrgeometers (Kipp CG1, The Netherlands). The sensible and latent heat fluxes were measured by the Eddy Correlation (EC) technique using a 3D sonic anemometer (Campbell, CSAT3, USA) and a fast humidity sensor (Li-Cor, Li-7500, USA), mounted at a height of 3 m.

The temperature profile was monitored at 0.5 m and 1.5 m with aspirated psychrometers (Pt-100 resistance thermometers). Wind speed was measured at two heights (2 and 5 m) with small sensitive microcup anemometers (length distance 1.2 m). Soil temperatures were measured at 2, 50 and 100 mm depths with Pt100 (platinium wire) home-made resistance thermometers. Soil surface temperature was monitored with a pyrometer (Heimann KT15, Germany).

Four pairs of manual microlysimeters (Boast and Robertson 1982), 30 mm deep and 70 mm in diameter, were installed along a 32 m transect running from the flat playa to the upper dune slope. The first pair (MLS-1) was next to the Playa Load Cell, the second set (MLS-2) near the dune footslope (13 m away from the Playa Load Cell), the third set (MLS-3) next to the Load Cell on the dune midslope (11 m above MLS-2), and the fourth pair (MLS-4) 8 m further upslope. In total, 16 overnight measurements were carried out using the manual microlysimeters.

3.5 Results and Discussion

An example of the Load Cell performance is provided in Fig. 3.4a, together with relevant meteorological data (Fig. 3.4b).

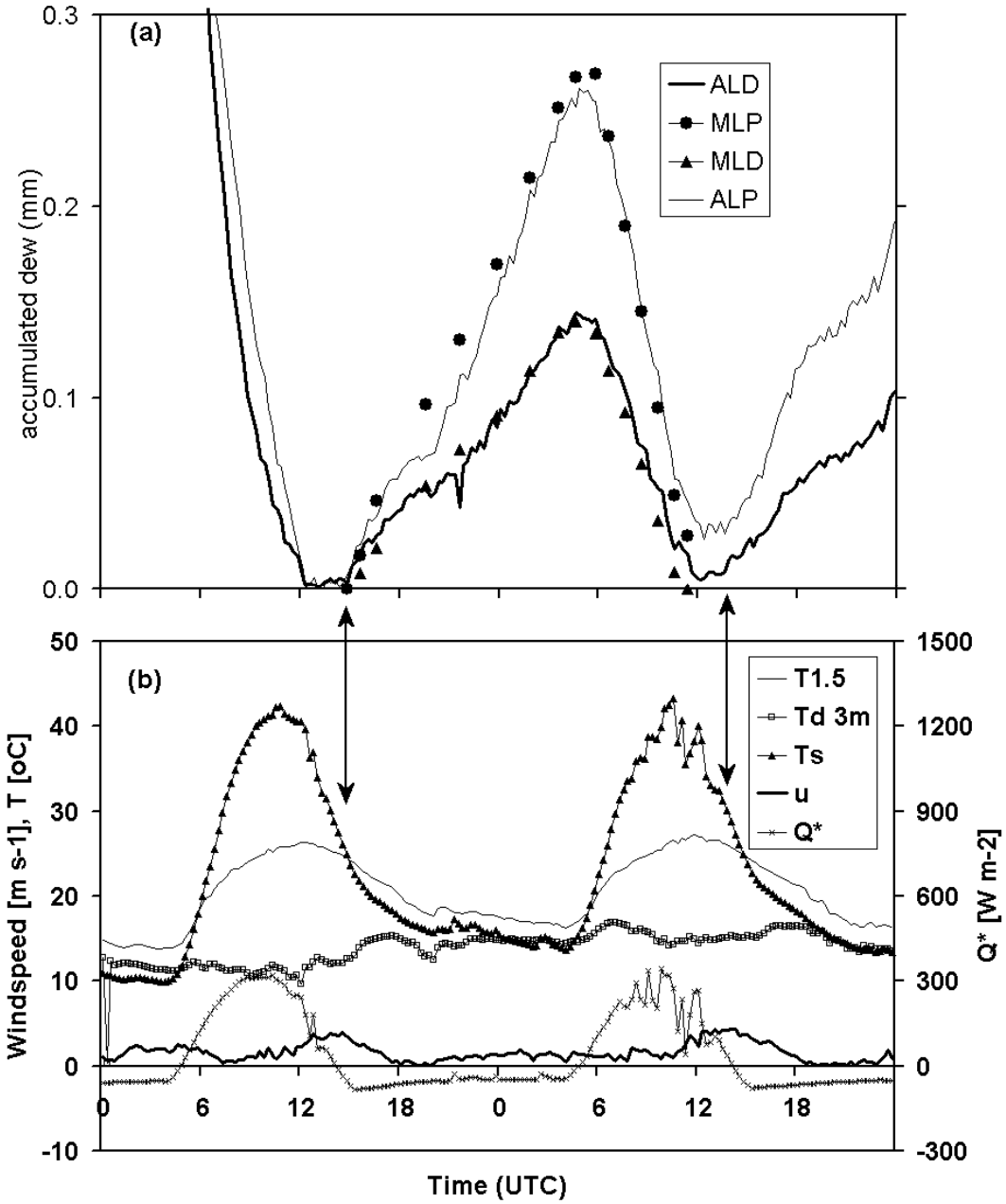

Figure 3.4 ***a*:** Automatic microlysimeter on dune midslope (ALD), automatic microlysimeter on the playa (ALP), manual microlysimeter on dune midslope (MLD), manual microlysimeter on the playa (MLP), 16-17 Oct. 2000. ***b*:** Meteorological data for 18-19 Oct. 18-19. T1.5 air temperature at 1.5 m, Td dew point at 3 m, u windspeed at 3 m, Q* net radiation. Solar time is UTC + 2 h 18 min.

The sensitivity of the LCM is demonstrated for DOY 290 (16 Oct 2000). This day experienced the first rain of the season, a drizzle of 0.3 mm followed by dew. This rain was not registered by the station's manual rain gauges or rain recorder, but was detected on both LCM's. The remaining water in the manual and LCM's could be

attributed to the water that did not evaporate on the less hot day after the dew night preceding the drizzle. The manual and recording microlysimeter data differ by less than 5%, Of interest is the difference between the playa and dune midslope dew accumulation amounts.

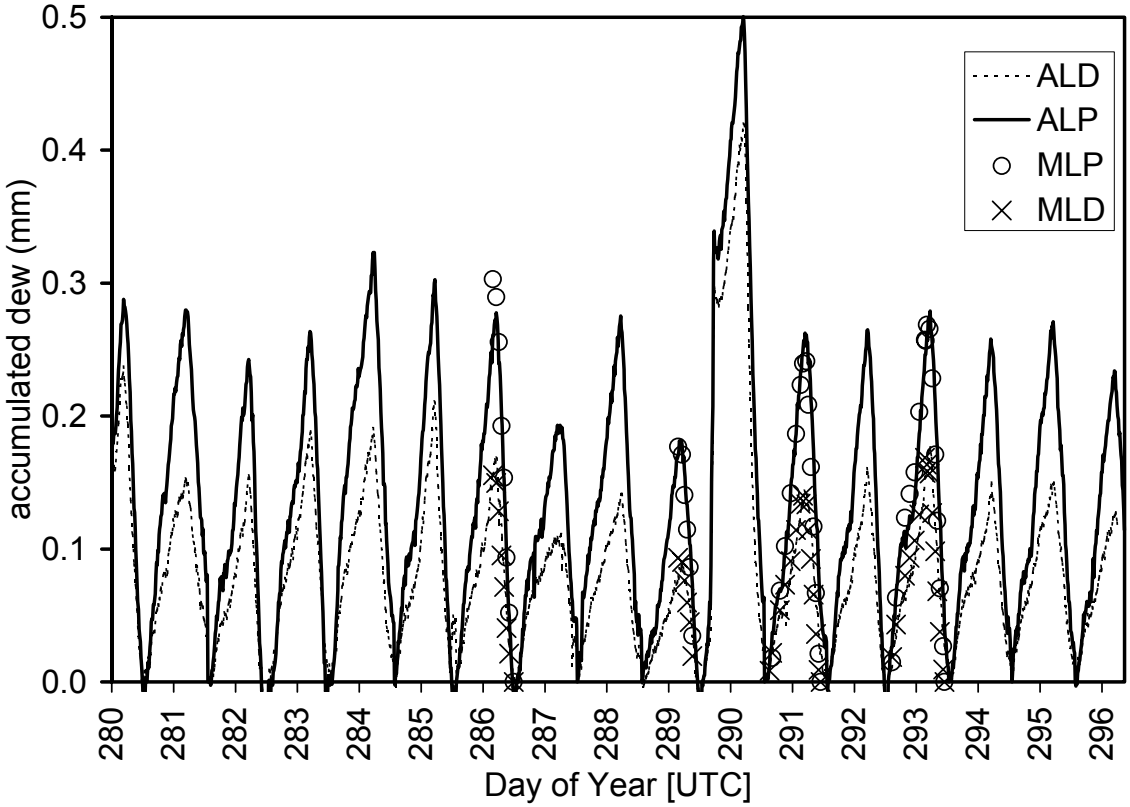

Figure 3.5: Daily dew formation and evaporation measured using the automatic microlysimeters. Automatic microlysimeter on dune midslope (ALD), automatic microlysimeter on the playa (ALP), manual microlysimeter on the playa (MLP), manual microlysimeter on dune midslope (MLD).

The dune midslopes receive about 40% less dew than on the playa soil (Figs. 3.5 and 3.6). We attribute this to the fact that the playa surface contains clay and silt, and high salinity levels due to surface ponding by rain and subsequent evaporation. The dry soil and the salt are able to attract and absorb moisture. The dune slope surfaces, in contrast, have the surface salts washed out by rain and only the thin curst contains some silt and clay from aeolian dust deposition. The grain size distribution of the 2 to 4 mm thick crust shows a concentration of silt and clay. The grain size distribution medians are 90um for the crust and 230 um for the sand below the crust (Verrecchia et al. 1993). The dew formation process is controlled by the available energy (i.e. net radiation minus soil heat flux) and the vapor pressure deficit (Monteith, 1957). The vapor pressure deficit is dependent on the soil moisture content

near the surface. The vapor pressure deficit is less for high dew episodes (> 0.2 mm) and it results in smaller differences between the two soil types (Fig. 3.6). This could be attributed to the filling up of the finer soil capillaries, resulting in a reduced vapour pressure reduction effect in the soil pore air. This is also the reason that dew formation already starts at a low relative humidity of the free atmosphere <<100%. See for example Fig. 3.4, where the dew formation process starts already (see arrows), at a free atmosphere dew point temperature of more than 10 degrees below the soil surface temperature.

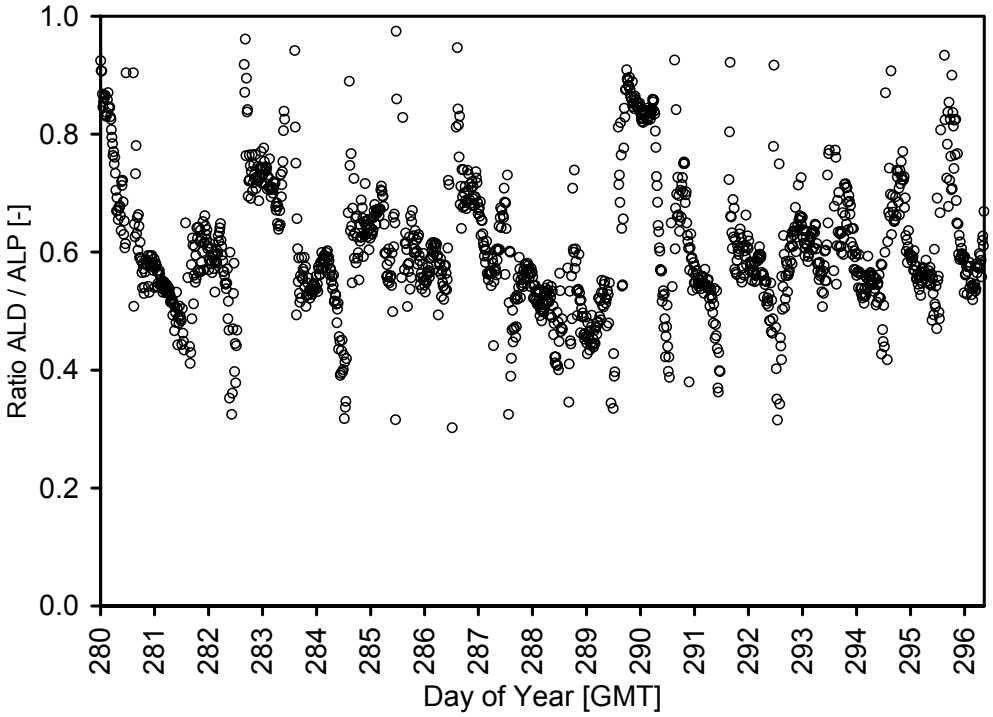

Figure 3.6: Ratio between automatic microlysimeter on dune midslope (ALD) and automatic microlysimeter on the playa (ALP)

To establish that soil composition, and not microclimatic conditions, was the source of this difference, a playa soil sample in a manual microlysimeter was transposed with one from the dune slope The playa sample placed on the midslope recorded, in terms of dew amount, the same relatively higher values as at the playa location, and the relatively lower value for the midslope sample placed on the playa. This phenomenon, as well as "surface dew patches" in the research site that can be detected visually, will be discussed in a companion paper (Berkowicz et al. 2005).

3.6 Conclusions

The development of inexpensive and portable recording microlysimeters to study minor changes in near-surface soil moisture content can make a valuable contribution to dew research. The total accuracy of the LCM tested here, as based on

manufacturer's specifications and oven testing, was ±0.02 mm of equivalent dew. The LCM's compact size and light weight allows the sensor to be installed in a variety of settings and landscapes, and not just on flat surfaces.

This Load Cell microlysimeter revealed, or provided independent data to show that dew formation on bare soil is highly dependent on the soil composition and it occurred on almost every evening during the field experiment. The daily dew variation ranged from 0.1 to 0.2 mm on stable dune slopes but up to 0.4 mm on the playa. This difference is attributed to the playa's high silt and clay content and salinity and it becomes less with increasing soil moisture content. The soil composition is also the reason that dew formation already starts while the soil surface temperature is more than 10 degrees higher than the dewpoint temperature of the free atmosphere.

Acknowledgments

We thank the Minerva Arid Ecosystems Research Centre of the Hebrew University of Jerusalem, the Dutch Organisation for Scientific Research (NWO), and the Wageningen University Meteorology and Air Quality Group for supporting the Negev desert field campaigns in 1997 and 2000.

References

Berkowicz, S.M., Heusinkveld, B.G., and Jacobs, A.F.G., 2001: Dew in an arid ecosystem: Ecological aspects and problems in dew measurement. Proc., 2nd International Conference on Fog and Fog Collection,15-20 July 2001, St. John's, Newfoundland, Canada. pp 301-304.

Berkowicz, S.M., 2003: Nizzana rainfall data summary. Unpublished internal report. Arid Ecosystems Research Centre, Hebrew University of Jerusalem, Jerusalem, Israel.

Berkowicz, S.M., Heusinkveld, B.G., Felix-Henningsen, P., and Jacobs, A.F.G., 2005: Dew patches in an arid environment. (Manuscript).

Boast, C.W., and Robertson, T.M. 1982: A micro-lysimeter method for determining evaporation from bare soil: description and laboratory evaluation. *Soil. Sci. Am. J.*, 46, 689-698.

Brackenbury, J.H., 1997: Spider webs: dew loading of the linyphid sheet-web. *J. Zool. London*, 242, 131-136.

Broza, M., 1979: Dew, fog and hygroscopic food as a source of water for desert arthropods. *J. Arid Environ.*, 2, 43-49.

Daamen, Carl C., Simmonds, L. P., Wallace, J.S., Laryea, K.B., and Sivakumar, M.V.K., 1993: Use of microlysimeters to measure evaporation from sandy soils. *Agric. Forest Meteorol.*, 65, 159-173.

Danin, A., Bar-Or, Y., Dor, I., and Yisraeli, T., 1989: The role of cyanobacteria in stabilization of sand dunes in southern Israel. *Ecologia Mediterranea*, XV: 55-64.

Evenari, M., Shanan, I., and Tadmor, N., 1982: *The Negev: Challenge of a Desert*. University Press, Cambridge Mass., 284 pp.

Evett, S.R., Warrick, A.W., and Matthias, A.D., 1995: Wall material and capping effects on microlysimeter temperatures and evaporation. *Soil Sci. Soc. Am. J.*, 59, 329-336.

Grimmond, S.B., Isard, S.A., and Belding, M.J., 1992: Development and evaluation of continuously weighing mini-lysimeters. *Agric. Forest Meteorol.*, 62, 205-218.

Gutterman, Y., and Shem-Tov, S., 1997: Mucilaginous seed coat structure of *Carrichtera annua* and *Anastatica hierochuntica* from the Negev Desert highlands of Israel, and its adhesion to the soil crust. *J. Arid Environ.*, 35, 695-705

Harel, Y., Ohad, I., and Kaplan, A., 2004: Activation of photosynthesis and resistance to photoinhibition in cyanobacteria within biological desert crust. *Plant Physiology*, 136, 3070-3079.

Heusinkveld, B.G., Jacobs, A.F.G., Holtslag, A.A.M., and Berkowicz, S.M., 2004: Assessing the soil heat flux component in the surface energy balance of a desert region. *Agric. Forest Meteorol.* 122, 21-37.

Heusinkveld, B.G., Jacobs, A.F.G., Holtslag, A.A.M. and Berkowicz, S.M., (2005). Dew water movement in a sand dune ecosystem with a biological crust. (manuscript).

Jackson, D.W.T., 1996: A new, instantaneous aeolian sand trap design for field use. *Sedimentology*, 43, 791-796.

Jacobs, A.F.G., Heusinkveld, B.G., and Berkowicz, S.M., 1999: Dew deposition and drying in a desert system: a simple simulation model. *J. Arid Environ,*. 42, 211-222.

Jacobs, A.F.G., Heusinkveld, B.G., and Berkowicz, S.M., 2000a: Dew measurements along a Longitudinal Sand Dune Transect, Negev Desert, Israel. *Intl. J. Biometeorol.,* 43, 184-190.

Jacobs, A.F.G., Heusinkveld, B.G., and Berkowicz, S.M., (2000b). Force restore technique for surface temperature and surface moisture in a dry desert system. *Water Resources Research* 36, 1261-1268.

Jacobs, A.F.G., Heusinkveld, B.G., and Berkowicz, S.M., 2002: A simple model for potential dew-fall in an arid region. *Atmospheric Res*., 64, 287-297.

Larmuth, J., and Harvey, J., 1978: Aspects of the occurrence of desert plants. *J. Arid Environ.*, 1, 129-133.

Littmann, T., and Ginz, D., 2000: Eolian transport and deposition in a partially vegetated linear sand dune area (northwestern Negev, Israel). *Z. Geomorph. N.F. Suppl.-Bd*.,121, 77-90.

Malek E., McCurdy G.D., and Giles B., 1999: Dew contribution to the annual water balance in semi-arid desert valleys. *J. Arid Environ.,* 42, 71–80.

Moffett, M.W., 1985: An Indian ant's novel method for obtaining water. *National Geographic Res.*, 1, 146-149.

Monteith, J.L. (1957): Dew. Quart. J. Roy. Meteorol. Soc., 83:322-341.

Munne-Bosch S., and Alegre, L., 1999: Role of dew on the recovery of water-stressed Melissa officinalis L-plants *J. Plant Physiol*., 154, 759-766.

Munne-Bosch, S., Nogues, S., and Alegre, L., 1999: Diurnal variations of photosynthesis and dew absorption by leaves in two evergreen shrubs growing in Mediterranean field conditions. *New Phytologist*, 144, 109-119.

Nevo, E., Bar-El, C., Bar, Z., and Beiles, A., 1981: Genetic structure and climatic correlates of desert landsnails. *Oecologia (Berl),* 48, 199-208.

Pfisterer, U., Blume, H.-P., and Beyer, B., 1996: Distribution pattern, genesis and classification of soils of an arid dune area in northern Negev. *Z. Pflanzenernähr. Bodenk*., 159, 419-428.

Richards, K., 2004: Observation and simulation of dew in rural and urban environments. *Prog. Physical Geog.*, 28, 76–94.

Scott, D., Bayfield, N.G., Cernusca, A. and Elston, D.A., 2002. Use of a weighing lysimeter to assess the effects of trampling on evapotranspuiration of montane

plant communities. *Can. J. Botany*, 80, 675-683.

Sharon, D., Margalit, A., and Berkowicz, S. M., 2002: Locally modified surface winds on linear dunes as derived from directional raingauges. *Earth Surf. Processes Landforms*, 27, 867-889.

Sear,D.A., Damon,W., Booker, D.J., and Anderson, D.G., 2000: A load cell based continuous recording bedload trap. *Earth Surf. Processes Landforms*, 25, 659-672.

Steinberger, Y., Loboda, I., and Garner, W., 1989: The influence of autumn dewfall on spatial and temporal distribution of nematodes in the desert ecosystem. *J. Arid Environ.*, 16, 177–183.

Storlie, C.A., and Eck, P. 1996: Lysimeter-based crop coefficients for young Highbush blueberries. *Hort. Sci.*, 31, 819-822.

Tielbörger, H., 1997: The vegetation of linear desert dunes in the north-western Negev, Israel. *Flora,* 192, 261-278.

Verrecchia, E., 1993: Physical properties of the psammophile cryptogamic crust and their consequences to the water regime of sandy soils, north-western Negev Desert, Israel. *J. Arid Environ.*, 29: 427-437.

Wallin, J.R., 1967: Agricultural aspects of dew, *Agric. Meteorol*., 4, 85-102.

Zangvil, A., 1996: Six years of dew observations in the Negev desert Israel. *J. Arid Environ.*, 32, 361-371.

4 A new remote optical wetness sensor and its applications

reprinted from*

B.G. Heusinkveld[a], S.M. Berkowicz[b] , A.F.G. Jacobs[a], W. Hillen[a], A.A.M. Holtslag[a]

[a*] *Meteorology and Air Quality Group, Wageningen University, Droevendaalsesteeg 4, Atlasgebouw, P.O. Box 47, 6700 AA Wageningen, The Netherlands*

[b] *Arid Ecosystems Research Centre, Hebrew University of Jerusalem, Institute of Earth Sciences, Edmond Safra Givat Ram Campus, Jerusalem, Israel 91904*

*Published in Agricultural and Forest Meteorology (2008), doi:10.1016/j.agrformet.2007.11.007

Abstract

An Optical Wetness Sensor (OWS) was developed for continuous surface wetness measurements. The sensor is an all-weather instrument that does not interfere with the surface wetting and drying process and is unaffected by solar radiation. It is equipped with its own light source with which it can scan a surface and analyse its spectral reflectance. The backscattered radiation is detected around two wave bands: 1.70 µm (170 nm waveband) and 1.94 µm (80 nm waveband). The optical design is such that the ratio of the two signals is not dependent on the sampling distance, hence making it possible to study leaves under field conditions. Field and lab testing showed that the OWS was also capable of resolving small changes in surface soil water content such as from dew. In addition, the change of leaf water content could be detected (accuracy 5%). The OWS was also capable of measuring small changes in water content in the upper soil layer (<2 mm) of a loamy and fine sandy soil. For plant leaves it must be noted that the OWS responds to both internal and external water and thus cannot always discern between them.

Keywords: surface wetness, remote sensing, optical wetness sensor, dew, soil moisture, leaf water content.

4.1 Introduction

The ability to detect and measure moisture upon surfaces has intrigued scientists for decades. Concise reviews covering several aspects of this issue are contained in Berkowicz et al. (2001), Richards (2004) and Agam & Berliner (2006). If the source of the moisture is dew (and to some extent fog), then surface properties will heavily influence the formation, rate and amount of condensation. Soils, tree/plant leaves, rocks, and man-made materials (cement, ceramic, metals, glass) have different inherent thermal and physical properties. Surfaces moistened by rain may also be of interest.

Attempts to directly detect/measure surface moisture have been greatly hindered by a lack of suitable sensors. Over the past 50 years, much attention has been given to the development of techniques (i.e. numerical models) and instruments to make reliable estimates of dew amounts and leaf wetness duration (Wallin, 1963; Burrage, 1972). Such instruments are based, however, on indirect approaches. For example, dew drops forming on wooden blocks (e.g. Duvdevani, 1947), electrical resistance grids (e.g. Gillespie & Kidd, 1978), and artificial leaves equipped with a TDR (Time Domain Reflectometry) sensor (Decagon Devices Inc. USA; http://www.decagon.com) have been used as leaf proxies.

Techniques requiring sampling are destructive and prevent repetitive measurements on the same sample. Surface measurements involving sensitive balances will interfere to some extent with the measurements, and for many surfaces sampling may not be an option. In the last decade, technological developments have generated new possibilities and have greatly reduced the size and cost of electronic components, paving the way for remote sensing instrumentation.

There are many practical applications for a remote sensing surface wetness sensor. In agriculture, leaf surface wetness is well-known for contributing to the development of plant pathogens, foliar bacteria, crop epidemics and pests (Baier, 1966, Bass et al., 1991; Hatefield & Thomases, 1982; Huber & Gillespie, 1992; Jacobs et al., 1990; Lou & Goudriaan, 2000; Wallin, 1963, 1967), with severe economic repercussions. *Botrytis-spp.* in lilies and *Phytophthora infestans* in potatoes are feared for their rapid destructive work (Doornik & Bergman, 1974; Shoemaker & Lorbeer, 1977; Royle & Butler, 1986). Farmers avoid crop risks by preventive spraying of costly fungicides/pesticides on a very regular time schedule. These sprayings can be considerably reduced if reliable prognostic estimates can be made of actual leaf wetness duration (e.g. Norman, 1982; Weiss & Norman, 1987) and can be applied to both field crops and greenhouses. This would decrease farming costs and reduce the amount of chemicals introduced into the environment.

Surface wetness has a great effect on evaporation and surface temperature, (Monteith, 1981; Holtslag et al., 1988). Kiondo (1990) showed how the partitioning of the surface energy balance components depends on soil moisture content. Satellite

observations of vegetation and for monitoring of agricultural crops can be affected by early morning dew (Lin & Minnis, 2000; Pinter, 1986; Wood et al., 2002). In addition, such data are confined to the daylight period. Satellite remote sensing cannot use certain spectra of solar radiation because of interference with the atmosphere (water vapour absorption features).

In urban settings, high concentrations of pollutants found in dew can lead to surfaces being damaged, such as on cars and vegetation (Khare et al., 2000; Pierson et al., 1986; Takenaka et al., 2003).

Surface wetness is an important parameter in arid to Mediterranean ecosystems, where dew and/or fog are usually the only source of water input during the hot or rainless periods. In the Negev desert, observations by Evenari et al. (1982) and Zangvil (1996) have shown that dew occurs about 200 times per year and can add up to the equivalent of 30 mm of precipitation Although the daily input does not contribute to an increase of water to deeper layers of soil, this moisture can nevertheless be critical for small animals and micro-organisms that have adapted to survive under moisture stress (Broza, 1979; Moffett, 1985; Steinberger et al., 1989). Arid and semi-arid sand dune ecosystems may contain biotic crusts, up to several mm thick, composed of cyanobacteria, mosses, lichens, and algae (Lange et al., 1992). Temperature, light and moisture are essential elements for crust photosynthesis. Dew contributes to the water balance of this very thin soil layer. The crusts help stabilize the dunes (Danin et al., 1989), inhibit rain infiltration (Yair, 1990) as well as evaporation from the soil due to its protective cover (Jacobs et al., 1999, 2000a). Measuring the surface moisture on such crust surfaces is important for studying crust hydration and dehydration cycles (Heusinkveld et al., 2006).

Recent studies on dew deposition, plant water relations, and diurnal variations of photosynthesis in some Mediterranean shrubs and plants found that the leaves were able to absorb dew and thus restore plant water status (Munne-Bosch et al., 1999; Munne-Bosch & Alegre, 1999). Dew can affect understorey plant species in forests (Barradas & Glez-Medellin, 1999). Measurements of leaf water content could improve fire risk management decision systems (Wittich, 2002). The golf industry is sensitive to potential damage by pathogens to the turfgrass used in many courses (Madeira et al., 2001; Williams et al., 1998). In contrast, there is great interest in the water-repelling behaviour of some plant leaf surfaces and the mechanism of water beading off (Otten & Herminghaus, 2004).

Aeolian sand transport is highly dependant on soil surface moisture. Wiggs et al., (2003) investigated the influence of changes in surface moisture content on sand entrainment and transport on a meso-tidal beach. Such research can benefit from a remote surface moisture meter.

Advances in infrared spectroscopy have made it possible to study the reflectance spectra of soils of different composition and soil moisture contents

(Chang et al., 2001; Eshel et al., 2004; Lobell & Asner, 2002; Weidong, 2002). These studies demonstrated that the soil water content could be derived from the spectral reflectance signature of the soil. Mouazen et al., (2004) developed an online soil moisture content meter based on near infrared reflectance spectroscopy. Their sensor is mounted inside a soil spoiler (plough) and measures the soil water content of the soil in contact with the sensor optics. Ayalew & Ward (1999) designed a prototype infrared reflectance moisture meter to measure milled peat. However, these sensors have a common limitation in that they were not designed to work under full sunshine conditions. Bruckler et al. (1988) developed a near-surface soil moisture meter based on microwave measurements. Since microwaves penetrate the soil far deeper than near infrared, it is less suited to measure soil moisture content at the soil surface. Cessato et al. (2001) demonstrated that Leaf Water Content (LWC) can be measured by analyzing the reflectance spectra in a laboratory set-up but did not find a uniform relationship between LWC and leaf reflectance spectra.

The objective of the present study is to present a new sensor that remotely measures surface wetness without interfering with the wetting/drying process and that can operate in the field and also under full sun conditions. Of special interest is the ability to assess moisture content on soil surfaces and on plant leaves.

4.2 Theoretical background

A remote sensing field sensor for detecting and measuring the amount of surface water can be based on determining the reflectance signature of reflected incident radiation from a given surface. Two kinds of surfaces can be identified; a porous surface where the water is locked inside its porous structure and a closed surface with water deposition on top.

4.2.1 Water detection of water in a porous surface

Examples of a porous surface include soils and leaves with a porous cuticle. The reflectance of incident radiation on a surface is affected by water. For soils, the solar radiation reflection coefficient (albedo) decreases as soil humidity increases. This phenomenon arises from the fact that air fills the space between the particles in a dry soil. Reflectance is then linked to the refraction index of the air-particle interfaces. When the soil is wet, water fills part of the micro-pores. As the water-particle index of refraction is lower than the air-particle index of refraction, reflectance is thus lower.

Many ideas have been proposed to quantify soil moisture using the change in albedo. Graser & Van Bavel (1982) summarized research using light absorption by water to find a relationship between soil water content and the albedo and concluded that no uniform relation existed between them. They also noted that some of the

relations found could be a measurement artifact due to strong moisture gradients near the surface.

Dry soils have the highest reflectance with the maximum reflectance depending on soil type; sandy soils have a higher reflectance than loamy soils. Until the hygroscopic (absorbed) moisture content is reached, there is almost no change of albedo. Additional moisture (above the hygroscopic limit) results in a marked decrease of reflectance caused by the excess water that surrounds the soil particles and fills the voids between particles. The change from high to low reflectance depends on the soil type. For sandy loams, the change occurs between 0 to 3% of moisture capacity in the sample (Ben-Dor et al., 1997).

A careful selection of certain light wavebands that are sensitive to water can improve detection of water in porous media. Soil texture and soil composition have a great influence on the albedo. It is expected that by using selective wave bands, the dependence of moisture detection on soil composition can be reduced. By using the spectral reflectance signature of a surface, one can estimate soil surface moisture content. Bowers et al. (1965) demonstrated this by measuring the light reflection from a soil sample in the 0.5 to 2.6 μm range of an equilibrated moist soil sample placed under a spectrometer. The water absorption bands in the reflected spectra were evident around 1.45 and 1.93 μm. In satellite remote sensing these wavebands cannot be used because the solar radiant energy at these wave bands is being absorbed in the atmosphere. Although the shape of Bowers et al. (1965) reflectance curve, as a function of wavelength and soil moisture content, is not characteristic for all soil types, it was typical for Newtonia silt loam. However, various soils exhibit a similar spectral dependence around the water absorption bands.

Lobell & Asner (2002) measured the spectral reflectance of thin samples (1 mm) of four different soil types while drying them on a balance. They found that shortwave infrared was more suitable for volumetric water content detection than visible wavelengths because of its enhanced sensitivity for soil water contents above 20%. They found that the reflectance could be parameterised with a simple exponential reflectance model, with little variation in constant C among soils, when using the soil water saturation data θ/θ_{sat} instead of θ only (Eq. 4.1):

$$R_\lambda = R_{\lambda,s} + (R_{\lambda,d} - R_{\lambda,s})e^{(-C_\lambda \frac{\theta}{\theta_s})} \qquad (4.1)$$

where R_λ is the reflectance at wavelength λ, $R_{\lambda,s}$ is the reflectance at λ at saturated water content, $R_{\lambda,d}$ is the reflectance at λ for a dry soil, θ is the soil volumetric moisture content and θ_s is the saturated volumetric soil moisture content. The model is reasonable because the mechanism to explain the decrease of reflectance with increasing soil water content follows the Beer law of exponential extinction of light passing through an absorbing medium. Weidong et al. (2002) measured the spectral reflectance of a much thicker soil sample (15 mm) under slow-drying conditions.

Their results were different and may have artifacts because a soil under drying conditions will have a strong moisture gradient near the surface (Graser et al., 1982).

Cessato et al. (2001) did not find a uniform relationship between LWC and leaf reflectance spectra but demonstrated that a calibration can work for a specific leaf. An important factor in selecting a water absorption band is that it should not be sensitive to possible O-H bonds in the substrate. Leaves have a high percentage of O-H bonds but the 1.93 μm wave band is not sensitive to these O-H bonds. Simultaneous detection of a second wave band of light near the absorption band is essential to serve as a reference, but which is insensitive to water and also insensitive to these O-H bonds. The ratio between these two wave bands determines the band depth absorption. Using this technique, the response will be less sensitive to chemical surface composition. A suitable wave band exists around the 1.70 μm, where the reflectance changes in relation to soil moisture content or LWC content is low.

4.2.2 Closed surfaces

The percentage of surface area covered with water will depend on certain characteristics of the surface. This wettability will depend on the contact angle between the water and the surface. Hydrophobic surfaces have high contact angles whereas hydrophilic surfaces have contact angles approaching zero. In the case of water condensation or dew, the ratio between a wet and a dry area will increase in time and stabilize at a maximum value. This maximum value will be dependent on the contact angle only (Beysens, 1995). A liquid is considered to wet a solid only if the contact angle is zero.

This raises the question of how to define surface wetness in meteorological problems. In chemistry, liquid on a surface with a contact angle greater than 90° is said not to wet the solid. In such cases drops of liquid tend to move about easily on the surface and do not enter capillary pores. A plant surface usually has a contact angle of less than 90°, although there are plant surfaces with contact angles of >100°.

In meteorology it is common to define surface wetness as the appearance of water droplets or layers of water on a surface. Spherical droplets with large contact angles are included. Wettable surfaces with contact angles of less than 90° will also retract surface water in surface pore holes. Such water is not always visible to the human eye. Furthermore, water in these pores may have a lower vapour pressure because vapour pressure above a concave surface is reduced by the curvature of that surface. This will permit condensation above the dew point temperature. Such surface water is harder to detect since the surface surrounding the pore remains quite dry. What precedes the formation of visible wetness is the formation of a water layer with a thickness of a few molecules.

Note that the optical detection of surface leaf wetness is complicated by the fact that the leaf also responds to LWC change. If LWC change has a time scale of days

and leaf surface wetting/drying a time scale of hours then it might be possible to discern between the two by implementing a dry/wet base-line moving average.

The Optical Wetness Sensor (OWS) described below is based on using the optical interaction of incident light with a surface to detect surface wetness. To understand the potential of this technique, it is important to understand the processes involved in reflectance. A surface can reflect, absorb and transmit incident radiation. The surface reflectance characteristics will also depend on surface roughness. Reflectance can be diffuse, specular (mirror-like) or a combination of both. Penetration of radiation into the surface can also be reflected back to the surface. A substrate covered with a layer of water (contact angle = 0) will reflect light at the air-water interface and at the water substrate interface. The light absorption in the water layer will be a function of wavelength and water depth. The transmission path will also depend on the angle of incidence. The spectral reflectance signature contains information about the reflecting surface.

To test the possible use of water absorption bands in the infrared, an experiment was carried out using a Varian Cary 5E UV-Vis-NIR spectrophotometer (Cary, NC, USA) with a diffuse white integrating sphere attachment. There is a small hole for a light detector and 2 small holes for the 2 input light beams. The leaf was attached inside the integrating sphere. The spectrometer detector collected all diffuse and specular components of a light beam reflecting off the leaf as well as collecting light from a reference beam that was directed at the white sphere. In Fig. 4.1 the reflected light leaf spectrum of a leaf with a wet surface was divided by the spectrum of the same leaf with a dry surface. Major light absorption bands for water are noticeable in Fig. 4.1. Water has a weak absorption band around 0.93 μm and some strong absorption bands around 1.45 μm and 1.93 μm. There are even stronger absorption bands at longer wavelengths, but these wavelengths are harder to detect and so are impractical for use in surface wetness detection.

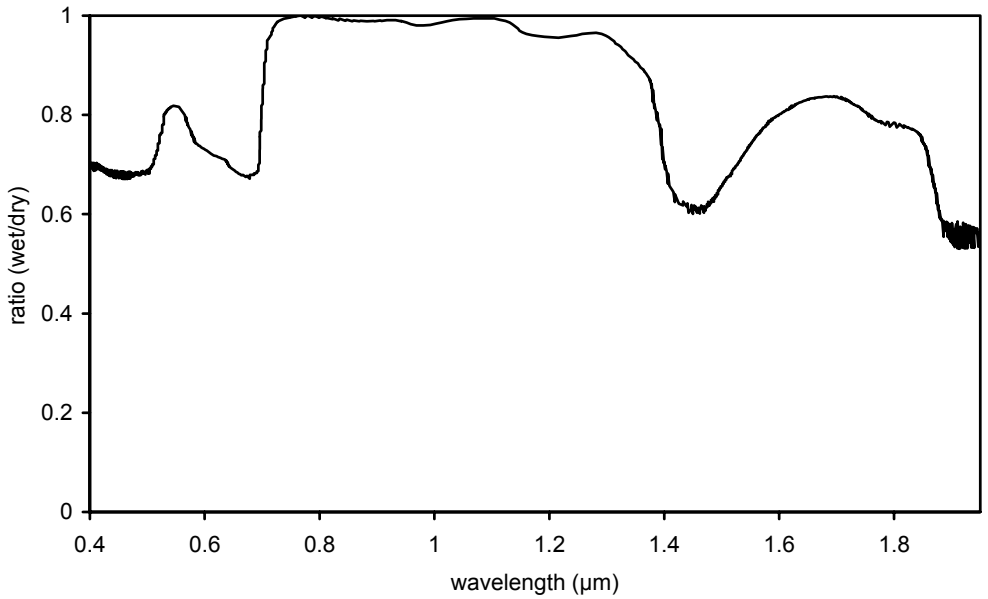

Figure 4.1: Ratio of hemispherical reflectance ratio between a fresh leaf with and without water drops on its surface.

A major challenge was to design an OWS that would also permit continuous surface wetness monitoring under field conditions without being affected by solar radiation. This can only be achieved by an active sensor with its own light source. The location of this light source in relation to the detector is a prime concern and can be illustrated by the following example. A set-up with a detector and emitter combination, aligned such that a specular component will be measured, will detect Fresnel reflectance. The reflectance would approach 100% at gazing angles. No light will penetrate the water surface and hence no light absorption would occur in the water layer. The Fresnel reflectance is usually much stronger than the diffuse reflected energy. Selection of the proper detection angles with respect to the surface and emitter positions is crucial. This presents a major difficulty since it is not possible to fix a leaf in the field without disturbing its environment. A further complication is that spherical droplets will always have specular components, regardless of the orientation. However, with proper calibration it is indeed possible to detect layers of water in a diffuse reflectance set-up. A porous medium, such as soil, does not have these limitations as long as it is not saturated, thus making the set-up less critical for specular components in the reflected light. A leaf surface can also be porous as water will be adsorbed in the cuticle. In such a case no problem occurs with specular reflectance by water, as for non-saturated soils.

4.3 Materials and Methods

The OWS is based on spectral reflectance spectroscopy. An all weather instrument that will not interfere with the wetting and drying process requires careful design considerations and the use of absorption bands in the infrared requires special optics. A key obstacle is that the emitted radiation of the OWS is a fraction of the emitted radiation of the sun, thus the sensor should be insensitive to ambient light conditions. This can be achieved with a modulated light source, taking into account that overexposure (saturation) of the light detectors to the reflected solar radiation must be avoided and that such precautions should not interfere with the measurements. The need for a small sensor is obvious as it should minimize the radiation balance interference with the surface to be measured. This requires a small sensor head, i.e. the ratio between the diameter of the sensor and the sensing distance should be low. Figure 4.2 shows the design implementation of the developed OWS. The OWS light source is collimated onto a surface and the reflected radiant energy is collected and coupled into an optical fiber. This fiber splits the light equally into two beams that pass through a band pass filter and are projected onto a light detector. The two detector signals are synchronously demodulated and then go through a low pass filter with a time constant of 1 second.

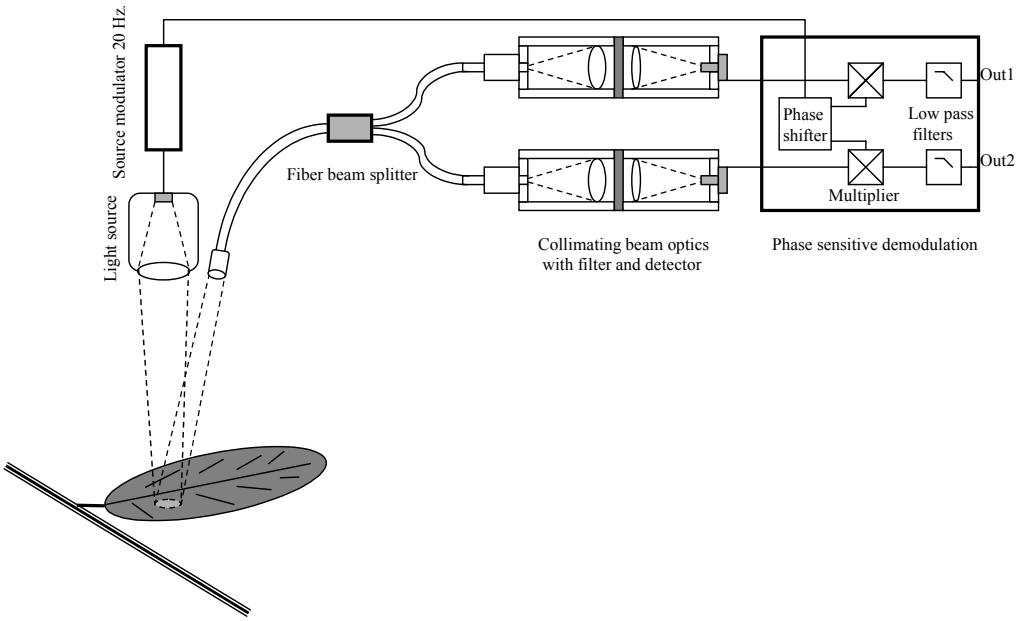

Figure 4.2: Optical Wetness Sensor schematic design (not to scale).

4.3.1 Optics

It is difficult to find a light source that emits sufficient energy in the strong water absorption bands. In addition, the reflected light should be detected with a unit that measures both light wave band reflections from the same surface under conditions where the sampling distance is not a constant. The collected optical output power is reduced by a power of 2 when doubling the distance, which limits the sampling distance. There are several solutions but all required finding a source that would emit enough radiation in the reference and water absorption wave band and optics to couple the reflected light onto a light detection system. One option is to select two narrow band sources and couple these into one fiber such that both sources illuminate the same surface and detect the reflected light with one detector. Alternatively, one broadband source can be selected, but using a double detector design with optical narrow band filters and an optical system such that the detectors are coupled to the same surface.

The light source selection criteria were based on two requirements: strong light emission around 1.9 μm and electronic modulation capability to reduce noise and discriminate reflected light from solar radiation. Mechanical light modulation would make the design too bulky. As a light source, LED's (Light Emitting Diodes) are available in these wave bands (Telcom devices, USA) but their optical power is very weak and limited to less than 200 μW over a 100 nm bandwidth. A further complication over the use of LED's is that it is difficult to couple the optical power into a fiber with a diameter of 400 μm and 25° input angle; less than 3% of the power would be coupled into these fibers. As this is too low, another option was investigated. Halogen lamps can be modulated with a mechanical chopper wheel but this results in a bulky design and produces too much heat. A solution was found using a new light source from Ion optics (USA, model: PulsIR). The source is a surface emitting film with a special rough surface (30 mm^2). This roughness treatment enhances infrared emissivity to a value close to one. The efficient radiative heat loss and low thermal mass enables the source to quickly lose its heat and thus its temperature drops rapidly after an electrical current pulse. The source can be modulated at 20 Hz with a temperature modulation of more than 350° C. The maximum temperature will be around 850° C. This results in a radiant intensity of more than 0.5 mW nm^{-1} around the 1.93 μm wave length (see Fig. 4.3). The optical power of this source was calculated using Planks formula for blackbody spectral exitance (M_λ):

$$M_\lambda = c_1 \lambda^{-5} (e^{\frac{c_2}{\lambda T}} - 1)^{-1} \qquad (4.2)$$

where c_1 is $3.74 \cdot 10^{-16}$ Wm^2, c_2 is $1.44 \cdot 10^{-2}$, λ is wavelength in meters, T is absolute temperature in K.

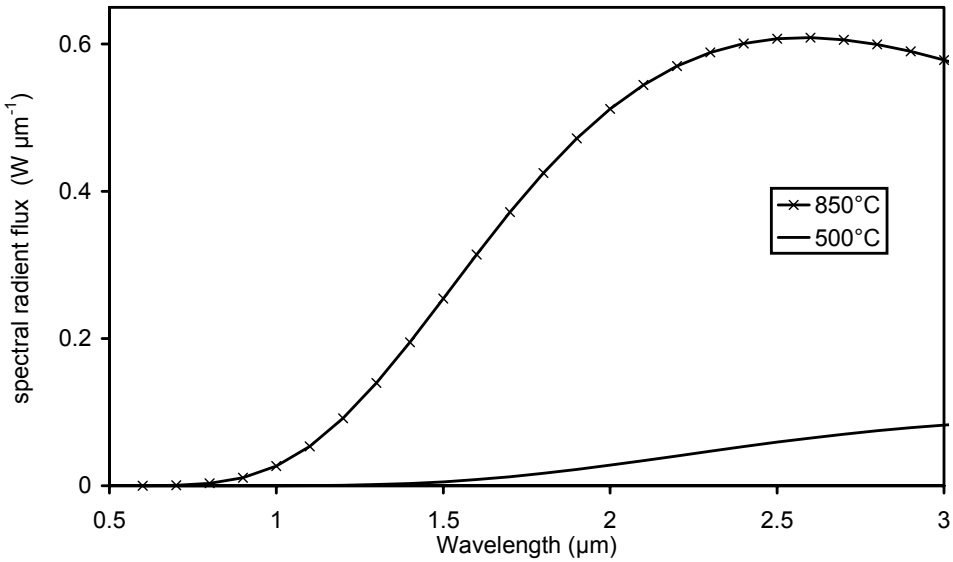

Figure 4.3: Output of the filament source used in the Optical Wetness Sensor.

It was decided to use interference filters with two detectors to detect a wave band in the water absorption band and a wave band nearest to the absorption band but insensitive to water. The optical bandpass interference filters have their peak transmission wavelength around 1.70 µm (Half-power Wave Band (HWB): 10%) for the reference and 1.94 µm (HWB: 4%) for the water absorption band. It is very important to have both detectors looking at the same surface. This was achieved with a Y-shaped optical fiber splitter (Ocean Optics, USA) composed of three separate optical fibers (400 µm each) and epoxied at the nexus of the Y-shaped assembly. In this way the detected light could be split onto the two optical benches containing the bandpass filters, light focussing lenses and detectors so that the sensor head could be kept small. A drawback of using a single 400 µm optical fiber is that the input aperture is very limited. The view angle of the optical fiber is small, which makes it difficult to equip it with a large aperture (light gathering) collimating lens. Therefore the light collected through the 2.4 mm input lens is low and this restricts its detection distance from a given surface. The result is that the probe head can readily assess an area of 21 cm^2 from a distance of 30 cm (Fig. 4.2). The optical losses on the emitter side can be kept low because the source is directly positioned at the probe head since it is small and hence without fiber coupling problems. A large aperture (30 mm) collimating lens with short focal distance is able to effectively focus the source. The reflected light is effectively coupled into a fiber splitter that equally splits the light energy onto two detectors. Coupling light from the fiber onto the detector is achieved with an imaging beam probe. The probe projects an enlarged image of the optical fiber end onto the detector.

For light-gathering potential it would have been better to have a larger aperture detector, but this was not possible due to the limited diameter of the glass fibers. The probe head size could not be made smaller because the PulsIR output is not focussed it has an almost Lambertian surface and its surface area is large (30 mm^2). This makes it difficult to collimate and project the light beam onto the surface area that the detector is sensing with a small lens. However, the OWS sensor head (4 x 6 cm with rounded edges) still manages to minimize the sky view obstruction (0.33 % at 30 cm distance) that would affect the radiation balance of the sampling surface. In addition, no matter how the distance varies, both detectors will always be looking at the same surface. This means that the ratio of the two signals will not be affected by a moving sampling surface such as leaves.

4.3.2 Electronics

A modular design was considered that could be split into the following sub-components. A pulse driver circuit modulates the light source at 20 Hz. This ensures optimal modulation depth at highest possible modulation frequency. The two output signals of the OWS are not affected by ambient light variations such as from the sun. This is achieved by a phase sensitive multiplier (lock-in amplifier) and is able to recover signals from very high noise levels (<100 dB).

The detector types suitable for the light spectral range (1.6 - 2.0 µm) are limited, hence a new type wavelength-enhanced InGaAs-diode light detector was selected (Hamamtsu, Japan). Its infrared spectral response peaks around 1.95 µm. The detectors have build-in peltier coolers and they are cooled to -5° C for more stable operation.

A measurement sequence (Fig. 4.4) where the source is on for a limited time is introduced to achieve 3 goals:

-Minimize power consumption

-Minimize sample surface heating

-Reduce noise

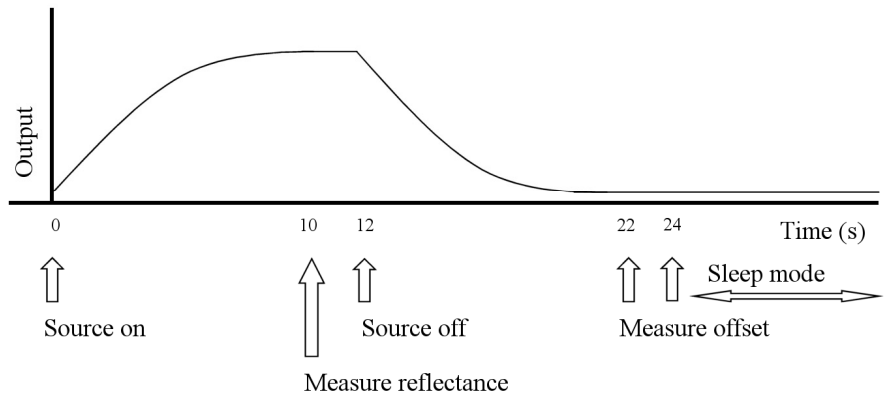

Figure 4.4: Optical Wetness Sensor measurement sequence suppresses noise and reduces power consumption.

The total power consumption of the OWS is 11 W when the source is on and only 6 W when the source is switched off. The transmitter source which emits 200 mW radiation is on only for a limited time to minimize sample heating. This is important because the source emits more than 200 mW radiation. The incident radiation could warm the surface and influence the dew formation or drying processes. The surface heating was tested on a dry leaf by leaving the light source on and measuring the temperature distribution across the leaf (in still air) using an infrared camera (Infrared Solutions, USA, Model IR-Snapshot). Although the sensitivity of the camera was high enough (noise equivalent delta temperature of 0.07 °C), it was not possible to measure a 'hot spot' on the leaf. Some heat production in the sensor head is needed to keep the sensor free from condensation.

Noise reduction is achieved by averaging and by measuring the offsets in the electronic signal during the off time of the source. Since the wetting and drying is a slow process (time scales are tens of minutes), the signals can be averaged over a few minutes. A measurement cycle consists of a period of 24 seconds (Fig. 4.4) and is controlled by a datalogger (Campbell USA, model 23X). The instrument source is switched on during the first 10 seconds. During this time the outputs with a time constant of 1 sec will become stable by the end of the 10 second period and the output of the low pass filtered lock-in amplifier can be recorded with a datalogger. Next, the light source is switched off by opening an electronic switch in series with the light source. The lock-in amplifier will remain synchronized since the synchronization signal is still there. Ten seconds later the final output will show the internal DC offsets introduced after the demodulator circuit. These offsets will be subtracted from the reflectance signal during later analysis. The offset signal will also contain additional low frequency noise in cables and in the digitization process inside the

datalogger. After one measurement cycle the instrument can enter a sleep mode. More measurements result in less noise. If sufficient power is available, the measurements can be repeated without a significant sleep mode time. Thus about 37 measurements can be taken per 15 minutes. This results in a maximum power consumption of 8.1 W and approaches 6 W using a very long measurement interval time (long sleep mode).

It was estimated that the calculated noise equivalent optical power at the detector is comparable with the detector specifications. This means that the electronics contribute little to the total noise figure.

To insure that the temperature variations outdoor would not affect the OWS measurements, the OWS was first tested in an oven. The temperature varied from 20 to 65° C while the OWS was sampling a white spectralon reference panel (Ocean Optics U.S.A.). The ratio of the output signal changed by less than 1%.

4.4 Measurements

The OWS was calibrated under lab conditions for two soil types that were totally different in colour and grain size distribution (Fig. 4.5) and on grass leaves to measure leaf water content. The OWS was tested in the field on both a biological sand crust and a desert shrub, *Anabasis articulata*.

Figure 4.5: The two soil types used in the soil calibration; left, a loamy soil and right, a fine sandy soil.

4.4.1 Soil Calibration

The sensor response was tested on a fine sandy soil and a loamy soil (bulk densities: $1.40 \cdot 10^3$ and $1.63 \cdot 10^3$ kg m^{-3}) (Fig. 4.5). The loamy soil can retain more water at high suction levels than the fine sandy soil and was selected because of easy mixing at various moisture concentrations. The soil water retention curve was determined in the soil laboratory by a hanging water column method for soil water pressures up to 0.1 m. The 10 m and 160 m values were determined by a pressure plate extractor (Dane & Hopmans, 2002) (Fig. 4.6).

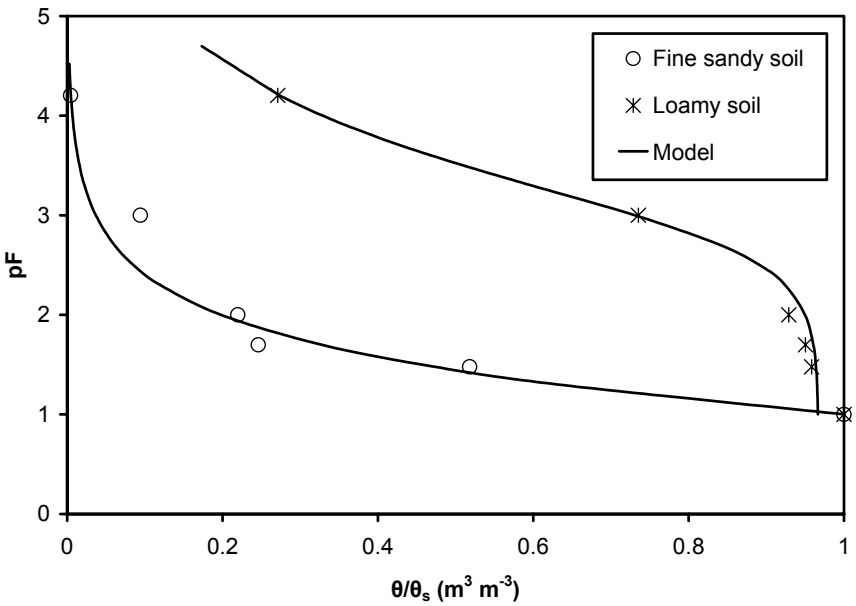

Figure 4.6: Soil water retention curve of the loamy and fine sandy soil (*h* (m), *pF=log(100h)* is the water column equivalent soil pore pressure). Model lines based on Van Genuchten model (1980) $\frac{\theta}{\theta_s} = \frac{\theta_s}{(1+\alpha(-h)^n)^{1-1/n}}$.

The OWS soil calibration procedure was as follows. Two containers were filled with soil and mixed with a fixed amount of water (near field capacity). The sample was placed on an accurate 3-decimal place balance (Mettler PM1200) with an OWS aimed into the container. The samples were left to dry and the output of the OWS and the soil sample weights were recorded each minute. During the drying of the soil, a vertical moisture gradient was present and thus the OWS would underestimate the soil moisture content since it only detects moisture in the upper mm of the topsoil. Therefore careful manual mixing of the samples with a metal spoon was necessary just before the measurement cycles started (data were then averaged into 1 minute means). The spoon was included in the weight measurement because not all soil could be removed quickly form the spoon. After mixing, the soil was compacted by

stamping it with a fixed force (about 10 N cm^{-2}). Sample points consist of 2 or 3 one minute averages that were in turn averaged. If the first and second 1 minute averages were found not to differ by more than 3%, the data were accepted. The procedure is needed to insure that the moisture gradient during calibration is minimal. If the measurements are too far apart, it suggests surface evaporation and/or condensation have occurred thus causing both the soil surface water content and the reflection ratio to change. However, the bulk soil water content as measured by the balance will remain almost unchanged. In the wet region the noise is caused by a ponding effect since it is impossible to compact the soil with the same pressure at each calibration point. The OWS reflectance measurement was calibrated using a white spectralon panel (Ocean Optics U.S.A.) and the calibration was repeated after the soil measurements. The signal drift of the OWS was less than 0.05% during the calibration, which lasted a full day.

To demonstrate the importance of soil sample homogeneity during the calibration (Graser et al., 1982), a calibration was made of the OWS similar to the measurement procedure by Weidong (2002), i.e. without sample mixing before each measurement but with a slowly drying sample (4 mm thickness). This gave a totally different calibration curve (Fig. 4.7) than the well-mixed sample measurement procedure as outlined above (result in Fig. 4.8). Figure 4.7 is the OWS signal response to a wet soil sample that was drying very slowly over a 48-hour period. Since the soil dries from above, the reflection signal soon becomes too high and does not even change below 6% soil water saturation (compare with Fig. 4.8).

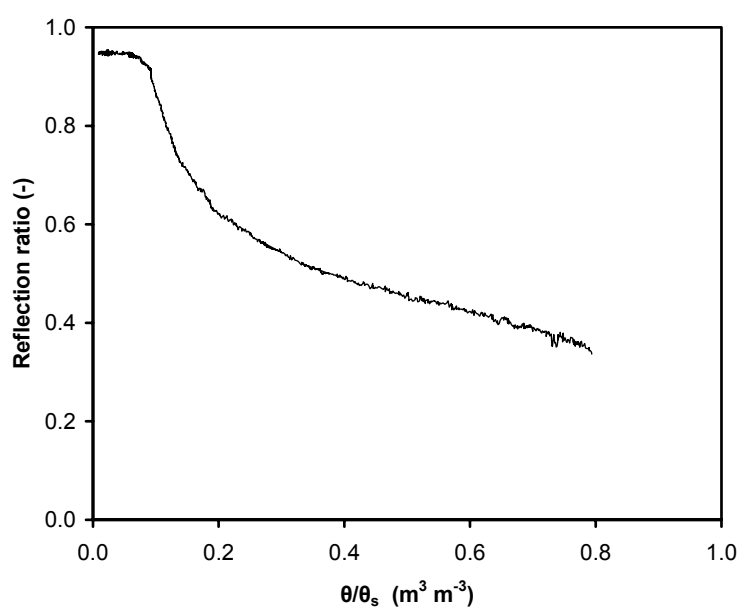

Figure 4.7: Optical Wetness Sensor response on a 4 mm fine sandy soil layer drying slowly.

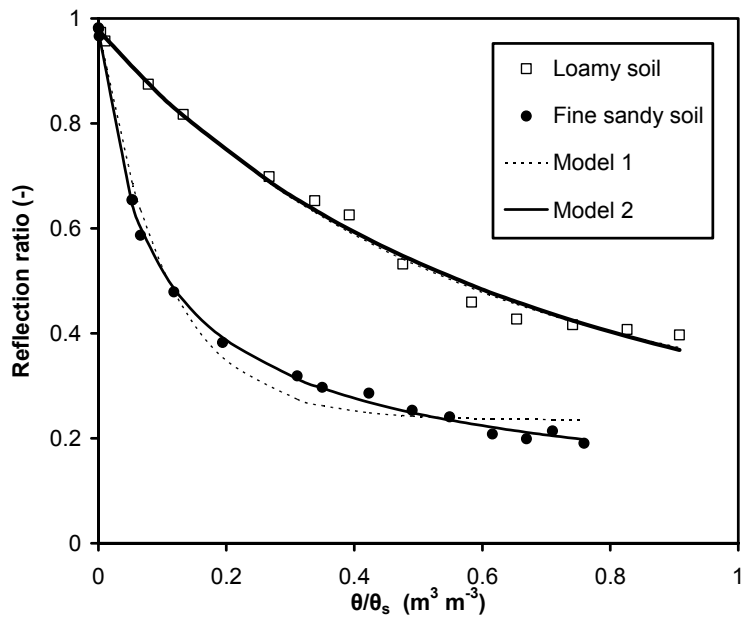

Figure 4.8: Optical Wetness Sensor response on a loamy soil and on a fine sandy soil (the soil was mixed before every measurement).

Using the correct measurement procedure (mixing), Fig. 4.8 shows that the OWS is very capable of detecting soil water content and that it is most sensitive in the drier region. The two soils responded differently. At air dry, a matrix water potential of -30 kJ kg^{-1}, the loamy soil contains much more water. The OWS seems to be less sensitive to water content change in the loamy soil, probably due to water in the much finer soil pores. Figure 4.8 demonstrates that a set of calibration curves for a specific soil is very well possible. Equation 1 was fitted through the measurements of the reflection ratio and not of the reflection at one wave band, since the ratio is insensitive to distance variations (input for Eq. 4.1: $R_\lambda = \frac{R_{1.93\mu m}}{R_{1.45\mu m}}$, $R_{\lambda,s} = \frac{R_{1.93\mu m,s}}{R_{1.45\mu m,s}}$ and $R_{\lambda,d} = \frac{R_{1.93\mu m,d}}{R_{1.45\mu m,d}}$, see model 1 in Fig. 4.8). However, for fine sandy soil, a better result could be obtained with the following model (Eq. 4.3, input $R = \frac{R_{1.93\mu m}}{R_{1.45\mu m}}$) using the same number of parameters (model 2 in Fig. 4.8)):

$$R = A(\frac{\theta}{\theta_s} - B)^{C^*} \qquad (4.3)$$

The results are shown in Fig. 4.8 and Table 4.1. It is interesting to note that the calculated $\frac{R_{1.93\mu m,s}}{R_{1.45\mu m,s}}$ does not represent the $\frac{R_{1.93\mu m,s}}{R_{1.45\mu m,s}}$ extrapolated from the

measurements, especially for the loamy soil. It is not clear why but it is to be expected that the measurements at high saturation could be contaminated by specular reflectance. However, most applications for the OWS will involve the study of soil wetness below field capacity. From Fig. 4.8 it is clear that the OWS is very sensitive to soil moisture changes over the soil moisture range from field capacity to oven dry. The fitted parameters of Eq. 4.1 suggest that only one parameter (*C*) is needed to characterize a soil. Comparing Figs. 4.6 and 4.8, it seems that *C* is a function of soil pore size distribution since pore size distribution is directly related to the soil water retention curve. Additional soil types would have to be tested to verify this.

	$\frac{R_{1.93\mu m,s}}{R_{1.45\mu m,s}}$	$\frac{R_{1.93\mu m,d}}{R_{1.45\mu m,d}}$	**C**	**r^2**	**s.e.e.**	**A**	**B**	**C***	**r^2**	**s.e.e.**
Loamy soil	0.24	0.98	1.87	0.99	0.018	1.25	-1.16	-1.69	0.99	0.021
Fine sandy soil	0.24	0.98	9.87	0.98	0.033	0.176	-0.0458	-0.558	1.0	0.011

Table 4.1: Model parameters reflection ratio estimation using Eq. 4.1 (R_s, R_d, C) and Eq. 4.3 (A, B, C*), *s.e.e.* is the standard error of estimate.

According to the calibration, the OWS can be used to measure soil surface moisture. Its greatest sensitivity and accuracy is achieved from the dry range up to half saturation, a very interesting range in evaporation and ecosystem studies. It is estimated that the total accuracy in this range will be better than 5%.

4.4.2 Grass calibration

A plastic container (12 cm diameter, 4 cm depth) was filled with fresh *Lolium perenne* grass leaves. The grass leaves were cut and their length ranged between 1 and 4 cm (width approximately 4 mm). The grass leaves were mainly horizontally aligned in the plastic container (3 cm layer) and placed on an accurate 3-decimal place scale (Mettler PM1200) in a laboratory. Initially two OWS sensors were aimed at this grass sample from a height of 0.20 m. A complication was found in that the grass dried mainly from above (as did the soil samples). This means that the OWS sees a dryer grass than what the balance measures (water content). To overcome this problem, it was decided to turn the grass at frequent intervals and omit data where this was not done. Figure 4.9 presents the data. The OWS accuracy is not the limiting factor; the scatter is mainly due to evaporation from above and the limited mixing by turning at fixed intervals. Hence the calibration accuracy will be around 10%.

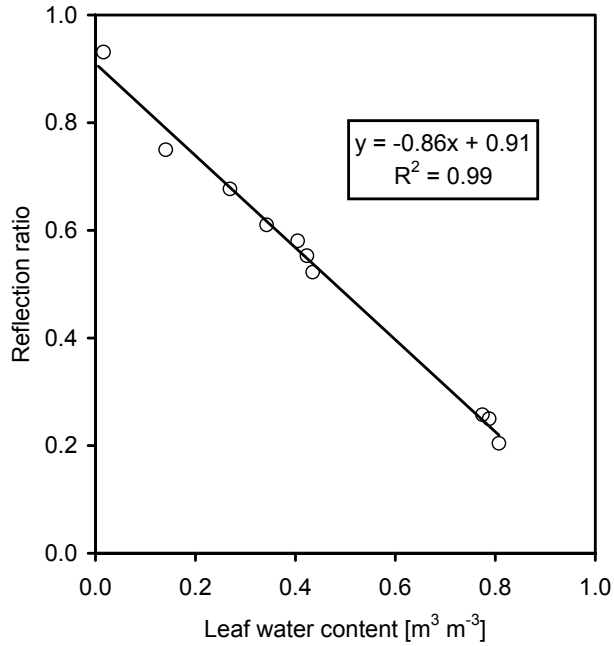

Figure 4.9: The sensitivity of the Optical Wetness Sensor to variations in leaf water content.

4.4.3 Field experiment

The sensor was tested on a biological sand crust and on plant leaves in the framework of a dew study in a desert ecosystem, NW Negev, Israel. The sensor head was aimed at the soil surface form a height of 30 cm scanning a round surface area of 21 cm^2. The leaves of the *Anabasis articulata* desert shrub are thin (3 mm) and the OWS scans a volume of leaves overlapping each other from a distance (nearest leaves were 25 cm away) (Fig. 4.10). The measurements were carried out within a linear sand dune system near the end of the hot and rainless summer period. The purpose of the Negev dew experiment was to assess the occurrence and duration of free surface water on plant leaves and soils covered with a biological crust (Jacobs et al., 1999, 2000a, 2000b; Heusinkveld et al., 2006). A recording microlysimeter was used to measure the dew input and evaporation (cup diameter 154 mm, depth 35 mm) (Heusinkveld et al., 2006). These measurements were combined with gravimetric soil water content measurements and *in situ* meteorological data collection. Gravimetric techniques were used to determine soil water content in the dune slope crusts. Surface crust samples were scraped off using a stainless steel spatula and placed into small containers. The samples were weighed, dried in an oven (105 deg. C, for 24 hours), and the weight difference provided the soil water volume. Repetitive measurements on the same sample cannot be made, thus for each sampling interval three different sampling points were chosen separated by several cm. This was carried out for 2 dew nights at fixed time intervals with 3 close locations sampled at each time interval.

This approach is very time consuming, but provides a very direct and accurate independent measure of soil water content.

Figure 4.10: Optical Wetness Sensor installed above an *Anabasis articulata* plant.

The OWS aimed at an *Anabasis articulata* desert shrub indicated a moisture response (Fig. 4.10) despite no visible dew detection on the plant leaves. The strong response of the OWS can be seen in Fig. 4.11c. It appears that the dew diffuses inside the leaf or remains in the thick cuticle. However, there could also be a water recharge by the root system or a combined effect.

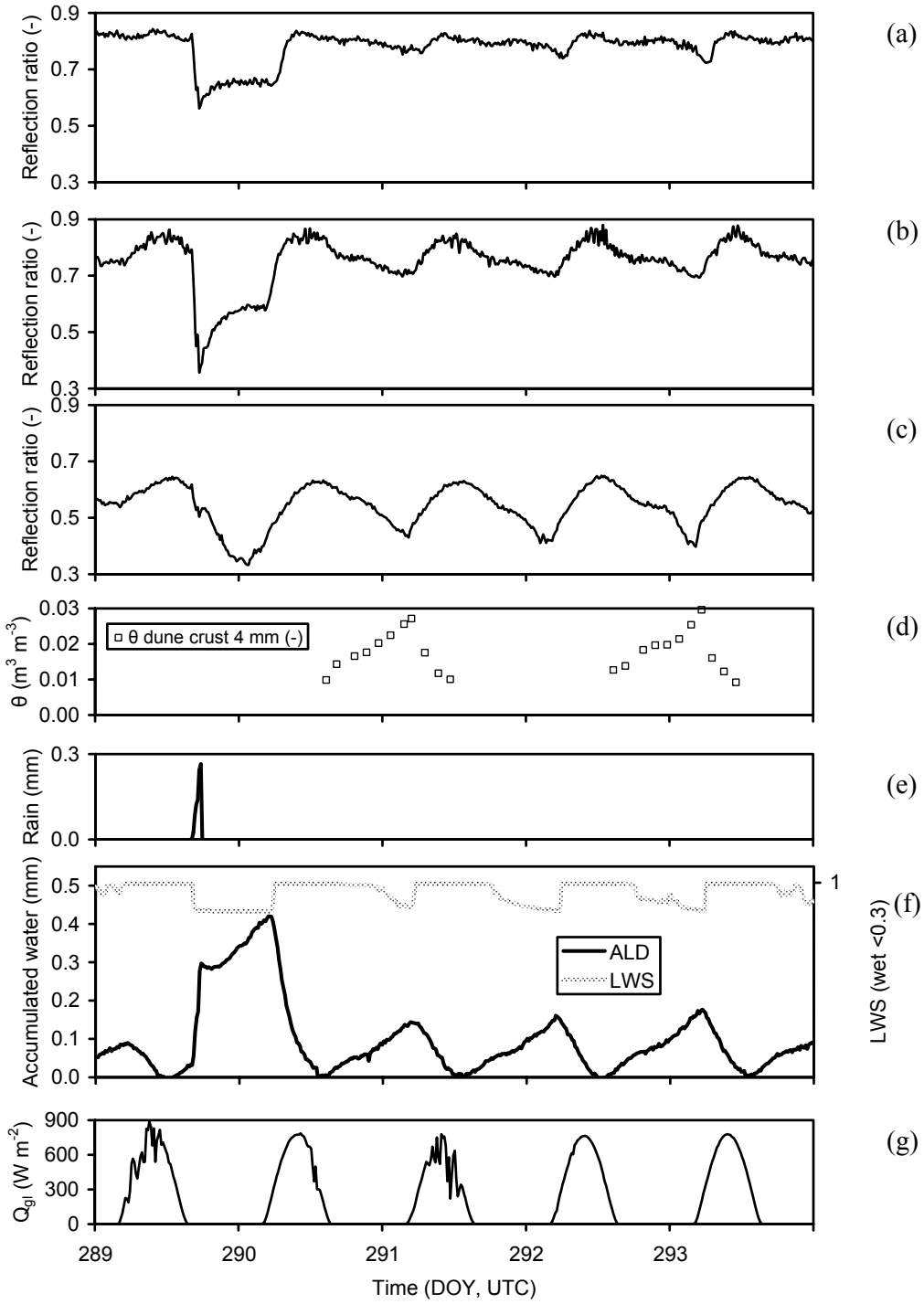

Figure 4.11: Measurements on a sand dune slope with a crust (15-19 Oct. 2000). Optical Wetness Sensor response on a 4 mm crust (a), 2 mm crust (b) and *Anabasis articulata* plant (c). Manual gravimetric soil moisture measurements of the dune crust (4 mm) (d), rain event (e), artificial Leaf Wetness Sensing grid (LWS) and a recording weighing lysimeter (ALD) (f), solar global radiation (g).

The amount of dew water on sand dune slopes with a biological crust can be seen in Fig. 4.11f, as measured by the microlysimeters. The dew water diffuses into the soil and increases the water content of the crust (Fig. 4.11d). By comparing the gravimetric soil moisture data with the microlysimeter data, it appears that around half the dew amount remains in the upper crust of the 4 mm samples. To indicate day length, global radiation data is provided in Fig. 4.11g. A standard leaf wetness sensing grid coated with a latex paint was mounted near the soil surface and can also respond to high humidity (Fig. 4.11f). However, wetness periods can still be estimated by using a wet/dry value; below 0.3 we considered the grid to be wet.

It is interesting to see the response of the OWS sensor to a light rain on both the biological sand crusts and the plant (Fig. 4.11a, b, c, e). The OWS on a thin crust of 2 mm (Fig. 4.11b) responded much stronger than the OWS on the thick crust (4 mm) (Fig. 4.11a). This can be explained from the fact that a similar amount of water is redistributed by diffusion over a larger soil volume and thus the soil moisture content of a thick crust is less than that of a thin crust. This is an interesting finding because it might indicate that initial growth and development of newly formed biological crusts can profit more from the available dew. Only a small percentage of the dew water diffuses into the soil below the crust since the diffusion coefficient for a coarse sandy soil is much lower than for a biological crust.

From the reflection data the soil crust moisture content could be calculated by using the gravimetric soil moisture measurements of the crust as a reference. Such an analysis was left out because the integrated sampling depth of the OWS is far less than 4 mm. With an operational wavelength of around 2 um, its light penetration depth will mainly depend on soil surface grain size distribution and type and to some extent on soil moisture concentration. A laboratory calibration with an undisturbed crust with homogeneous soil moisture profiles would be needed.

4.5 Concluding remarks

The OWS is the first all weather field sensor capable of studying surface wetness both day and night. Care in the optical alignment must be taken to avoid specular reflection from water layers ponding on a soil surface or leaf, as this might cause false readings. The OWS is not sensitive to OH bonds in the chemical composition of a surface but responds strongly to water in soil pores. This enables the detection of soil water content in the upper mm of the soil. The soil calibrations show that the OWS is very sensitive to changes in soil water content over the soil moisture range between oven dry and field capacity. The OWS can also be applied towards measuring leaf water content directly, especially when not confounded by dew, fog or rain deposition**.** This is possible under field conditions, since the optics were designed such that the scanning distance is allowed to fluctuate without affecting the reflection ratio. For enhanced accuracy of quantitative measurements, it is preferable to do a

calibration. Our tests show that this could be achieved for the soils and plants selected for study here. For plant leaves it must be noted that the OWS responds to both internal and external water and the difference cannot always be distinguished. Further work is planned to find possible universal calibration curves as a function of soil composition.

Acknowledgements

This research was funded in part by the Dutch Technology Foundation (STW). We thank the Micro-spectroscopy center of the Wageningen University for facilitating the spectroscopy measurements in Fig. 4.1. We thank Dr. Jos van Dam for the soil analyses carried out at the Wageningen University soil physics laboratory. The Hebrew University Arid Ecosystems Research Centre of the Hebrew University of Jerusalem supported the field experiment carried out in Israel. Co-author SMB is grateful to the M. Sim Foundation for support during the preparation of the manuscript.

References

Agam, N., Berliner P.R., 2006. Dew formation and water vapor adsorption in semi-arid environments- A review. J. Arid Environ. 65, 572-590.

Ayalew, A., Ward, S.M., 2000. Development of a prototype infrared reflectance moisture meter for milled peat. Computers Electron. Agric. 28, 1-14.

Baier, W., 1966. Studies on dew formation under semiarid conditions. Agric. Meteorol. 3, 103-112.

Barradas, V.L., Glez-Medellin, M.G., 1999. Dew and its effect on two heliophile understorey species of a tropical dry deciduous forest in Mexico. Int. J. Biometeorol. 43, 1-7.

Bass, B., Savdie, I., Gillespie, T.J., 1991. Simulation of leaf wetness duration for field corn. Agric. For. Meteorol. 57, 69-84.

Ben-Dor, E., Irons, J.R., Epema, G.,1996. Remote sensing for the earth sciences. Manual of Remote Sensing, vol. 3. In: A.N. Rencz (ed.), Soil Reflectance. Wiley, New York, pp. 111-189.

Berkowicz, S.M., Heusinkveld, B.G., Jacobs, A.F.G., 2001. Dew in an arid ecosystem: Ecological aspects and problems in dew measurement. Proceedings, 2nd International Conference on Fog and Fog Collection, 15-20 July 2001, St. John's, Newfoundland, Canada, pp. 301-304.

Beysens, D., 1995. The formation of dew. Atmos. Res. 39, 215-237.

Bowers, S.A., Hanks, R.D., 1965. Reflection of radiant energy from soils. Soil Science 100, 130-138.

Broza, M., 1979. Dew, fog and hygroscopic food as a source of water for desert arthropods. J. Arid Environ. 2, 43-49.

Bruckler, L., Witono, H., Stengel, P., 1988. Near surface soil moisture estimation from microwave measurements. Remote Sens. Environ. 26, 101-121.

Burrage, S.W., 1972. Dew on wheat. Agric. Meteorol. 10, 3-12.

Cessato, P., Flasse, S., Tarantola, S., Jacquemoud, S., Gregoire, J.M., 2001. Detecting vegetation leaf water content using reflectance in the optical domain. Remote Sens. Environ. 77, 22-33.

Chang, C.W., Laird, D.A., Mausbach, M.J., Hurburgh, C.R., 2001. Near-infrared reflectance spectroscopy-principal components regression analyses of soil properties. Soil Sci. Soc. Am. J. 65, 480-490.

Dane, J.H., Hopmans, J.W., 2002. Hanging water column, pressure plate extractor. In: Dane, J.H. & Topp, G.C. (eds.), Methods of Soil Analysis, Part 4-Physical Methods. Wisconsin, USA: Soil Sci. Soc. America, Inc. Madison, pp. 680-698.

Danin, A., Bar-Or, Y., Dor, I., Yisraeli, T., 1989. The role of cyanobacteria in stabilisation of sand dunes in southern Israel. Ecol. Mediter. XV, 55-64.

Doornik A.W., Bergman, B.H.H., 1974. Infection of tulip bulbs by botrytis-Tulipae originating from spores or contaminated soil. J. Horticult. Sci. Biotech. 49, 203-207.

Duvdevani, S., 1947. An optical method of dew estimation. Quart. J. Royal Met. Soc. 73, 282-296.

Eshel, G., Levy, G.L., Singer, M.J., 2004. Spectral reflectance properties of crusted soils under solar illumination. Soil Sci. Soc. Amer. J. 68, 1982-1991.

Evenari, M., Shanan, L., Tadmor, N., 1982. The Negev: Challenge of a Desert. Harvard University Press, Cambridge, Mass., 2nd. Edn., 437 pp.

Gillespie, T.J., Kidd, G.E., 1978. Sensing duration of leaf moisture retention using electrical impedance grids. Can. J. Plant Sci. 58, 179-187.

Graser, E.A., Van Bavel, C.H.M., 1982. The effect of soil moisture upon soil albedo. Agric. Meteorol. 27, 17-26.

Hatefield, J., Thomases I., 1982. (eds.). Biometeorology in Integrated Pest Management. Academic Press, New York. 491 pp.

Heusinkveld, B.G., Berkowicz, S.M., Jacobs, A.F.G., Holtslag, A.A.M., Hillen, W.C.A.M., 2006. An automated microlysimeter to study dew formation and evaporation in arid and semi-arid regions. J. Hydrometeorol. 7, 825-832.

Holtslag, A.A.M., DeBruin, H.A.R., 1988. Applied modeling of the nighttime surface-energy balance over land. J. of Appl. Meteorol. 27, 689-704.

Huber, L., Gillespie, T.J., 1992. Modelling leaf wetness in relation to plant disease epidemiology. Annual Rev. Phytopathology 30, 553–77.

Jacobs, A.F.G., Van Pul, W.A.J., Van Dijken, A., 1990. Similarity dew profiles within a corn canopy. J. Applied Meteorol. 29, 1300-1306.

Jacobs, A.F.G., Heusinkveld, B.G., Berkowicz, S.M. 1999. Dew deposition and drying in a desert system: a simple simulation model. J. Arid Environ. 42, 211-222.

Jacobs, A.F.G., Heusinkveld, B.G., Berkowicz, S.M., 2000a. Dew measurements along a longitudinal sand dune transect, Negev Desert, Israel. Intl. J. Biometeorol. 43, 184-190.

Jacobs, A.F.G., Heusinkveld, B.G., Berkowicz, S.M., 2000b. Force-restore technique for ground surface temperature and moisture content in a dry desert system. Water Resour. Res. 36, 1261-1268.

Khare, P., Singh, S.P., Kumari, K.M., Kumar, A., Srivastava, S.S., 2000. Characterization of organic acids in dew collected on surrogate surfaces. J. Atmos. Chem. 37, 231-244.

Kiondo, J., Saigura, M., Sato, T., 1990. A parametrerisation of evaporation from bare soil surfaces. J. Appl. Meteorol. 29, 385-389.

Lange, O.L., Kidron, G, Büdel, B., Meyer, A., Kilian, E., Abeliovich, A., 1992. Taxonomic composition and photosynthetic characteristics of the 'biological crusts' covering sand dunes in the western Negev desert. Functional Ecology 6, 519-527.

Lin, B., Minnis, P., 2000. Temporal variations of land surface microwave emissivities over the atmospheric radiation measurement program southern Great Plains site. J. Appl. Meteor. 39, 1103-1116.

Lobell, D.B., Asner, G.P., 2002. Moisture effects on soil reflectance. Soil Sci. Soc. Am. J. 66, 720-727.

Lou, W., Goudriaan, J., 2000. Dew formation on rice under varying durations of nocturnal radiative loss. Agric. For. Meteorol. 104, 303–313.

Madiera, A.C., Gillespie, T.J., Duke, C.L., 2001. Effect of wetness on turfgrass canopy reflectance. Agric. For. Meteorol. 107, 117-130.

Moffett, M.W., 1985. An Indian ant's novel method for obtaining water. National Geographic Res. 1, 146-149.

Monteith, J.L., 1981. Evaporation and surface temperature. Quart. J. Roy. Meteor. Soc. 107, 1-27.

Mouazen, A.M., 2004. Towards development of on-line soil moisture content sensor using a fibre-type NIR spectrophotometer. Soil Tillage Res. 80, 171-183.

Munne-Bosch, S., Nogues, S., Alegre, L., 1999. Diurnal variations of photosynthesis and dew absorption by leaves in two evergreen shrubs growing in Mediterranean field conditions. New Phytologist 144, 109-119.

Munne-Bosch, S., Alegre, L., 1999. Role of dew on the recovery of water-stressed Melissa officinalis L-plants. J. Plant Physiol. 154, 759-766.

Norman, J. M., 1982. Simulation of microclimates. In: J. Hatefield & I. Thomases (eds.), Biometeorology in Integrated Pest Management. Academic Press, New York, pp. 65-99.

Otten, A., Herminghaus, S. 2004. How plants keep dry: A physicist's point of view. Langmuir 20, 2405-2408.

Pierson, W.R., Brachaczek, W.W., Gorse, R.A., Japar, S.M., Norbeck J.M., 1986. On the acidity of dew. J. Geophys. Res. Atmos. 91D3, 4083-4096.

Pinter, P.J. Jr., 1986. Effect of dew on canopy reflectance and temperature. Remote Sens. Environ. 19, 187-205.

Richards, K., 2004. Observation and simulation of dew in rural and urban environments. Prog. Phys. Geog. 28, 76–94.

Royle, D.J., Butler, D.R., 1986. Epidemiological significance of liquid water in crop canopies and its role in disease forecasting. In: P.G. Ayres & Boddy, L. (eds.), Water, Fungi and Plants. Cambridge Univ. Press, Cambridge, pp. 139-156.

Shoemaker, P.B., Lorbeer, J.W., 1977. Role of dew and temperature in epidemiology of botrytis leaf-blight of onion. Phytopathology 67, 1267-1272.

Steinberger, Y., Loboda, I., Garner, W., 1989. The influence of autumn dewfall on spatial and temporal distribution of nematodes in the desert ecosystem. J. Arid Environ. 16, 177-183.

Takenaka, N., Soda, H., Sato, K., Terada, H., Suzue, T., Bandow, H., Maeda, Y., 2003. Difference in amounts and composition of dew from different types of dew collectors. Water Air Soil Pollut. 147, 51-60.

Van Genuchten, M.Th., 1980. A closed form equation for predicting the hydraulic conductivity of unsaturated soils. Soil Sci. Soc. Am. J. 44, 892–898.

Wallin, J.R., 1963. Dew, its significance and measurement in phytopathology. Phytopathology 53, 1210-1216.

Wallin, J.R., 1967. Agrometeorological aspects of dew. Agric. Meteorol. 4, 85-102.

Weidong, L., Baret, F., Xingfaa, G., Qingxi, T., Lanfenb, A., Bing, Z., 2002. Relating soil surface moisture to reflectance. Remote Sens. Environ. 81, 238-246.

Weiss, A., Norman, J. M., 1987. Comparison of field measurements and numerical simulations of leaf wetness durations in a bean canopy. 18th AMS Conf. on Agricultural and Forest Meteorology, 13-18 Sept. 1987. Amer. Meteorol. Soc., Boston, Mass. pp. 52-53.

Wiggs, G.F.S., Baird, A.J., Atherton, R.J., 2004. The dynamic effects of moisture on the entrainment and transport of sand by wind. Geomorphology 59, 13-30.

Williams, D.W., Powell, A.J. Jr., Dougherty, C.T., Vincellie, P., 1998. Separation and quantification of the sources of dew on creeping bentgrass. Crop Sci. 38, 1613-1617.

Wittich, K.P., 2002. Waldbrandgefahren-Vorhersage des Deutsche Wetterdienstes. AFZ/Der Wald 53, 321-324.

Wood, D., MacNairn, H., Brown, R.J., Dixon, R., 2002. The effect of dew on the use of RADARSAT-1 for crop monitoring: Choosing between ascending and descending orbits. Remote Sens. Environ. 80, 241-247.

Yair, A., 1990. Runoff generation in a sandy area – The Nizzana sands, western Negev, Israel. Earth Surf. Processes Landforms 15, 597-609.

Zangvil, A., 1996. Six years of dew observations in the Negev desert, Israel. J. Arid Environ. 32, 361-371.

5 Dewfall and soil water flow in a sand dune ecosystem possessing biological soil crusts

Manuscript intended for publication

B.G. Heusinkveld[a], S.M. Berkowicz[b] , A.F.G. Jacobs[a], P. Felix-Henningsen[c], A.A.M. Holtslag[a]

[a] *Meteorology and Air Quality Group, Wageningen University, Droevendaalsesteeg 4, Atlasgebouw, P.O. Box 47, 6700 AA Wageningen, The Netherlands*

[b] *Arid Ecosystems Research Centre, Hebrew University of Jerusalem, Institute of Earth Sciences, Edmond Safra Givat Ram Campus, Jerusalem, Israel 91904*

[c] *Institut für Bodenkunde und Bodenerhaltung, Justus Liebig Universität Giessen Heinrich-Buff-Ring 26, D-35392 Giessen, Germany*

Abstract

The contribution of dew to the water balance of a desert soil is intriguing since, apart from fog, it is the only source of water for organisms during the hot rainless period. We define dew as a vapour flux towards the surface, where it can be adsorbed by the porous soil. Since a large part of the adsorbed water is strongly bound to the soil, there is a need to quantify the amount of dew available for biological activity, defined here as Free Available Dew (FAD). This study also focuses on dew water movement in the soil since this will also affect the FAD and total dew. The study area is in a linear sand dune belt situated near Nizzana, NW Negev, Israel. Extensive soil moisture and micrometeorological data were collected during a six-week field experiment at the end of the dry season in 2000. The soil measurements included standard gravimetric soil moisture measurements and sensors that measured soil pore humidity directly. Automated microlysimeters monitored dew on the soil surface. Measurements revealed that a soil covered with a biological sand crust 'collects' most of the dew water in the top soil layer during the night, and that daily amounts of dew are more than double the potential dew even though the FAD is less. These amounts can be estimated from standard weather station data, using a modified version of the standard Penman equation and an additional measurement of the soil pore relative humidity near the surface. A physical multi-layer soil model was constructed to simulate movement of dew water in the soil, especially moisture in the top soil layers. Our soil moisture measurements and model results reveal that daily dew water can penetrate into the the first cm of the soil. The difference in hydraulic properties of the crust and the underlying soil concentrates moisture in the crust. The upper half of the crust experiences a prolonged wetness period of 20% of the time where FAD for cyanobacteria might be available.

Keywords: desert; sand dunes; dew; evaporation; biological soil crust

5.1 Introduction

In the Negev desert, Israel, dew and fog are the only sources of atmospheric water during the hot dry season (April to October). Dew amounts are usually very small, but not negligible. This study focuses on dew in the NW Negev desert in a linear sand dune system near Nizzana. The study area consists of stable linear dunes with slopes covered by a layer of biological soil crusts only a few mm thick. The upper first mm, where light can penetrate, contains a dense growth of organisms such as cyanobacteria and algae. These organisms not only influence the behavior of water in the soil, but also contribute substantially to nitrogen and carbon fixation (Lange *et al*., 1992). Furthermore, crusts protect the dunes from wind erosion, affect the germination and establishment of phanergams (seed plants), influence the nitrogen balance, and serve as a sink for carbon since they contain chlorophyl (Danin *et al*., 1989; Verrecchia *et al*., 1993). The crust can be defined as a miniature boundary (Belnap, 2003) and highlights the importance of the frequently neglected finer-scale boundaries that influence ecosystem fluxes and processes. Crusts serve as an interface between the atmosphere and soil surface, areas of dramatically different physical environments.

Jacobs *et al.* (1999) and Heusinkveld *et al*. (2006) showed that the average daily water input caused by dew in the Nizzana region is around 0.1 to 0.4 mm. They used manual and recording microlysimeters to measure the daily variation of soil water content in the upper few cm of the soil layer. These amounts can be significant for the activity of biological crusts during the dry season (Lange, 1992). However, the microlysimeters do not provide information, nor data, of how deep moisture diffuses into the soil nor provide data on the availability of this dew water for biological activity. Such data are important for desert ecosystem functioning. For example, dew will be more effective if it remains concentrated in a relative small layer of the topsoil. The impact of dew water on biological crusts activity will depend, in part, on the dew water movements into the soil. Part of the dew water will be bound to the capillary forces within the soil pores, also referred to as the matrix potential (J kg^{-1} or kPa). Dew formation, with no visible water on the surface, has been referred to as vapour adsorption (Kosmas et al., 1998, 2001; Agam and Berliner, 2004, Verhoef et al., 2006), although strictly speaking the result of vapour adsorption is still liquid water.

As a large part of this liquid water is locked inside the soil pores, the force to release this water will be too great for biological activity. Therefore it is important to further define what this soil dew is. From a meteorological viewpoint, dew can be defined as a water vapour flux in the atmosphere towards the soil. Note that lysimeters will also detect a water flux from the atmosphere to the soil surface. Dewfall occurs when the temperature of the condensation surface drops below the

dewpoint temperature of the free atmosphere. However, if we define dewfall as a vapour flux to the surface, then there are conditions whereby dewfall can take place when the surface temperature is higher than the dewpoint temperature of the air at a reference height. This effect can occur when a surface is a porous medium; the capillary size and its size distribution will reduce the vapour pressure within the soil pores. Therefore the hydraulic properties of a soil greatly influence the amount of dew and its distribution within the soil. The reduction in vapour pressure is a function of the radius of the concave meniscus water in the capillaries, and was first described by the Kelvin relation e.g. Hillel, 1980:

$$\ln \frac{e_0}{e} = \frac{2\sigma}{\rho r R_v T} \tag{5.1}$$

where e_0 (Pa) is the vapour pressure of a flat water surface, e (Pa) is the actual vapour pressure of a curved water surface, ρ (kg m^{-3}) is the density of water, r (m) is the radius of the water curvature, R_v (462 J kg^{-1} K^{-1}) is the specific gas constant for water vapour, T is the absolute temperature (K), and σ (J m^{-2}) is the surface tension of water. When soil dries out, the remaining soil water in the small capillaries has a very concave meniscus. These concave water surfaces cause a further reduction in vapour pressure, which can be described in terms of soil water potential (Philip, 1957):

$$h = e^{(\frac{\Psi g}{R_v T})} \tag{5.2}$$

where h (-) is the relative humidity of the soil pores, ψ (J kg^{-1}) is the soil water potential representing the matrix forces by which water is retained in the soil, and g is the acceleration due to gravity (m s^{-2}).

In desert ecosystems studies, it is therefore preferable to define soil dew as a combination of Free Available Dew (FAD) and Adsorbed Water (AW). The FAD is the amount of water available (including dew droplets) with the limit of the FAD as a percentage of soil dew determined by the biological activity under investigation. These values, for example, differ among plant species or cyanobacteria. In general, a soil water matrix potential of -1.6 kJ kg^{-1} (-1.6 MPa or pF 4.2) is the limit for vascular plants to extract water from a soil, also called the wilting point. This is equivalent to a relative humidity of the soil pores close to 100%. However, cyanobacteria as found in biological crusts have a very high resistance to water stress. Palmer and Friedmann (1990) measured photosynthetic activity of cyanobacteria at a matrix water potential larger than -6.9 kJ kg^{-1} at 20° C. This means that cyanobacteria are capable of extracting moisture from an atmosphere or soil capillary with a relative humidity of >

95% (at 20 °C). They also reported even larger soil water potential tolerances for cryptoedolithic lichens that begin to photosynthesize at a matric water potential > -46.4 MPa, which is equivalent to a relative humidity of >71% at 20°C . Therefore one can conclude that for cyanobacteria the FAD will be larger than for vascular plants. Such information is useful in assessing crust optimum survival conditions.

Another intriguing question is to what extent dew can penetrate into the soil. The factors controlling water movements are the microclimate at the soil-atmosphere interface and several soil factors. These factors include the soil matrix potential as a function of water content, also called the soil moisture retention curve (SMRC) or pF curve, and the general soil physical properties. The differences among SMRC's are attributed primarily to the differences in pore size distribution of soils. A soil with a biological crust will have a cover consisting of cyanobacteria, sand grains and aeolian dust particles. Thus it can be expected that the soil pore size distribution within the crust will show a higher amount of capillaries less than 10 µm, and therefore a higher field capacity than the sand below the crust. This modifies the soil moisture retention curve such that the soil with a biological crust layer will hold more water under higher temperatures. However, there is a negative aspect for biological activity in that this dew water will only be available at a higher volumetric soil moisture concentration. These crusts range from 1 to 4 mm in thickness, thus their water-holding capacity can be substantial. Pore size distribution measurements of the Nizzana study area were previously made with a mercury pore size meter (Verrecchia *et al*., 1995). Cyanobacteria influence the pore size because they tend to reduce the larger capillaries by means of swelling as they absorb water. Since the soil moisture content in a desert soil is so low (during the dry season), moisture transport in the soil mainly takes place in the unsaturated zone. The evaporation and condensation process at the soil-atmosphere boundary takes place through the soil pores.

5.2 Experimental site and set-up

The experiment was carried out in the Hebrew University Arid Ecosystems Research Centre sand dune field station, which is situated within a linear dune system near Nizzana, Israel (30° 56'N, 34° 23'E, elevation 190 m a.s.l.). The annual average rainfall is about 100 mm, occurring mainly between November and March, with a coefficient of variation of about 40%. The linear sand dunes in the study site trend several km west to east, partly a reflection of the winds >5 m s^{-1} blowing from the SW, W and NW directions (Sharon *et al.,* 1997). The interdune spaces are about 50-125 m apart and the dunes themselves are about 10-25 m high.

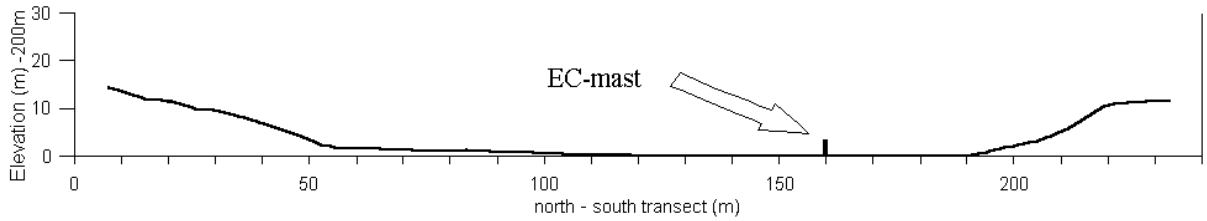

Figure 5.1 North-south transect between two linear dunes in the Nizzana experimental site. Biological sand crusts appear on both slopes from about 10-55 m and 190-220 m. Meteorological data were collected near the Eddy Covariance (EC) mast.

Within this landscape, three different zones can be identified (Fig. 5.1).

1. Mobile dune crests largely unvegetated (0-10 and 220-230 m).
2. Interdune area, generally flat with some hummocks, experiencing fluvial deposition from slope runoff, and which may contain a playa (55-190 m).
3. Stable dune slopes, partly vegetated (north-facing more vegetated than south-facing). The north-facing slopes are covered by a biological crust up to 4 mm thick (Fig. 5.2), while the south-facing slope crusts tend to be less than 2 mm thick (10-55 and 190-220 m).

Figure 5.2: A 3 mm thick biological crust covering the sand. The photo capsule (50 mm length) provides a scale. The crust is malleable when moistened by dew. A spatula is used to remove the crust.

The main meteorological data were collected in zone 2, adjacent to a north-facing dune slope:

- Radiation budget, shortwave and longwave, type CM5 and CG1, both incoming and outgoing (Kipp and Zonen, the Netherlands). The longwave radiation sensors were equipped with window heating to avoid dew formation.
- Sensible and latent heat fluxes from a 3 m tower using an ultrasonic anemometer and thermometer CSAT3 (Campbell Scientific, USA) and open path infrared gas analyser Li7500 (Licor, USA). The mast is depicted in Fig. 5.1.
- Wind, temperature and moisture profile (microcup anemometers and shielded psychrometers, produced in the Wageningen University meteorology workshop).

The ventilated psychrometers were adapted for dry desert conditions and equipped with a pumping system to wet the wet bulb wick; excess water was pumped away from the end of the wick by means of an air pump. The psychrometers were tested against a respirated reference Assmann psychrometer inside a well-mixed climate chamber and the system proved reliable. A test of the importance of the excess water pump showed that when switched off, errors in wet bulb depression of up to 0.6 K at a wet bulb depression of 8 K. When the pump was operating, no detectable differences could be found between Assman and MAQ psychrometers (<0.05 K).

Gravimetric techniques were used to determine soil water content in the playa and dune slope. The soil water distribution in a vertical profile was determined using soil sampling cups (30 mm diameter and 50 mm depth). Fresh shallow soil profiles were cut and the cups were then driven perpendicular into the exposed profile. Surface crust samples were scraped off using a stainless steel spatula and placed into similar cups. In both cases, the samples were weighted, dried in an oven (105° C, for 24 hours), and the weight difference data provided soil water volume. The gravimetric method is simple but time-consuming and destructive. Repetitive measurements on the same sample cannot be made, therefore for each sampling time a different sampling location was chosen several cm away. This was carried out for 4 dew nights at fixed time and soil depth intervals. By measuring three new profiles at each sampling time, the quality of the data could be improved. The method is very time consuming, but provides a very direct and accurate measure of soil water content.

Manual and recording microlysimeters were used to measure the dew input and evaporation, integrated over a certain depth. Microlysimeters of various depths were first tested to determine the optimal depth and 3.5 cm was found sufficient (Jacobs et al., 1999). Specially designed recording microlysimeters were used, based on a Load Cell, with a cup diameter of 154 mm and a depth of 35 mm. A strain gauge balance measures the weight change of the Load Cell. The strain gauge was temperature compensated. The design was further optimised by burying the strain

gauge and its housing at a depth of 250 mm in the soil. Here the temperature variations were considerably damped (less than 5 K) even during the heat of a summer day (Heusinkveld *et al*., 2006).

Figure 5.3: Placement of a relative humidity probe underneath the crust

The soil moisture affects the relative humidity of the soil pores (Eq. 5.2). As the soils are very dry, it is thus difficult to measure soil water potential. Plotting the relative humidity against the soil matrix potential shows that the greatest sensitivity occurs in a dry region. Thus a new approach was chosen, whereby the soil pore relative humidity is measured directly. In this way the osmotic potential is also included in the measurement. A standard atmospheric capacitive relative humidity sensor (Vaisala HMP45, Finland) was buried below the biological crust (Fig. 5.3), accuracy 2% at relative humidity 0-90% and 3% above 90%. This sensor has a diameter of 1.5 cm and the sensor head is equipped with a membrane filter. Although the filter makes the sensor element waterproof and protects it from contamination, the electronics housing might not withstand wetting during rainy periods.

The surface wetness was monitored by a new type optical wetness sensor (Heusinkveld et al., 2008). The optical method enables remote soil surface wetness measurements and is most sensitive in dry (pF < 5) to moist range.

Home-made soil thermometers (Pt100 sensor elements installed in 4 mm diameter stainless steel tubes, absolute accuracy <0.1 °C) were installed at fixed depths of 50 and 100 mm below the dune slope crust. The soil surface temperatures were determined with a pyrometer (Heiman KT15, Germany, +/- 0.5 °C) and PT100 thermometers buried near the surface. All data were collected using Campbell 21X dataloggers equipped with external relay multiplexers to expand the number of

channels. Datalogger measurements were performed every 5 seconds and averaged to 15 minute intervals.

5.3 Dewfall

A simple atmospheric model was tested to obtain a better understanding of the dew formation process, and which could be compared with field measurements. Dewfall can be estimated from standard meteorological measurements using a simple Penman approach (Monteith, 1981). Water vapour transport in the atmosphere towards and from a (wet) surface is proportional to the vapour pressure gradient, divided by a resistance:

$$L_v E = \frac{\rho C_p}{\gamma} \frac{e_o - e}{r_{at}} \tag{5.3}$$

where L_vE is the latent heat flux (W m^{-2}), C_p is the specific heat of air at constant pressure (J kg^{-1} K^{-1}), γ is the psychrometric constant (Pa K^{-1}), e_0 is the vapour pressure at the surface (Pa), e is the vapour pressure at reference height (Pa), and r_{at} (s m^{-1}) is the sum of the aerodynamic resistance r_a (s m^{-1}) plus the boundary layer resistance r_b (s m^{-1}). Penman solved this equation for a wet surface by extrapolating the atmospheric saturated vapour pressure to the surface by a Taylor expansion series:

$$e_o(T) = e_w(T) + s(T_0 - T) \tag{5.4}$$

where $e_w(T)$ is the saturated vapour pressure at reference height (Pa), s is the derivative of the saturated vapour pressure (Pa K^{-1}), T_0 is the soil surface temperature and T is the air temperature at reference height.

The resistances to heat and vapour fluxes are assumed to be equal. A similar expression can be found for the sensible heat flux:

$$H = \rho C_p \frac{T_s - T}{r_{at}} \tag{5.5}$$

Here the temperature gradient between the temperature of the surface and that of a reference height in the atmosphere surface layer is proportional to the sensible heat flux H (W m^{-2}). Combining Eqs. 5.3-5.5 with the surface energy balance equation gives the standard Penman equation for a wet surface:

$$L_v E = \frac{s(Q^* - G) + \frac{\rho C_p}{r_{at}}(e_w(T) - e)}{s + \gamma} \tag{5.6}$$

where G is the soil heat flux and Q^* is the net radiation (W m^{-2}). The Penman equation (Eq. 5.6) is very practical because it only requires measurements of one level to calculate dew and evaporation from a wet surface. In a saturated atmosphere, Eq. 5.6 reduces to:

$$L_v E = \frac{s(Q^* - G)}{s + \gamma}. \tag{5.7}$$

Monteith (1963) called this the potential rate of nocturnal dew formation. Applying Eq. 5.6 to a bare soil is not straight-forward. These relations were established for a saturated surface, or adapted with an additional resistance to estimate evaporation of a canopy where the free water is behind stomata gates. A dry soil behaves differently, namely that the free water is held by matrix potential forces in the soil pores. Although some researchers have introduced a skin resistance through which the soil water has to pass through a dry layer to the free atmosphere, analogous to leaf stomata resistance, it is only useful to study general evaporation from deeper soil layers (Kondo et al, 1990). Introducing a soil resistance here would have no relationship to the transport process at this fine scale. Thus instead of using Eq. 5.4 to derive the Penman equation, the vapour pressure reduction of the soil can be taken into account by:

$$e_o(T_0) = h_s(e_w(T) + s(T_0 - T)) \tag{5.8}$$

where h_s is the relative humidity of the soil pores. We then arrive at the following modified Penman equation for a bare soil:

$$L_v E = \frac{h_s s(Q^* - G) + \dfrac{\rho C_p}{r_{at}}(h_s e_w(T) - e)}{h_s s + \gamma}. \tag{5.9}$$

Note that for $h_s = 1$ the usual Penman equation is achieved. Under dry soil conditions the dew formation will be enhanced by the second term, in contrast to Eq. 5.6, where dew formation on a free water surface is reduced by the second term, because the saturation deficit of the atmospheric surface layer rarely approaches zero. The modified Penman equation (Eq. 5.9) can be practical if there are simple techniques to directly measure the saturation level of the soil pores.

5.4 Soil water flow

To investigate dew water flow in the soil, a fine one-dimensional multilayer numerical soil model was constructed, simulating temperature and soil water flow up to 3 m depth. It is assumed that soil properties change with depth only. With the model, it becomes possible to study the effects of soil crusting and dew water movements within the soil. The main soil water transport is in the vapour phase, since the soil moisture content is low at the end of the dry season. The soil moisture transport and heat diffusion model is based on Van Wijk & De Vries (1963) and Philip & De Vries (1957). They introduced the heat equation for a moist and unsaturated soil, which includes the latent heat transport by distillation/condensation (Hillel, 1980, p. 301):

$$C_v \frac{\partial T}{\partial t} = \lambda^* \frac{\partial^2 T}{\partial z^2} - L_v \frac{\partial}{\partial z}(D_{\theta v} \frac{\partial \theta}{\partial z}) \tag{5.10}$$

where T is the soil temperature (°C), z is the soil depth (m), C is the volumetric soil heat capcity (J m^{-3} K^{-1}), L_v is the latent heat of vaporisation (J kg^{-1}) and is a weak function of temperature (Fritschen & Gay, 1979). Thus

$$L_v = 2.4903 \cdot 10^6 - 2259.4T \qquad (T \text{ in °C}) \qquad (5.11)$$

and λ^* is the apparent thermal conductivity (W m^{-1} K^{-1}) incorporating transfer of latent heat by vapour movement under the influence of a temperature gradient (De Vries, 1986). De Vries (1963) developed a method of estimating soil thermal conductivity from soil texture, bulk density, and water content. The method includes the most important soil properties affecting conductivity but it requires additional knowledge of parameters called "shape factors" that describe the shape and packing together of the soil particles:

$$\lambda^* = \lambda' + \rho D_{Tv} L_v \qquad (5.12)$$

where λ' is the conductivity of a soil, $\rho D_{Tv} L_v$ is a distillation term caused by a temperature gradient and D_{Tv} (m^2 s^{-1} K^{-1}) is the vapour diffusivity for a temperature gradient. Hysteresis in the soil moisture characteristic curve (Eq. 5.25) would also affect the apparent thermal conductivity but is not considered in the present study.

The soil moisture transport in a porous medium can be described by a similar diffusion equation (Philip & De Vries, 1963):

$$\frac{\partial \theta}{\partial t} = \frac{\partial}{\partial z}(D_\theta \frac{\partial \theta}{\partial z} + D_T \frac{\partial T}{\partial z}) \qquad (5.13)$$

where D_θ (m^2 s^{-1}) is the soil moisture diffusivity for a moisture gradient, and θ is the volumetric soil water content (m^3 m^{-3}). The general diffusion coefficients include vapour and liquid transport caused by a temperature and soil moisture gradient:

$$D_\theta = D_{\theta v} + D_{\theta l}$$

$$D_T = D_{Tv} + D_{Tl}$$

To derive the vapour diffusivities $D_{\theta v}$ and D_{Tv}, the vapour velocity in the soil can be written as (Van Wijk & De Vries, 1963):

$$v_v = -\alpha(\theta_s - \theta)\frac{DM_v}{\rho_l RT}\frac{P}{P-e}\frac{\partial e}{\partial z} \qquad (5.14)$$

where v_v is the vapour velocity (m s^{-1}), α is a tortuosity value (-), θ_s is the saturated volumetric soil water content (m^3 m^{-3}), D is the diffusion coefficient for water vapour in still air (m^{2}s^{-1}), P is the ambient air pressure (Pa) and e is the vapour pressure (Pa). There is a more extended model to calculate vapour flow (Parlange et al., 1998), in which an additional soil pore air flow is included in Eq. 5.14 to account for convective transport driven by the diurnal thermal expansion and contraction of the soil air. The complexity of the biologically active soil layer and the limited understanding of the biological material and its interaction with soil moisture lead to the implementation of Eq. 5.14 only. As an example, a biological crust expands with

increasing moisture content thereby blocking the larger soil (Verrecchia, 1995). That is the reason why in the present study we omitted this convection driven vapour flow.

The vapour pressure gradient is a function of temperature and moisture gradients:

$$\frac{\partial e}{\partial z} = h\frac{\partial e_s}{\partial z} + e_s\frac{\partial h}{\partial z} \tag{5.15}$$

or

$$\frac{\partial e}{\partial z} = h\frac{\partial e_s}{\partial T}\frac{\partial T}{\partial z} + e_s\frac{\partial h}{\partial T}\frac{\partial T}{\partial z} + e_s\frac{\partial h}{\partial \theta}\frac{\partial \theta}{\partial z} \tag{5.16}$$

Combining Eq. 5.15 and 5.13 the vapour diffusion coefficients become:

$$D_{Tv} = \alpha(\theta_s - \theta)\frac{DM_v}{\rho_l RT}\frac{P}{P-e}(h\frac{\partial e_s}{\partial T} + e_s\frac{\partial h}{\partial T}) \tag{5.17}$$

$$D_{\theta v} = \alpha(\theta_s - \theta)\frac{DM_v}{\rho_l RT}\frac{P}{P-e}e_s\frac{\partial h}{\partial \theta} \tag{5.18}$$

For the liquid diffusion coefficient a similar approach applies. The velocity of the liquid flux component according to Darcy's law (Hillel, 1980) is:

$$v_l = -K\frac{\partial \psi}{\partial z} \tag{5.19}$$

where K is the hydraulic conductivity (s) and ψ is the soil water potential (J kg^{-1}).

$$v_l = -K(\frac{\partial \psi_m}{\partial z} + \frac{\partial \psi_g}{\partial z}) \tag{5.20}$$

where ,ψ_m is the soil matrix potential and ψ_g is the soil gravity potential.

$$v_l = -K(\frac{\partial \psi_m}{\partial z} + g) \tag{5.21}$$

where g is the acceleration due to gravity (m s^{-2}).

Since matrix potential is a function of moisture content and temperature, Eq. 5.20 can be rewritten as:

$$v_l = -(K\frac{\partial \psi_m}{\partial \theta}\frac{\partial \theta}{\partial z} + K\frac{\partial \psi_m}{\partial T}\frac{\partial T}{\partial z} + Kg) \tag{5.22}$$

The diffusion coefficients for liquid water now become:

$$D_{\theta l} = K\frac{\partial \psi_m}{\partial \theta} \qquad (\mathrm{m^2\,s^{-1}}) \tag{5.23}$$

$$D_{Tl} = K\frac{\partial \psi_m}{\partial T} \qquad (\mathrm{m^2\,s^{-1}\,K^{-1}}) \tag{5.24}$$

The model can be forced with soil surface temperature coupled with soil surface moisture flux measurements from the microlysimeters.

A simple power relation for modelling the soil moisture characteristic curve was chosen (Clapp and Hornberger, 1978), which links soil water potential to soil water content:

$$\psi_m = \psi_e (\frac{\theta}{\theta_s})^{-b} \tag{5.25}$$

where ψ_e is the air entry water potential and b is a fit parameter (-) which follows the relationship (Campbell, 1985):

$$b = 1.0 d_g^{-\frac{1}{2}} + 0.2\sigma_g \tag{5.26}$$

where 1.0 ($mm^{0.5}$) and 0.2 (mm^{-1}) are fitting constants, d_g (mm) is the geometric mean particle diameter (mm) and σ_g (mm) is the geometric standard deviation. The air entry potential is (Campbell, 1985):

$$\psi_e = -0.5 d_g^{-0.5} \tag{5.27}$$

Horizon:	Cryptogamic crust	Soil below crust
Depth (mm)	0 – 4.0	>4.0
Particle size distribution		
Clay fraction <2 (μm)	0.06	0.005
Silt fraction 2..50 (μm)	0.28	0.015
Sand >50 (μm)	0.66	0.98
Parameters derived from particle size distribution		
d_g (μm)	87.6	268
σ_g (mm)	19.9	1.265
ψ_e (J kg^{-1})	-1.69	-0.96
b (-)	7.4	2.18
Hydraulic conductivity at saturation K_s (s)	$3.1 \cdot 10^{-6}$	$1.3 \cdot 10^{-6}$

Table 5.1: Properties of the soil as used in the soil model (except *b*).

Verrecchia et al. (1995) analyzed the Nizzana dune slopes and presented the grain size distribution curves for the biological crust and the sand below it. The organic material was chemically removed. From these curves the soil properties in Table 5.1 were derived. The soil hydraulic properties were modelled with (Clapp and Hornberger, 1978):

$$K = K_s (\frac{\theta}{\theta_s})^{2b+3} \tag{5.28}$$

The saturated hydraulic conductivities K_s were taken from Rijtema (1969). The cryptogamic crust can be characterised as Type 8 loamy fine sand and the soil below the crust as Type 3 medium fine sand (see Table 5.1).

5.5 Analysis of the experiments and models

Soil properties

Bulk density, porosity and organic matter were determined in the University of Giessen soil physics laboratory and are provided in Table 5.2.

Horizon:	Cryptogamic crust	Soil below crust
Depth (mm)	0 – 4.0	>4.0
Bulk density (kg m^{-3})	$1.70 \cdot 10^6$	$1.54 \cdot 10^6$
Total porosity (m^3 m^{-3})	0.40	0.42
Organic matter	0.01	0

Table 5.2: Properties of the soil as used in the soil model.

The dry desert soil requires reliable soil water characteristics for modelling water transport in the extreme dry range (pF > 4.2). The complication is that the relationship between pore size and water holding capacity breaks down at soil water potentials in the range $-10^4 < \psi_m < -10^3$ J kg^{-1} or 5 > pF > 4 (Campbell, 1985). Pore size and grain size are related and therefore the coefficients for the soil water retention curve (Eq. 5.25) may not be valid. Hajnos et al. (2006) showed that the Kelvin relation to predict soil water potential from soil pore size is valid above 35% soil pore humidity (>-149 10^3 J kg^{-1}) and that below 35% adsorption processes dominate. Ten Berge (1986) suggests using adsorption isotherms for the dry range instead of using standard soil water characteristic curves. Such standard curves are often based exclusively on measurements at higher moisture contents (of wilting point pF 4.2 and below) and extrapolating these curves is not valid. However, the unique in situ measurements of soil relative humidity (Fig. 5.4) and soil water content makes it possible to expand the soil moisture characteristic model (Eq. 5.25) for the dry range.

The soil moisture retention curve (Eq. 5.25) and the parameters determined in Table 5.1 can be tested with the manual measurements of gravimetric soil moisture content over several layers and the soil relative humidity measurements obtained from the buried Vaisala relative humidity probe. The soil relative humidity is linked to soil water potential by Eq. 5.2. Two soil types can be tested; the playa soil in the interdune region and the dune slope soil below the biological crust (Fig. 5.4).

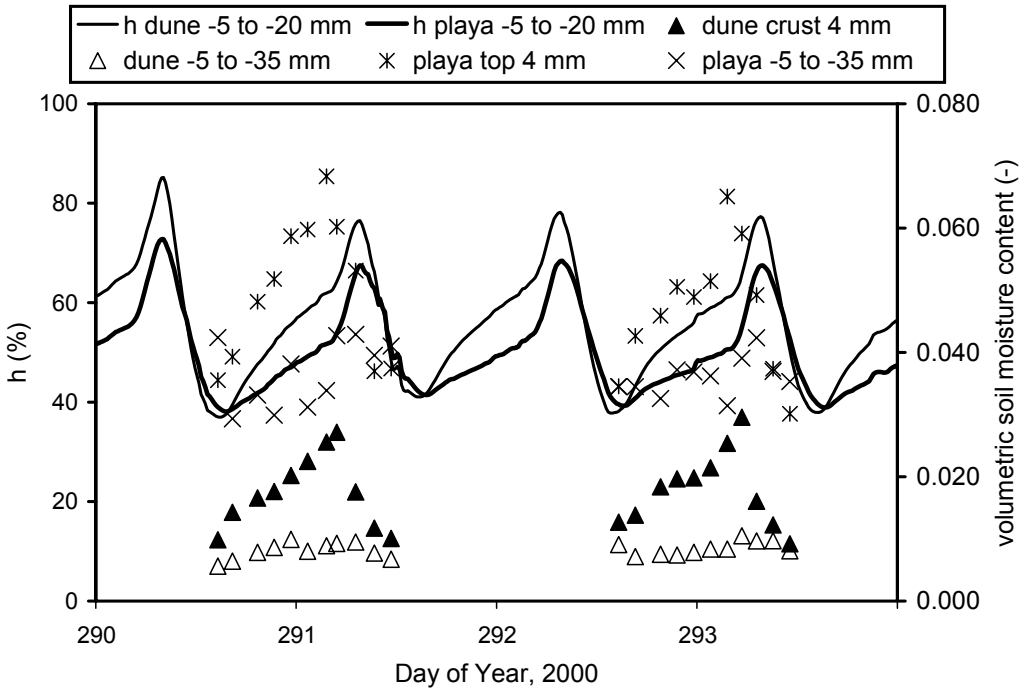

Figure 5.4: Triangles and crosses: Manual moisture measurements by sampling and drying on an interdune playa soil and sand dune slope (north-facing). Straight lines: relative humidity probe measurements in the soil.

There is a strong diurnal variation of soil moisture content especially in the top soil. The Vaisala relative humidity probe was buried in the soil and measures the relative humidity within 5 to 35 mm inside the soil. The relative humidity also shows a strong diurnal variation in contrast to the soil moisture content. It is to be expected that the relative humidity plotted against the soil moisture content should compare with Eq. 5.25 (calculating soil pore humidity from Eq. 5.2) (Fig. 5.5). Here it was decided to plot relative humidity and not soil water potential since the relative humidity was measured directly.

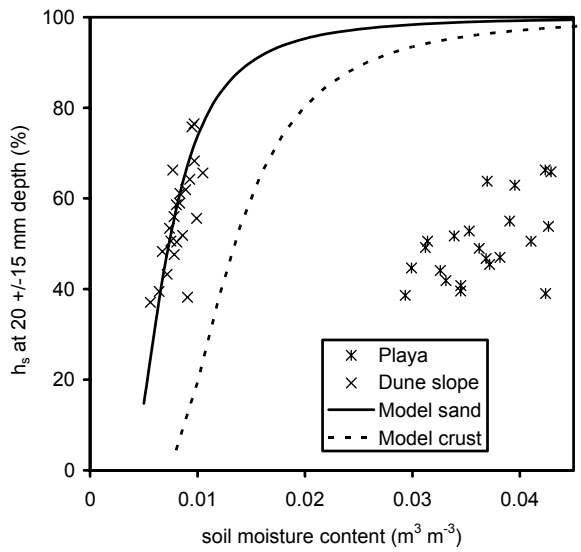

Figure 5.5: The measured and modelled daily variation in soil air relative humidity (model uses 20 °C), as a function of soil water content (1400h GMT 16 Oct. to 17 Oct. 1400 GMT and 1400 Oct. 18 to 1100 19 Oct. 2000).

There was a strong deviation between Eq. 5.25 using parameters from Table 5.1 and the measurements of soil relative humidity of the soil below the crust. Using these parameters for the soil moisture curve and calculating the soil matrix potential would give a very high soil pore relative humidity at the measured soil moisture contents. Therefore, it was decided to adjust the coefficient b in Eq. 5.25 of the soil below the crust by using the relative humidity measurements and to link these to the gravimetric volumetric soil moisture measurements (Eq. 5.2). See also Fig. 5.6 where the measurements of Fig. 5.4 and laboratory measurements of soil pore size distribution derived pF values are combined. This resulted in a fitted b_{sand} value of 2.83 (about 30% higher).

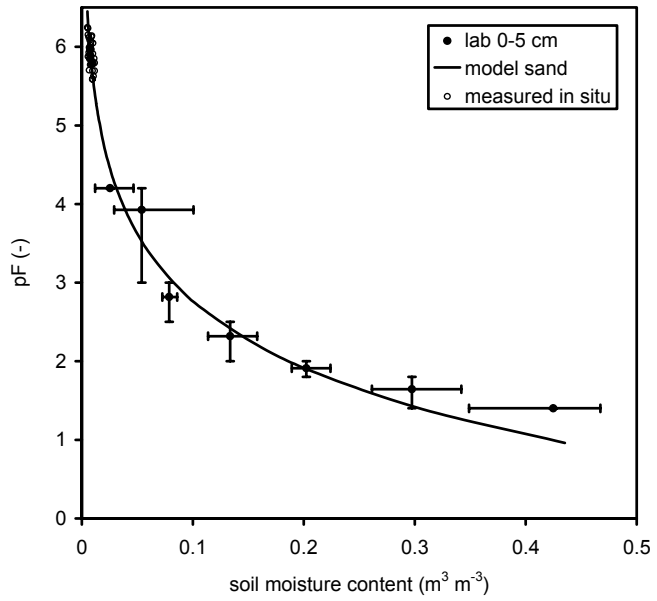

Figure 5.6: Soil matrix potential of sandy soil below the crust, as a function of soil water content. Straight line: Model of soil moisture characteristic curve, Circles: experimental in situ measurements, dots and error bars derived from pore size laboratory data, horizontal error bars represent the variation between 10 samples, and vertical error bars represent a soil pore size range.

Regarding the test of the parameters (Table 5.1) of the soil water retention curve for the crust, a major limitation was that only the relative humidity of the sandy soil under the biological crust could be measured due to the size of the probe, hence the parameters for the crust (Eq. 5.25) could not be tested directly. However, in addition to the sand dune measurements the relative humidity in the nearby playa soil (Fig. 5.1 area 2) was measured and it can be assumed that the fine playa soil material is partly intercepted by the biological crust. The crust *b* value from Table 5.1 would even be too high to describe the playa material. Therefore, the hydrological properties will lie somewhere in between the sand and playa material (Fig. 5.4 and 5.5). An iterative procedure was used to find the optimum value for b_{crust} and soil water diffusion model was used to do so. The upper boundary of the water diffusion model was forced with the latent heat flux derived from the weight change of the microlysimeters and the soil surface temperature. The soil model was first initialized with a measured temperature and moisture profile. Since these profile measurements were limited, the model was run several times for similar days and the resulting profiles were used to re-initiate the model runs until a stable situation was reached. The soil moisture variation averaged over the soil layers representing the crust and soil below should compare with the manual crust soil moisture measurements in Fig. 5.4. Best results could be achieved with a value of 3.17 and this differs considerably

from Table 5.1. As mentioned before, this deviation could be related to the complexity of the biologically active soil layer and the limited understanding of the biological material and its interaction with soil moisture.

5.5.1 Atmosphere

The dew formation process in an arid zone is influenced by several factors. As radiative heat loss cools the surface, the soil starts to adsorb water vapour (Fig. 5.4) long before the soil surface reaches the dewpoint temperature. While the radiative cooling continues, the downward moisture flux will dry the lower air layers and turbulence is needed to transport fresh air downwards. The turbulence can be suppressed by the stable temperature stratification of the atmosphere. Two days have been selected here to illustrate the processes involved. Both days are typical of the strong NW winds (noon to sunset) caused by the sea breeze circulation that predominates during the mainly rainless, warm to hot months (Littmann, 1997) (Fig. 5.7c).

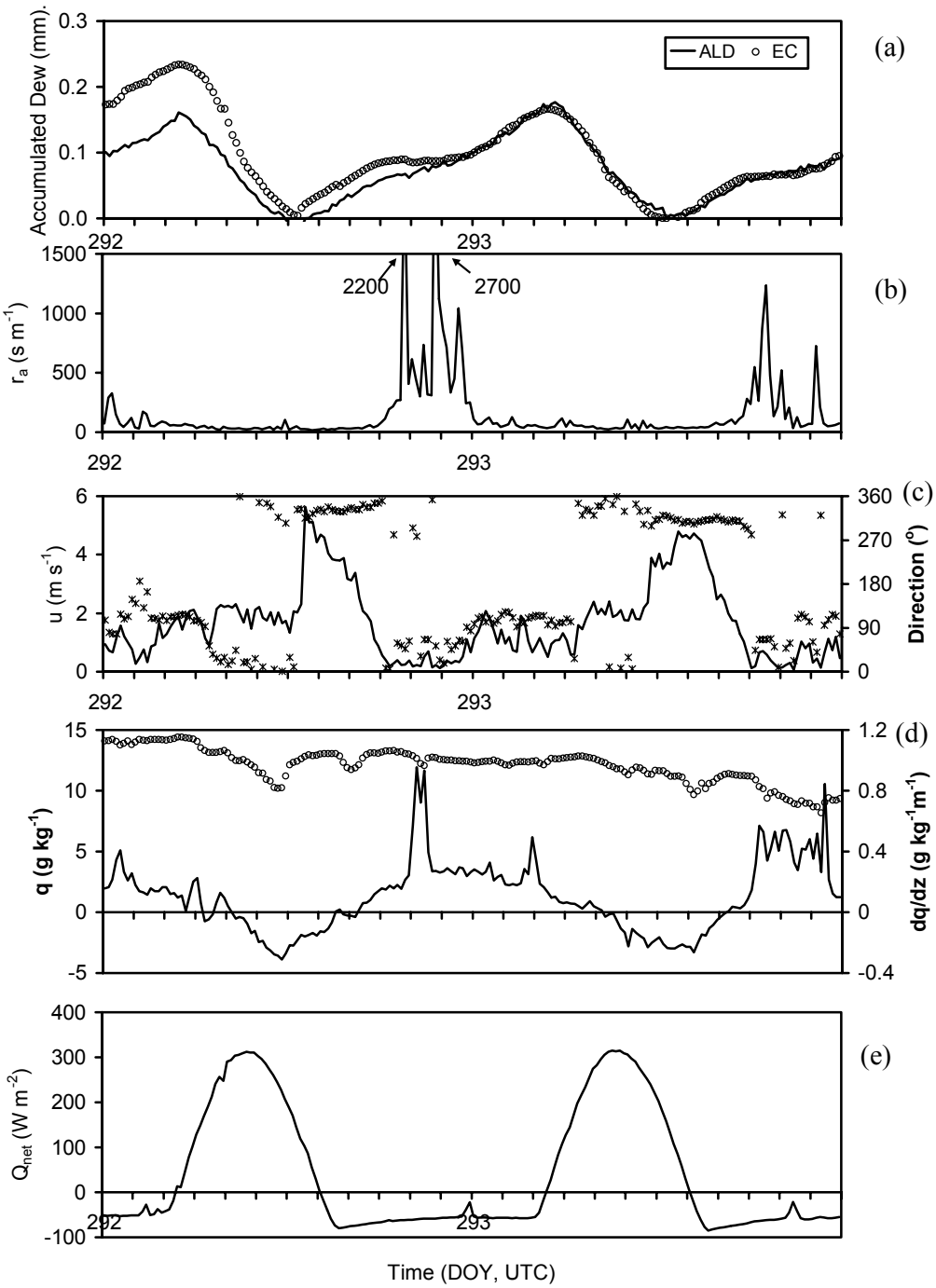

Figure 5.7: Measurements of radiative heating and cooling net radiation (e), specific humidity at 1.5 m and moisture gradient between 0.5 and 1.5 m height (d), wind speed and direction (c), aerodynamic resistance (b), accumulated dew from eddy covariance measurements and microlysimeter (a) DOY 292 and 293, 2000.

Starting with the daytime situation of DOY 292 there is a sudden increase in windspeed from the sea breeze, which is a thermally driven wind circulation generated by the temperature difference between Mediterranean sea and land surface. The peak in the windspeed arrives later in the afternoon due to the distance from the coast, near the coast the peak would occur earlier (Fig. 5.7c). This sea breeze brings in moist air (Fig. 5.7d) and cools the soil surface temperature. This cooling directly increases relative humidity near the soil surface and, while this is linked to soil water potential (Eq. 5.2), this will raise soil moisture content near the surface (Fig. 5.5). Meanwhile, the radiative heat loss starts cooling the soil surface. The microlysimeters detect a weight increase (Fig. 5.7a), which is the adsorption of water vapour into the upper soil layers. To demonstrate that the microlysimeter weight change is not related to saltation of sand grains, the accumulated dew (Eq. 5.29) from the eddy covariance measurements (EC) are also plotted (Fig. 5.7a).

$$Dew = -L_v^{-1} \int L_v E dt \qquad (5.29)$$

Both measurements start detecting a downward moisture flux at around the same time. The accumulated dew from the EC measurements (Eq. 5.29) on the interdune area compares well with the microlysimeter weight gain on the dune slopes. This conflicts with the measured microlysimeter ratio between dune slope and interdune as this ratio is around 0.6 during these days (Fig. 3.6) (Heusinkveld et al., 2006). A likely explanation is that the EC system is installed at a height of 3 m and this could lead to an underestimation of the downward latent heat fluxes. The low turbulence and stability of the atmosphere during large parts of the dew episodes decouples the 3 m measurements from the surface. However, the EC morning evaporation sometimes shows a larger evaporation which compares well with the microlysimeter measurements from the interdune area (not shown). As the windspeed declines, the specific humidity gradient increases and the atmosphere becomes stably stratified. The aerodynamic resistance increases rapidly and thus slows the vapour flux to the surface (Figs. 5.7a,b,c,d). The vapour flux is also reduced by the filling of the finer soil pores, which increases vapour pressure at the surface. Around 00:00, a light katabatic wind from the land takes over and a SE flow towards the coast starts to develop. This is an interesting period because the turbulence generated by the katabatic wind is sufficient to reduce the strong stratification that limits moisture transport to the air near the surface (Figs. 5.7a,b,c). This increase of turbulence leads to an increase in the vapour flux to the soil again despite the on-going increased soil moisture content (larger vapour pressure at the soil surface).

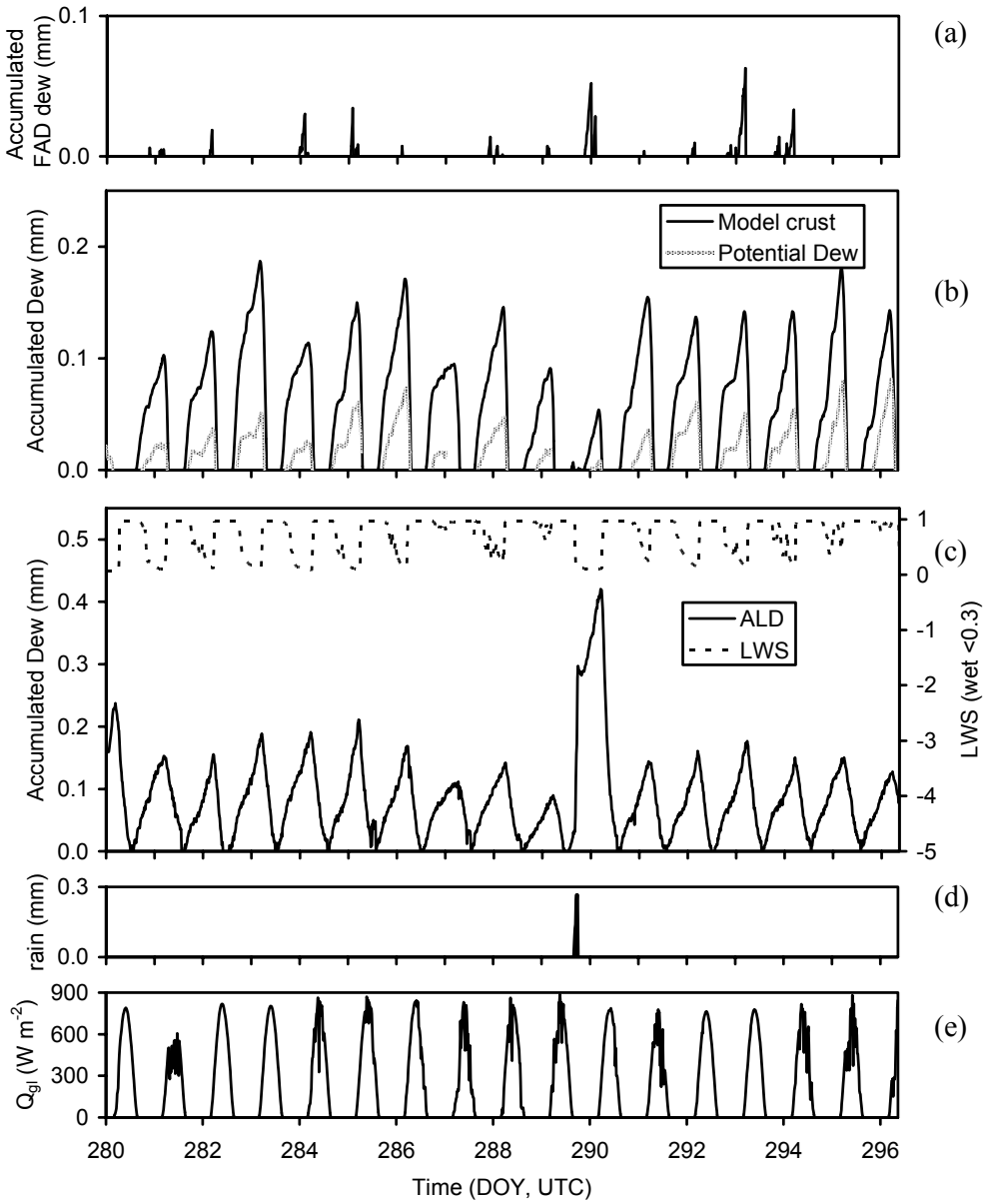

Figure 5.8: Accumulated Potential dew and the model output, compared with the recording microlysimeter measurements on north-facing dune slope (ALD) (6 Oct. – 22 Oct., 2000). The leaf wetness sensor (LWS) indicates a wet surface when its value drops below 0.3 mm. The peak on day 289-290 reflects a light drizzle of 0.3 mm rain.

To illustrate how the situation deviates from a normal dew night for a vegetated surface, the potential dew is plotted in Fig. 5.8b. The actual water accumulation in the soil is much higher than the potential dew; see microlysimeter

data in Fig. 5.8c. The next step is to test if introducing a vapour pressure reduction coefficient for the soil surface moisture (Eq. 5.9) can predict these larger dew quantities. The input for this simple model is the vapour pressure and temperature at reference height 0.5 m, and the relative humidity as measured by a temperature and humidity probe buried below the crust. The turbulence was measured using a sonic anemometer (CSAT3, Campbell USA) at 3m height (Fig. 5.7b). Figure 5.8b-c shows that the model compares well with the microlysimeter measurements. However, the boundary resistance had to be increased to correct for the relative humidity sensor depth. It can be expected that the relative humidity at the surface has a maximum during dew episodes and will be greater than the measurements below the crust, since the soil moisture concentration is higher near the surface during a dew episode. The aerodynamic resistance was measured by the eddy covariance system and an additional boundary layer resistance was added to compensate for the fact that the soil pore relative humidity was not measured at the surface (Eq. 5.30). The additional resistance was derived from an iterative procedure in which the accumulated latent heat flux (Eq. 5.9) was compared with the microlysimeter weight change. The high boundary layer resistance represents the resistance along the soil diffusion path to the depth of the relative humidity probe:

$$r_{at} = 800 + \frac{u}{u*^2} \tag{5.30}$$

where u is the windspeed (m s^{-1}) and u* is the friction velocity (m s^{-1}).
The advantage of this approach is that standard weather station data with an additional soil relative humidity probe can be used to estimate dewfall. A procedure to derive fluxes from standard weather station data can be found in De Rooy et al. (1999), and this technique can be incorporated into the presented model.

The standard Penman equation was also tested however with this equation no dew could be simulated. The reason is that the inclusion of soil relative humidity measurements is not included in this equation which is a main omission.

A simple approach can be used to find FAD (Free Available Dew) by selecting periods where the microlysimeter weight gain coincides with a soil surface and dewpoint temperature difference of less than 1 K (Fig. 5.8a). The accuracy of measurement is not high enough to be more specific. In this case the FAD would mean the available water for vascular plant species (pF < 4.2). Setting the difference at 1 K, instead of at 0 K, accounts for possible measurement errors. Moreover, the atmosphere moisture measurements were situated within the interdune area, which dries the air because of the 50% stronger latent heat flux. Dew formation will also limit the soil surface temperature drop thus it is favourable to avoid the ideal 0 K. The FAD appears to be a small fraction of the available dew (Fig. 5.8a-c).

5.5.2 Dew water movement in the soil

To analyze the detailed water movement in the soil of the dune slopes the coupled soil temperature and water diffusion soil model (Eq. 5.10 and 5.13) is used to study the dew water distribution as a function of depth and time. The model was run with a bare sandy soil covered with a 4 mm biological crust (Table 5.2). The model is forced with the microlysimeter flux measurements and the soil surface temperature. The soil model was first initialized with a measured temperature and moisture profile. Since these profile measurements were limited, the model was run several times for similar days and the resulting profiles were used to re-initiate the model runs until a stable situation was reached.

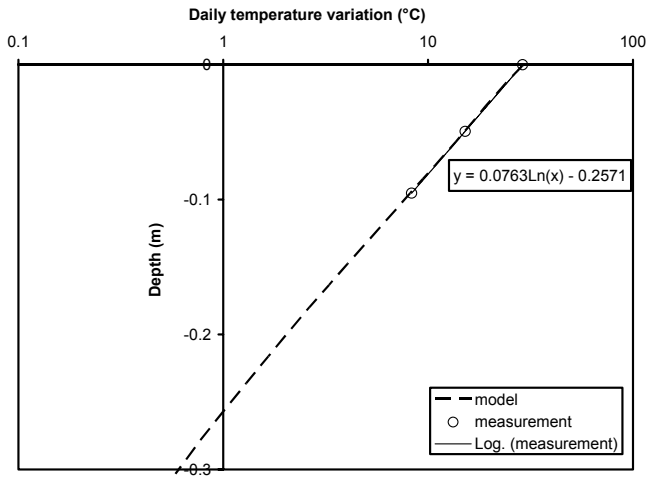

Figure 5.9: Amplitude of daily temperature wave as function of depth (DOY 290-292, 2000).

The temperature amplitude variation compares well with the measurements (Fig. 5.9) but the modelled thermal conductivity had to be increased by 20% to achieve these results. Such deviations are probably related to an uncertainty in the soil particle arrangement or a tolerance in temperature sensor placement. The soil damping depth (m) for daily temperature variations can be derived from these measurements and was found to be 7.6 cm +/-5% (Fig. 5.9).

The next step was the model validation of the soil moisture content (Fig. 5.10).

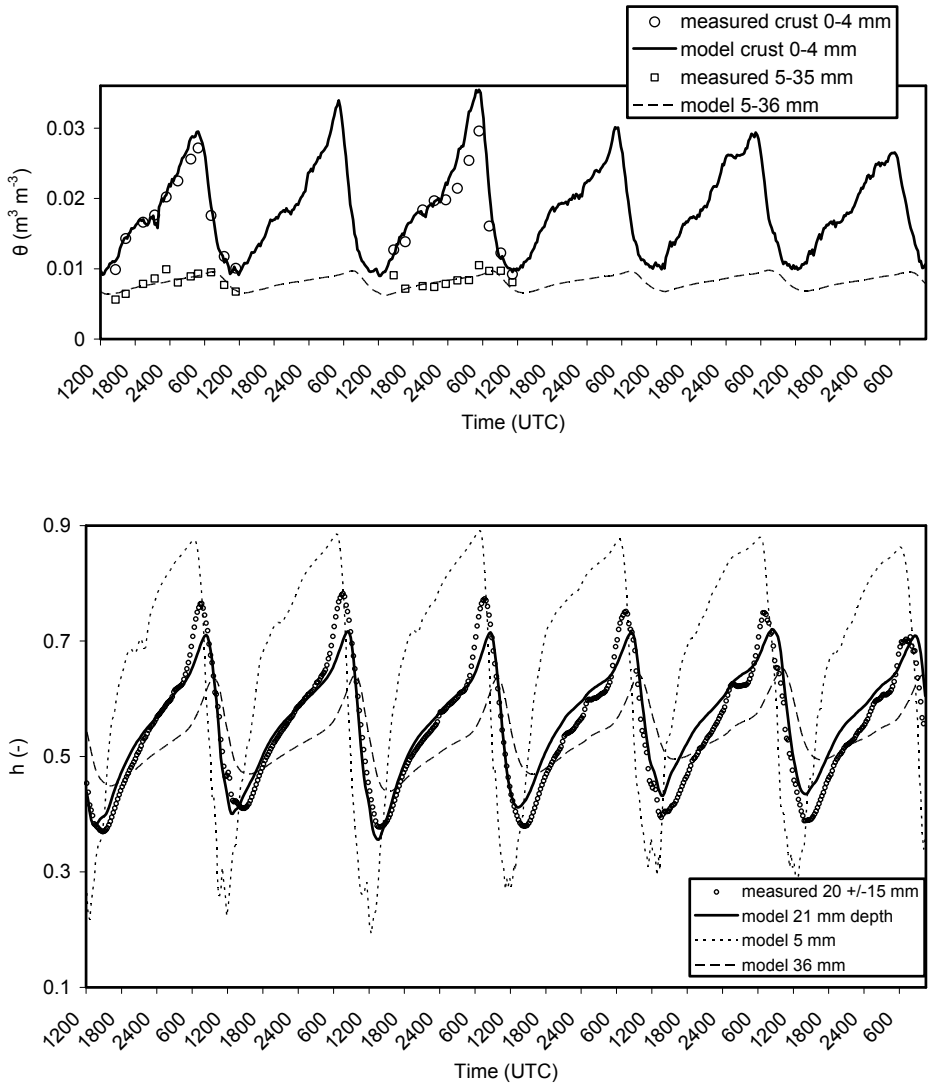

Figure 5.10: Measured and modelled soil moisture (upper panel) and relative humidity (lower panel) variation over 6 days (DOY 290-296, 2000).

The depth averaged crust model layers soil moisture content and the soil moisture content below the crust averaged of the depth of the soil sampling cups was compared with the gravimetric moisture content measurements (Fig. 5.10 upper panel). The comparison shows that the major soil moisture diffusion is confined to the crust only. The lower panel of Fig. 5.10 shows the model run compared with the relative humidity probe measurements. The soil relative humidity compares well considering the limitations in the measurements. The size of the probe limits a perfect comparison.

The probe size also affects soil heat flux. To show how dynamic the relative humidity is along the depth of the probe, also the upper and lower probe depth model layers were plotted. In theory it seems better to average the soil water potential over these model layers and calculate the relative humidity but this seems not relevant considering the size of the probe which modifies the soil.

A damping depth for soil moisture can be considered analogous to the damping depth of daily temperature variations. The simulations revealed that the daily soil moisture variation penetrates to a limited depth (15 mm). Fig. 5.11 shows that the soil moisture variation is mainly confined to the crust only.

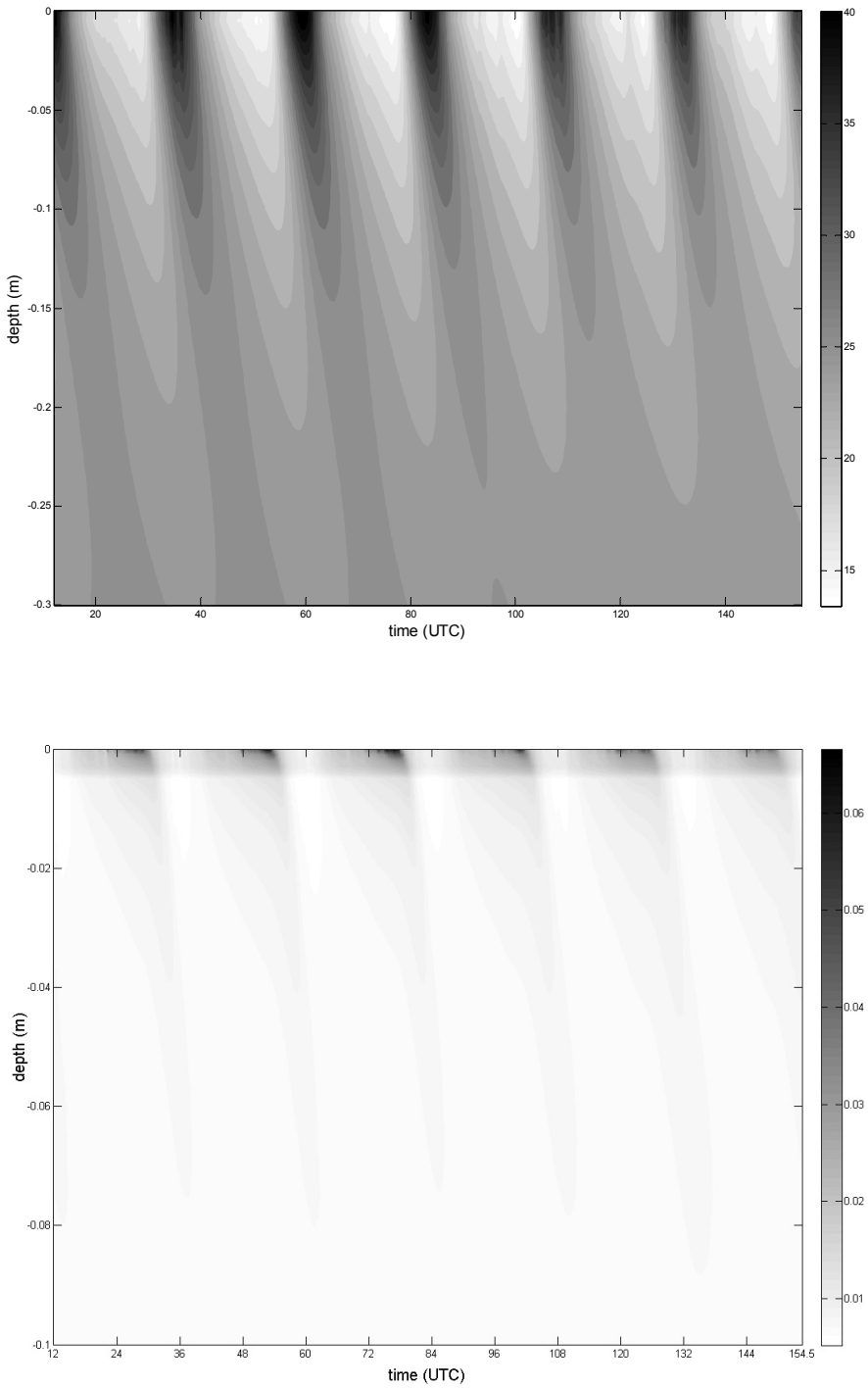

Figure 5.11: Contour plot of the evolution of temperature (top) and moisture content (bottom) in the soil (note the different depth scales) (6 day period: DOY 290-296, 2000).

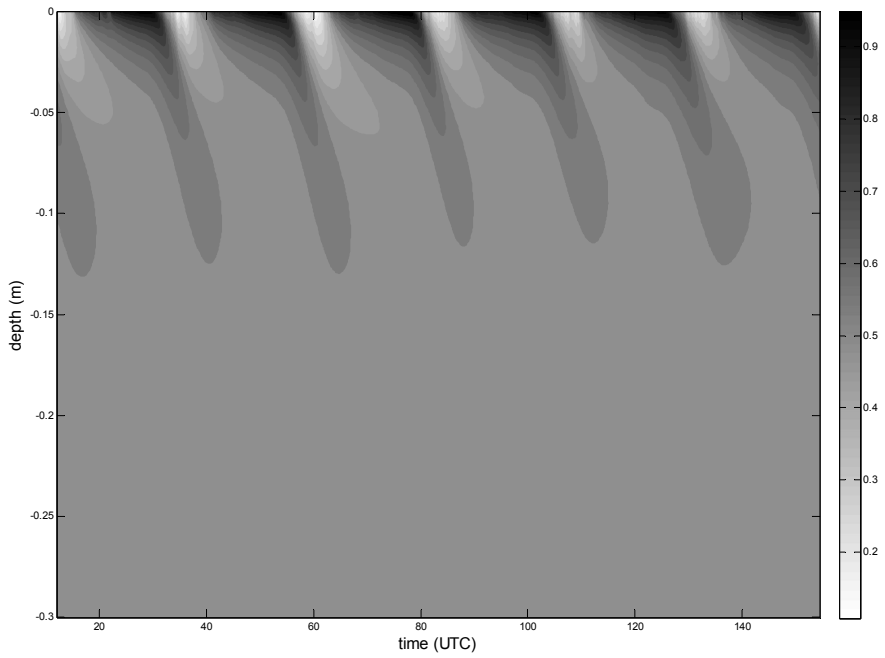

Figure 5.12: Contour plot of the evolution of soil pore relative humidity over 6 days (DOY 290-296, 2000).

The damping depth (daily cycle) for dew penetrates only about 15 mm into the soil, which is in agreement with Jacobs *et al.* (2000). In particular, the soil pore relative humidity peaks in the top part of the crust, during and just after sunrise. The dew formation process usually peaks and continues for about 1 hour after sunrise. Soil water mainly moves in its vapour phase through the soil pores (Fig. 5.12), since the dew amounts are small. The soil water diffusion goes in two directions; into the air and into the ground. The heating of the surface releases soil moisture into the soil pore air. This moisture that was initially locked in the matrix potential of the soil can move freely up or down. The water availability for photosynthetic activity lasts longer in the lower part of the crust around sunrise. Although the overall FAD period is shorter at that location, it might be more relevant (Fig. 5.13).

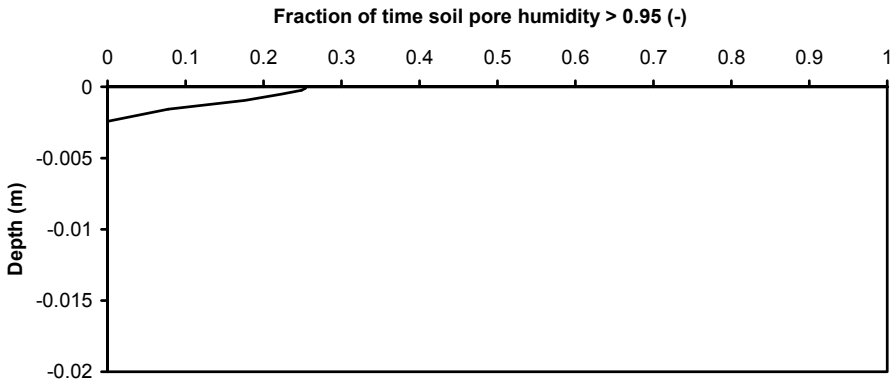

Figure 5.13: The soil wetness fraction where soil pore humidity is larger than 0.95 (evaluated for 6 days: DOY 290-296, 2000).

The model results show that the dew water input results in an increase in soil moisture, in a narrow top layer, for a prolonged period of time after sunrise. This is supported by the gravimetric soil moisture measurements (Fig. 5.11 and 5.12). The period of time that FAD is available for cyanobacteria can be calculated from the model results by calculating the time fraction of soil pore humidity > 95%. It seems that only the upper half of the crust has FAD during a certain percentage of time (Fig. 5.13).

The optical wetness sensors measured only a limited response to dew however the response of the sensor is small below 0.97 soil pore humidity (see Fig. 4.11). However, it is very interesting to note that the response on thinner crusts was higher, indicating that the amount of dew was distributed over a smaller volume. This resulted in a higher soil moisture concentration than that of the thicker crust and suggests that a thinner crust might benefit more from dew than a thick crust. A coupled soil atmosphere model is needed to verify this. In the analysis we show that the distribution of dew water greatly depends on the soil composition, i.e. thickness of the crust. Again, the daily available dew within a thin crust could be more effective than in a thicker crust.

5.6 Concluding remarks

The downward atmospheric vapour flux can be more than twice the potential dew. A certain percentage of this water will be Free Available Dew (FAD) suitable for biological activity and this amount is species-dependant. The remaining part will

be locked in the micro soil pores and at surface soil particles as adsorbed water. It is important to make this distinction, especially in desert ecosystem studies. The vapour flux towards the soil can be estimated from standard weather station data coupled with additional measurements of soil relative humidity. However, a calibration is needed to estimate the transfer coefficients because a measurement at the soil surface moisture is difficult. A soil specific calibration for an optical wetness sensor might provide additional information of surface conditions (pF < 4.5) but this needs further testing.

The presented coupled heat and moisture soil model presented here shows that the moisture transport is confined mainly to the crust. Allthough the soil physical and hydrological data was not highly detailed, nevertheless the simulations compared well with the measured soil moisture content and soil pore relative humidity measurements. It must be noted though that soils can be more complex along the dune slopes because there are areas where new crusts develop on old crusts covered by aeolian sand and this way several layers can develop. The model presented here might be able to simulate such soils also because the model is not limited to a two layer problem.

On the sand dune slopes, initial soil crusting might increase both the amount of dew and the soil moisture content near the surface. The FAD might be higher on a thinner than on a thicker crust, mainly because the soil moisture originating from dew remains more concentrated near the soil surface. The moisture differences between a thick and a thin crust were detected by the optical wetness sensor, although the differences were not large. A coupled atmosphere soil model is a logical step forward. This coupling was not needed in the present study because the focus was on the movement of soil water. With such a model the effects of crust formation and growth and the interplay between dew and soil water movement can be studied. Of special interest would be the transect across a rainfall gradient, starting at the mediteranian coast and moving inland.

Measurements indicate a longer wetness period for a thinner crust but there were too much unknowns, especially the soil composition. If true, this would suggest that the initial formation and growth of a biological crust might benefit more from dew.

References

Belnap J. Jayne Belnap . Susan L. Phillips . Mark E. Miller, 2004: Response of desert biological soil crusts to alterations in precipitation frequency. Oecologia (2004) 141: 306–316, DOI 10.1007/s00442-003-1438-6

Belnap J (1995) Surface disturbances: their role in accelerating desertification. Environ Monit Assess 37:9–57

Blume, J.P., Yair, A., Yaalon, D.H. (1995). An initial study of pedogenic features along a transect across longitudinal dunes and interdune areas, Nizzana region, Negev, Israel. Advances in GeoEcology 28: 51-64.

Campbell G.S. (1985). Soil Physics with BASIC. Developments in Soil Science 14. Elsevier. 150 pp.

Campbell, G. S., Jungbauer, J. D., Bidlake, W. R., Hungerford, R. D. (1994). Predicting the effect of temperature on soil thermal conductivity. *Soil Sci.,* 158(5):307–313.

Clapp, R.B., Hornberger, G.M. (1978). Empirical equations for some soil hydraulic properties. *Water Resour. Res.* 14: 601–604.

Danin, A., Bar-Or, Y., Dor, I., Yisraeli, T., 1989. The role of cyanobacteria in stabilisation of sand dunes in southern Israel. Ecol. Mediter. XV, 55-64.

De Vries, D. A., (1963), *Thermal Properties of Soils; Physics of Plant Environment*, W. R. Van Wijk, ed., John Wiley and Sons, NY, pp. 210–235.

De Vries, D. A. (1963). Thermal properties of soil. In Physics of Plant Environment. W. R. van Wijk (ed.) North Holland Pub. Co. Amsterdam, pp. 210-235.

De Rooy, W.C., Holtslag, A.A.M. (1999). Estimation of surface radiation and energy flux densities from single-level weather data. Journal of Applied Meteorology: 38, pp 526-540.

De Vries, D.A. (1987). The theory of heat and moisture transfer in porous media revisited. *Int. J. Heat Mass Transfer. Vol.30, No.7, pp.1343-1350.*

Fritschen, L.J. Gay, L.W. (1979). Environmental Instumentation. Springer Verlag, New York, pp 216.

Heusinkveld, B.G., S.M. Berkowicz, A.F.G. Jacobs, W.C.A.M. Hillen (2006). An automated microlysimeter to study dew formation and evaporation in arid and semiarid regions. *J. Hydrometeol.*, 7: 825–832.

Hillel, D (1980) Fundamentals of Soil Physics. Academic Press Inc. San Diego 413 pp.

Hopmans, J.W. and Dane, J.H. (1986). Thermal conductivity of two porous media as a function of water content, temperature, and density. *Soil Sci. 142/4:187-195.*

Hopmans, J.W. , Dane, J.H. (1986). Thermal conductivity of two porous media as a function of water content, temperature, and density. *Soil Sci. 142/4:187-195.*

Jacobs, A.F.G., Heusinkveld, B.G., Berkowicz, S.M. (1999). Dew deposition and drying in a desert system: a simple simulation model. *J. Arid Environ.* 42: 211-222.

Jacobs, A.F.G., Heusinkveld, B.G.,Berkowicz,, S.M. (2000). Force-restore technique for ground surface temperature and moisture content in a dry desert system. *Water Res. Resoures 36*: 1261-1268.

Kiondo, J., Saigura, M., Sato, T. (1990). A parameterisation of evaporation from bare soil surfaces. *J. Appl. Meteorol.* 29: 385-389.

Monteith, J.L. (1981). Evaporation and surface temperature. *Q.J.R. Meteor. Soc.* 107: 1-27.

Palmer, R.J., Friedmann, E.I. (1990). Water relations and photosynthesis in the cryptoendolithic microbial habitat of hot and cold deserts. *Microbial Ecology,* 19:111-118.

Philip, J.R., De Vries, D.A. (1957). Moisture movement in porous materials under temperature gradients. *Trans. Am. Geophys. Union* 38: 222-231.

Rijtema, P.E. (1969). Soil moisture forecasting. The Institute for Land and Water Management Research (ICW) nota 513, Wageningen; 18 pp.

Ten Berge, H.F.M., 1986, Heat and water transfer at the bare soil surface. Thesis Wageningen UR.

Verhoef, A., Diaz-Espejo, A., Knight, J.R., Villagarcía, L., Fernández, E. (2006). Adsorption of water vapor by bare soil in an olive grove in southern Spain. *J. Hydromet*. 7: 1011-1027.

Verrecchia, E, Yair, A., Kidron, G.J., Verrecchia, K. , 1995. Physical properties of the psammophile cryptogamic crust and their consequences to the water regime of sandy soils, north western Negev Desert, Israel. *J. Arid Environ. 29: 427-437.*

6 Observations and model calculations for dew collection on a flat surface in the NW Negev desert, Israel

Manuscript intended for publication

Bert G. Heusinkveld[(1)], Adrie F.G. Jacobs[(1)], Simon Berkowicz[(2)]

[1] *Meteorology and Air Quality Group, Wageningen University, Droevendaalsesteeg 4, Atlasgebouw, P.O.Box 47, 6700 AA Wageningen, The Netherlands*

[2] *Arid Ecosystems Research Centre, Hebrew University of Jerusalem, Institute of Earth Sciences, Edmond Safra Givat Ram Campus, Jerusalem, Israel 91904*

Abstract

A passive flat-plate dew collector (3 m^{-2}) was constructed and placed 15 cm off the ground during a meteorological field experiment carried out in the NW Negev desert, Israel, at a site about 40 km away from the Mediterranean coastline. The average dew yield was 0.05 L m^{-2} day^{-1} with a large variation of ±0.04 L m^{-2} day^{-1} over a 7 day period. The low thermal mass of the dew collector and effective insulation from below enabled dew formation although the air never reached saturation (at 2.5 m height). A numerical dew formation model was constructed to study the atmospheric conditions favouring dew. The model is compared with the surface temperature, an electronic surface wetness sensing grid plate and manual dew yield measurements obtained from the collector. The differences in dew yield between measurement and model are explained and can be related to the low placement of the collector near the soil. The soil is very hygroscopic leading to the drying of the air near the surface and thus a large reduction in dew yield. It is expected that a much larger collector placed higher above the hygroscopic soil would increase dew yield. The effect of changing the angle of the collector was simulated with the model and it shows that the output is reduced by up to 24% when placed at a 30° angle. Improving the collector insulation would increase dew yield by a maximum of 15%. Model simulation shows that dew yield would be 2 times larger near the sea if the air were saturated.

6.1 Introduction

During the last 15 years, dew research has investigated dew collecting as a supplemental water source for drinking, washing, or emergency purposes. This is of particular interest for islands, rural regions, and hot, dry climates where rainfall is sparse or restricted. Nilsson et al. (1994) and Nilsson (1996) designed an inclined flat plate dew collector using a special foil as a condensing surface, and tested its performance in diverse locations such as Tanzania and Sweden. Several recent studies (Beysens et al., 2003, 2005, 2006, Jacobs et al., 2008, Muselli et al., 2006, Sharan et al., 2007) examined passive dew collection on inclined surfaces, again testing substrates that would enhance dew drop gravity flow. An angle of 30° from the surface was found to be optimal in terms of the amount of water collected.

Modeling of passive dew collecting on an inclined surface is challenging, as one must include the effect of wind speed and direction on the collecting surface as well as the difference in height above the ground along the course of the collector surface. In addition, because the dew drops run off, the dynamics of the radiation balance on the collection surface must be considered.

In this study, a dew collector was studied in an arid setting. The purpose was to measure and model dew on an artificial surface set parallel to the ground at 15 cm height. This would maximize radiative cooling because of the optimal sky view and simplify the calculations and replications that would otherwise be needed for an inclined surface. Of interest was the extent a dry soil could influence the degree of dew formation on a large flat artificial surface placed just above the ground, and the possibility of edge effects on the artificial surface. A dew collection model can be constructed and calibrated to estimate factors affecting dew input and such a model can then be used to test dew yield at other locations such as at the coast.

The study area is situated in Nizzana (NW Negev desert, Israel) near the Egyptian border, about 40 km away from the Mediterranean coastline (N 30°56', E 34° 22', 190 m a.s.l.). This region consists mainly of linear sand dunes aligned west-east, in the direction of the prevailing wind vector. The Nizzana region receives about 100 mm of rain per year, mainly between November to February. The mean annual minimum and maximum temperatures are 12·5 and 25.9 ^{0}C, respectively. The linear sand dunes here are 50-200 m apart and about 10-25 m high.

Duvdevani (1947,1953) established an extensive network of dew observation stations in Palestine/Israel, He recognized the importance of dew in terms of plant disease and introduced a simple device as a proxy for the daily amount of dew that could occur on a plant. It consisted of a painted wooden block with dimensions 0.32 x 0.05 x 0.025 m that could be placed above the ground surface at levels from 2.5 cm to 1 m. The amount of dew was estimated from the optical comparison of dew drop size/shape on the wooden block to a set of reference photographs that had been

calibrated for mm equivalent depth of dew. His work revealed that there is a high frequency of dew nights even in the desert.

From a dewfall distribution map of the region prepared by Ashbel (1949), one can derive a rough dewfall gradient along a line from the Mediterranean coastline moving southeast into the Negev desert. Near the sea the number of dew nights per year was found to be between 200-250 and the annual dew amount over 100 mm. Moist air is the source for dew and it can be expected that near the sea this is not a limiting factor. There is a gradual drop in dew amount of around 20% for every 10 km away from the coastline in the direction of the Negev desert. Although Duvdevani's annual amounts of dew are now known to be greatly overestimated (see i.e. Zangvil, 1996), the dew frequency observations are a unique set of historical data. The modeling carried out, below, will help assess the dew differences between the NW Negev and a nearby Mediterranean coastal location.

6.2 Experimental set-up

A dew collector was constructed to assess and model the collection of dew from a flat surface. The collector (Fig. 6.1) consisted of 4-cm thick isolation styrofoam (1.20 x 2.50 m) covered with a pigmented common plastic foil with a shortwave abosrptivity of 0.15. The sheet facilitated dew harvesting at sunrise. To reduce heat conduction from the soil, the collector was placed on stakes 10 cm above the soil. Radiative heat exchange with the soil was minimized using an aluminium foil attached under the collector. Aluminium foil has a low emissivity in the thermal infrared and a low aborption coefficient for shortwave radiation.

Figure 6.1: Dew collector plate with infrared thermometer above, and Duvdevani wooden dew block in the foreground resting on short supports.

Nilsson et al. (1994) recommended that the collector surface be hydrophobic and clean to facilitate runoff. On an inclined collecting surface, droplets that start running will coalesce with other drops, thereby enhancing the removal of water into a collecting container at the base. Dust and dirt, however, will accumulate on the surface and thus reduce the dew drop flow efficiency. Another potential disadvantage is that when placing the collector at an angle, the open sky view factor is reduced. This may increase the soil view factor (or vegetation view factor) and thus reduce the net radiative heat loss (cooling power).

In the present set-up we used a common inexpensive plastic foil in place of a special hydrophobic surface. The collection plate was placed horizontally to maximize radiative heat loss. At sunrise the collector was hand-dried with water absorbent tissues, which were then placed in a sealed plastic container of a known dry weight. The container was weighed immediately in the field using an on-site shielded sensitive balance (Mettler, PM1200, Switzerland, 0.001-g accuracy) that had been placed inside a box to protect against wind effects. As the dry tissue weight was also measured beforehand, the weight change of the cloth from the collected dew could be calculated in equivalents of mm day^{-1} (kg m^{-2} day^{-1}).

During the field experiment a complete set of meteorological measurements were made (Table 6.1). Theses measurements were sampled at 0.1 Hz and averaged

over 15 min and stored on a data logger (Campbell 21X). The instruments and data loggers were powered by car batteries and recharged using solar panels.

A Duvdevani wooden dew block (Duvdevani, 1947) was placed near the dew collector (Fig. 6.1). Dew drops that develop on the block are compared with a set of drop photos that have an indicated equivalent in mm of dew. The blocks serve as a general proxy of dew on a wooden surface, but cannot realistically be projected to other substrates. No dew was detected on the Duvdevani block during the experimental period.

Variable	**Instrument**	**Heights,depths (m)**
Temperature, humidity and wind speed		
u	Cup anemometer, Wageningen University	1, 2.5, 6
T_a, T_w	Psychrometer	1, 2.5
T_s	Soil thermometers	-0.01, -0.015, -0.034, -0.05, -0.10, -0.15, -0.2, -0.3
Radiation, infrared thermometry		
R_s	Pyranometer, CM14, Kipp and Zoonen, Delft, Netherlands	
$R_{L\downarrow}$, $R_{L\uparrow}$	2 Pyrgeometers, CG1, Kipp and Zoonen	
T_s, T_c	Soil and collector surface temperature, infrared thermometer, KT14, Heimann, Germany.	
Water, Surface wetness		
	LWS (Leaf Wetness Sensor) coated grid, Model ES-460, Omnidata	0.4 m, 0.4 m, -0.002 m (soil)
Dew total soil	15 Micro-lysimeters, depth: 0.03 m, width: 0.07 m.	

Table 6.1: A list of the meteorological variables sampled, instrument type, measurement height or depth.

6.3 Energy balance model of a dew collector

An energy balance model of a collector was developed based on the collected dew, collector surface temperature and meteorological data. The energy balance of a wet surface (Eq. 6.1) was used to calculate the onset, duration, accumulated dew amount and surface temperature. The collector receives longwave and shortwave radiation from the sky; at night the longwave radiation ranged from 350 Wm^{-2} down to 250 Wm^{-2} (Fig. 6.4). The collector also emits longwave radiation, resulting in a net radiative heat loss. This heat loss will be compensated with heat flux from the air to the collector and by condensation when the collector temperature drops below the

dew point temperature. On certain nights during the experiments, the collector temperature dropped more than 10 K below the air temperature at 2.5 m.

The collector energy balance is:

$$aR_s + \varepsilon R_{L\downarrow} - L_v E - \varepsilon R_{L\uparrow} - H + G_c = 0 \tag{6.1}$$

where α is the shortwave absorption coefficient of the collector (-), R_s is the global radiation (W m^{-2}), $R_{L\downarrow}$ is the incoming longwave radiation (W m^{-2}), ε is the emissivity of the collector surface (-), $\varepsilon R_{L\uparrow}$ is the emitted longwave radiation (W m^{-2}) and G_c is the heat conduction through the insulation towards the collector surface (W m^{-2}):

$$G_c = \lambda_c \frac{T_s - T_c}{d_c} \tag{6.2}$$

where λ_c is the thermal conductivity of the insulation foam of the collector (0.05 W m^{-1} K^{-1}), T_s is the soil temperature, d_c is the thickness of the insulation foam under the collector (m).

The sensible heat flux can be written as (W m^{-2}):

$$H = h_c (T_c - T_a) \tag{6.3}$$

where T_c is the collector surface temperature, T_a is the air temperature at reference height and h_c is the heat transfer coefficient (W m^{-2} K^{-1})

The latent heat flux can be written as (W m^{-2}):

$$L_v E = \frac{M_w}{M_a} \frac{L_v}{P} h_w (e_s - e_a) \tag{6.4}$$

where h_w is the water vapour transfer coefficient (kg s^{-1} m^{-2}), M_w is the molar weight of water (kg mol^{-1}), M_a is the molar weight of air (kg mol^{-1}), P is the ambient air pressure (Pa), e_s is the saturated vapour pressure of a wet collector surface (Pa), e_a is the ambient vapour pressure (Pa) and L_v is the latent heat of vaporisation. A negative sign of L_vE indicates the condensation of dew onto the collector.

Rewriting Eq. 6.1:

$$aR_s + \varepsilon R_L - \frac{M_w}{M_a P} h_w (e_s - e_a) - \varepsilon \sigma T_c^{\,4} - h_c (T_c - T_a) + G_c = 0 \tag{6.5}$$

The temperature of the collector is not known, but the temperature deviation with respect to the air temperature can be expressed in Eqs. (6.4) and (6.5) (Taylor expansion) as:

$$L_v E = \frac{M_w}{M_a P} h_w \left(\frac{de_s}{dT}(T_a)\Delta T + e_s(T_a) - e_a\right) \tag{6.6}$$

$$R_{L\uparrow} = 4\sigma T_a^3 \Delta T + \sigma T_a^4 \tag{6.7}$$

and $\Delta T = T_c - T_a$ (6.8)

This leads to an expression for the unknown collector surface temperature:

$$T_c = \frac{aR_s + \varepsilon R_L + \lambda_c \dfrac{T_s - T_a}{d} - \dfrac{M_w}{M_a P} h_w (e_{sa} - e_a) - \varepsilon\sigma (T_a)^4}{h_c + 4\varepsilon\sigma (T_m)^3 + \dfrac{M_w}{M_a P} h_w \dfrac{de_s}{dT_m} + \dfrac{\lambda_c}{d}} + T_a \tag{6.9}$$

where T_m is the average temperature of collector surface (T_c) and air temperature (T_a). Equation 6.9 can be solved numerically and the result is obtained within a few iterations.

The total dew amout is calculated from the following procedure:

$D_{i+1} = D_i - E_i \Delta t$ while $D_{i+1} \geq 0$

$D_{i+1} = 0$ if $D_i - E_i \Delta t < 0$

Heat and mass transfer through a boundary layer can be described by general transport equations as a conductance times a gradient, as is common in molecular diffusion in still air. A flat plate in a laminar flow develops a boundary layer that at first will be laminar and, depending on plate dimensions and wind speed, will grow and become turbulent over some distance along its characteristic dimension. The transport within a laminar boundary layer is by diffusion. It is easiest to use an integrated form of the boundary layer conductance along the characteristic length of the plate to be able to evaluate exchange processes of the whole surface. It is also easier to work with the ratio of the characteristic dimension over the equivalent boundary thickness, i.e. the Nusselt number dimensionless group (*Nu*). The equivalent boundary layer thickness is equivalent to a still air boundary layer with a certain thickness that would have the same conductance as the turbulent boundary layer. Dimensionless groups are introduced to find universal relationships for transfer coefficients (Ede, 1967; Monteith et al, 1990). The Reynolds number is a dimensionless group characterising the flow:

$$\mathrm{Re} = \frac{ud}{\nu} \tag{6.10}$$

where u is the wind speed (m s^{-1}), d is the characteristic dimension in the direction of the flow (m), ν is the kinematic viscosity of air (m^2 s^{-1}). he heat transfer coefficient (W m^{-2} K^{-1}) is found using Nusselt numbers which is a function of Re numbers:

$$h_c = Nu \frac{\lambda}{d} \tag{6.11}$$

where λ is the thermal conductivity of air (W m^{-1} K^{-1}), *Nu* is the dimensionless Nusselt number, and d is the characteristic dimension (*m*).

Nusselt numbers were experimentally determined for various shapes in wind tunnel experiments (Ede, 1967; Monteith et al, 1990) and they are a function of

Reynolds number under forced convection. Within a certain Reynolds number range they generally have the following shape:

$$Nu = C_1 \, \mathrm{Re}^{C_2} \tag{6.12}$$

where the C_1 and C_2 constants are determined experimentally (Table 6.2 or 6.3).

It is important to note that outdoor wind conditions differ from wind tunnel generated winds. Within wind tunnels, considerable effort goes into minimizing turbulence in the wind flow. Outdoors there will always be turbulence and will thus enhance the exchange coefficients. A discussion of this aspect can be found in Jones (1983) where it is suggested to increase the exchange coefficients by a factor of 1.5. Mitchell (1976) investigated animal shapes but the exchange coefficients seem to be less affected by this difference (only 15%). The reason might be that a round shape has a large surface area directly confronting the wind, whereas a flat plate is aligned with the wind so that a small change in the wind attack angle will immediately affect the boundary layer of the whole plate. Sparrow and Tien (1977) studied heat exchange of flat plates oriented into the wind.

Boundary layer	Range of *Re*	C_1	C_2
Streamline flow	$<2\cdot10^4$	0.60	0.5
Turbulent flow	$>2\cdot10^4$	0.032	0.8

Table 6.2: Nusselt coefficients $Nu = C_1 \, \mathrm{Re}^{C_2}$ for forced convection over flat plates.

Temperature differences between plate and air flow can inhibit free convection and these forces can dominate over forced convection at low wind speeds. Nusselt numbers for free convection are determined using Grasshof numbers:

$$Gr = \frac{d^3 g \beta \Delta T}{\nu^2} \tag{6.13}$$

where g is the gravity constant (m s^{-2}), β is the thermal expansion coefficient (for a gas it is T^{-1} (K^{-1})), and ΔT is the temperature difference between the plate surface and air temperature.

Boundary layer	Range of *Gr*	C_1	C_2
Laminar flow	$<2\cdot10^5$	0.50	0.25
Turbulent flow	$>2\cdot10^5$	0.13	0.33

Table 6.3: Grashoff numbers $Nu = C_1 Gr^{C_2}$ for free convection over flat plates.

Mixed convection is considered to take place between $0.1 < \frac{Gr}{\mathrm{Re}^2} < 16$ and the largest Nusselt number is chosen, either forced or free convection. For numbers greater than this range, free convection dominates; less than this range forced convection is dominant.

Nilsson (1996) suggested calculating the heat exchange coefficient using the same approach as for meter-scale plates as is used in performance studies of solar cells (Duffie and Beckmann, 1991):

$$h_c = 2.8 + 3.0u \tag{6.14}$$

where u is the mean wind speed at condenser height (m s^{-1}).

However Eq. 6.10 is only limited for plates of a size around 0.5 m^2 and it does not provide a detailed analysis for mixed and free convection cases. A comparison with the procedure outlined above shows that both methods compare well for this size of plate.

Applying heat exchange coefficients of plates to large collectors has some limitations. The collectors differ from a plate in that they will only exchange heat and water along one side, as the other side is insulated. A complication is the exchange coefficients for free convection. A cool or hot plate will always generate a density driven flow. However, a dew collector placed horizontally will not have an increased exchange while being cold from above since the bottom side is insulated. Therefore the free convection case will only be considered when the plate is hotter than the air. It could well be that a cold plate suppresses turbulence but this needs further study.

The determination of the wind speed at condenser plate height (0.15 m) is not measured directly. However, there were wind measurements at 3 heights; 1, 2.5 and 5 m. For every time step a function can be fit through the 3 measurement heights.

$$\ln(z) = Au + \ln(z_0) \tag{6.15}$$

where z is the height (m), A is a constant (m^{-1} s) and z_0 is the roughness length (m).

Note that the solution of Eq. 6.15 will give a correct roughness length only during near-neutral conditions. Since the terrain was smooth (z_0 = 0.5 mm) it can be assumed that the extrapolation of the wind speed to 0.15 m height is acceptable.

The mass transfer coefficient for water vapour can be found assuming similarity between heat and mass transfer and correcting for the difference between temperature and water vapour boundary layer thickness. The correction coefficient is the Lewis number Le (-), and it is the ratio between the diffusion coefficients of air ($D_a = 20.8\ 10^{-6}$ m^2 s^{-1}) to that of water vapour ($D_v = 23.4\ 10^{-6}$ m^2 s^{-1}):

$$h_w = Le^{\frac{-2}{3}} \frac{1}{C_p} h_c \tag{6.16}$$

where h_w is the vapour transfer coefficient (kg m^{-2} s^{-1}) and C_p is the specific heat of air (J kg^{-1} K^{-1}).

For inclined plates the convective heat transfer coefficients are larger. A wind tunnel study by Sparrow et al. (1979) on rectangular plates at various orientations found the following correlation over the Reynolds number range of $2\cdot 10^4 - 9\cdot 10^4$:

$$Nu = 0.86\,\mathrm{Re}^{1/2}\,\mathrm{Pr}^{1/3} \qquad (6.17)$$

where the characteristic length in the *Re* number is four times the plate area divided by the plate perimeter and *Pr* is the Prandl number.

6.4 Measurements, model validation and discussion

For each time step the input variables for the model were the windspeed at 1 m height, the incoming global radiation, the incoming longwave radiation, the air temperature and wet bulb temperature (2.5 m.) (Figs. 6.2 a-c) and soil surface temperature. The constants used for the collector are in Table 6.4.

Collector constant	symbol	value	units
Thermal conductivity	λ	0.05	W m^{-1} K^{-1}
Insulation thickness	d_c	0.04	m
Shortwave absorption coefficient	α	0.15	-
Emissivity	ε	1	-
Height above surface		0.15	m
Characteristic dimension	d	2.5	m

Table 6.4: Collector constants used in the model.

After sunrise the condenser dries quickly. The model sets the latent heat exchange coefficient to zero as soon as the condenser becomes completely dry. The onset of dew was calculated with a second model run where the latent heat exchange coefficient is not set to zero. This procedure enabled an accurate surface temperature simulation of a wet and a dry collector. The model was validated with the surface temperature measurements and the dew yield. The temperature calculated from Eq. 6.9 was compared with the surface temperature as measured with the infrared thermometer (Fig. 6.2e).

Heat exchange coefficients derived from Nusselt numbers of heat transfer theory were calculated from the wind speed derived from the wind profile measurements. The wind speed measurements were not located at the collector height (1 m instead of 0.15 m) and therefore a simpler approach could give better results. Equation 6.14 was tested to calculate exchange coefficients; it is interesting to note that good results from Equation 6.14 were obtained from the data of the 1 m wind speed sensor if the constant in Equation 6.14 was omitted. The reason for this could be related to the fact that the micro-cup anemometers have a very low dynamic and

static starting speed (dynamic: 0.1 m s^{-1}). The 1 m wind speed measurements might be a good scalar for the large-scale motions that govern the exchange processes at 0.15 m height. The soil surface around the collector was very smooth, however the large-scale motions can be related to the larger scale roughness of the terrain affected by the adjacent linear dune slopes.

The calculated surface temperature was not always in line with the measurements during daytime (Fig. 6.2e). The reason might be the small variation in the shortwave absorption coefficient due to dust accumulation on the collector. The soil surface albedo is around 0.35 (shortwave absorption coefficient 0.65), therefore the soil surface temperature becomes hotter than the collector. Dust on the collector surface would raise the temperature during daytime. On the last days of the measurement period, the difference deviated more since there was no dew and thus no surface cleaning. The nocturnal simulations show less deviation from measurements since they are not affected by shortwave radiation.

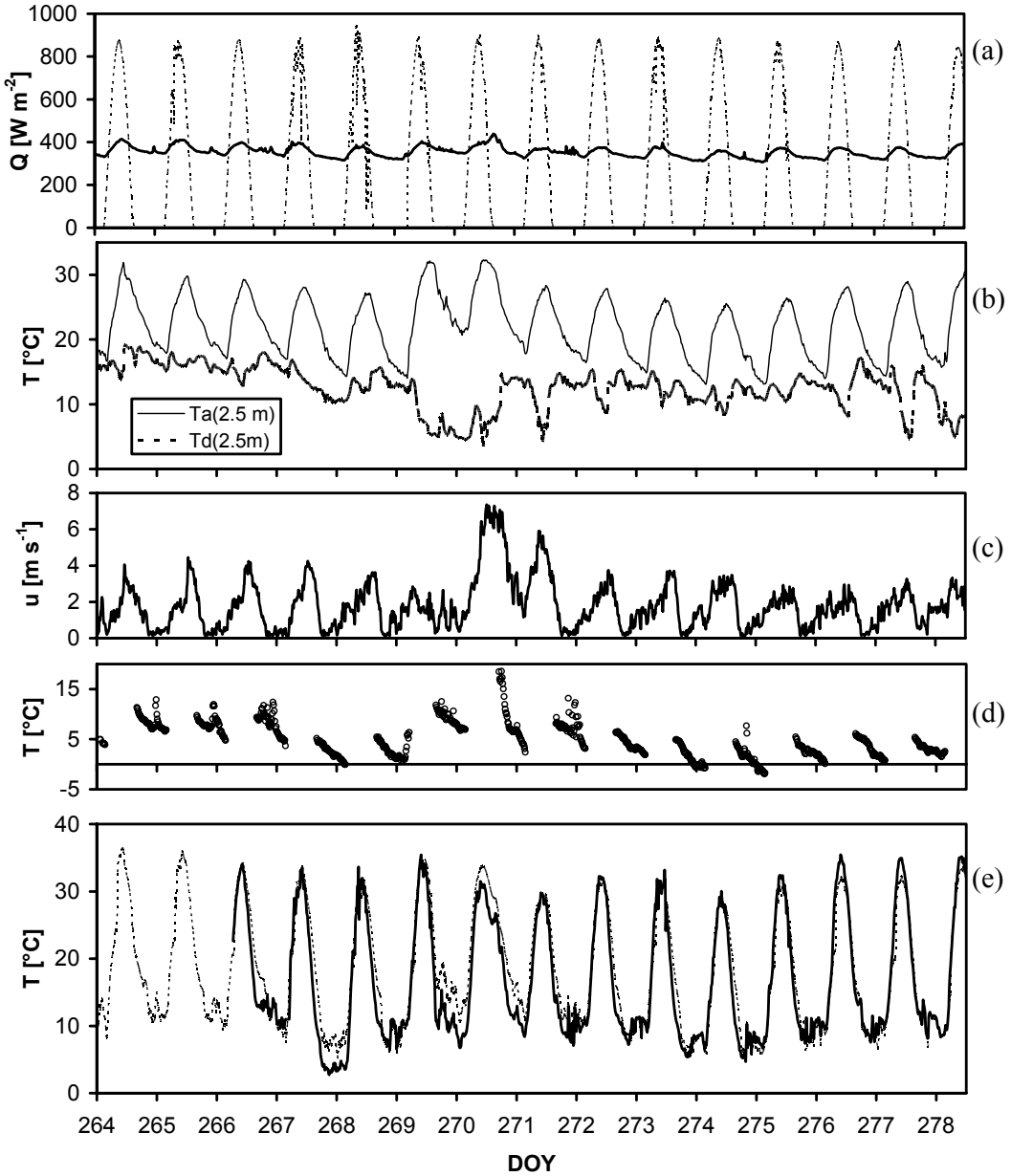

Figure 6.2: (a) dashed line: Incoming global radiation (R_s) and solid line: longwave incoming radiation ($R_{L\downarrow}$), (b) Air (T_a) and dewpoint (T_d) temperature at 2.5m, (c) windspeed at 1 m., (d) nocturnal effective sky temperature (assuming emissivity of 1), (e) measured and modelled (dashed line) collector surface temperature. The collector temperature measurements began on day of year 264. DOY 264 – 276 is 23 September - 3 October 1997.

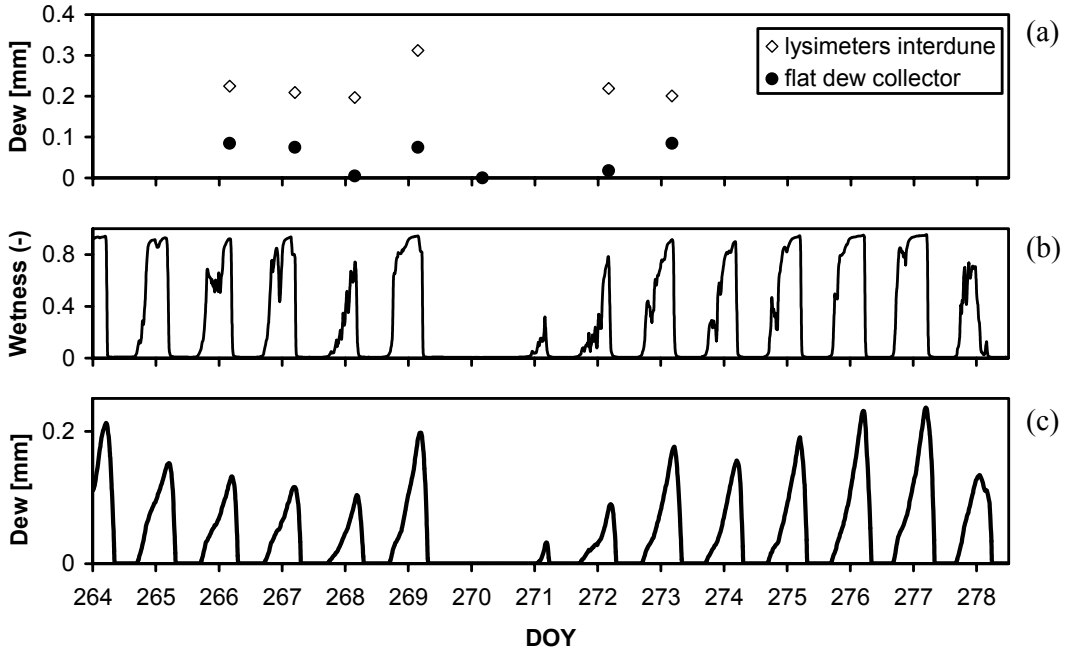

Figure 6.3: (a) Measured accumulated dew on collector and in the soil (microlysimeters), (b) wetness measurements from a leaf wetness sensor, where the output changes when moisture accumulates on its surface (a printed circuit board, 100 x 60 mm at 0.4 m height) and (c) simulated dew on the collector.

The next step was to test the modelled wetness periods and dew yields. The wetness periods compare well with the artificial leaf wetness sensor (Figs. 6.3b, c). The wetness measurement output quickly rises when the surface becomes wet, thus it is not an accurate method for quantifying dew. In addition, the hygroscopic paint (Latex) on the leaf wetness sensor responds to high relative humidity. Therefore the sensor surface can be considered wet only at a certain wetness level. By fully wetting the surface, the signal level is around 0.8 (-). The scale of the wetness sensor plate did not compare with that of the collector and was located higher, at 0.4 m. height. The leaf wetness sensor, however, did collect dew because of its much higher placement above the ground surface. Duvdevani (1953) tested wetness sensing blocks at several heights and found that a block placed higher above the ground surface yielded much more dew if the soil was dry.

Dew was collected at sunrise from the collector using absorbent cloths and the dew amount was obtained by weighing for 7 mornings. The average dew yield was 0.05 mm per night with a maximum of 0.085 mm, with one day without dew (Fig. 6.3a). Dew formation is absent during a dry spell where a mesoscale wind system develops from the east and suppresses the sea breeze circulation (see Fig. 6.2b,c, afternoon day 269 till end of day 270). Model simulations over the same period show an overestimation by a factor of 2.2 (Fig. 6.3c).

Why did the surface temperature simulations perform so well? The reason why the modelled temperature compared well with the infrared thermometer (IRT) could be related to the limited view factor (0.3 x 0.3 m.) of the IRT, so only a central spot was measured. This central spot might also have a dew amount similar to the simulated amount. This means that the simulations might be correct for the central collection surface only. This is also supported by visible inspection that revealed that dew amounts were smaller near the edges in the morning hours. The collection method leads to an underestimation because a small portion is lost by evaporation from the cloth during wiping in the morning hours.

Measurements with microlysimeters showed that the amount of dew on the soil surface surrounding the collector was much higher than on the collector itself (Fig. 6.3a), even though the soil did not always cool below the dew point temperature of the air above. The explanation is that a very dry soil surface combined with a higher salt content on its surface could reduce the vapour pressure and thereby dew formation will take place below a relative humidity of 100%. The soil is so dry that it acts similar to a dessicant. The model overestimation was also a result of the low placement of the collector. At a level of only 0.15 m. above the ground, the air reaching the collector can have contact with the soil, which results in some drying of the air and may have a large effect near the collector edges. The condenser itself acts as a kind of oasis, i.e. a cold spot being 5 to 10 K colder than the surrounding soil. The collector was too small to neglect these edge effects. A second proof for these edge effects is that the small Duvdevani block, which was placed at the same height, did not collect any dew during the selected period. Duvdevani (1953) also shows that for a dry soil there is a strong dew gradient with height, but not when the soil is wet. This supports the view that the soil acts as a dessicant. Duvdevani made observations from 0.025 m to 1 m height and showed that the largest amounts above dry soil were on the 1 m high Duvdevani block. A much larger dew collector would reduce the edge effects and increase accumulated dew (mm). It can be expected that the higher yields as predicted by the model could be more realistic for larger plates, thus part of the overestimation can be attributed to the limited size of the collector (Figs. 6.3a, c).

Selecting a foil with a lower shortwave absorption coefficient would increase dew duration. Simulation shows that this could extend the dew duration by 1 hour.

A flat plate collector is not practical for passive water collection because it does not initiate drop runoff. A collector placed at an angle, a set-up as used by Nilsson et al. (1994) and Beysens et al. (2006) can now be simulated. The cooling power will be reduced somewhat because the total sky view will be less and the collector will see part of the desert soil. The soil surface temperature measurements were used to calculate the additional infrared radiation load onto the collector. This was inserted into the collector model and the output drops 24% at a slope angle of

30°. Arranging collectors in a way such that the surfaces face each other could help improve their collective cooling power by reducing the ground view factor.

Another consideration is that there is a limited wind range for optimal collector performance. High wind speeds will limit the resulting temperature drop from radiative cooling and will increase sensible heat towards the collector, whereas very low wind speeds will limit transport of moist air. By simulating the behaviour at different wind speeds it became evident that a higher and windier exposure in the experimental site would have been better. Model simulations show an increase of 10% for a location 5 m higher (wind effect only, on top of a dune). This location would also generate fewer problems with interdune soil which dries the air as discussed previously. A wind speed of around 1 m s^{-1} seems optimal.

The cooling power depends on the emissivity of the collector surface and it was chosen as 1. This is true for a wet surface, but before any water condenses it must cool down to the dew point temperature. This will depend on emissivity but also on the thermal mass of the collector. Since the collector consists of styrofoam and a plastic sheet, it has a low thermal mass and might not be too critical. However, Nilson (1993) suggested using a special pigmented foil to enhance longwave emissivity. A closer look at the condensing surface reveals that there are always dry areas and wet areas, since the dew water collects in droplets on the hydrophobic surface. Drop coalescence will release dry surface area so the area occupied by water droplets remains constant after some time. The contact angle between the water drops and the surface determines the final wet/dry ratio of the total collector surface (Beysens, 2006). This surface distribution has an effect on the average emissivity of the total surface so a pigmented foil might still enhance cooling during dew formation if the surface is not hydrophilic. A hydrophilic surface would have one smooth layer of water. A collector placed at an angle would profit more from a high emissivity foil since dew water constantly runs off. A simulation with a lower emissivity shows that the dew yield depends linearly on the emissivity, i.e. a surface with an emissivity of 0.9 collects 10% less.

The soil surface remains warmer than the dew collecting surface during the evening, thus good insulation between the soil and the collector is important. The heat leakage through the insulation is a function of the temperature difference between collector surface and the underside of the collector. It is not straightforward to calculate the temperature of the underside of the collector. The model calculated the heat leakage towards the collecting surface by assuming that the bottom side of the collector has a temperature equivalent to that of the soil surface. This is the worst case, since the collector is not in contact with the soil and has a radiation shield (aluminium foil) present between the soil and collector. In reality the temperature gradient will be smaller. To test the importance of good insulation, the model was rerun with an ideal insulator (λ=0) and resulted in a dew yield increase of 15%.

6.5 Simulating dew collector performance for conditions close to the sea

Daily dew amounts in a coastal desert also depend on the distance from the sea as discussed in the introduction. More dew yield can be expected near the coastline. According to Ashbel (1949), who prepared a dew distribution map for Israel using long-term results from a Duvdevani wooden block observation network, a 20% drop in dew yield per 10 km from the sea is predicted, with annual dew yield for Nizzana projected to be around 80 mm. Although this amount is far too high as compared to more recent measurements (Zangvil, 1996; Jacobs et al., 2000), Ashbel's annual dew frequency map is based on daily observations and represents a rare set of dew occurrence data. The Nizzana measurements were 40 km south of the coastline so dew yield should theoretically be 2.5 times greater near the sea. A coastal location was thus simulated with the model. Comparable coastal meteorological data is lacking from that period, however a dataset was obtained for an Israel Ministry of Agriculture meteorological station 8 km from the coastline (Azrikam, 31 45' N, 34 42' E) but without incoming longwave radiation data. In practice, the net radiative heat loss will be reduced in a moist atmosphere and this can be estimated by modelling the longwave incoming radiation (Brunt (1932); Kustas et al. (1989)). According to Kustas et al. (1989):

$$Q_{l\downarrow} = 0.642\left(\frac{e_a}{T_a}\right)^{\frac{1}{7}} \sigma T_a^{\,4} \qquad (6.18)$$

where e_a is the vapour pressure (Pa) at reference height and T_a is the temperature at reference height (K).

The estimate by using the Brunts model was found to have an error of about 7% for clear days, thus we used Eq. 6.18. This form compared well with the measured data on clear days (within 2%) (Fig. 6.4).

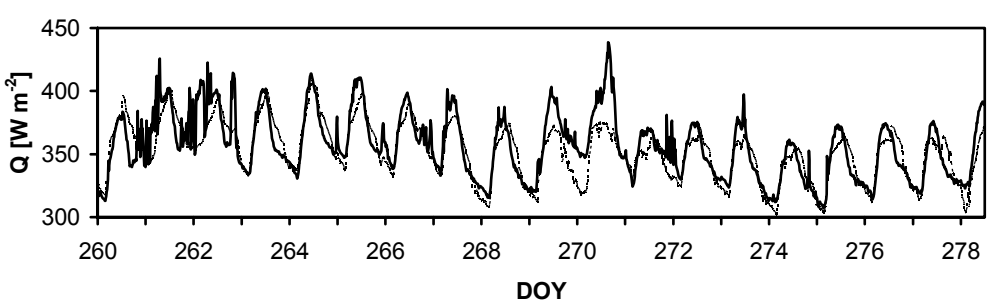

Figure 6.4: Longwave incoming radiation (straight line) and modelled radiation (dashed line) using weather station temperature, humidity data, and assuming clear skies.

The deviations in the first 3 days can be attributed to clouds, and the large underestimations around days 269-270 were caused by a sand storm (Figs. 6.4 and 6.2a,b,c).

The dew collector model was run twice to estimate differences in dew yield between Nizzana and the Azrikam station 8 km away from the coast. The initial run was with Nizzana conditions and with modelled longwave incoming radiation according to Equation 6.12 in order to make a fair comparison. The second run included the Azrikam conditions, with the modelled longwave radiation (Eq. 6.12). The modelled yield at Azrikam increases 15% or 0.008 mm day^{-1}, which is less than than the dew gradients between the coastal region and the inland desert as documented by Ashbel (1949) and others. By running the collector model (and longwave radiation model) again with the Azrikam data, but assuming a saturated atmosphere during the night, one can test the gain if atmospheric moisture was not a limiting factor. The increase in dew yield then becomes a factor of 2 higher. It seems that the Azrikam station receives air from a katabatic wind direction (during the night), which might explain why the specific humidity does not differ much from the Nizzana location. Kidron (1999) reported that dew in the Negev desert increases between 0.015 and 0.03 mm day^{-1} 100 m^{-1} at higher altitudes despite the longer distance from the sea. He compared the Nizzana location with two stations further inland and at higher altitude: Sede Boker (at 500 m altitude) and Har Harif (about 40 km south of nizzana at 1000 m altitude). Therefore the coastal distance reduction might be only valid for low altitude locations. The reduction of incoming longwave radiation at higher altitudes would be a reasonable explanation for this increase. Kidron (1999), however, used a house-hold absorbent cloth to measure dew and thus the amounts could be questioned.

It is interesting to note that the Nizzana dew yields calculated with the modelled longwave radiation data were almost identical with the model run with the measured longwave radiation. This seems unusual, but the large underestimation of the modelled longwave radiation occured during dust-storm conditions where no dew would be generated by the model.

6.6 Concluding remarks

During the experimental campaign, the passive flat-plate dew collection (3 m^{-2}) experienced an average dew yield of 0.05 L m^{-2} day^{-1} with a large variation of ±0.04 L m^{-2} day^{-1}. Modelling of a large flat collector in the Nizzana area with improved insulation and placed at a higher elevation away from the interdune, showed that more than 0.2 mm day^{-1} of dew could be generated on an average dew night. Runing the model with a dataset of a meteorological station 8 km from the coast show a 15% increase. The model simulations show that 0.14 mm dew day^{-1} averaged over 18 days (which included a dry spell) is possible. However this amount can only be

attained at a location high enough away from dry soils and exposed to a wind speed of around 1 m s^{-1}. In Nizzana the air humidity is a limiting factor. Running the dew collector model for a location at the coast, and assuming a saturated atmosphere during the night, gives a dew yield increase by a factor of 2. In reality this value will be lower, since the coastal winds will not be saturated during nocturnal conditions.

Acknowledgements

This research was funded in part by the Dutch Technology Foundation (STW). The Arid Ecosystems Research Centre of the Hebrew University of Jerusalem supported the field experiment carried out in Israel.

REFERENCES

Ashbel, D., 1949. Frequency and distribution of dew in Palestine. 1949. Geogr. Rev. 34:291-297.

Beysens, D., Milimouk, I., Nikolayev, V., Muselli, M. and Marcillat, J. 2003. Using radiative cooling to condense atmospheric vapor: A study to improve water yield. J. Hydrol. 276: 1-11.

Beysens, D., Muselli, M., Nikolayev, V., Narhe, R.. and Milimouk, I., 2005. Measurement and modelling of dew in island coastal and alpine areas. Atmospheric Research 73: 1-22.

Beysens, D., Muselli, M., Milimouk, I., Ohayon, C., Berkowicz, S., Soyeux, E., Mileta, M. and Ortega, P., 2006. Application of passive radiative cooling for dew condensation. Energy 31; 1967-1979.

Beysens, D., (2006) Dew nucleation and growth. C.R. Physique 7, 1082-1100, Academie des sciences. Published by Elsevier Masson SAS.

Beysens, D., Muselli, M., Milimouk, I., Ohayon, O., Berkowicz,S.M., Soyeux, E., Mileta, M., Ortega, P. (2006). Application of passive radiative cooling for dew condensation. Energy. 31:1967-1979. doi.10.1016/j.energy.2006.01.006.

Duvdevani, S. 1947. An optical method of dew estimation. Q. J. Royal Meteorol. Soc. 73: 282-296.

Duvdevani, S. 1953. Dew gradients in relation to climate, soil and topography. Proc. Intl. Symp. Desert Research. Research Council of Israel. Special publ No. 2; 136-152.

Heusinkveld, Bert G., 1998: preprint 10th Symposium on meteorological observations and instrumentation, p.300.

Muselli, M., Beysens, D., Marcillat, J. and Milimouk, I. 2006. A comparative study of two large radiative dew water condensers. J. Arid Environ. 64: 54-76.

Duffie, J.A., Beckman, W.A. (1991).Solar Engineering of Thermal Processes (Wiley, NY).

Ede, A.J. (1969). An Introduction to Heat Transfer (Pergamon Press Ltd, London)

Jacobs, A.F.G., Heusinkveld, B.G. and Berkowicz, S.M. 2008. Passive dew collection in a grassland area, The Netherlands. Atmospheric Research 87: 377-385, doi:10.1016/j.atmosres.2007.06.007.

Jones, H. G.: 1983, *Plants and Microclimate*, Cambridge University Press, Cambridge, p. 323.

Kidron G.J., 1999. Altitude dependent dew and fog in the Negev desert, Israel. Agricultural and Forest Meteorology, Vol. 96, 1-4

Kustas W.P., R.D. Jackson and Asrar, G., (1989). Estimating surface energy-balance components from remotely sensed data, *Theory and applications of optical remote sensing*, G. Asrar Ed., John Wiley & Sons, New York, pp. 604-627.

Mitchell, J.W., 1976. Heat transfer from spheres and other animal forms. Biophysical J., 16, 561.

Monteith J.L., Unsworth M.H., 1990. Principles of Environmental Physics. Chapman and Hall, New York, 291 pp.Nikolayev, V., Beysens,D., A. Gioda, A., Milimouk, I., Katiushin, E. and Morel, J.P. 1996. Water recovery from dew. J. Hydrol. 182: 19-35.

Nilsson, M.J., 1994: Thesis 'Optical Scattering Properties of Pigmented Foils for Radiative Cooling and Water Condensation: theory and Experiment'

Nilsson, T., Vargas, W.E., Niklasson, G.A., Grangvist, C.G., 1994. Condensation of water by radiative cooling. Solar Energy 5, 310–317.

Nilsson, T. 1996. Initial experiments on dew collection in Sweden and Tanzania. Sol. Energy Mater. Sol. Cells 40: 23-32.

Nilsson, T., Vargas, W.E., Niklasson, G.A. and Granqvist. C.G. 1994. Condensation of water by radiative cooling. Sol. Energy 5:310-317.

Pedro, M.J., Jr. and Gillespie, T.J., 1982: Estimating dew duration. II. Utilizing standard weather station data. Agric. Meteorol. 25: 297-31

Sharan, G., Beysens, D. and Milimouk-Melnytchouk, I. 2007. A study of dew water yields on galvanized iron roofs in Kothara (North-West India). J. Arid Environ. 69: 259-269.

Sparrow, E.M. and Tien K.K. (1977).Forced Convection Heat Transfer at an Inclined and Yawed Square Plate - Applications to Solar Collectors. J. Heat Transfer, 99 (4): 507-512.

Steinberger, Y., 1989: The influence of autumn dewfall on spatial and temporal distribution of nematodes in the desert ecosystem. J.Arid Environments 16-177-183.

7 Effect of open path gas analyzer wetness on eddy covariance flux measurements; a proposed solution

Accepted by Agricultural and Forest Meteorology

Bert G. Heusinkveld, Adrie F. G. Jacobs, and Albert A. M. Holtslag

Wageningen University, Meteorology and Air Quality Group, P.O.Box 47, 6700AA Wageningen, The Netherlands

Abstract

Open path gas analyzers are popular in eddy covariance flux measurements of trace gasses (i.e. CO_2). The quality of the data, however, may be influenced by several factors. Exposure in an outdoor environment invariably causes the instrument to become colder or warmer than the air temperature. Instruments with internal temperature regulation and/or from heat generated by active electrical components can also influence the sensor temperature. In addition, sensors can have condensation problems on their optical windows thus affecting the quality of the measurement. Unreasonable measurements have been widely discussed, especially in moist, high-latitude regions. As this is a very important research problem facing flux studies, we examined how wetness (dew and raindrops) on the surface of the focus lens of the popular LI-COR LI-7500 infrared gas analyzer may affect flux measurements from the open-path eddy-covariance system. Field experiments showed that additional sensor heating may inhibit dew formation yet greatly improve the quality of flux measurements. A detailed energy balance approach was used to model the gas analyzer window temperature under environmental conditions and dew effect through a pair of LI-COR LI-7500, with and without heated treatment, in a grassland ecosystem in the Netherlands. With the proposed model, existing datasets can be filtered for dew events. Data from three different flux measurement sites were then used to assess the magnitude of dew effects on longer time-sales; two years from the Netherlands and three weeks of data from an arid coastal desert. About 30% of the measurements were affected by dew in the grassland area versus 4% in the arid region during the dry season. Sensor heating suppresses dew formation but might lead to errors in trace gas fluxes evaluated over long periods, thus we analyzed how sensor heating or cooling affects trace gas flux measurements. Additions to a recent (2006) correction and application to a horizontally and vertically oriented LI-COR LI-7500 are presented as they deal with sensor heating problems in eddy covariance systems. The sensor energy balance model, together with the proposed modified sensor heating corrections, were used to estimate sensor temperature effects on long-term scale CO_2 flux measurements and showed that additional heating does affect the turbulent trace gas CO_2 fluxes but is very minor, especially for a horizontally mounted LI-COR LI-7500 gas analyzer. Further efforts are urgently needed to improve the data quality and quality of flux measurements.

Keywords: Eddy covariance, CO_2 flux measurement, density correction, open path gas analyzer, condensation problems

7.1 Introduction

Open path gas analyzers directly measure the density of a gas component in the atmosphere. Such analyzers, in combination with a fast 3-dimensional wind sensor, can be used to measure turbulent fluxes of trace gasses (Fig. 7.1). Fluxes can be evaluated over a certain time interval and are calculated from the covariance of fast measurements of vertical wind speed and concentration of the trace gasses: $F = \overline{w'\rho'}$, where w is the vertical wind speed (m s^{-1}) and ρ is the density (kg m^{-3}) of the trace gas.

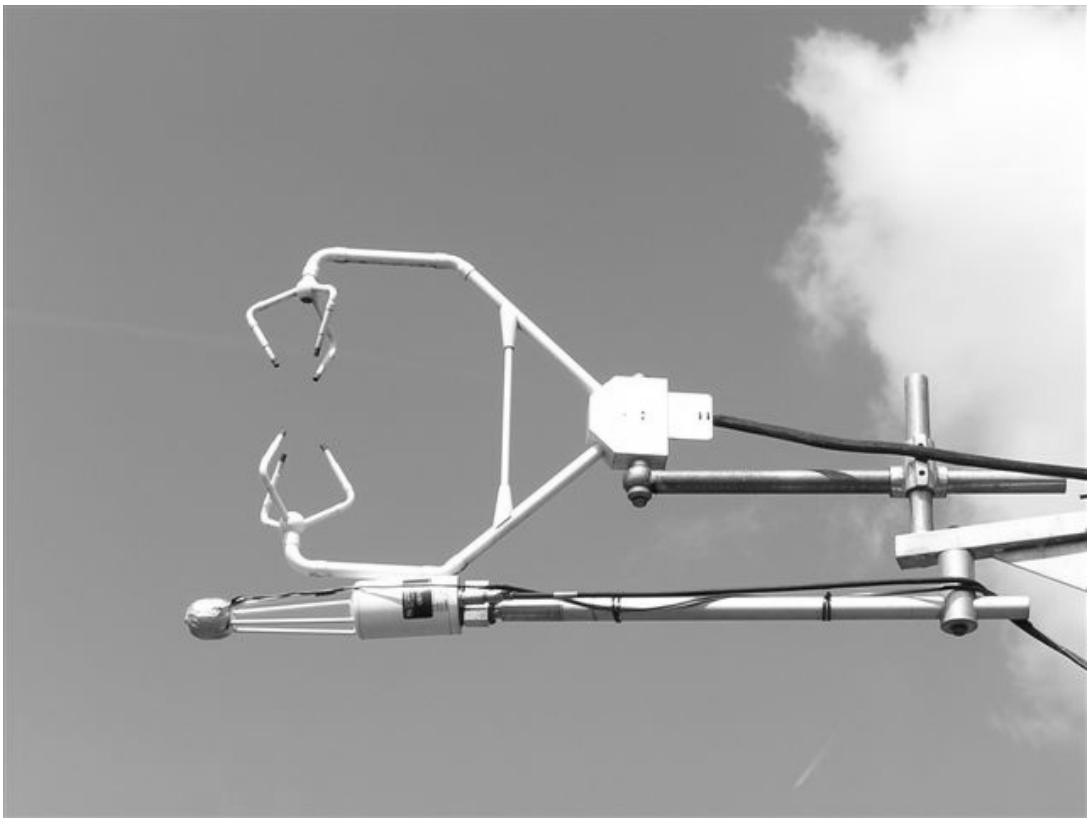

Figure 7.1: Eddy covariance set-up with a sonic anemometer located above a LI-7500 CO_2 and H_2O open path gas analyzer with an additional 0.7 Watt heating element attached to the detector housing (left part) using a low emissivity aluminium tape.

The LI-COR LI-7500 (USA) gas analyzer, the focus of this study, is a widely-used instrument for studying CO_2 exchange processes (Fig. 7.2). It is important that the optical path and windows of these analyzers remain free of contamination. The LI-7500 instrument manual states that water droplets (dew) on the windows can be tolerated to a certain extent; the automatic gain value will increase, but the calibration is unchanged. This is probably due to the differential measurement technique whereby double wave bands are used for each gas (one reference and one sensitive to the gas of interest). In essence, LI-COR assumes that infrared light does not penetrate the water

droplets. In this study the effects of dew are investigated since light in both reference and absorption bands might still pass through a very thin layer of water where the water absorption band is less transparent. Hence problems may arise that might be avoided by installing an extra heating element. This possibility and the impact of extra heating were tested in the present paper.

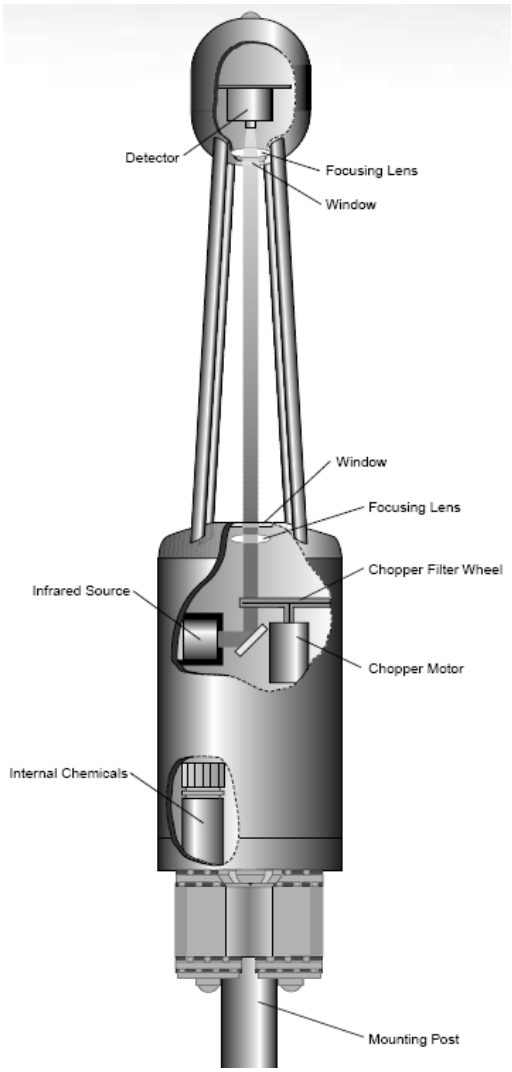

Figure 7.2: LI-COR LI-7500 open path infrared gas analyzer with detector housing (top part, diameter 0.045 m, length: 0.053 m) and main cylindrical housing containing chopper and infrared source (diameter: 0.064 m, length: 0.116 m) (picture courtesy LI-COR USA).

The separate turbulent eddies that transport trace gasses also transport heat and water vapor. This transport has an effect on the air density and, since these density changes are correlated to the vertical wind speed, a correction is needed to compensate. This correction was first outlined by Webb et al. (1980), called the Webb-Pearman-Leuning correction (WPL), and stressed the importance of avoiding

artificial heat sources near the eddy covariance system. The LI-7500 does have some internal heating and an additional heating element could affect the measurements. According to LI-COR only some heating occurs inside the main cylindrical sensor head but not inside the small detector housing at the tip of the sensor head. This is very well illustrated by Amiro et al. (2006) in which they included a picture of a LI-7500 in a cold environment. In the photo rime and frost cover the detector housing but not the cylindrical housing containing the source and chopper, i.e. clear evidence of heating. The warm surface of the open path sensor creates a boundary layer of warmer air just above the sensor surface and affects the measured concentration. Accordingly, one cannot simply install a heating element at the sensor head detector housing to avoid dew and rime.

A sensor heating correction as suggested by Burba et al. (2006a), hereafter called the BAXD1 correction, might provide a correction. Burba et al. (2006a) appear to have explained the differences found between flux stations equipped with a closed path analyzer and flux stations operating with an open path analyzer. The BAXD1 correction was later modified, hereafter called the BAXD2 correction (Burba et al., 2006b). The effect is rather small and almost zero on flux corrections evaluated over hourly intervals. However, the BAXD1 and 2 corrections might bridge the differences found in Net Ecosystem Exchange (NEE) budgets for CO_2 between open and closed path analyzer equipped flux stations when evaluated over a full year. The BAXD1 and 2 corrections seems to correct the apparent off-season CO_2 uptake according to Burba et al. (2006a,b). Amiro et al (2006) found CO_2 uptake during winter months that could not be explained, and thus tested the BAXD1 correction concept. As they did not have detailed sensor temperature data, estimates were made but without real improvements.

A solution to dew problems may require an additional heating element and create a possible problem in flux measurements. An evaluation of possible errors and an analysis and possible refinement of the BAXD2 correction for horizontally or vertically oriented open path analyzers is presented here. These refinements are important since they incorporate environmental conditions, such as radiative cooling and dew, and can make the correction universally applicable to all types of open path gas analyzers with our without internal heating.

7.2 Open path sensor head temperature

To avoid condensation problems, the temperature of the sensor head windows should remain above the dew point temperature. In order to detect condensation problems in existing data sets one needs a model to calculate the temperature of both windows of the sensor head. These temperatures can also be used to apply possible corrections to trace gas flux measurements. The widely-used open path analyzer LI-7500 in Fig. 7.2 (LI-COR, USA) is evaluated here but can also be applied to other sensors. The LI-7500 sensor head consists of two housings with the detector housed in

the top (Fig. 7.2), hereafter called the detector-housing (11.6 x 6.4 cm), with the cylindrical housing containing the infrared source and chopper, hereafter called the source-housing (5.3 x 4.5 cm) (Fig. 7.2). The temperatures of both elements of the LI-7500 sensor head can be found by solving the energy balance of these two housings:

$$P_s + R_{in} = A_s(H + L_v E + R_{Ls}) \tag{7.1}$$

where P_s is the power consumption of the instrument (J s^{-1}), R_{in} is the short- and long-wave radiation balance on the housing (J s^{-1}), A_s is the total surface area of the cylindrical surface area of the housing which is almost cylindrical (m^2), H is the sensible heat flux (W m^{-2}), L_vE is the latent heat flux (W m^{-2}), and R_{ls} is the longwave radiation emission of the housing (W m^{-2}). The internal power consumption is negligible for the detector-housing as explained by Burba et al. (2006a), but the source-housing does have internal heating. Part of the internal heating is due to a temperature regulation system in the source housing (Burba et al. 2006a) and partly due to electronic power dissipation (chopper engine, semi conductor circuits, source, etc.). The heating increases at low temperatures ($P_s = 4.8\ e^{-0.040T}$), where T is temperature in °C. This was tested in a climate chamber between -10 and +25 °C by measuring the power consumption of the instrument. The power consumption is lower for newer generation electronics ($P_s = 3.2\ e^{-0.036T}$). The power consumption measurements might not have been accurate because it was not possible to measure the electrical currents only to and from the sensor head. Thus for each measurement the difference was taken between the power consumption with and without the sensor head attached (total error estimate +/- 20%). However, the results do not differ too much from published values (Burba et al. 2006a).

The radiation balance of the instrument, R_{in}, is composed of direct, diffuse and reflected shortwave radiation, incoming longwave radiation, $R_l^{\downarrow}$ (W m^{-2}), and emitted longwave radiation, $R_l^{\uparrow}$ (W m^{-2}), from the surface below:

$$R_{in} = \frac{A_s}{2}\varepsilon(R_l^{\downarrow} + R_l^{\uparrow}) + A_e(1-\alpha_s)R_b + \frac{A_s}{2}(1-\alpha_s)R_d + \frac{A_s}{2}\alpha(1-\alpha_s)R_s \tag{7.2}$$

where A_e is the instrument cross-section surface area (m^2), R_s is the incoming global solar radiation (W m^{-2}), R_d is the diffuse solar radiation (W m^{-2}), R_b is the direct solar radiation (W m^{-2}), α is the albedo of the underlying land surface, α_s is the albedo of the sensor, and ε is the emissivity of the instruments housing.

The direct solar radiation mainly heats the equivalent cross-section area A_e, whereas the diffuse shortwave incoming and the land surface reflected global radiation, assuming a lambertian surface, receives radiation over an area of $0.5A_s$. The sensible and latent heat fluxes can be expressed as (Monteith and Unsworth, 1990):

$$H = h_c(T_s - T_a) = h_c \Delta T \tag{7.3}$$

$$L_v E = \frac{0.622}{P} h_w(e_s(T_s) - e_a) \tag{7.4}$$

and emitted longwave radiation:

$$R_{ls} = \varepsilon\sigma T_s^4 \tag{7.5}$$

where h_c is the heat exchange coefficient (W m^{-2} K^{-1}), T_s is the housing surface temperature (K), T_a is the air temperature (K), h_w is the exchange coefficient for water vapor (W m^{-2}), e_s is the saturated vapor pressure (Pa), e_a is the ambient vapor pressure (Pa), and ΔT is the temperature difference between the air and the housing (K).

To find the temperature of the housing, the temperature deviation with respect to the air temperature can be expressed in Eqs. (7.4) and (7.5) (Taylor expansion) as:

$$L_v E = \frac{0.622}{P} h_w \left(\frac{de_s}{dT}(T_a)\Delta T + e_s(T_a) - e_a\right) \tag{7.6}$$

$$R_{ls} = 4\varepsilon\sigma T_a^3 \Delta T + \varepsilon\sigma T_a^4 \tag{7.7}$$

By combining Eqs. (7.2), (7.3), (7.6), (7.7) into (7.1) and after some rearranging, the housing surface temperature is given by:

$$T_s = \frac{P_s + R_{in} - \frac{0.622}{P} h_w A_s (e_s(T_a) - e_a) - \varepsilon\sigma (T_a)^4 A_s}{h_c A_s + 4\varepsilon\sigma (T_a)^3 A_s + \frac{0.622}{P} h_w \frac{de_s}{dT}(T_a) A_s} + T_a \tag{7.8}$$

Equation 7.8 must be solved iteratively since the heat exchange coefficient h_c is a function of the difference between housing temperature and the free atmosphere, T_a,and this affects T_s. The iteration starts with a sensor temperature equal to ambient temperature. Within the iteration procedure the outcome of Eq. 7.8 is inserted into Eq. 7.1 and tested for imbalance. The imbalance converges to near zero after only a few iterations.

The heat transfer coefficients can be calculated using non-dimensional Nusselt numbers (*Nu*) (Monteith and Unsworth, 1990):

$$Nu_f = 0.32 + 0.51 Re^{0.52} \qquad Re < 10^3 \tag{7.9}$$

$$Nu_f = 0.24 Re^{0.6} \qquad Re > 10^3 \tag{7.10}$$

where *Re* is the Reynolds number for the sensor:

$$Re = \frac{ud}{\nu} \tag{7.11}$$

where u is the wind speed at sensor height (m s^{-1}), d is the characteristic diameter (m), and ν is the kinematic viscosity of air (m^2 s^{-1}). Grasshof numbers are used to determine free or mixed convection cases:

$$Gr = \frac{d^3 g\beta |T_s - T_a|}{\nu^2} \tag{7.12}$$

where g is the acceleration of gravity (m s^{-2}) and β is the expansion coefficient (K^{-1}).

Free convection occurs if $\frac{Gr}{Re^2} > 16$ then $Nu = 0.48Re^{0.25}$ and mixed convection if $0.1 < \frac{Gr}{Re^2} \leq 16$ then

$$Nu = 0.48Re^{0.25} \text{ if } Nu_f < 0.48Re^{0.25} \text{ otherwise } Nu = Nu_f \tag{7.13}$$

The transfer coefficient for heat is then given by (W m^{-2} K^{-1}):

$$h_c = \frac{Nu\lambda}{d} \tag{7.14}$$

and the transfer coefficient for evaporation (W m^{-2}):

$$h_w = 1.07\frac{L_v(T_a)}{C_p}h_c \tag{7.15}$$

where L_v is the latent heat of vaporisation (J kg^{-1}) and λ is the thermal conductivity of air (W m^{-1} K^{-1}).

The model cannot differentiate between a dry and a wet sensor and therefore two runs are required. The Li-7500 has a white paint estimated to have an albedo of 0.85 but which drops to 0.50 when wet. The emissivity was set to one. The first model run assumes an always wet sensor while the second model run was repeated with a zero latent heat exchange coefficient (always dry sensor). Next, the latent heat fluxes from the first run are accumulated (negative numbers mean dew formation) and if all dew evaporates from the surface the accumulated dew remains zero until new dew appears. Using this approach the H, L_vE and T_s for each time sample were selected from the wet or dry model runs based on the accumulated dew (dew on sensor uses results from first run; if dry, use second run).

Note that further model refinements are possible:

- Improvement of the cylindrical model for heat exchange coefficients for various angles of attack.
- Including effect of dirt or snow accumulation affects on albedo and emissivity.
- Including radiative heat exchange between the 2 sensor housings.
- Including uneven heat distribution and thermal conductivity of various components inside sensor housings.
- Determining heat exchange of the four stems connecting the sensor housings.
- Including advection by snow or raindrop impaction.

7.3 Sensor heating or cooling corrections for trace gas flux measurements

The theory developed by Burba et al. (2006a, b) to correct trace gas flux measurements from eddy covariance measurements using heated open path gas analyzers was considered for a vertically oriented sensor head (BAXD1 and 2). They tested the sensor temperature in a laboratory set-up and in the field as a function of air temperature but did not provide a numerical solution for the outdoor sensor temperature. Their main concern was the heating of the instrument due to internal power dissipation. One of their field tests already revealed a problem with radiative cooling. Usually the sensor head is slightly angled to accommodate water droplet runoff, but which complicates this correction. Although they acknowledge this, they do not provide a solution for an angled set-up. As sensor heating or cooling, H_s (W m^{-2}), affects air density it is best to start with the original WPL correction:

$$F_{WPL} = \frac{m_a}{m_v}\frac{\overline{\rho_c}}{\overline{\rho_a}}\overline{w'\rho_v'} + (1+\frac{\overline{\rho_v}}{\overline{\rho_a}}\frac{m_a}{m_v})\frac{\overline{\rho_c}}{\overline{T}}\overline{w'T'} \qquad (7.16)$$

where m_a and m_v are molecular weights of air and water vapor, w is the vertical wind speed (m s^{-1}), ρ_d is the dry air density (kg m^{-3}), ρ_v is the water vapor density (kg m^{-3}), ρ_a is the density of air and ρ_c is the density of CO_2 (ρ_v and ρ_a measured by the LI-7500). The challenge is how to include density effects introduced by H_s for various sensor orientations.

The original proposed BAXD1 correction assumes that there is a difference in heating between upward and downward eddies passing through the analyzer because horizontal wind speed (u) is negatively correlated to the vertical wind speed (w). Upward eddies remain longer in the optical path and exchange more heat than the faster (larger u) downward eddies. This would be valid for all sensor orientations. The correction was implemented by adding a small fraction of the sensor temperature flux $\frac{H_s}{\rho_a c_p}$ (c_p is specific heat of air, (J kg^{-1} K^{-1})) to the $\overline{w'T'}$ term in Eq. 7.16. However, this approach was not included in the BAXD2 correction (Burba et al. 2006b).

The BAXD2 correction by Burba et al. (2006b) used a different approach in which they no longer mention the wind speed asymmetry effect and now assume that all H_s passes through the sampling volume. This seems very unlikely considering the fetch of an EC-system such that eddies not in contact with the LI-7500 heat flux will pass through the instrument. However, this approach would probably be valid for a fraction of H_s of the source housing (can) only. Burba et al. (2006b) also add the temperature flux from both housings to the WPL correction but this might not be correct for a vertical oriented Li7500. The reason is that H_s from the upper housing is a heat flux originating from above the sampling volume and therefore $\frac{H_s}{\rho_a c_p}$ should be subtracted

from $\overline{w'T'}$ in Eq. 7.16. This would suggest that for an upright orientation it is preferable to have a LI-7500 with both housings heated equally to cancel each other.

An additional term not mentioned by Burba et al. (2006a,b) is the change of average gas sample temperature (T_g) inside the LI-7500 path as it differs from that in the sonic path where temperature is usually measured. This correction is needed for all sensor orientations. The WPL correction assumes the temperature measured is the same in the LI-7500 and sonic path, therefore the temperature difference $\delta\overline{T} = T_g - T$ must be inserted into the WPL correction and the WPL corrected flux needs to be adjusted by a factor $\frac{(\overline{T}+\delta\overline{T})}{\overline{T}}$. This leads to the following sensor heat flux included WPL correction (F_{SWPL}):

$$F_{SWPL} = \frac{m_a}{m_v}\frac{\overline{\rho}_c}{\overline{\rho}_a}(\overline{w'\rho_v'}) + (1+\frac{\overline{\rho}_v}{\overline{\rho}_a}\frac{m_a}{m_v})\frac{\overline{\rho}_c}{\overline{T}+\delta\overline{T}}(\overline{w'T'} + c_1\frac{a_c H_{sc} - a_b H_{sb}}{\rho_a c_p}) \quad (17)$$

where H_{sc} and H_{sb} are the sensible heatflux (Eq. 7.3) from the source housing (can) and detector housing (ball), a_c and a_b are the surface area on window side of the can or ball over land surface area (m^2 m^{-2}), and c_1 is an orientation factor of 0 for a horizontally oriented LI-7500 and 1 for a vertically oriented LI-7500 (-).

The corrected CO_2 flux (F_c) now becomes (all sensor orientations):

$$F_c = (\overline{w'\rho_c'} + F_{SWPL})\frac{(\overline{T}+\delta\overline{T})}{\overline{T}} \quad (7.18)$$

A horizontally oriented LI-7500 would be exposed to H_s from the sides and therefore only $\delta\overline{T}$ must be considered (Eq. 7.17, c_1 = 0), which greatly simplifies corrections. The gas sample temperature change is a function of the sampling volume, the wind speed (u), and the heat transported (Eq. 7.3) to the sampling volume. This leads to the following expression:

$$\delta\overline{T} = \frac{(A_{sc}H_{sc} + A_{sb}H_{sb})L_p}{\rho_a c_p V_s \overline{u}} \quad (7.19)$$

where V_s is the sampling volume (m^3), A_{sc} and A_{sc} are the heat exchanging surface areas of can and ball, and L_p is the gas sample path length in the wind direction (m). The sampling volume length for a vertically mounted sensor is the width of the open path. For a horizontally mounted LI-7500 it depends on the direction of the wind (m):

$$L_p = |l_1 \cos\gamma| + |l_2 \sin\gamma| \quad (7.20)$$

where γ is the angle between horizontal wind speed (u) and length axis through LI-7500 (horizontal orientation, Fig. 7.1), l_1 is the optical path length (m), and l_2 is the sampling volume average cross section (0.0545 m).

Another unmentioned correction is that any open path sensor will dampen temperature fluctuations of eddies passing through its open path because of its thermal

inertia (copper will have a larger effect than plastic), especially the four stems supporting the ball housing. A correction scheme has yet to be proposed for this.

How well is H_s represented in Eq. 7.17? The flux originating from an upright source housing should be equivalent to a land surface sensible heat flux. The fetch of the gas chamber to its own heat flux is unknown, since the boundary layer above the windows is not fully developed across the entire gas sample path (l_1). This is similar to the problem of measuring turbulent heat exchange above a canopy where the area around the EC-system should be homogeneous (in a radius of about >30 times the height of the EC-system above the canopy).

To understand the impact on flux measurements when a heated or cooled open path gas analyzer is involved, consider an imaginary flux measurement (set-up in Fig. 7.1) with the following cases as depicted in Fig. 7.3. For simplicity, the example is above a dry surface with dry air (no condensation) and no CO_2 exchange. Case 1 shows an isothermal atmosphere, thus the density as measured by the open path gas analyzer is unaffected by temperature variations of the turbulent eddies. The measurements of covariance between horizontal wind speed (w, m s^{-1}) and trace gas density (CO_2), $\overline{w'\rho_c'}$ (kg m^{-3} s^{-1}), will read a zero flux. No density correction is needed. In Case 2 there is an upward sensible heat flux affecting the gas density measurements resulting in an apparent CO_2 uptake because the downward eddies have a higher density whereas the upward eddies have a lower density (CO_2). For all cases (L_vE = 0) and dry air reduces Eq. 7.17 to the Eq. depicted on the right hand side of Case 1, thus the WPL corrected CO_2 flux will give the correct zero flux (Case 2).

In Cases 3 and 4 a heated LI-7500 is introduced (same heating for both ball and can). This leads to an under-estimation of the CO_2 flux, and cannot be corrected by the BAXD1 or 2 corrections. To correct Case 3 a sensor temperature correction in the WPL and a correction factor for the final flux is proposed in Eqs. (7.17) and (7.18). F_{SWPL} is the WPL CO_2 flux (kg m^{-2} s^{-1}) including sensor heating. Case 4 is just a combination of Cases 2 and 3.

All cases: $F = F_{CO_2} = 0$, $L_vE = 0$, $\delta T = T_{gas_sample} - T$	Downdraft	Updraft	Flux calculation
Case 1 $\overline{w'T'} = 0$, $\delta\overline{T} = 0$	w = -1 ↓ $\rho_C = 1$, $T_s = 295$	w = 1 ↑ $\rho_C = 1$, $T_s = 295$	$F = \overline{w'\rho_c'}$
Case 2 $\overline{w'T'} = 10$, $\delta\overline{T} = 0$	w = -1 ↓ $\rho_C = 1.035$, $T_s = 285$	w = 1 ↑ $\rho_C = 0.967$, $T_s = 305$	$F_{WPL} = \overline{w'T'}\frac{\overline{\rho}_c}{\overline{T}}$ $F = \overline{w'\rho_c'} + F_{WPL}$
Case 3 $\overline{w'T'} = 0$, $\delta\overline{T} = 3$, $H_{sc} = H_{sb}$	w = -1 ↓ $\rho_C = 0.99$, $T_s = 298$	w = 1 ↑ $\rho_C = 0.99$, $T_s = 298$	*Horizontal Li-7500:* $F_{SWPL} = \overline{w'T'}\frac{\overline{\rho}_c}{\overline{T} + \delta\overline{T}}$ *Vertical Li-7500:* $F_{SWPL} = (\overline{w'T'} + \frac{\delta_T^*}{l_1}\frac{H_{sc} - H_{sb}}{\rho_a c_p})\frac{\overline{\rho}_c}{\overline{T} + \delta\overline{T}}$
Case 4 $\overline{w'T'} = 10$, $\delta\overline{T} = 3$, $H_{sc} = H_{sb}$	w = -1 ↓ $\rho_C = 1.024$, $T_s = 288$	w = 1 ↑ $\rho_C = 0.958$, $T_s = 308$	$F_c = (\overline{w'\rho_c'} + F_{SWPL})\frac{(\overline{T} + \delta\overline{T})}{\overline{T}}$

Figure 7.3: Four illustrative cases of measurements of turbulent transport in a dry atmosphere using an open path gas analyzer to demonstrate needed corrections. The dashed circle depicts the eddy size of the first case for comparison. In all cases there is no exchange of CO_2 (or H_2O) between surface and atmosphere as indicated in the top left corner (*F* is the CO_2 flux).

7.4 Experiments and results

An experiment to compare two eddy covariance systems at a height of just over 3 m, with (Fig. 7.1) and without heated LI-7500 detector housings, was carried out at the Wageningen University meteorological station situated in a grassland area in the Netherlands (lat 51^0 58.28' N; lon $5^0$38.49' E; elevation 7 m a.m.s.l.). The climate can be described as a mid-latitude coastal climate with a high number of annual dew nights (average 250) (Jacobs et al., 2006b). The air temperature (PT100) and relative humidity were measured inside a Stevenson screen. The relative humidity sensor, a Vaisala HUMICAP Humidity and Temperature Transmitter HMP337, has a warmed sensor head to improve accuracy during moist conditions (accuracy 3%). The incoming global and outgoing short-wave radiation of the grassfield were measured

by one albedo meter (Kipp & Zonen, Delft, Netherlands CM14) which consists of 2 CM11 short-wave thermopile radiometers with a spectral range of 305 to 2800 nm and an overall error of <3%. The long-wave radiation components were also measured separately using two Kipp CG1 long-wave radiometers. Spectral range is from 5 to 50 μm with an overall error of 3%. An additional Kipp & Zonen CM11 short-wave radiometer was used to measure diffuse incoming global radiation (short-wave) by installing a shadow-ring over the instrument. The shadow-ring was adjusted or checked manually on a daily basis. The direct solar beam incoming short-wave radiation (R_b) was derived by subtracting the diffuse global radiation from the incoming global radiation and dividing the result by the sine of the calculated solar altitude.

The two eddy covariance systems were installed on masts 25 m apart (in each mast: Li-7500 at 3.18 m, Sonic at 3.44 m and a pitch angle of 228 relative to north). The only difference between the two systems was that a heating resistor was installed on the detector housing of the LI-7500 open path gas analyzer (Fig. 7.2). The heat dissipation was less than 0.7 W. The heating element (cylindrical resistor, 11 x 4 mm, 220 Ω ±1%) was glued to the side of the sensor ball and covered with 0.5 mm layer of thick plastic tape and the ball (including the resistor) was covered with aluminium tape to reduce radiative heat loss (low emissivity). There were slight differences in calibration constants, but it is clear from Fig. 7.4 that dew is a serious problem for the non-heated LI-7500.

It seems that the LI-7500 has fewer problems with raindrops than with dew on its surface (Fig. 7.4, rain around 20:00 GMT). The LI-7500 uses the ratio of two light waveband transmissions through the optical path to determine the gas concentration; one light waveband is absorbed by the gas concentration while the other light waveband is insensitive to gas concentration. In this way the measurements are not influenced by partial obstruction of the optical path so long as the light absorption or blocking affects both the absorption and reference bands in an equal manner. A thick rain droplet on the surface totally blocks both light wavebands and therefore does not affect measurement quality. Raindrops are problematic only if they form layers, since light in both light wavebands will not reach the light detector. The dew problem might be related to the build-up of very thin layers of water molecules preceding the formation of visible dew drops. In addition, these layers may also remain in-between the visible dew drops. These layers would not absorb light in the water and CO_2 absorption wave bands in the same amount as in the reference light wavebands for both gasses and would therefore cause too high readings (i.e. morning hours 00:00-08:00 GMT).

The LI-7500's automatic gain control (AGC) measurement can be used to find light-blocking cases. However, since the LI-7500 manual states that the calibration is still valid while the AGC approaches 100%, it would not detect many of the dew

related measurement errors sinc these occur at a AGC<100% when the water layers are thin. We can not validate this statement as AGC data were missing, thus we strongly recommend repeating the experiment using such data.

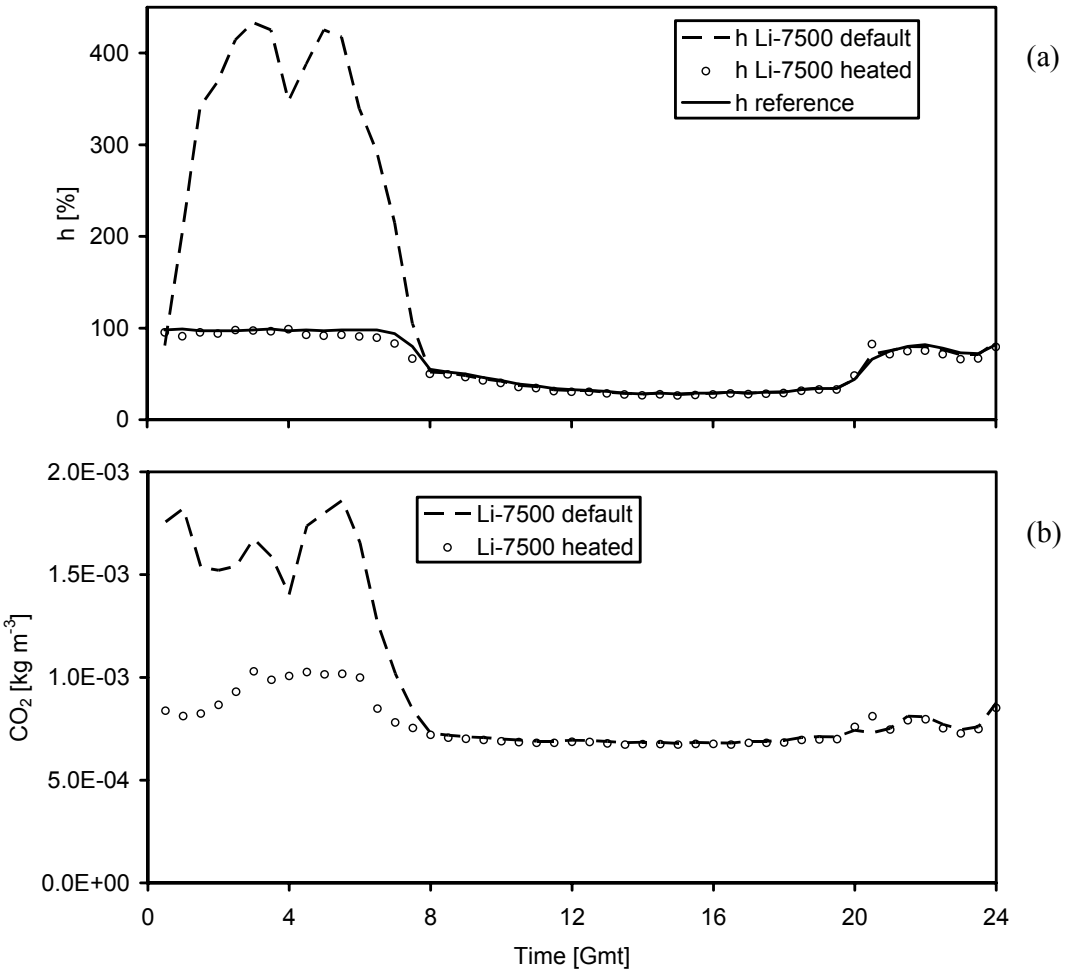

Figure 7.4: Two eddy covariance flux stations, one equipped with a LI-7500 with a heated sensor head tip (+0.6 W) and one complete flux station without additional heating (default). Panel A shows the relative humidity signals of the two LI-7500 sensors at 3 m (using air temperature at 1.8 m to calculate percentage saturation) and reference humidity sensor at 1.8 m; panel B shows the CO_2 signals (24 April 2003).

The LI-7500 exposure to the separate components of the radiation balance at the field station on April 24, 2003 (Fig 7.5c), leads to radiatve heat loss of the Li-7500 from 00:00-08:00 GMT. During the evening hours it started to rain (Fig. 7.5b) but this hardly affected the measurements. It could, however, cause an output failure if a window is accidentally fully covered with a thick layer of rain water.

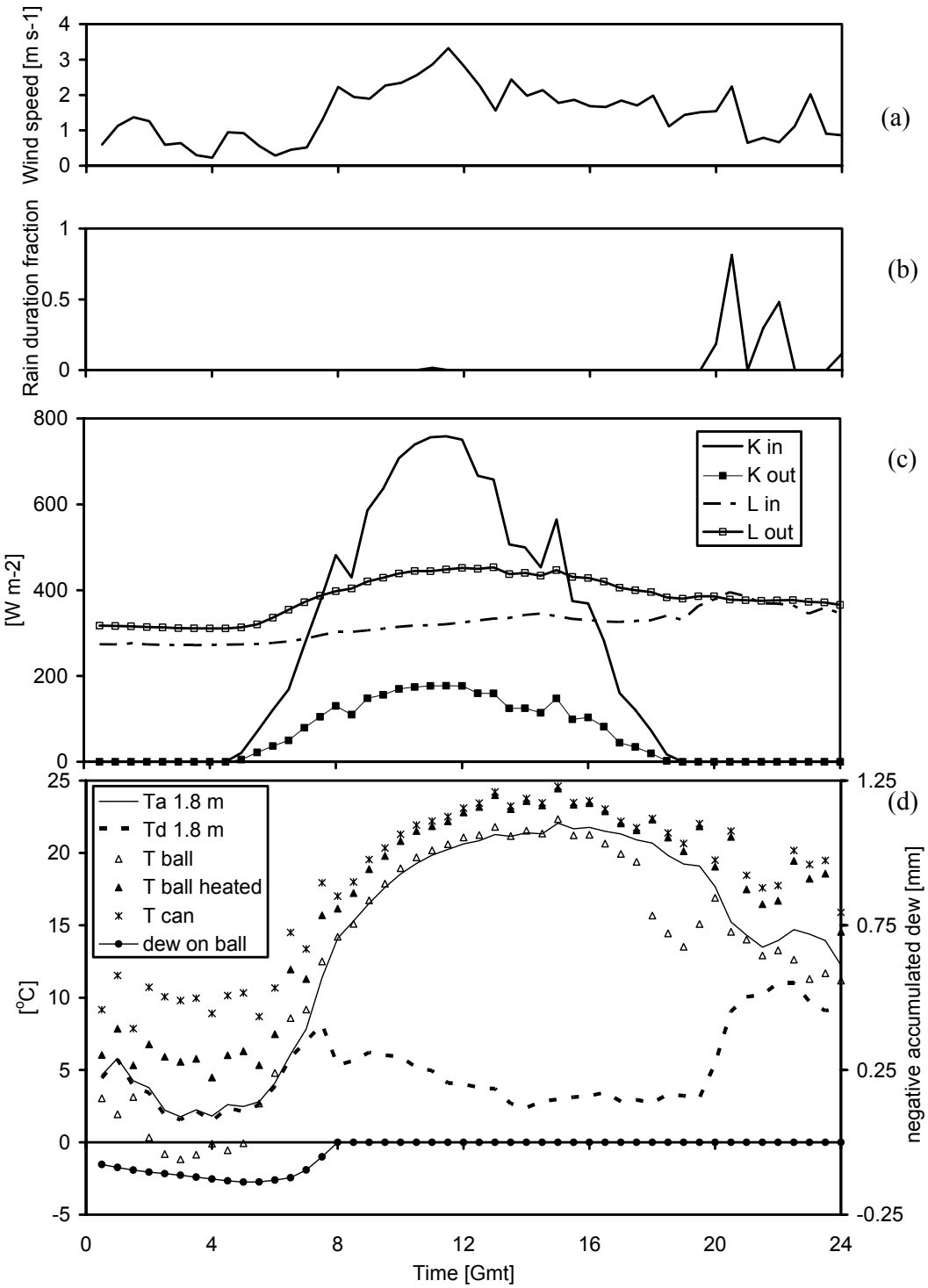

Figure 7.5: Panel A: Horizontal wind speed. Panel B: Rain duration (% of 30 minute intervals). Panel C: Separate components of the radiation balance. Panel D: Air and dew point temperature at 1.8 m, calculated temperature of a standard LI-7500 sensor head consisting of a ball (tip of sensor head containing the light detectors) and a can (containing a light source and chopper and electronics), calculated temperature of a heated ball of a second LI-7500, and calculated dew amounts on a non-heated ball (24 April 2003).

The results of the model (T_s and accumulated dew, Fig. 7.5d) show that during the very early clear sky and calm morning hours the temperature of the sensor housing dropped up to 4 °C below dew point temperature, thus the air needed to be much dryer to avoid condensation on the detector window. After sunrise the dew evaporated rapidly. For the presented case, the can was always warmer than T_d and the heated ball was warmer than T_a but not the un-heated ball.

Processing fluxes from these dew-contaminated gas density measurements will not be accurate. Both Eddy covariance flux stations were processed with the same software (Van Dijk et al., 2004) and include density corrections (WPL), planar fit axis rotation, sensor separation and spectral loss corrections, etc, but no sensor heating correction (illustrated in Figs. 7.6 and 7.7). Fluxes are not accurate for the reference station during moisture condensation (see also Fig. 7.5d). The noise during the rain episode (around 20:00 GMT) did affect the heated station more than the default station, but this is because the ultrasonic anemometer and the LI-7500 are both sensitive to water droplets and, by coincidence, the heated station might have been more affected. The LI-7500 manual warns for spikes in the data while droplets (or pollen, etc.) fall through the optical path. This affects the measurement differently than from a large water drop on a window because the operating principle of the LI-7500 is that it measures the four light wavebands one by one (in the same path). A thick water droplet on the window would not affect calibration if the drop is motionless, but if a droplet falls through the optical path it will block the beams unequally due to the speed of the water droplet passing by. This leads to spikes especially in the flux data (Figs. 7.6 and 7.7).

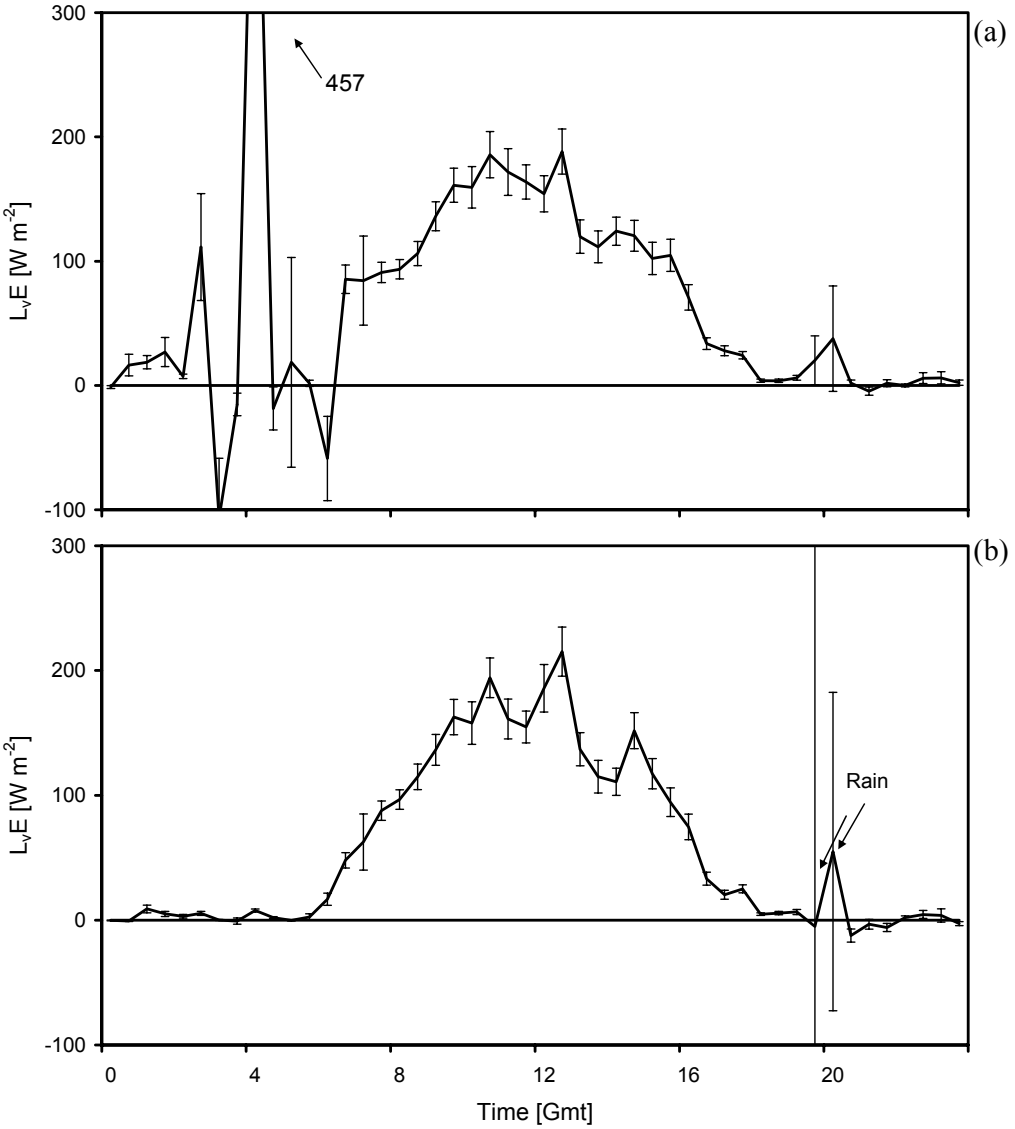

Figure 7.6: EC-system with a LI-7500 without heating (panel A) and an EC-system equipped with a LI-7500 with a 0.7 Watt heating element on the sensor head (panel B). Error bars indicate the tolerance of the flux measurements (24 April 2003).

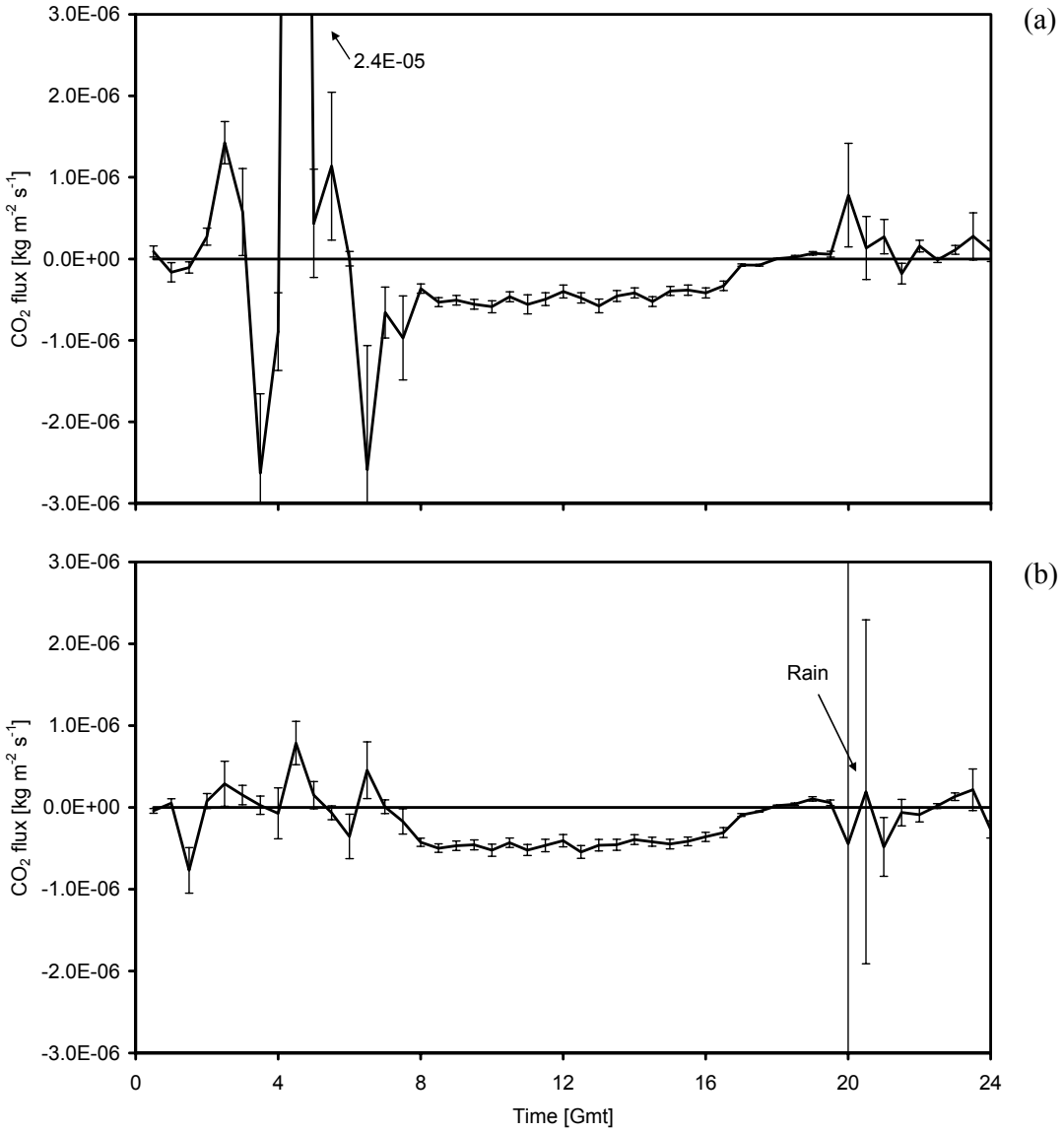

Figure 7.7: EC-system CO_2 flux measurements with a standard LI-7500 (panel A), and one with a heated LI-7500 (panel B). Error bars indicate the tolerance of the flux measurements (24 April 2007).

Of interest is that the NEE (CO_2) was 5% less for the heated system during CO_2 uptake between 08:00 – 16:00 h for this day. We believe that this could be attributed to the noisier signal and slowly evaporating water layers on the default LI-7500. The NEE is 5% higher on the previous, quite similar day (not shown).

The dew-contaminated night-time fluxes in the reference station (without heating) (00:00–08:00 h) have no meaning and are too noisy to compare. This clearly shows the advantages of window heating. It is important to be able to identify the problematic condensation periods and this can only be done with a careful analysis of

all components that contribute to the energy balance of the sensor head (Eq. 7.1). The conditions favoring condensation usually occur during calm conditions and it is already standard procedure to omit EC-data during such situations. This is because the EC-system would still measure fluxes at its measurement height but they are no longer related to the fluxes near the surface. Such cases can be tested with a u^* criteria: for a $u^* < 0.1$ m s^{-1} the measurements are decoupled from the surface (Jacobs et al., 2006a). However, still condensation conditions or dew remnants cannot be detected with a u* criterion alone.

Three datasets were selected to calculate the percentage of time experiencing possible condensations problems (Table 7.1) and to find the minimal heating needed to avoid this. Two datasets were obtained from the Wageningen University Haarweg Meteorological station and includes all meteorological conditions during the years 2003 and 2006 (Jacobs et al., 2006a). A third dataset, of an arid climate in the Negev desert, Israel, was obtained for a six-week dry period in September-October 2000 (lat $30^0$56' N; lon $34^0$23' E; elevation 190 m a.m.s.l.). The latter is different form the first two datasets in that the CO_2 exchange was minimal. A description of the Negev experiment can be found in (Heusinkveld, et al., 2004). The precipitation duration at Haarweg station was detected with a precipitation monitor (Niederschlagswächter, Thies-clima, Germany). It uses an IR-light barrier that responds to precipitation particles larger than 0.3 mm. Both detector- and source-housing temperatures were calculated using Eqs. (7.1-7.8). The aerodynamic exchange coefficients were not corrected for sensor orientation with respect to wind direction but were assumed to be a good estimate for this study, although improvements are possible. The albedo was found not to be a very critical parameter in the model. When running the model again with a 10% change in the wet state albedo, the wetness period changed by only 0.3% on an annual basis. This procedure was repeated for the exchange coefficient; a 10% change had an inverse effect on the calculated wet period by only 1%. The projected surface area for various solar angles was considered constant (largest cross section) for the Fig. 7.1 orientation. This was a safe assumption since it mainly affects the shortwave radiation balance and the albedo model parameter is not critical. The model was not optimized for wind angle of attack. A wind blowing perpendicular to the cylindrical housing was assumed (horizontal LI-7500) and this affects the exchange coefficients. Probably the wetness duration would be extended a bit because wind from the front/back would result in a small reduction in the heat exchange coefficient. As the ball housing is rather symmetric, only a wind direction from the can side or from the connector side can be problematic (Fig. 7.1) and it is the ball housing that has a major condensation problem.

The sensor housing was assumed to have no temperature gradients because the housing is made of good heat conducting material (metal), although refinements are possible. The model calculates a steady-state solution for each time step and since

time intervals are at a 30 min basis (for the Negev dataset 15 min) it was assumed that heat storage is of minor importance. In addition, the heat generated inside the housing is considered to be distributed equally, although in reality the situation is a bit more complex. Radiative heat exchange between top and bottom housing were omitted. The heat transport through the 4 stems connecting the two parts (ball, can) of the housing was considered not to affect the sensor housing. This is a fair assumption since the stems are thin and therefore heat transport between ball and can is minimal. Evidence for this can be found in Burba et al. (2006a) who showed that there was a near perfect one-to-one relationship inside a climate chamber between chamber temperature and detector housing (ball). Under certain environmental conditions the additional surface area of the stems and the radiative surface cooling might contribute to a slight increase in wetness periods of the ball. The important point is that the model will provide a tool to estimate possible dew episodes with a reasonable accuracy (<5%). Keep in mind that the major driving force for cooling is the radiative heat loss. With the calculated accumulated dew on the sensor, the percentage of time with a highly probable wet sensor could be approximated (Table 7.1). In the Netherlands the detector housing could be moistened by dew more than 30% of the year. Even in the Negev field experiment, although the air was not very moist, the detector housing was still not free of condensation problems (3.7% of the time).

		Haarweg year 2003	Haarweg year 2006	Negev desert 6-22 October 2000
Moist conditions in fraction of time (e/e_s >0.9)		0.29	0.25	0
Precipitation in fraction of time		0.064	0.066	≈0
Fraction of time sensor housing moist by dew only (model)	Source housing	0	0	0
	Detector housing	0.34	0.27	0.037
Minimal heating needed to prevent condensation problems (>0.99 time) on detector housing (W)		0.7	0.52	0.18

Table 7.1: The three datasets used to calculate the fraction of time with condensation problems, and the amount of sensor heating needed to avoid this.

Based on our calculations, we used a maximum 0.7 W heating element to minimize heating effects on flux measurements (Table 7.1, bottom line). However, more heating would be safer to keep the sensor housing, and especially the windows,

above the dew point temperature. It was not possible to mount the heating element inside the housing, thus thermal heat transfer could be less optimal according to the way the heating element was installed.

Technical issues unrelated to sensor performance reduced data availability for the first two datasets by 34% in 2003 and 18% in 2006 (Table 7.2). Only 128 days in 2003 and 183 days in 2006 of the CO_2 flux data had an acceptable accuracy. Dew-related gaps occured during characteristic conditions leading to a bias in gap frequency. In order to derive annual estimates of CO_2 exchange, these gaps must be filled and this may lead to systematic biases because the data basis used for gap-filling contains little information on fluxes during dew periods. The NEE analysis of the Haarweg dataset of 2003 (Jacobs et al., 2006a) shows that large gap-filling was needed and how difficult this was (but no sensor heating corrections). The sum of the remaining 128 days of acceptable CO_2 flux measurements are -1671 g of CO_2 m^{-2} and after gap-filling only -791 g CO2 m^{-2} y^{-1} remain in the year 2003 (Table 7.2).

location	Haarweg grass cover		Negev desert
Measurement period	2003	2006	6-22 October 2000
Accepted period with a CO_2 flux tolerance <20%	35%	50%	98%
Data loss CO_2 flux tolerance >20%	10.8%	16.7%	1%
Data loss, due to operational problems (power loss, calibration, etc)	34%	18%	0%
Data loss Sonic (tolerance >10%)	3%	3.7%	0%
Data loss Li-7500 (e/e_s >1.1)	3.6%	6.7%	0%
Data loss Sonic and Li-7500 data (tolerance >10%)	13.6%	4.9%	1%
NEE ($\sum F_{CO_2}$ with a tolerance <20%), no H_s correction	-1671 g m^{-2} in 128 days	-1925 g m^{-2} in 183 days	-11 g m^{-2} in 16 days
NEE with gap filling (ref. Jacobs et al, 2006a) (g m^{-2} y^{-1}), no H_s correction	-791	-772 (estimate)	

Table 7.2: Data collected during the three measurement campaigns and the loss of data due to various causes.

The effect of the proposed sensor heating correction for a horizontally and vertically oriented LI-7500 (Eqs. 7.17 and 7.18) and the proposed sensor temperature model were tested on the three datasets (Tables 7.1 and 7.2). The main goal was to

investigate the size of the contribution of the different corrections. The corrections were calculated using the sensor housing temperature model and Eqs. (7.17) and (7.18). The NEE corrections (row 3, Table 7.3) are for the horizontally mounted sensor housing temperatures calculated with the proposed model. Only the average temperature change over the flux averaging interval of the open path gas chamber volume is needed. The model results show that the gas chamber volume temperature rise is 0.6°C maximum, thus corrections are small. This was also the case for the heated LI-7500, so the corrections can be neglected.

Location		Haarweg grass cover				Negev desert	
Measurement period		2003		2006		6-22 October 2000	
Units		g m^{-2} in 128 days		g m^{-2} in 183 days		g m^{-2} in 16 days	
modified Li-7500 (0.7 Watt heating element in detector housing)		No	yes	no	yes	no	yes
1. BAXD2, if the sensor was mounted vertically (approximate)	can	4.66	4.66	7.05	7.05	0.16	0.16
	ball	-0.18	1.70	-0.39	2.32	-0.012	0.12
	sum	4.48	6.36	6.65	9.37	0.15	0.28
2. Corrected BAXD2, if the sensor was mounted vertically (approximate)	can-ball	4.84	2.97	7.44	4.73	0.17	0.041
$\delta\overline{T}$ correction, if the sensor was mounted vertically (approximate)	can	-0.10	-0.10	-0.10	-0.10	≈0	≈0
	ball	-0.008	-0.046	-0.009	-0.045	≈0	≈0
	sum	4.73	2.82	7.33	4.58	0.17	0.17
3. Eqs 7.17 and 7.18, horizontal sensor (Fig. 7.1), modeled sensor temperature	can	-0.21	-0.21	-0.21	-0.21	≈0	≈0
	ball	-0.016	-0.095	-0.017	-0.091	≈0	≈0
	sum	0.23	-0.31	-0.23	-0.30	≈0	≈0

Table 7.3: Impact of sensor heating correction to Net Ecosystem Exchange of CO_2, evaluated over long periods. The LI-7500 sensor housing comprises of a "can" containing the source and a "ball" containing the detector (negative sign of NEE means CO_2 uptake by land surface).

For a standard installment the sensor is usually mounted vertically but slightly tilted to support water droplet runoff as recommended by LI-COR. Such an orientation will behave more like a vertically than a horizontally oriented sensor, but no solution is given. A small numerical experiment showed that corrections become

more significant when the sensor is mounted vertically. The original BAXD2 (row 1, Table 7.3) is calculated and the detector housing temperature deviation increases the NEE uptake (CO_2). This is in agreement with what was found by the condensation experiment (Fig. 7.5) because there are lengthy time intervals when the sensor-housing temperature is lower than the air temperature. The reduction in NEE uptake, caused by the heating of the source-housing, is partially compensated by the cool detector housing. The proposed modifications reduce the BAXD2 correction (row 2, Table 7.3), and it becomes almost zero for a heated LI-7500 in the Negev experiment. However, a comparison experiment between an open path and a closed path gas analyzer eddy covariance set-up is needed to verify the H_s corrections and proposed modifications. This is challenging since the corrections seem very small.

Sensor orientation still remains an important issue in calculating the exact correction since the H_s correction is highly dependant on the size of the boundary layer thickness (and therefore local temperature) that develops above the windows of the housing.

7.5 Summary and conclusion

Dew forms when an object's surface temperature is reduced to below the dew-point temperature. This process is driven mainly by radiative cooling and open path sensors exposed to radiative cooling risk condensation on their optical windows. An independent comparison between a heated and a non-heated LI-7500 based EC-system shows that additional heating to inhibit dew formation greatly improves the quality of measurements during typical mid-latitude maritime weather conditions. A method to calculate sensor temperature is presented based on the description of the energy balance of the sensor. Calculations and measurements show that sensor temperature colder than T_a is possible under certain environmental conditions, even if there is some heating inside the instrument. Dew affects the accuracy of the LI-7500 measurements and can form at air humidities far less than 100%, especially during calm nights. For such dew nights, the sensor can also remain wet following sunrise for a considerable time, depending on the amount of evaporation. This has been included in the proposed sensor dew model and can be used to filter existing datasets for dew events. The heat needed to keep the LI-7500 windows above dew-point does not seem to introduce significant errors when measuring fluxes. The proposed average gas sample heating/cooling correction can be applied to vertical and horizontal sensor orientations. Sensor orientation is important to consider because the BAXD2 correction is not needed for a horizontally mounted LI-7500, and the remaining correction is small (modeled NEE correction for the evaluated datasets <1 g CO_2 on an annual basis). However, for a vertically mounted LI-7500 the errors would be smaller than assumed by the BAXD2 correction especially if sensor heating is applied

to the detector housing (annual NEE (CO_2) correction for a mid-latitude grassland <10 g CO_2).

The BAXD2 correction including the suggested modification and additions should also be applied to non-heated sensors because environmental conditions can lead to a colder or warmer sensor, and both directions can influence flux measurements. However, the correction for old datasets can only be applied correctly with a dedicated model to calculate sensor temperatures as presented. Note that the corrections could even change sign for a cooler sensor and, under certain conditions, for a vertically oriented sensor the temperature effects of detector- and source-housing can compensate each other (in the LI-7500).

Although the LI-7500 can withstand some rain, dew is a serious problem for night-time measurements. In addition, daytime measurements could be affected during low solar angles, clear skies, low wind speed and moist air. It is shown that dew can be avoided by installing a small heater on top of the detector housing.

From the analysis of sensor temperature simulations under environmental conditions, condensation problems can be reduced using a sensor coated with a low thermal emissivity with a minimal amount of internal heating. It is still favorable to use a high albedo surface coating to reduce solar heating effects.

Avoiding condensation on the LI-7500 windows is a serious issue in mid-latitude climates because it introduces large errors in flux measurements or causes the measurements to become invalid during moist periods. The simulations show that periods resulting in a moist sensor window were >27 % in 2003 and 2006, and thus the lack of reliable data during those wet periods will have a serious impact on the final measurement quality of NEE (CO_2) annual estimates. This could result in an overestimation of NEE uptake for CO_2 because the wet periods usually coincide with periods where the respiration dominates over photosynthesis. However, even in arid environments one should be careful with moist conditions. This is demonstrated in the Negev experiment where moisture problems occurred 3.7% of the time (Table 7.1). When evaluating NEE over longer periods one should carefully analyze the data and keep in mind that condensation problems should be checked carefully. With the proposed calculation scheme for LI7500 surface temperature, such events can be isolated.

Further model optimizations are possible (see bulleted list, Section 2), but the sensor housing albedo and heat exchange coefficients are not very critical.

Acknowledgements

This research project was performed in the framework of the Dutch National Research Programme *Climate Changes Spatial Planning* (www.klimaatvooruimte.nl). It is co-funded by the Dutch Ministry of Agriculture. The authors are grateful to the Dutch Organization for Scientific Research (NWO), and the Arid Ecosystems

Research Centre of the Hebrew University of Jerusalem for assistance in carrying out the field campaign in the Hebrew University Nizzana Experimental Station. The authors thank Simon Berkowicz for valuable comments and support.

References

Amiro, B., Orchancsky A., Sass A, 2006. A perspective on carbon dioxide flux measurements using an open-path infrared gas analyzer in cold environments. In: Conference proceedings AMS annual meeting P4.7, San Diego, 2006.

Burba, G.G., Anderson D.J., Xu L., McDermitt, D.K., 2006a. Correcting apparent off-season CO_2 uptake due to surface heating of an open path gas analyzer: progress report of an ongoing study. In: Conference proceedings AMS Annual meeting, San Diego, 2006.

Burba, G.G., Anderson, D.J., Xu, L., McDermitt, D.K., 2006b. Additional term in the Webb-Pearman-Leuning correction due to surface heating from an open-path gas analyzer. Eos Trans. AGU 87 (52), Fall Meet. Suppl., C12A-03.

Heusinkveld, B. G., Jacobs, A. F. G., Holtslag, A. A. M., Berkowicz, S. M., 2004. Surface energy balance closure in an arid region: role of soil heat flux. Agric. Forest Meteorol., 122, 21-37.

Jacobs, A.F.G., Heusinkveld, B.G., Holtslag A.A.M., 2006a. Seasonal and interannual variability of carbon dioxide and water balances of a grassland area. Climatic Change. DOI 10.1007/s10584-006-9182-7.

Jacobs, A.F.G., Heusinkveld, B.G., Wichink Kruit, R.J., 2006b. Contribution of dew to the water budget of a grassland area in the Netherlands. Water Resour. Res., DOI:10.1029/2005WR004055.

Monteith J.L., Unsworth M.H., 1990. Principles of Environmental Physics. Chapman and Hall, New York, 291 pp.

Tennekes, H. and Lumley, J.L., 1972. A First Course in Turbulence. MIT Press, Cambridge, MA, 399 pp.

Webb E.K., Pearman, G.I., Leuning, R., 1980. Correction of flux measurements for density effects due to heat and water vapour transfer. Quart. J. Roy. Meteorol. Soc. 106: 85-100.

Van Dijk, A., Moene, A.F., De Bruin, H.A.R., 2004. The principles of surface flux physics: theory, practice and description of the ECPACK library Internal Report 2004/1, Meteorology and Air Quality Group, Wageningen University, Wageningen, the Netherlands, 99 pp.

8 Summary and perspectives on future research

In this thesis dew and related microclimate conditions were investigated within a coastal desert system in the NW Negev desert, Israel. The study was motivated by the fact that although dew plays a varied role in many ecosystems and environmental settings (as outlined in the previous Chapters), no standard instrumentation exists to measure dew and, hence, there has been limited quantitative research on dew formation, deposition and drying. This is especially the case in desert ecosystems where dew can serve as the primary source of moisture for microorganisms and small faunae during the lengthy rainless periods, and where the wetting/drying process can accelerate bacterial breakdown of seed coats (for germination).

The research in this thesis is directed at:

1. The role of soil heat flux in the energy balance in a coastal desert ecosystem,
2. Quantifying (through sensor development and measurements) dew deposition and evaporation in a coastal desert ecosystem,
3. Analyzing the conditions that favour dew formation,
4. Developing and validating a numerical model to investigate dew water flows at a soil surface.

8.1 Objective 1: The role of soil heat flux in the energy balance in a coastal desert ecosystem

Energy balance studies highlight the delicate interplay between radiative forcing Q^*, and resulting turbulent and soil heat fluxes. The accurate measurement of soil heat flux G, is often neglected in energy balance studies. Because in a desert G can be as high as the sensible heat flux H, this omission will lead to large errors in the calculations. During the night these fluxes (G, H, Q^*) are especially dominant. A dry soil will quickly dampen the daily temperature wave to such an extent that an adequate correction for a buried soil heat flux sensor becomes very difficult and necessitates many additional measurements.

Chapter 2 introduced a new soil heat flux measurement approach. The weather conditions experienced during the long, hot and rainless summers, coupled with the sparse or absent vegetation in the flat interdune area, provided the conditions for a unique experiment whereby the soil heat flux could be measured almost at the surface. The near-surface placement essentially removes the need for depth corrections. Harmonic analysis and a calorimetric method are used to obtain the soil surface heat flux in comparison with observations near the surface. It appears that the approach proposed here provides realistic soil heat fluxes at the surface. The correctness of the

measured near surface soil heat fluxes is confirmed by the perfect closure of the soil surface energy balance under dry desert conditions. The surface energy balance closure test gives less scatter with the directly measured surface soil heat flux measurements than with the corrected data of the two conventional techniques described in Chapter 2. This nearly perfect closure supports the placement of the soil heat flux sensor very close to the surface. In a dry bare soil with a very high soil heat flux, we advise burying the sensor as close as possible to the soil surface.

Future research for Objective 1:

The partitioning of the separate components of the energy balance at the surface reveals the necessity for high-quality soil heat flux measurements. The very good energy balance closure found in the present study shows that the turbulent fluxes of H and L_vE can be trusted, at least for high Bowen ratios. The numerous papers reporting on an energy balance closure gap rely, in fact, on measurements from evaporating vegetated surfaces and raise the issue whether evaporation had been measured correctly. Jacobs et al. (2008) used a detailed analysis of all separate components of the energy balance and found that careful corrections would lead to a good closure. However, corrections still remain large, and hence there is a practical need to do controlled field experiments with low Bowen ratios and an instrumental set-up that avoids large corrections. Such a controlled experiment would require measurements above a moist surface devoid of vegetation. It would be very interesting to apply the soil heat flux measurement concept for such an experiment if the soil heat flux plates would not obstruct evaporation. Tiny soil heat flux plates exist nowadays but they might not be adequate. Perhaps a better approach is to use lysimeters to provide an independent measure of evaporation. Moist soils require a much deeper lysimeter than introduced in Chapter 3, but are technically possible. The experimental site used in this thesis might provide an opportunity to study the energy balance for low Bowen ratios. A suitable period would be at the end of the winter rain period, where the 100 mm (average) annual rainfall recharges soil moisture and could enable energy balance closure studies under moist conditions.

8.2 Objective 2: Quantifying (through sensor development and measurements) dew deposition and evaporation in a coastal desert ecosystem

The research here focused on four different surfaces; an interdune area, dune slopes with biological soil crusting, plant leaves, and a dew collection experiment on a flat surface. The following sensing methods were developed or used to quantify dew:

- manual and automated microlysimeters
- visual observations of dew

- eddy covariance measurements
- optical wetness sensors
- leaf wetness sensing grids
- gravimetric water content determination by manual soil sampling
- relative humidity measurements of soil pores
- artificial dew collector

The new microlysimeter design (Chapter 3) was motivated by the fact that existing methods to estimate accumulated dew amounts have relied on proxy surfaces and may not represent the actual dew amounts on the soil surface. A microlysimeter directly measures the moisture gain/loss by weight measurement. An innovation is the loadcell placement, which is located far deeper than the sample cup depth to minimize measurement errors introduced by the daily soil temperature wave. The measurements revealed that there is a significant daily exchange of moisture between soil and atmosphere.

The total accuracy of the microlysimeter tested here, as based on manufacturer's specifications and oven testing, was ±0.02 mm of equivalent dew. The microlysimeter's compact size and light weight allows the sensor to be installed in a variety of settings and landscapes, and not just on flat surfaces.

This Load Cell microlysimeter revealed, or provided independent data to show that dew formation on bare soil is highly dependent on the soil composition. The daily dew variation ranged from 0.1 to 0.2 mm on stable dune slopes but up to 0.4 mm on the interdune playa. This difference is attributed to the playa's high silt and clay content and salinity and it becomes less with increasing soil moisture content. The soil composition is also the reason that dew formation already starts while the soil surface temperature is more than 10 degrees higher than the dewpoint temperature at reference height. The dune slopes showed a 60% smaller diurnal variation than the interdune area for average dew nights.

A new surface optical wetness sensor (OWS) was constructed to study the dew wetting/drying cycles of a surface and leaf water content. The OWS is the first all weather field sensor capable of studying surface wetness both day and night. The soil calibrations show that the OWS is very sensitive to changes in soil water content over the soil moisture range between oven dry and field capacity, and without interfering with the surface. Without calibration, the OWS can qualify soil surface wetness. The OWS could follow the soil moisture variation in the upper part of a biological soil crust because the detection light waveband uses the light water absorption feature around 1.9 μm. The idea is that the OWS sensing depth is equivalent to the photosynthetically active layer of the biological soil crust. The model simulations of dew water flow within the crust showed that only the upper crust portion has the longest free available dew period for possible photosynthetic activity of

cyanobacteria. The variation of soil moisture could be detected by the OWS but the diurnal variation is small. A very light rain of 0.3 mm on Day of Year 289 (2000) showed that the signal for liquid water is stronger than the amount caused by dew input. However, cyanobacteria are capable of photosynthesis at soil water potentials far lower than at saturated water potential. The OWS can also be applied towards measuring leaf water content directly, especially when not confounded by dew, fog or rain deposition. For plant leaves it must be noted that the OWS responds to both internal and external water and the difference cannot always be distinguished.

Eddy covariance (EC) flux measurements were used to measure the turbulent transport of moisture. There is a difficulty that the open path infrared gas analyzer (Li-7500) is sensitive to moisture on its window. Avoiding condensation on the Li-7500 windows is a serious issue in mid-latitude climates because it introduces large errors in flux measurements or causes the measurements to become invalid during moist periods. The simulations show that periods resulting in a moist sensor window were >27 % for a mid-latitude location above grass (Netherlands). The lack of reliable data during those wet periods will have a large impact on the final measurement quality of net ecosystem exchange (NEE) of CO_2 estimates on an annual basis. This uncertainty could result in an overestimation of NEE uptake for CO_2 because the wet periods usually coincide with periods where the respiration dominates over photosynthesis. However, even in arid environments one should be careful with moist conditions. This is demonstrated in the Negev experiment where moisture problems occurred 3.7% of the time (Table 7.1). When evaluating NEE over longer periods one should carefully analyze the data and keep in mind that condensation problems on the windows should be checked carefully. With the proposed calculation scheme for Li-7500 window surface temperature, such events can be isolated. In the end, the direct measurement of moisture exchange by the microlysimeters was the preferred method. The EC underestimated the latent heat transport when compared to the microlysimeters. The stratification of the atmosphere and the measurement height of 3 m is probably the cause for this underestimation of accumulated dew. The EC measurements were useful for testing the onset of dew formation and to compare the different rates of dew deposition with the microlysimeters.

Future research for Objective 2:

The depth of the microlysimeter sampling cup, 35 mm, was limited but sufficient to measure the diurnal variation. This sufficient depth was confirmed by parallel manual microlysimeter measurements at various depths. Such a shallow depth may not be adequate at the end of the rain season while there is still a moisture supply from deeper soil layers. The dew formation at the start of the dry season will be different because the soil water content is larger and dew rise may become an

important factor. Dew rise is the migration of soil water to the surface, which could moisten the air and lead to dew formation on plant leaves also.

With the optical wetness sensor it becomes possible to measure minute changes in surface moisture content. A careful calibration is needed to quantify the moisture concentration in a porous surface and this could be fine-tuned for biological soil crusts.

8.3 Objective 3: Analyzing the conditions that favour dew formation

The measurements show that there is strong soil moisture variation in the upper 30 mm of the soil. Typical meteorological conditions are described in Chapter 5 and are typical for a dew night. It is shown that the downward atmospheric vapour flux can be more than twice higher than the potential dew. The vapour flux towards the soil can be estimated from standard weather station data coupled with additional measurements of soil relative humidity.

A large flat collector in the study site, with improved insulation and placed at a higher elevation, could generate more than 0.2 mm day^{-1} of dew on an average dew night. The model simulations show that the dew yields near the coast are 2.5 times *greater if moisture supply is not limited*. The model simulations show that 0.14 mm dew day^{-1} averaged over 18 days (which included a dry spell) is possible. However this amount can only be attained at a location high enough away from dry soils and exposed to a wind speed at collector height of around 1 m s^{-1}. In the study site, the air humidity is a limiting factor. With the same model set-up applied to a coastal setting the yields can increase by a factor of 2.5. In practice this value will be lower, since the coastal winds will not always be saturated during nocturnal conditions.

Future research for Objective 3:

There are numerous coastal deserts with topographic gradients heading towards a significant water body and the combined effect of a sea breeze and nocturnal katabatic flow needs more attention. As such it is recommended to explore the use of meso-scale models to study air masses that transport moisture and favour dew formation conditions. Chapter 6 analyzes the effect of incoming radiation, moisture and wind on dew yield of an artificial collector. The model simulations need to be tested for higher elevations. In the present research these simulations were omitted because of a lack of data. The model needs more validation to test the combined effect of increased radiative heat loss due to a drop in incoming longwave radiation at higher elevations and a reduction in specific humidity at a farther distance from the Mediterranean coast.

8.4 Objective 4: Developing and validating a numerical model to investigate dew water flows within a soil surface

Chapter 5 outlines the conditions for dew formation and provided an analysis of the water content within the soil. The measured moisture input into the soil begins before sunset, continues till sunrise, and is far larger than the amount of water available for biological activity. The reason is that part of it remains locked in the soil matrix potential. The dynamics of the exchange of water between the soil surface and the atmosphere under very dry conditions are strongly coupled to the soil moisture characteristics. Literature about this topic, however, is limited. One reason is that soil moisture content in drylands (beyond wilting point, pF > 4.2) has been of little interest to agriculture or mid-latitude regions. The strong daily temperature variations of the top soil in the NW Negev desert, or desert soils in general, shows that the soil desiccates the air during the evening hours. A downward latent heat flux will increase moisture content of the upper soil layers or wet the surface of leaves. The first process is usually called vapour adsorption and the second is called dew formation. A soil surface will adsorb water until visible water will appear onto its surface, or until this water will be available for biological activity. The point at which this happens will depend on the soil composition and soil water content. The concept of free available dew, as proposed in Chapter 6, is important when validating dew contribution to an ecosystem. The free available dew can be defined as the amount of accumulated water after the soil moisture level has risen above the wilting point. The wilting point differs among plant or cyanobacteria types, and the latter is much more drought resistant. This must be analyzed further for specific ecosystems.

A numerical multilayer model was designed to simulate water flows during condensation and evaporation. Cyanobacteria would be the first organism to become photosynthetically active when water concentration rises high enough at sunrise. The wilting point for cyanobacteria is much lower than for vascular plants, therefore the term Free Available Dew (FAD) was introduced. This would be the amount of dew suitable for biological activity (species specific). The dew as detected by the microlysimeters is the FAD plus a remaining part that is locked in the soil pores as adsorbed water. It is important to make this distinction, especially in desert ecosystem studies.

On sand dune slopes, initial biological soil crusting increases both the amount of dew and the soil moisture content near the surface. The FAD might be higher on a thinner crust than on a thick one, mainly because the soil moisture originating from dew remains more concentrated near the soil surface. Moisture differences between a thick and thin crust could be detected by the optical wetness sensor, although the differences were not large.

Future research for Objective 4:

There is a need to improve the soil water characteristic curves for the crust and soil below the crust. The extreme dry range is the driving force governing downward vapour flux, as observed by the microlysimeters. Soil water characteristic curves beyond wilting point based on adsorption isotherms for water on different clay minerals may be an improvement (see Chapter 5.5). The question is how biological crust activity can be modelled accurately. Issues as discussed in Chapter 5 include the swelling of the biological crust and the expected hysteresis. Research on the meteorological and soil conditions affecting photosynthetic activity of biological crusts under natural conditions would improve our understanding of sandy arid ecosystems.

A coupled atmosphere-soil model would be a next step towards study the differences between thin and thick crusts. Simulations did not reveal a longer wetness period for thinner crusts but there were many unknowns, especially the soil composition. If true, this would suggest that the initial formation and growth of a biological crust might benefit more from dew.

Samenvatting

Dit proefschrift bestudeert dauw en gerelateerde micrometeorologische condities van een woestijn nabij de kust van de noordwestelijke Negev woestijn in Israel. De studie is gemotiveerd door het feit dat hoewel dauw een gevarieerde rol speelt in veel ecosystemen (zoals beschreven in de voorgaande hoofdstukken), er nog geen standaard instrument om dauw te kunnen meten. Het onderzoek naar dauw formatie, depositie en drogen is daarom beperkt. Dit is uitdrukkelijk het geval voor woestijn ecosystemen waarbij dauw een primaire rol als watervoorziening voor microorganismen en kleinschalige fauna gedurende de lange regenloze periodes kan spelen of waarbij het nat/droog proces bacteriele afbraak van zaad coatings kan versnellen (voor ontkieming).

Het onderzoek in dit proefschrift is gericht op:

1. De rol van de bodemwarmtestroom in de energiebalans van een kust woestijn ecosysteem,
2. Quantificeren (via sensor ontwikkeling en metingen) van dauw depositie en verdamping in een kust woestijn ecosystem,
3. Analyse van de condities die waarbij dauw formatie optreedt,
4. Ontwikkeling en validatie van een numeriek model om het dauw water transport te onderzoeken nabij het bodemoppervlak.

8.1 Doelstelling 1: De rol van de bodemwarmtestroom in de energiebalans van een kust woestijn ecosysteem

Energiebalans studies benadrukken het delicate samenspel tussen stralingsforcering Q^*, en de resulterende turbulente en bodemwarmte fluxen. De meetnauwkeurigheid van bodemwarmtetransport G wordt vaak verwaarloosd in energieblans studies. Omdat in een woestuijn G net zo hoog kan worden als het voelbare warmtetransport H, zal het verwaarlozen van de G metingen leiden tot grote fouten in de berekening. Gedurende de nacht zijn de fluxen (G, H, Q^*) erg dominant. Een droge bodem zal snel de dagelijkse temperatuurgolf zodanig dempen dat een adequate correctie voor een begraven bodemwarmtestroom sensor erg moeilijk wordt en veel additionele correcties nodig worden.

Hoofdstuk 2 introduceert een nieuwe benadering om bodemwarmtestroom te meten. De meteorologische condities gedurende de lange hete en regenloze zomers, gekoppeld met de spaarse of afwezige vegetatie in de vlakke gebieden tussen de duinen, vormen een condities voor een uniek experiment waarbij de bodemwarmtestroom gemeten kon worden bijna direct aan het oppervlak. De plaatsing zo dicht bij het oppervlak heeft tot gevolg dat de dieptecorrecties niet meer nodig zijn. De Harmonische analyse en calorimetrische methode werden gebruikt om

deze directe metingen te vergelijken met traditionele methoden. Het blijkt dat de benadering zoals hier voorgesteld een realistische bodemwarmtestroom meting aan het oppervlak oplevert. De correctheid is ook bevestigd door het perfect sluiten van de bodemoppervlakte energiebalans onder droge woestijn condities. De oppervlakte energiebalans sluiting test geeft minder scatter met de direct gemeten bodemwarmtestroom dan uit de gecorrigeerde data van twee conventionele methodes zoals beschreven in hoofdstuk 2. De bijna perfecte sluiting ondersteunt de plaatsing van bodem warmtstroom sensoren nabij het oppervlak. In een droge kale bodem met een erg hoge bodemwarmtestroom adviseren we om de sensor zo dicht als mogelijk is nabij het oppervlak te plaasten.

Toekomstig onderzoek voor doelstelling 1:

De spliting van de separate componenten van de energiebalans aan het aardoppervlak maakt duidelijk dat hoge kwaliteitsmetingen van de bodemwarmtestroom noodzaak zijn. De zeer goede energiebalans sluiting zoals gevonden in de huidige studie laat zien dat de turbulente flux metingen van H en LvE betrouwbaar zijn, in ieder geval voor hoge Bowen verhoudingen. Het grote aantal publicaties dat rapporteert over het gat in de energiebalans sluiting zijn gebaseerd op metingen boven verdampende vegetatie en de vraag rijst dan ook hoe betrouwbaar de verdampingsmetingen zijn. Jacobs et al. (2008) gebruikte een gedetailleerde analyse van alle afzonderlijke componenten van de energie balans en vond dat een nauwkeurige correctie leidt tot een goede sluiting. Echter, correcties blijven groot, en daarom is er een noodzaak om onder gecontroleerde omstandigheden met lage Bowen verhoudingen en een instrumentele opstelling te meten die grote correcties uitsluit. Een dergelijk gecontroleerd exepriment zou dan plaats kunnen vinden boven een nat oppervlak zonder vegetatie. Het zou zeer interessant zijn om de bodemwarmtestroom meetmethode zoals hier is voorgesteld toe te passen als er geen obstructie ontstaat voor verdamping. Tegenwoordig zijn er zeer kleine bodemwarmtestroom sensoren beschikbaar maar deze zijn waarschijnlijk niet adequaat genoeg. Een betere benadering is waarschijnlijk het gebruik van lysimeters om onafhankelijk de verdamping te kunnen meten. Vochtige bodems benodigen een veel diepere lysimeter dan die geintroduceerd is in hoofdstuk 3, maar technisch is dit zeker mogelijk. De experimentele onderzoekslocatie zoals gebruikt in de Negev woestijn zou een mogelijkheid kunnen bieden om de energiebalans te onderzoeken bij lage Bowen verhoudingen. Een geschikte periode zou het einde van de winterregens kunnen zijn, waarbij de 100 mm (gemiddelde) jaarlijkse neerslag het bodemvocht tekort weer aanvult en zo energiebalans sluitingsstudies mogelijk maken onder vochtige condities (bodem).

8.2 Doelstelling 2: Quantificeren (via sensor ontwikkeling en metingen) van dauw depositie en verdamping in een kust woestijn ecosystem

Het onderzoek hierbij focusseerde op 4 verschillende oppervlaktes; het relatief vlakke gebied tussen de zandduinen, de duinhellingen met biologische korstvorming, plantenblaadjes en een dauw verzamelingsexperiment op een vlak oppervlak. De volgende detectiemethodes werden gebruik of ontwikkeld om dauw te quantificeren:

- handmatige en automatische microlysimeters
- visuele observaties van dauw
- eddy covariantie metingen
- optische sensoren die de natheid van een oppervlak meten
- kunstblad met electrisch weerstandsgrid metingen
- gravimetrisch watergehalte determinatie via handmatige bodembemonstering
- relatieve vochtigheidsmetingen in de bodem porien
- kunstmatige dauwcollector

Het nieuwe microlysimeter ontwerp (Hoofdstuk 3) werd gemotiveerd door het feit dat bestaande methodes om dauwhoeveelheden af te schatten berustten op het detecteren van dauw op een kunstmatig oppervlak wat vaak niet representatief is voor de hoeveelheid dauw op de bodem zelf. Een microlysimeter meet op een directe manier de toename of afname aan vocht via een weegmethode. De metingen toonden een significante dagelijkse uitwisseling van vocht tussen bodem en atmospfeer.

De totale nauwkeurigheid van de microlysimeter zoals hier getest is gebaseerd op de fabrikant specificaties van de weegbrug en de testen in een oven en was ±0.02 mm dauw equivalent. De compacte afmetingen en het lage gewicht laten toe dat de sensor geinstalleerd kan worden in een complex landschap, en niet alleen op een vlak oppervlak.

De microlysimeter laat zien dat dauw formatie op kale grond sterk afhangt van de bodemcompositie. De dagelijkse dauw variatieert van 0.1 tot 0.2 mm op stabiele duinhellingen en loopt op tot 0.4 mm op de vlakke bodem tussen de duinen. Dit verschil wordt verklaard uit het feit dat de bodem tussen de duinen een hoog silt en klei gehalte en verhoogde saliniteit heeft. Het verschil wordt minder naarmate de bodem vochtiger wordt. De bodem samenstelling is ook de reden dat dauw formatie al start als de bodem oppervlakte temperatuur nog 10 graden hoger is dan de dauwpuntstemperatuur op waarnemingshoogte. Tijdens een gemiddelde dauw nacht vertoonden de duin hellingen een 60% lagere dagelijkse variatie dan het gebied tussen de duinen.

Een nieuwe optische oppervlaktevocht sensor (OWS) werd ontwikkeld om het bevochtigen/drogen door dauw van een oppervlak of bladvocht gehalte te kunnen bestuderen. De OWS is de eerste optische veld sensor die dag en nacht onder allerlei weerscondities kan werken. De bodem kalibraties tonen aan dat de OWS erg gevoelig

is voor veranderingen in bodem vochtgehalte in een bodemvocht range die loopt van zeer droog tot aan veld capaciteit. De bodem wordt niet verstoord tijdens de metingen (contactloos). Zonder kalibratie kan de OWS al quantificeren of een oppervlak droog dan wel nat is. De OWS kan de vocht variatie in de bovenste laag van een biologische bodem kost volgen omdat de licht detectiebanden gebruik maken van een water absorbtieband rond de 1.9 µm golflengte. De benadering is dat de OWS gevoelig is voor tot een meetdiepte equivalent aan de fotosynthetisch actieve laag van de biologische korst. Model simulaties van bodemvocht transport in de biologische korst tonen aan dat slechts het bovenste deel van de biologische korst vrij water ter beschikking heeft voor mogelijke fotosynthese aktiviteit van cyanobacteriën. Bodemvocht variatie kon gedetecteerd worden door de OWS maar de dagelijkse variatie is smal. Een klein regenbuitje van 0.3 mm tijdens het veldexperiment in de NW-Negev woestijn op dagnummer 289 (jaar 2000) laat zien dat het signaal voor vloeibaar water sterker is dan de intensiteit veroorzaakt door dauw. Echter, cyanobacteriën zijn in staat om fotosynthese te bedrijven bij bodemwater potentialen ver onder het verzadigde bodemwater potentiaal. De OWS kan ook toegepast worden om watergehalte in bladeren te meten, indien niet verstoord door dauw, mist of regen interceptie. Voor planten bladeren moet opgemerkt worden dat de OWS reageert op intern en extern water en dat het verschil niet altijd eenduidig onderscheiden kan worden.

Eddy covariantie (EC) transport metingen werden gebruikt om het turbulente transport van vocht te meten. Het probleem is dat open pad infrarood gas analysatoren (LI-COR, LI-7500) gevoelig zijn voor vocht op de lensjes. Dauw op de LI-7500 lensjes is een serieus probleem op de klimaatzones op de gematigde breedte omdat het grote fouten in flux metingen introduceert en vaak zijn de metingen helemaal niet meer betrouwbaar gedurende vochtige episodes. De simulaties tonen aan dat vochtige lensjes door dauw meer dan 27% van de tijd voorkomen op een gematigde breedte locatie boven gras (Nederland). Het tekort aan betrouwbare metingen gedurende deze dauw episodes hebben een grote invloed op de uiteindelijke kwaliteit van de metingen van de netto ecosysteem uitwisseling (NEE) van CO_2 gemeten op jaarbasis. Deze onzekerheid resulteert in een overschatting van de opname van CO_2 vanwege de natte periodes omdat deze vaak samenvallen met periodes waarbij de respiratie domineert over fotosynthese. Het blijkt dat zelfs in een ariede omgeving opgepast moet worden voor vochtige condities door dauw op de lensjes. Dit wordt gedemonstreerd aan de hand van het Negev experiment waarbij vocht problemen 3.7% van de tijd optraden (Tabel 7.1). Bij de evaluatie van NEE over langere periodes wordt aangeraden de data nauwkeurig te analyseren op condensatie problemen op de lensjes. Met het voorgestelde berekeningsschema voor de oppervlaktetemperatuur van de LI-7500 lensjes kunnen zulke periodes gevonden worden. Uiteindelijk verdiende de meting voor uitwisseling vocht tussen bodem en atmosfeer van de microlysimeters de

voorkeur tijdens de experimenten in de NW-Negev woestijn. De EC methode onderschatte de verdamping in vergelijking tot de microlysimeters. De stratificatie van de atmosfeer en de meethoogte van ongeveer 3 m is waarschijnlijk de reden voor de onderschatting van de geaccumuleerde dauw. De EC metingen waren wel nuttig bij het bepalen van de start van het dauwvormingsproces en om de verschillen tussen dauw depositie snelheid met die van de microlysimeters te vergelijken.

Toekomstig onderzoek voor doelstelling 2:

De diepte van het microlysimeter monster bakje van 35 mm was beperkt maar voldoende voor het meten van de dagelijkse bodemvocht variatie. De adequate diepte werd bevestigd door parallelle handwaarnemingen met microlysimeters van verschillende dieptes. Waarschijnlijk is de gevonden minimale diepte te weinig na een regenperiode omdat er juist dan een vochtaanvoer vanuit diepere lagen kan plaats vinden. De dauw formatie aan het begin van het droge seizoen zal afwijken want het bodemvocht is lager en dauw stijging kan een belangrijke factor worden. Dauw stijging is de migratie van bodemvocht naar het oppervlak, hetgeen de lucht kan bevochtigen en ook kan leiden tot dauw formatie op planten.

Met de OWS wordt het mogelijk om zeer kleine verschillen in bodemvocht te meten. Een nauwkeurige kalibratie is nodig om dauw op die manier te kunnen kwantificeren in poreuze media en dat zou geoptimaliseerd kunnen worden voor een biologische korst.

8.3 Doelstelling 3: Analyse van de condities waarbij dauw optreedt

De metingen laten zien dat er een sterke bodemvocht variatie is in de bovenste 30 mm van de bodem. Typische meteorologische condities zijn beschreven in hoofdstuk 5 en zijn karakteristiek voor een dauw nacht. Aangetoond werd dat het neerwaartse vochttransport meer dan 2 keer hoger is dan de potentiele dauw. Het vochtransport richting de bodem kan afgeschat worden met behulp van standaard weerstation data met additionele metingen van de relatieve vochtigheid in de bodem.

Een grote vlakke collectorplaat, op de meetlocatie in de Negev woestijn, met additionele isolatie aan de onderkant en geplaatst op een grotere hoogte kan meer dan 0.2 mm per dag aan dauw inzamelen gedurende een gemiddelde dauwnacht. Model simulaties laten zien dat 0.14 mm dew per day gemiddeld over 18 dagen (inclusief een droge periode) mogelijk is. Echter, deze hoeveelheid kan alleen bereikt worden op grotere hoogtes verder weg van de droge bodem en blootgesteld aan een wind van rond de 1 m s^{-1}. Op de studie locatie de luchtvochtigheid was een beperkende factor. Hetzelfde model toegepast op een kustlocatie laat zien dat dauw hoeveelheden 2.5 keer hoger zijn indien vocht niet een beperkende factor is. In de praktijk zal deze waarde lager zijn, omdat de zeewind niet verzadigd zal zijn gedurende de nacht.

Toekomstig onderzoek voor vraagstelling 3:

Er zijn vele kust woestijnen met topografische gradienten richting een groot wateroppervlak en het gecombineerd effect van een zeebries en een nachtelijke katabatische wind verdient meer aandacht. Aldus is het aanbevelingwaardig om het gebruik van mesoschaal modellen te onderzoeken ter bestudering van luchtmassa's die vocht transporteren en optimale dauwcondities verschaffen. Hoofdstuk 6 analyseert het effect op inkomende straling, vocht en wind op de dauw opbrengst van een kunstmatige collector. De model simulaties moeten getest worden voor hoger gelegen locaties. In het huidige onderzoek werden deze simulaties weggelaten vanwege het tekort aan data. Het model moet verder gevalideerd worden om het gecombineerde effect van toegenomen stralingswarmte verlies veroorzaakt door een reductie in inkomende langgolvige straling op grotere hoogtes en de reductie van specifieke vochtigheid door de toegenomen afstand tot de Mediterrane kust te kunnen testen.

8.4 Doelstelling 4: Ontwikkeling en validatie van een numeriek model om het dauw water transport te onderzoeken nabij het bodemoppervlak

Hoofdstuk 5 gaat in meteorologische condities waarbij dauw formatie plaats vindt en maakt een analyse van het bodemvocht. Het gemeten vocht transport vanuit de atmosfeer naar de bodem begint al voor zonsondergang en gaat door tot zonsopkomst en is veel groter dan de hoeveelheid water beschikbaar voor biologische activiteit. De reden is dat een groot deel van het bodemvocht opgesloten wordt in het bodem matrix potentiaal. De dynamica van de uitwisseling van water tussen het bodemoppervlak en de atmosfeer onder erg droge condities is sterk gekoppeld aan de bodemvocht karakteristieken. Literatuur hierover is echter beperkt. Een reden daarvoor is dat bodemvocht concentraties in droge gebieden (boven het verwelkingspunt, pF >4.2) weinig interesse vanuit de landbouw of gematigde breedtes trokken. De sterke dagelijkse tempeatuursvariatie van de bovenlaag van de bodem in de NW Negev woestijn, of een woestijn in het algemeen, laat zien dat de bodem de lucht droogt gedurende de nachtelijke uren. Een neerwaarts gerichte latente warmtestroom zal de bodemvochtigheid nabij het oppervlak doen toenemen of plantendelen doen bevochtigen. Het eerste proces wordt vaak water adsorptie en het tweede proces wordt dauw genoemd. Een bodem oppervlak zal water adsorberen totdat zichtbaar water verschijnt op het oppervlak, of totdat water beshikbaar komt voor biologische activiteit. Het moment waarop dit plaats vindt zal afhangen van de bodemsamenstelling en het vochtgehalte. Het concept van vrij beschikbare dauw, zoals voorgesteld in Hoofdstuk 6, is belangrijk bij de validatie van de dauw bijdrage aan een ecosysteem. Vrij beschikbare dauw kan gedefinieerd worden als de

hoeveelheid geaccumuleerd water nadat het bodemvocht is gestegen tot voorbij het verwelkingspunt. Het verwelkingspunt verschilt tussen plant of cyanobacterie types en de laatste is veel vocht resistenter. Dit moet verder geanalyseerd worden voor specifieke ecosystemen.

Een numeriek meerlaags model werd ontworpen om water transport gedurende vocht condensatie of verdamping in de bodem te kunnen simuleren. Cyanobacteriën zijn de eerste organismen die photosynthetisch actief worden wanneer de water concentratie hoog genoeg is gestegen gedurende zonsopkomst. Het verwelkingspunt voor cyanobacteriën ligt veel hoger dan dat van vasculaire planten en daarom werd de term vrij beschikbare dauw (FAD) geintroduceerd. Dit representeert de hoeveelheid dauw beschikbaar voor biologische activiteit (soorten specifiek). De dauw zoals gedetecteerd bij de microlysimeters is het FAD plus een deel dat nog opgesloten zit in de soil porien als geadsorbeerd water. Het is belangrijk om dit verschil te maken juist voor woestijn ecosysteem studies.

Op zandduin hellingen, initiele biologische korstvorming verhoogt de hoeveelheid dauw en bodemvocht concentratie nabij het oppervlak. Vocht variaties tussen een dikke en dunne biologische korst konden gedetecteerd worden met de OWS, hoewel de verschillen klein waren.

Toekomstig onderzoek voor doelstelling 4:

Er is een noodzaak voor het verbeteren van bodemvocht karakteristieken van de biologische korst en de bodem eronder. De extreem droge bodem is de drijvende kracht achter het neerwaartse vochttransport, zoals geobserveerd door de microlysimeters. Bodemvocht karakteristieken voorbij het verwelkingspunt zijn vaak gebaseerd op adsorbtie isotermen voor water op verschillende klei mineralen en zouden verbeterd kunnen worden (zie Hoofdstuk 5.5). De vraag is hoe de biologische korst activiteit succesvol gemodelleerd kan worden. Discussiepunten zoals beschreven in Hoofdstuk 5 bevatten het opzwellen van de bodem door vocht en de te verwachten hysteresis. Onderzoek naar de meteorologische en bodemkundige condities die de fotosynthese van een biologische korst beinvloeden onder natuurlijke condites zouden ons begrip van een aried woestijn ecosysteem kunnen verbeteren.

Een gekoppeld atmospfeer-bodem model is een volgende stap in de studie naar de verschillen tussen een dunne en dikke biologische korst. Simulaties (uit Hoofdstuk 5) vertoonden geen langere nat periode voor een dunne korst, maar er waren nog veel onzekerheden, zoals vooral bij de bodem compositie. Als dit verschil wel voorkomt, dan suggereert dit dat de initiatie en groei van biologische korsten meer van dauw profiteert.

Curriculum Vitae

Bernard Gerard Heusinkveld (Bert) werd geboren op 12 augustus 1965 te Hengelo (G.). Op de Jenaplan basisschool te Hengelo (G.) ontstond al interesse in de meteorologie (met dank aan meester Rhebergen) en werden de buitenlucht temperatuur en luchtvochtigheid afgelezen. Tevens werden snelle luchtdruk varieties waargenomen middels een zelfgebouwd soort weerglas. Na de MAVO en doorstroom naar de HAVO (Ulenhof college) in Doetinchem werd na veel wikken en wegen, want het interessegebied was zo breed, gekozen voor een technische opleiding aan de HTS richting Elektrotechniek in Arnhem. In het praktijk jaar werd een eerste stage gelopen bij TNO-metaal waarbij warmtestromen in metalen werden gesimuleerd. Een tweede stage bracht mij bij het KNMI alwaar ze nog in het trotse bezit waren van een groep instrumentele ontwikkeling. De ervaringen die ik daar opdeed bij het ontwikkelen en testen van een snelle vochtsensor zouden me later goed van pas komen. Er werd gekozen voor een buitenlandse stage in Zwitserland bij ABB. Het afstudeeronderzoek werd bij Lips in Drunen uitgevoerd naar het automatisch positioneren van zeeschepen bij boorplatforms. In 1991 begon ik mijn beroepsleven bij de vakgroep Meteorologie aan de Landbouw Universiteit, later genoemd Wageningen Universiteit in een elektronisch laboratorium voor instrumentele ontwikkeling. Ik maakte hierbij ook zelf enige ontwikkeling door en droeg mijn steentje bij tijdens Meteorologische veldexperimenten wereldwijd. Een van de hoogtepunten was de zelf ontworpen elektronica voor een scintillometer zodat de vakgroep er nu zelf een, en later vele, scintillometers had.

Inmiddels begon de klimsport opgang te maken wereldwijd en ook in Wageningen was er een klimmuur verrezen. Uiteindelijk ontwikkelde ik me door tot kliminstructeur van de NKBV en werd erelid bij Ibex.

Centralisatie van ondersteunende diensten en het zoeken naar nieuwe uitdagingen leidden uiteindelijk tot het aangaan van een 4/5 nieuw dienstverband als assistent in opleiding. Het promotieonderzoek werd gefinancierd door NWO-STW. Het onderwerp behelst in hoofdlijnen instrumentele ontwikkeling t.b.v. het onderzoek naar natheid van een oppervlak door o.a. dauw. Uiteindelijk bleek het ontwikkelde instrument een ingang te geven naar onderzoek in de Negev woestijn, Israël. Het opzetten van en uitvoeren van 2 veldexperimenten heeft een goudmijn aan gegevens opgeleverd en tot op de dag van vandaag worden hier nog steeds de vruchten van geplukt o.a. in de vorm van publicaties wat leidt tot een beter inzicht in de subtiele meteorologische processen die dauw, de stille neerslag, aansturen. To be continued!

Appendix Wageningen UR Scintillometer design

The Wageningen UR large aperture scintillometers were designed by Heusinkveld and Nieveen (1994), with the first author responsible for the electronics design. These scintillometers continue to be used in numerous measurement campaigns around the globe in over 16 countries and the electronics has remained unchanged to date. A scintillometer can perform path-averaged sensible heat flux measurements. The design has proven itself during unattended operation over a time span of several years. The design is commercialized and has been implemented in all recent Kipp and Zoonen (Delft, The Netherlands) scintillometers (LAS and X-LAS).

The electronics signal processing is a modified version of the original design by Ochs and Wilson (1993) (NOAA, Boulder, U.S.A.). These modifications include:

- One chip synchronous detection circuitry.
- Temperature compensation circuitry.
- Current feedback compensation for the light detector to improve signal to noise ratios during bright background light (midday).
- High quality Salen and Key second order band pass filtering.

A digital processing scheme was proposed to replace the analog computation of refractive index fluctuations (C_n^2). It is computed from the demodulated signal at the receiver and was successfully tested in a comparison field experiment in Crete (De Bruin et al., 1996).

References

De Bruin, H.A.R., J.P. Nieveen, S.F.J. de Wekker and B.G. Heusinkveld, 1996: Large aperture scintillometry over a 4.8 km path length for measuring areally-average sensible heat flux. Proc.22nd AMS Symposium on Agricultural and Forest Meteorology, 28 January- 2 February, Atlanta, Georgia, USA, J69-J71.

Heusinkveld, B.G., Nieveen, J.P. (1994). Wageningen university large aperture scintillometer design. *Internal publication Wageningen UR Meteorology group.*

Ochs, G.R. and Wilson, J.J. (1993). A second-generation large-aperture scintillometer. *NOAA Tech. Memo, ERL WPL-232. NOAA Environmental Research Laboratories, Boulder, Co.*

List of refereed publications (and submitted manuscripts) by Bert G. Heusinkveld

Scientific articles (and submitted manuscripts) in refereed journals

Heusinkveld, B.G., Berkowicz, S.M., Jacobs, A.F.G., Hillen, W., Holtslag, A.A.M. (2008) A new remote optical wetness sensor and its applications. *Agricultural and Forest Meteorol*ogy, doi:10.1016/j.agrformet.2007.11.007

Jacobs, A.F.G., **Heusinkveld, B.G**., Holtslag, A.A.M. (2008) Towards closing the surface energy budget of a mid-latitude grassland *Boundary-Layer Meteorology,* DOI 10.1007/s10546-007-9209-2.

Jacobs, A.F.G., **Heusinkveld, B.G.**, Berkowicz, S.M. (2008) Passive dew collection in a grassland area, The Netherlands. *Atmospheric Research*, 87: 377-385.

Paaijman, K.P., Jacobs, A.F.G., **Heusinkveld, B.G.** (2008) Diurnal temperature variations of shallow and clear water bodies in western Kenya. *Hydrological Processes* (submitted).

Paaijmans K.P, **Heusinkveld BG**, Githeko AK, Dicke M, Holtslag AAM, Takken W, Jacobs AFG (2008) Diurnal temperature variations of shallow and clear water bodies in western Kenya. *Hydrol. Processes* (submitted).

Jacobs, A.F.G., **Heusinkveld, B.G.,** Kraai, A., Paaijmans K.P., (2008) Diurnal temperature fluctuations in an artificial shallow water body. *Int. J. Biometeorology*. (submitted).

Mauder,M., Foken,T. Clement, R., Elbers,J.A., Eugster, W., Grünwald, T., **Heusinkveld, B.G.**, Kolle, O. (2007) Quality control of CarboEurope flux data – Part II: Inter-comparison of eddy-covariance software. *Biogeosciences Discuss.,* 4: 4067-4099.

Weber, S., Graf, A., **Heusinkveld, B.G.** (2007) Accuracy of soil heat flux plate measurements in coarse substrates-Field measurements versus a laboratory test. *Journal of Theoretical and Applied Climatology,* 89: 109-114.

Jacobs, A.F.G., **Heusinkveld, B.G**., Holtslag A.A.M. (2007). Seasonal and interannual variability of carbon dioxide and water balances of a grassland area. *Climatic Change,* DOI 10.1007/s10584-006-9182-7.

Heusinkveld, B.G., Berkowicz, S.M., Jacobs, A.F.G., Holtslag, A.A.M., Hillen, W.C.A.M**.** (2006) An automated microlysimeter to study dew formation and evaporation in arid and semiarid regions. *Journal of Hydrometeorology,* 7: 825-832.

Jacobs, A.F.G., **Heusinkveld, B.G**., Wichink Kruit, R.J., Berkowicz, S.M. (2006). Contribution of dew to the water budget of a grassland area, Netherlands. *Water Resources Res*earch, 42, W03415, doi:10.1029/2005WR004055.

Jacobs, A.F.G., **Heusinkveld, B.G**., Klok, E.J. (2006) Leaf wetness within a lily canopy. *Meteorological Applications*, 12: 193-198.

Beysens, D., Milimouk, I., Nikolayev, V.S., Berkowicz, S., Muselli, M., **Heusinkveld,** B.G., Jacobs, A.F.G. (2006) Comment on "The moisture from the air as water resource in arid region: Hopes, doubt and facts" by Kogan and Trahtman. *Journal of Arid Environments*, 67: 343-352.

Jacobs, A.F.G., **Heusinkveld, B.G**., Kessel, G.J.T. (2005) Simulating of leaf wetness duration within a potato canopy. *NJAS-Wageningen Journal of Life Sciences,* 53: 151-166.

Jacobs, A.F.G., **Heusinkveld, B.G.,** Paaijmans, K.P.M. (2005). Shallow water temperatures and malarial mosquitoes. *Bulletin of the American Meteorological Society,* 86: 25-26.

Heusinkveld, B.G., Jacobs, A.F.G., Holtslag, A.A.M., Berkowicz, S.M. (2004) Surface energy balance closure in an arid region: role of soil heat flux. *Agricultural and Forest Meteorology*, 122: 21-37.

Jacobs, A.F.G, **Heusinkveld, B.G**., Holtslag, A.A.M. (2003). Carbon dioxide and water vapour flux densities over a grassland area in the Netherlands. *International Journal of Climatology*, 23: 1663-1675.

Jacobs, A.F.G., **Heusinkveld, B.G**., Berkowicz, S.M. (2002) A simple model for potential dewfall in an arid region. *Atmospheric Research*, 64: 285-295.

Kohsiek, W., Meijninger, W.M.L., Moene, A.F., **Heusinkveld, B.G**., Hartogensis O.K., Hillen, W.C.A.M., de Bruin, H.A.R. (2002) An extra large aperture scintillometer for long range applications. *Boundary-Layer Meteorology*, 105; 119-127.

Jacobs, A.F.G., **Heusinkveld, B.G**., Berkowicz, S.M. (2000). Force restore technique for surface temperature and surface moisture in a dry desert system. *Water Resources Research*, 36: 1261-1268.

Jacobs, A.F.G., **Heusinkveld, B.G**., Berkowicz, S.M. (2000) Effect of wind on the formation of dew in the Negev. *Hydrology and Earth System Sciences (refereed article)*.

Jacobs, A.F.G., **Heusinkveld,** B.G., Berkowicz, S.M. (2000) Dew measurements along a longitudinal sand dune transect. *International Journal of Biometeorology* 43:184-190.

Jacobs, A.F.G., **Heusinkveld,** B.G., Berkowicz, S.M. (1999) Dew deposition and drying in a desert system: a simple simulation model. *Journal of Arid Environments*, 42: 211-222.

Jacobs, A.F.G., **Heusinkveld,** B.G., Nieveen, J.P. (1998). Temperature behavior of a natural shallow water body during a summer period. *Theoretical and Applied Climatology*, 59: 121-127.

Jacobs, A.F. G., **Heusinkveld,** B.G., Lucassen, D.C. (1998). Temperature variation in a class A evaporation pan. *Journal of Hydrology*, 206:75-83.

Jacobs, A.F.G., Jetten, T.H., Lucassen, D.C., **Heusinkveld, B.G**., Nieveen J.P. (1997) Diurnal temperature fluctuations in a natural shallow water body. *Agricultural and Forest Meteorology*, 88: 269-277.

Lloyd, C.R., Bessemoulin, P., Cropley, F.D., Culf, A.D., Dolman, A.J., Elbers, J., **Heusinkveld, B.G**., Moncrieff, J.B., Monteny, B., Verhoef, A. (1997) A comparison of surface fluxes at the HAPEX-Sahel fallow bush sites. *Journal of Hydrology*, 188-189: 400-425.

Moncrieff, J. B., Massheder J. M., de Bruin, H.A.R., Elbers, J., Friborg, T., **Heusinkveld**, **B.G.**, Kabat, P., Scott, S., Soegaard, H., Verhoef, A. (1997) A system

to measure surface fluxes of momentum, sensible heat, water vapour and carbon dioxide. *Journal of Hydrology*, 188-189: 589-611.

Verhoef, A., Allen, S.J., de Bruin, H.A.R, Jacobs, C.M.J., **Heusinkveld, B.G.** (1996) Fluxes of carbon dioxide and water vapour from a Sahelian savanna. *Agricultural and Forest Meteorology*, 80: 231-248.

Verhoef, A., van den Hurk, B.J.J.M., Jacobs, A.F.G., **Heusinkveld, B.G.** (1996) Thermal soil properties for vineyard (EFEDA-I) and savanna (HAPEX-Sahel) sites. *Agricultural and Forest Meteorology,* 78: 1-18.

Refereed book contribution

Veste, M., **Heusinkveld, B.G**., Berkowicz, S.M., Breckle, S.-W., Littmann, T., Jacobs, A.F.G. (2008). Dew formation and activity of biological soil crusts. In: Arid Dune Ecosystems - The Nizzana Sands in the Negev Desert. Breckle, S.-W. & A. Yair (Eds.). Springer, Ecological Studies. Vol. 200 (in press).

Professional publications

Jacobs, A.F.G., **Heusinkveld, B.G**., Holtslag, A.A.M. (2006). Dauw boven grassland. *Meteorologica,* 15.

Dalenoord, E., **Heusinkveld, B.G.,** Hage, J. van de, Jacobs, A.F.G. (2004). Elektrisch geleidende luchten.
Meteorologica 13 . - p. 12 - 14.

Heusinkveld, B.G., Jacobs, A.F.G., Bosveld, F.C. (1997). De opkomst en ondergang van ijs in een sloot.
Meteorologica 4 (1997) 4-8.

Jacobs, A.F.G.; **Heusinkveld, B.G.**; Holtslag, A.A.M. (2006). Dauw boven grasland
Meteorologica 15 (1). - p. 27 - 30.

Jacobs, A.F.G., **Heusinkveld, B.G.**, Berkowicz, S. (1997). Dew deposition in the Negev Desert: source of Life.
Annual Report Production Ecology 10.

Publications for the general public

DeBruin, H.A.R.; Jacobs, A.F.G.; **Heusinkveld, B.G.**; Holtslag, A.A.M. (2001). Het wonderbaarlijke ijs.
NVOX Tijdschrift voor Natuurwetenschap op School 3 (2001). - ISSN - p. 142 - 146.

Jacobs, A.F.G.; Paaijmans, K.P.; **Heusinkveld, B.G. (2006)**. Over malaria en de temperatuur van ondiepe wateren.
Vuurwerk 17 . - p. 14 - 19.

Jacobs, A.F.G.; **Heusinkveld, B.G. (2004)**. Occulte neerslag: De Fonteinboom
Vuurwerk 15 . - p. 4 - 5.

Cover photo; Flowering *Pancratium sickenbergeri* bulb, Nizzana sand dunes, NW Negev, Israel. Photo by B.G. Heusinkveld.